AGARD-LS-144

AGARD

ADVISORY GROUP FOR AEROSPACE RESEARCH & DEVELOPMENT

7 RUE ANCELLE, 92200 NEUILLY SUR SEINE FRANCE

AGARD LECTURE SERIES No. 144

Interaction between EMP, Lightning and Static Electricity with Aircraft and Missile Avionics Systems

NORTH ATLANTIC TREATY ORGANIZATION

NORTH ATLANTIC TREATY ORGANIZATION

ADVISORY GROUP FOR AEROSPACE RESEARCH AND DEVELOPMENT

(ORGANISATION DU TRAITE DE L'ATLANTIQUE NORD)

AGARD Lecture Series No.144

INTERACTION BETWEEN EMP, LIGHTNING AND STATIC ELECTRICITY WITH AIRCRAFT AND MISSILE AVIONICS SYSTEMS

The material in this publication was assembled to support a Lecture Series under the sponsorship of the Avionics Panel and the Consultant and Exchange Programme of AGARD presented on 29—30 May 1986 in Ankara, Turkey, 2—3 June 1986 in Oberpfaffenhofen, Germany and 5—6 June 1986 in The Hague, The Netherlands.

THE MISSION OF AGARD

The mission of AGARD is to bring together the leading personalities of the NATO nations in the fields of science and technology relating to aerospace for the following purposes:

- Exchanging of scientific and technical information;
- Continuously stimulating advances in the aerospace sciences relevant to strengthening the common defence posture;
- Improving the co-operation among member nations in aerospace research and development;
- Providing scientific and technical advice and assistance to the Military Committee in the field of aerospace research and development (with particular regard to its military application);
- Rendering scientific and technical assistance, as requested, to other NATO bodies and to member nations in connection with research and development problems in the aerospace field;
- Providing assistance to member nations for the purpose of increasing their scientific and technical potential;
- Recommending effective ways for the member nations to use their research and development capabilities for the common benefit of the NATO community.

The highest authority within AGARD is the National Delegates Board consisting of officially appointed senior representatives from each member nation. The mission of AGARD is carried out through the Panels which are composed of experts appointed by the National Delegates, the Consultant and Exchange Programme and the Aerospace Applications Studies Programme. The results of AGARD work are reported to the member nations and the NATO Authorities through the AGARD series of publications of which this is one.

Participation in AGARD activities is by invitation only and is normally limited to citizens of the NATO nations.

Published May 1986

ISBN 92-835-1528-5

Printed by Specialised Printing Services Limited
40 Chigwell Lane, Loughton, Essex IG10 3TZ

LIST OF SPEAKERS

Lecture Series Director: Prof. A.W. Biggs
University of Alabama
Electrical and Computer Engineering Dept.
Huntsville, AL 35899
USA

SPEAKERS

Dr F.M.Tesche
LuTech, Inc.
3742 Mt Diablo Boulevard
Lafayette, CA 94549
USA

Dr C.E.Baum
AFWL/NTAAB
Kirtland AFB, NM 87117
USA

Dr R.Sturm
Wehrwissenschaftliche Dienstelle der
Bundeswehr für ABC-Schutz
Postfach 1320
3042 Münster
Germany

Mr I.P.McDiarmid
British Aerospace plc
Military Aircraft Division
Warton Aerodrome
Preston, Lancs PR4 1AX
UK

Dr J.E.Nanevicz
Stanford Research Institute
333 Ravenswood Avenue
Menlo Park, CA 94025
USA

Dr P.A.Sevat
Physics and Electronics Laboratory TNO
PO Box 96864
2509 JG The Hague
The Netherlands

CONTENTS

	Page
LIST OF SPEAKERS	iii
	Reference
INTRODUCTION* by A.W.Biggs	1
INTRODUCTION TO CONCEPTS OF ELECTROMAGNETIC TOPOLOGY AS APPLIED TO EMP INTERACTION WITH SYSTEMS by F.M.Tesche	2
ELECTROMAGNETIC TOPOLOGY FOR ORDERING ELECTROMAGNETIC INTERACTION IN COMPLEX SYSTEMS by C.E.Baum	3
SHIELDING AGAINST LIGHTNING INDUCED CURRENTS AND VOLTAGES by I.P.McDiarmid	4
STATIC CHARGING EFFECTS ON AVIONIC SYSTEMS by J.E.Nanevicz	5
ALLEVIATION/TESTING TECHNIQUES FOR AIRCRAFT CHARGING by J.E.Nanevicz	6
SIMULATION OF AIRCRAFT TRAILING WIRE ANTENNA ACTION WITH TRANSIENT ELECTROMAGNETIC WAVES. MODELS FOR ADAPTIVE ANTENNA ARRAY RESPONSES TO TRANSIENT ELECTROMAGNETIC WAVES* by A.W.Biggs	7
SHIELDING AGAINST EMP INDUCED CURRENTS AND VOLTAGES, EMP SIMULATION AND TESTING AND EMP COUPLING TO CABLES by R.J.Sturm	8
BALANCED EMP-SHIELDING OF C^3-FACILITIES by P.A.A.Sevat	9A
INTRODUCING LARGE CURRENTS INTO CABLES by P.A.A.Sevat	9B
EMP INTERACTION WITH AIRCRAFT AND MISSILES: A DESCRIPTION OF AVAILABLE COUPLING, PENETRATION, AND PROPAGATION ANALYSIS TOOLS by F.M.Tesche	10
MEASUREMENT TECHNIQUES FOR TRANSIENT ELECTROMAGNETICS by C.E.Baum	11
BIBLIOGRAPHY	B

* Oral Presentation only – no paper.

INTRODUCTION TO CONCEPTS OF ELECTROMAGNETIC TOPOLOGY AS APPLIED TO EMP INTERACTION WITH SYSTEMS

Frederick M. Tesche

LuTech, Inc.
3742 Mt. Diablo Blvd.
Lafayette, CA 94549
USA

ABSTRACT

This paper reviews the concept of the electromagnetic shielding topology of an electrical system, and illustrates how such a system can be hardened against unwanted electrical interference arising from external transient or CW sources. This manner of viewing a system proves to be useful in estimating the possible system responses, in developing particular hardened designs for the system, and in defining suitable tests for the verification of the hardness design.

I. INTRODUCTION

Due to the complexity of modern electrical systems, it is virtually impossible to carry out a rigorous analysis of how the system would respond if excited by lightning or nuclear electromagnetic pulse (EMP). In many instances, however, it may be desirable to obtain rough estimates or bounds for the system response, either for the purpose of designing an electrically hard system, or for estimating the vulnerability of the system to an outside electromagnetic (EM) environment.

One way of doing this is to introduce the concept of an electromagnetic shielding topology, which is a description of the configuration and interconnection of the conducting surfaces in the system which act as EM shields for the system. This topic has been discussed previously by a number of investigators in references [1], [2], [3]. With a knowledge of such a shielding topology, it is possible to determine all points of entry (POEs) for EM energy into the system, and concentrate the EMP hardening activities at these particular locations. In this manner, the hardening of a system has been reduced to controlling the EM transmission properties of the POEs of the shields: the details of the internal cónfiguration of the system are not important.

Associated with the topological diagram is a signal flow graph, referred to as the interaction sequence diagram. This shows the major internal coupling and propagation paths inside of the system, and is used in obtaining rough estimates of the system response which, in turn, are used in designing the system.

This interaction sequence diagram has several uses. In the process of designing a new system, it permits a designer to determine the most important, or "critical" coupling path in the system, so as to decide which parts of the system should be hardened first against the external EM environment. An alternate use is in the area of hardness assurance. By examining the diagram, the important POEs can be identified, and suitable tests defined to determine if the various protection mechanisms in the system are functioning properly. A third use is in the analysis area, where the interaction sequence diagram may be used to estimate (roughly) what the responses of the system are in the EM environments.

In the system design process, electromagnetic topology plays a key role as indicated in Figure 1. The designer of the system has a set of functional requirements which must be met by the system. At the same time, there is an indication of the electrical stress (lightning, EMP, EMI, etc.) which can excite the system, and which should not adversely affect the normal operation of the system. In addition, there is a specified level of EM susceptibility for the components in the system. This may be a well defined set of numbers, such as, the known failure levels of all semiconductor devices within the system, or an approximate "noise level" of the internal system noise. The system EM topology provides a way of relating the behavior of the system to the outside stress and determining whether there will be a failure of the system. If it is estimated that a failure may occur, the design of the system must be modified to eliminate (or at least, reduce) the chance of a failure. Thus, the design process is an iterative one, often requiring several iterations through the analysis/design phase before a final system design is determined.

In this paper, the concepts of the system shielding topology and the associated interaction sequence diagram are introduced, and some simple hypothetical system examples are given. Section II of this paper discusses the elementary concepts of electromagnetic topology, and the interaction sequence diagram. In Section III, these are illustrated with a simple example. Section IV presents a brief discussion of how the electromagnetic topology concepts are used to develop hardness allocations for a system being designed, and Section V presents a summary of these discussions.

II. DEFINITIONS

In this paper the term electromagnetic topology, or simply topology is meant to refer to the collection of conducting surfaces within an electrical system which tend to impede the passage of electromagnetic fields. These are, in the most general sense,

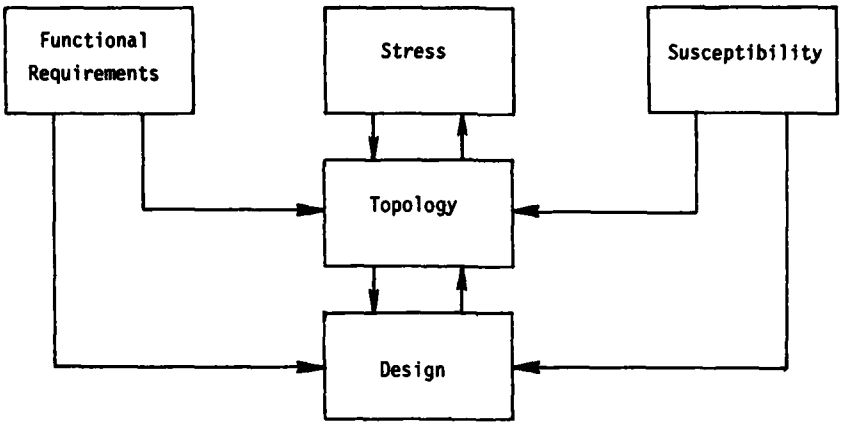

Figure 1. Role of electromagnetic topology in system design.

nothing more than Faraday cages.

Viewing the system in this manner is useful, because it is possible to concentrate the EM hardening activities at the surface, or "barrier", which should be closed and have a minimum number of penetrations, so as to provide the maximum shielding.

Often, a system consists of multiple, nested shielding surfaces. However, in every case of practical interest, there must be some form of penetration from the outside of the system to the interior. In these cases, it is important to identify each penetration point in the barrier, and add suitable EM protection, so as to maintain the internal electrical responses at some agreed upon safe level.

In defining the shielding topology for a system, it is important to realize that a system frequently can have different operational configurations, and hence, different electrical topologies. In these cases it is important to develop a topological representation for each system configuration, and perform the required hardening or EM interaction study for each configuration.

As an illustration of the topological shielding concept, consider a very simple example of a shielded system having three separate, nested electromagnetic barriers as shown in Figure 2. The volume outside the system is denoted as V_0, with V_1, V_2, and V_3 being the volumes inside, which are bounded by the surfaces $S_{0,1}$, $S_{1,2}$, and $S_{2,3}$.

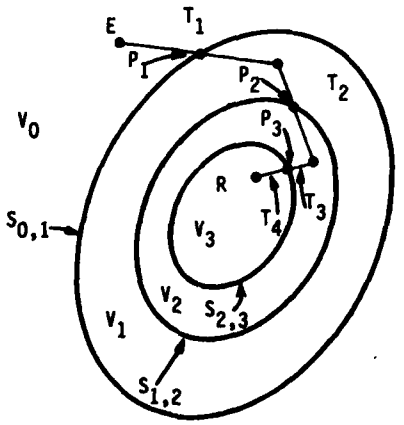

Figure 2. Simple electromagnetic topology for a system having three barriers.

Outside the system, it is assumed that there is some form of electromagnetic field excitation, and this is able to penetrate into the system, eventually arriving at the V_3 volume to create electrical responses. Although there may be many different individual paths within the system by which the external EM field is able to propagate to the response point, these paths are represented schematically in this discussion as a single path from the outside to the inside of the system. In this manner, the various internal responses to the outside EM stress can be viewed as a vector [R] which is related to the excitation fields through a series of matrix transfer functions as:

$$[R] = [T_4][P_{2,3}][T_3][P_{1,2}][T_2][P_{0,1}][T_1][E] \qquad (1)$$

In this expression, [E] represents a vector of excitations which account for the electromagnetic field outside the system, $[T_1]$ is a coupling and propagation matrix which provides a knowledge of the local excitation quantities at each of the penetration points on surface $S_{0,1}$, and $[P_{0,1}]$ is a matrix defining the penetration properties of the first barrier, $S_{0,1}$. Thus the product

$$[P_{0,1}][T_1][E] \qquad (2)$$

represents the electrical response at all of the points within volume V_1 which are contained on the interaction paths defined for the system.

Generally, the matrices defining the penetration properties of the system's shielding barriers, $[P_{i,j}]$, are sparse and diagonal, since the penetration process is local. However, the matrix defining the coupling and propagation properties of a volume, $[T_i]$ is usually not sparse, due to the wave nature of the electromagnetic field.

Evaluating the response of Eq.(1) exactly for anything but the most simple system e.g., a straight wire inside of a spherical shield having an aperture) is a very complex task. Consequently, it is desirable to approximate the general matrix equation by considering approximations to this interaction process. This is done by introducing the interaction sequence diagram which is a signal flow diagram associated with the system topological diagram. This diagram shows the major paths of EM energy propagation and penetration within the system.

The EM energy is able to penetrate into the system through three basic mechanisms: 1) direct (hard-wire) penetrations, 2) aperture penetrations, and 3) diffusion (see reference [4]). Once inside the system the energy can propagate along deliberate or inadvertent transmission line structures, or by direct radiation.

For simplicity, the EM propagation of energy within the system is assumed to propagate in only one direction. Hence, the linear graph representing the EM interaction sequence diagram is a directed graph. It is assumed that the direction of energy flow is from a region having large EM fields to one having smaller fields. Along each propagation path, there is a transfer function which describes the behavior of the EM signals. At any particular observation point in the system, there can be several paths contributing to the response.

The interaction sequence diagram is useful in designing a new system by permitting the definition of a "critical coupling path". This is the coupling path which provides the largest amount of excitation at a response point, and is used in determining which POEs of the system should be hardened first.

In developing the interaction sequence diagram, only a few of the most important coupling paths are initially considered. The rest, providing only small contributions to the total system response, are disregarded. However, as any one critical coupling path is eliminated (by locating suitable penetration protection devices such as filters, nonlinear elements, etc. at the penetration points in the topological surfaces), these previously unimportant coupling paths may then become critical in determining the system response. Hence, the interaction sequence diagram may change as the system becomes harder.

The propagation and penetration of energy along the interaction paths of the system are defined in terms of transfer functions. These relate the behavior of an observable quantity on one point in the system to that of another observable somewhere else in the system. In the present case, the possible observables are 1) current, 2) charge, 3) E field, or 4) H field. Normally, these transfer functions are complex-valued functions of the frequency. However, in the application of the interaction sequence diagram to practical problems, it is common to ignore this fact and develop a rough estimate of the transfer function magnitude at the primary frequencies of interest in the EMP or EMC regime.

III. AN EXAMPLE

Let us consider a simple example to illustrate the EM Topological approach for hardening a system, and compare it with a more conventional analysis procedure. Figure 3 illustrates a hypothetical communications facility which contains a UHF antenna and feeding coaxial line connected to load equipment which are located inside of two individual EM barriers. Within the first barrier, there is a filter vault sub-volume which contains any necessary EMP or EMI filters for the first layer penetration, and

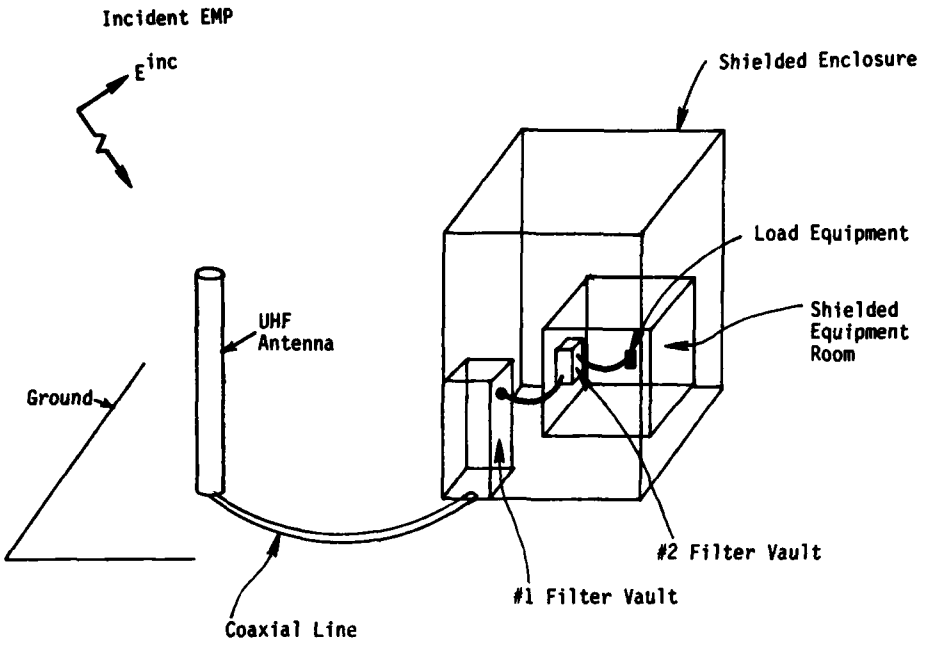

Figure 3. Hypothetical ground-based system.

consequently, keeps any large EM fields produced by the normal operation of these devices out of the first protected volume. Similarly, within the second EM barrier there is another filter vault for the same purpose.

It is assumed that an incident EMP excites the external regions of the system and that it is necessary to estimate the response of the load equipment. This response, which might be the voltage developed across the load impedance connected to the transmission line feeding the antenna, is usually calculated by using a detailed transmission line model, as shown in Figure 4. The interaction of the incident EMP field on the antenna can be modeled using simple antenna theory to yield an equivalent Thevenin circuit at point A-A'. With the use of the simple transmission line propagation relations and a knowledge of the filter designs, it is then possible to compute the load voltage.

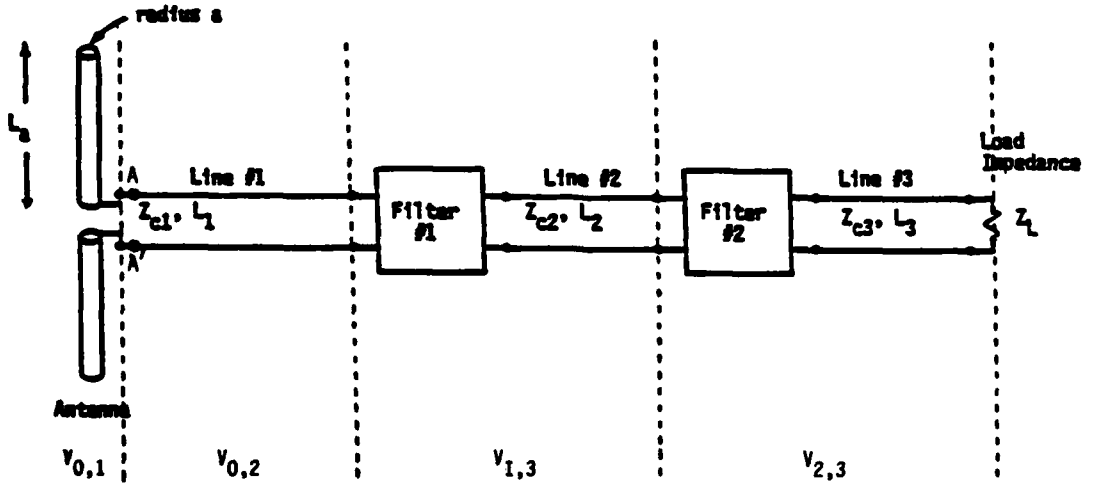

Figure 4. Conventional transmission line model for system.

Note that in the conventional equivalent circuit for this interaction path, there is little information regarding the nature of the system topology and how the interaction path penetrates through into the interior. This, however, may be accomplished by using the EM topological model. Figure 5a shows the system topology for this example.

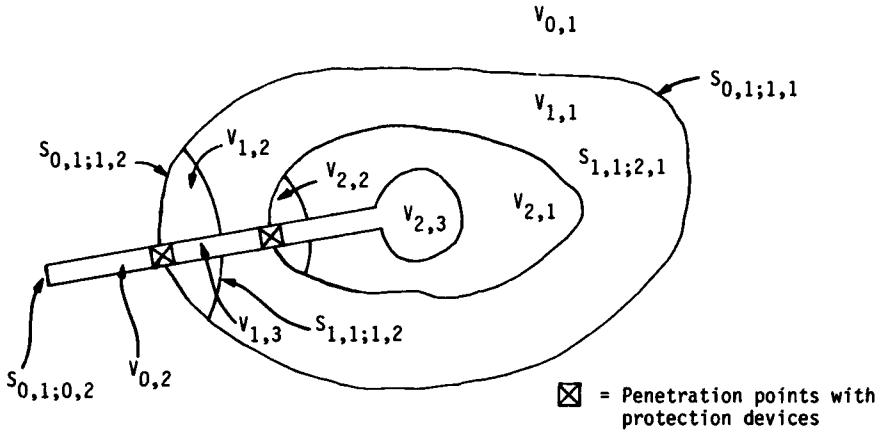

a. System Topology

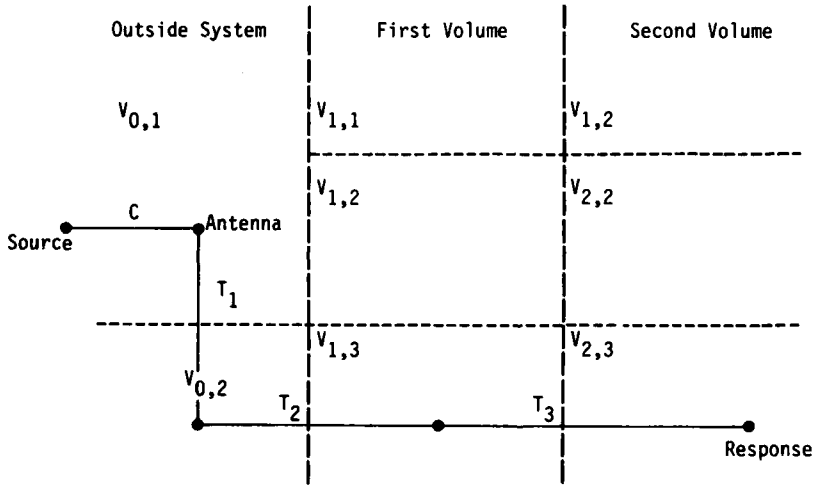

b. Interaction Sequence Diagram

Figure 5. System topological diagram (a) and interaction sequence diagram (b) for hypothetical system.

Because of the coaxial lines and two filter vaults being present in the system, it is necessary to adopt a slightly more complicated labeling scheme from that used in Figure 2, which had a very simple topology. Note that in addition to the volume completely outside of the system, there is another volume located inside the transmission line between the antenna and the first penetration point of the system. Because this volume is not protected at the antenna terminals, topologically it is also an external volume. To distinguish between these two external volumes, referred to as sub-volumes, it is necessary to introduce an additional subscript. Consequently, the volume completely outside the system is denoted as $V_{0,1}$, and that inside the coaxial line is $V_{0,2}$.

Within the first EM barrier in Figure 5a, it is seen that there are three sub-volumes: one inside the coaxial line region just past the first protective device, one inside the filter vault, and the other inside the remainder of the first barrier. For each of these sub-volumes, there is a minimum of one surface that must be traversed to pass from any of the outside regions (i.e., $V_{0,1}$ or $V_{0,2}$) to the region in question. These regions are denoted as $V_{1,1}$, $V_{1,2}$, and $V_{1,3}$, respectively.

The labeling of the system surfaces also becomes a bit more tedious in this case. Previously, the system surfaces were labeled by two numbers, as $S_{i,j}$, referring to the surface that divides volume V_i from V_j. With subvolumes $V_{i,j}$ and $V_{k,l}$, the corresponding bounding surface is denoted as $S_{i,j;k,l}$. The various surfaces for the example system are also shown in Figure 5a.

The interaction sequence diagram for the conducting antenna penetration path for the example system is illustrated in Figure 5b. The incident EM field strength, denoted by E, couples to the antenna in a manner represented by the transfer function denoted by C. This antenna response then propagates into the first coaxial cable through transfer function T_1. The transfer function T_2 represents the combined effects of the filter #1 and the second transmission line segment, and T_3 accounts for the second filter and line combination. In this manner, the response at the end of the line in the volume $V_{2,3}$ can be expressed as

$$R = T_3 \times T_2 \times T_1 \times C \times E \qquad (3)$$

Note that in the interaction sequence diagram, there is a clear indication of the various shielding levels in the system, and that the antenna interaction path only passes through a few of the many volumes. In a real system, there are usually other penetration points in the shielding topology, and we would expect there to be other interaction paths in the diagram. In this case, the response at the desired point would consist of a sum of terms like that in Eq.(3) above, one for each path.

Generally, the system topology diagram and the interaction sequence diagram is much more complicated than that shown in Figure 3. For example, Figure 6 presents a more detailed topological diagram for a realistic system having a three layer shielding topology. The corresponding interaction sequence diagram is shown in Figure 7. It is to be noted that in this system, the external field couples to several different external appendages of the system, and gives rise to a more complicated interaction process. Also, within the system there is propagation along various transmission lines which, if neglected, provides a unity transfer function. This can give rise to a substantial simplification of the interaction sequence diagram.

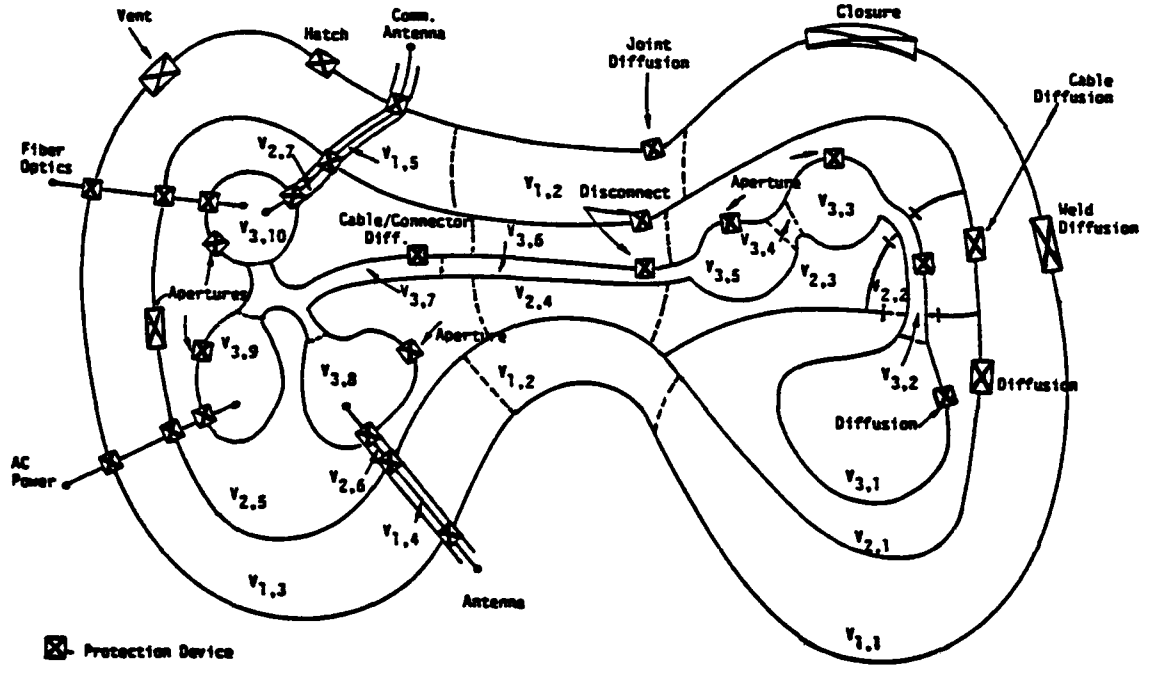

Figure 6. Example of a detailed system topology diagram for a complex, hypothetical system.

Further simplifications can be achieved, as previously noted, by neglecting those interaction paths which do not contribute greatly to the system response. Specifically, those paths which involve diffusion and aperture penetration typically do not provide the largest response in the system. The conducting (or hard-wired) penetrations are usually most important.

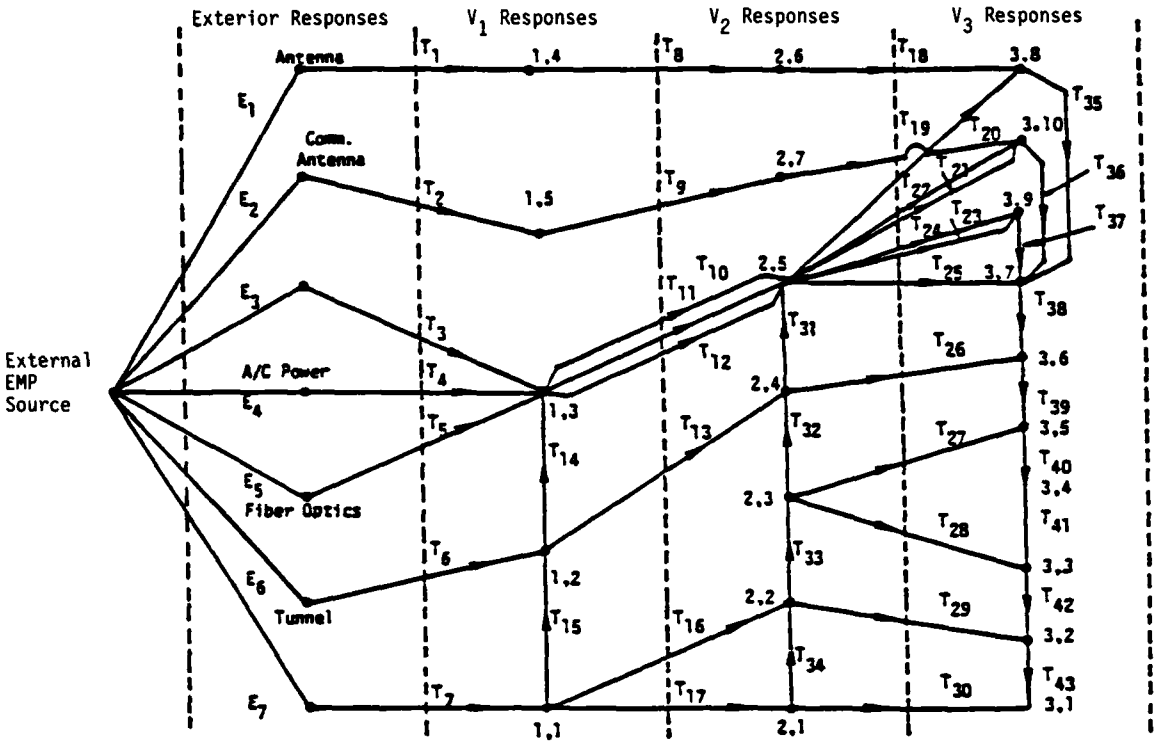

Figure 7. The interaction sequence diagram corresponding to Figure 6.

IV. DEVELOPMENT OF SYSTEM HARDNESS ALLOCATIONS

The interaction sequence diagram can be used in the design process of a system in allocating the required hardening at the various POEs in a system. This is done by estimating the EM-induced response inside the system, comparing it with some predetermined level and, if the response exceeds this level, the necessary amount of additional EM shielding or protection can be estimated.

The determination of the maximum permissible response level in the system is not an easy task. First, it is necessary to define exactly what is meant by "response". As previously discussed, a response can be any observable within the system, and may be considered either as a transient or spectral signal. Frequently, bounds on such responses are specified in design requirements provided by procuring agencies. Often, such bounds are related to the component failure or upset levels estimated for the system. An alternate, but overly conservative, approach for determining this signal level is to equate it to the ambient noise level in the system.

Estimating the required hardening for the system can be done in two ways. The first is by concentrating on the response at a point in the system on a path-by-path basis. By determining the critical coupling path, the important POEs in the path may be identified and suitably hardened.

The second approach is on a layer-by-layer basis, where all POEs in a particular shielding layer in the system are identified, and bounding estimates of the total EM energy penetrating into the shield made, using the concepts discussed in references [5] and [6]. Requiring that the bound of the penetrated response be lower than a certain amount leads to a definition of the shielding of the various POEs.

It is to be recognized that in the design of a practical system, there are other constraints than EMP hardness placed on the system. These include cost, weight, maintainability, etc., and these factors also affect the hardness allocation process. Hence, the development of detailed hardness requirements for the system is usually an iterative process, attempting to obtain the "best" design for all of these factors.

Once the various hardening levels have been specified, the topological diagram with its identification of the various penetration points can form the basis of a topological control plan for the duration of the system construction phase. Any modification of the system topology during the construction must be analyzed for possible adverse effects on the overall system hardness.

Having a system with a well-defined shielding topology and an interaction sequence diagram is also useful in attempting to define a series of measurements for the purpose of EM hardness validation, once the system is built. Since the major POEs are identified and controlled in the design of the system, the locations for possible measurements are also well defined, as are the observables. Such measurements, once performed on a hardened system, serve to form the baseline response useful for comparing subsequent measurements of the system response as the system ages.

V. SUMMARY

This paper has introduced the concept of electromagnetic topology for the purpose of designing an electrically hardened system. The topological concept provides a framework for viewing the EM interaction process in a structured manner. The design of a system first involves determining the various shielding surfaces in the system, and then identifying the penetration points in the system. This leads to a definition of the major EM coupling paths in the system which transmit the externally produced signals to the critical equipment on the system's interior. With an estimate of the susceptibility levels of components within the system, it is possible to determine the relative amounts of EM protection required at each penetration point.

It is important to keep in mind that this technique is more qualitative than quantitative. The transfer functions used in the interaction sequence diagram and the approximations used in defining the diagram are such that detailed time domain histories of internal responses are not calculable. Only rough estimates of internal responses are possible using this topological approach. However, this method of viewing a system provides useful guidance to system designers, many of whom are not accustomed to dealing with electromagnetic field problems.

REFERENCES

1. Tesche, F.M., "Topological Concepts for Internal EMP Interaction", IEEE Trans. EMC, Vol EMC-20, February 1978, pp. 60-64.

2. Vance, E.F., "On Electromagnetic Interference Control", IEEE Trans. EMC, November 1980, pp. 319-328.

3. Baum, C.E., "*Electromagnetic Topology:* A Formal Approach to the Analysis and Design of Complex Systems", Proceedings of the 1981 EMC Symposium, Zurich, Switzerland, 1981.

4. EMP Interaction: Principles, Techniques and Reference Data, K.S.H. Lee, editor, Air Force Weapons Laboratory Report, AFWL-TR-80-402, Kirtland AFB, New Mexico, 1980.

5. Yang, F.C., and C.E. Baum, "Use of Matrix Norms of Interaction Supermatrix Blocks for Specifying Electromagnetic Performance of Subshields", AFWL EMP Interaction Notes, Note 427, April 1983.

6. Baum, C.E., "Bounds on Norms of Scattering Matrices", AFWL EMP Interaction Notes, Note 432, June 1983.

ELECTROMAGNETIC TOPOLOGY FOR ORDERING ELECTROMAGNETIC INTERACTION IN COMPLEX SYSTEMS

Carl E. Baum
Air Force Weapons Laboratory
Kirtland AFB, New Mexico 87117-6008

ABSTRACT

For complex electronic systems such as missiles, aircraft, communication centers, etc., one would like to understand and control the interaction of electromagnetic fields (from EMP, lightning, and other sources) with the system. In general the system is much too complicated for a detailed understanding of every resulting signal everywhere in the system. However, the use of topological concepts allows one to control the signal levels, at least in a bounding sense, by concentrating attention on a set of closed surfaces (generalized shields) within the system and obtaining a norm of the appropriate measurable scattering parameters. This paper discusses both qualitative and quantitative aspects of EM topology as a tool for the design (and testing) of complex electronic systems for controlled EM response.

I. The subject of electromagnetic topology has grown considerably since its inception in 1974 [1]. There is already more than enough material to write a book on the subject. In this situation it was felt that the most useful function these lecture notes could serve would be to provide a bibliography of the important references on the subject; this is included herewith.

Note that electromagnetic topology has both qualitative (or descriptive) and quantitative aspects. The bibliography is divided into two parts to reflect the emphasis of the particular references. Note, however, that some references contain both aspects, in which case the appropriate category is uncertain.

Qualitative EM topology is concerned with the use of topology to describe the shielding (and other) macroscopic EM characteristics of a complex system (scatterer). It is concerned with things like the number of subshields, relative shielding orders between various volumes, equivalence of EM topology diagrams and special graphs known as interaction sequence diagrams, representations of grounding networks, etc. Its purpose is to provide concepts for the overall EM design of a system by identifying and ordering the important elements in a design which control the EM response.

Quantitative EM topology uses the quantities of qualitative EM topology (such as shields, layers, subshields, sublayers, etc.) to partition the EM interaction equations into parts associated with each of these for subsequent manipulation. The general interaction equation in scattering form is the BLT equation [9]. Partitioning introduces supervectors and supermatrices. Assuming that transfer functions through subshields are small leads to the good-shielding approximation. Application of norms leads to bounds on signals reaching various sublayers of the system. The uses of various kinds of norms in this context is growing. Initially the norms were for frequency-domain quantities [10]. More recently time-domain has been used as well [13].

II. BIBLIOGRAPHY

Part 1: Qualitative EM Topology

1. Baum, C. E., How to Think About EMP Interaction, Proc. 1974 Spring FULMEN Meeting (FULMEN 2), pp. 12-23, April 1974.

2. Baum, C. E., The Role of Scattering Theory in Electromagnetic Interference Problems, in P.L.E. Uslenghi (ed.), Electromagnetic Scattering, Academic Press, 1978.

3. Vance, E. F., On Electromagnetic Interference Control, Interaction Note 380, October 1979, and IEEE Trans. Electromagnetic Compatibility, November 1980, pp. 319-328.

4. Baum, C. E., Multiple Electromagnetic Topologies for Describing Various Aspects of Electronic Systems and Various System States, Proc. 1980 Spring FULMEN Meeting (FULMEN 4), March 1980, p. 33.

5. Lee, K.S.H. (ed.), EMP Interaction: Principles, Techniques, and Reference Data, EMP Interaction 2-1, December 1980, AFWL-TR-80-402 (available from NTIS).

6. Baum, C. E., Sublayer Sets and Relative Shielding Order in Electromagnetic Topology, Interaction Note 416, April 1982, and Electromagnetics, October-December 1982, pp. 335-354.

7. Baum, C. E., Topological Considerations for Low-Frequency Grounding and Shielding, Interaction Note 417, June 1982, and Electromagnetics, April-June 1983, pp. 145-157.

Part 2: Quantitative EM Topology (including transmission-line network theory, BLT equation, and norms)

8. Tesche, F. M., Topological Concepts for Internal EMP Interaction, IEEE Trans. Antennas and Propagation, January 1978, pp. 60-64, and IEEE Trans. EMC, February 1978, pp. 60-64.

9. Baum, C. E., T. K. Liu, and F. M. Tesche, On the Analysis of General Multiconductor Transmission-Line Networks, Interaction Note 350, November 1978, and also to appear in L. H. Leussen and J. E. Thompson (eds.), Advanced Electrical and Optical Diagnostics, Martinus Nijhoff, The Hague.

10. Baum, C. E., Electromagnetic Topology: A Formal Approach to the Analysis and Design of Complex Electronic Systems, Interaction Note 400, September 1980, and Proc. EMC Symposium, Zurich, 1981, pp. 209-214.

11. Agrawal, A. K., and C. E. Baum, Bounding of Signal Levels at Terminations of a Multiconductor Transmission-Line Network, Interaction Note 419, April 1983.

12. Yang, F. C., and C. E. Baum, Use of Matrix Norms of Interaction Supermatrix Blocks for Specifying Electromagnetic Performance of Subshields, Interaction Note 427, April 1983.

13. Baum, C. E., Black Box Bounds, Interaction Note 429, May 1983, and Proc. EMC Symposium, Zürich, 1981.

14. Baum, C. E., Bounds on Norms of Scattering Matrices, Interaction Note 432, June 1983.

15. Baum, C. E., Some Bounds Concerning the Response of Linear Systems with a Nonlinear Element, Interaction Note 438, June 1984.

16. Baum, C. E., On the Use of Electromagnetic Topology for the Decomposition of Scattering Matrices for Complex Physical Structures, Interaction Note to be published.

SHIELDING AGAINST LIGHTNING INDUCED CURRENTS AND VOLTAGES

by
I. P. MacDiarmid
British Aerospace, P.L.C.
Military Aircraft Division
Warton Aerodrome
Preston
LANCS PR4 1AX
UNITED KINGDOM

1. INTRODUCTION

In the past ten years there has been a rapidly growing need for the aircraft designer to consider the direct and indirect effects of lightning. The concern over the indirect effects of lightning arises because of the increasing use of electrical/avionic equipment on aircraft. This utilisation of electronics now involves those systems on which the safety of flight depends. It is clear that it is now essential for design engineers to consider the protection of equipment and systems from the indirect effects of lightning.

In addition to the changes in system technology cited above, the airframes in which the systems are contained, make use of increasing amounts of non-metallic material, in particular Carbon Fibre Composite (C.F.C.). The electrical conductivity of such material is much lower (<< 1/1000) than that of aluminium alloy - the traditional airframe material. To exacerbate the situation electrical contact to C.F.C. components is difficult, thus the electrical conductivity of a structure containing many components manufactured in C.F.C. can be very low. This greatly reduces the protection of the systems against the induced effects of lightning afforded by the structure. In addition the resilience of the structure to damage as a result of the direct effects of lightning is greatly reduced, although the protection of the structure against the direct effects of lightning is not covered in this lecture. The lecture will concentrate on the mechanisms involved in the coupling of the lightning currents which flow in the structure, with the systems, during direct lightning attachment to the airframe.

The problem is considered in three parts, this arises from a topological view of the coupling mechanisms. Lightning, attaching to the airframe, produces large currents in the structure, these currents have associated with them high electromagnetic field strengths. The electromagnetic fields couple with the cabling involved in the system contained within the airframe. The currents and voltages induced in the cables appear at the terminals of the equipment. The electronics in the system, if not protected, will be temporarily upset or permanently damaged. It can be seen that it is a three level problem; protection of the systems by the structure, protection of the cabling and equipment from the fields which penetrate the structure and finally protection of the equipment from the field-induced currents and voltages which finally appear at the terminals. All three areas of design effort, namely; the electrical performance of the airframe, the systems installation and the equipment are interdependent. The airframe manufacturer has direct control over the first two and by suitable specification must control the equipment design.

It can be seen that in order to obtain protection for the minimum weight/cost/volume penalty, including "cost of ownership" considerations, there is the concept of a "balanced protection strategy" (Ref. 1), in which the protection of the systems is suitably shared between airframe, systems installation and equipment design.

This lecture will cover the mechanisms involved in the indirect effects of lightning and will indicate the prime features of good, airframe, system and equipment design in order to protect against these effects.

2. THREATS AND VULNERABILITY

Before considering the mechanisms of the indirect effects of lightning, it is perhaps worthwhile obtaining orders of magnitude for the threat posed by the lightning to the equipment contained within the aircraft. A quantitative assessment of the threat can be obtained by approximately evaluating the voltages and currents on the cables and obtaining estimates of the values required to destroy or cause upset of the electronics.

Firstly, it is important to establish the fundamental parameters of the lightning. Lightning phenomenologists continue to debate this subject vigourously. The lightning parameters applicable to aircraft are those current and charge time

histories which, in general, exist at some point in the lightning channel, NOT at the ground. The majority of lightning measurements (Ref. 2 & 3) have until recently been made using ground based towers. The requirements and recommendations of Mil-Std 1757 (Ref. 4) CLM-R 163 (Ref. 5) and other similar aircraft design requirement documents are based on these types of measurements. The protection of modern aircraft is now a more precise design aim and accordingly it is felt that the threat against which the protection is designed must be more accurately known, hence much work (Ref. 6 & 7) is progressing to establish more accurately the threat values.

For the purposes of this lecture the lightning parameters are taken as those shown in Fig. 1. This diagram (taken from Ref. 8) is a collection of the worst case parameters, any one or more of whcih could occur in a lightning strike. It can be seen that the peak current is 200KA, the maximum rate of rise (occuring in the restrike phase) is 100KA/microsec. The maximum action integral, which is a measure of the energy available for dissipation, is $2*10^6$ A^2 s. The figures are enormous by any standards, it is little wonder that lightning poses a threat to airborne electronics!

The complete lightning event used as a basis for lightning protection design and described by Fig. 1. is not a function which can be conveniently described mathematically. The double exponential function:

$$I = I_L (e^{-t/\tau_1} - e^{-t/\tau_2}) \quad ..... \quad (2.1)$$

where I_L = 206KA; $\tau_1 = 5.8 \times 10^{-5}$ secs and $\tau_2 = 2.8 \times 10^{-7}$ secs.

is often taken as the 'driving function' for the purposes of analysis. This function is shown in Fig. 2.

The major parameters of the lightning have been described but it is the way in which these variations in time, of current and charge, in the lightning channel, manifest themselves as voltages and currents in the system, which is of significance.

The precise analysis of the coupling between the electromagnetic fields arising from the lightning currents in a particular structure and the systems contained within that structure is an extremely complex subject, however, in order to illustrate the magnitude of the threat, reference can be made to some analysis work reported in Ref. 9. The peak threat voltages and currents arising at the terminals of the equipment are shown in Fig. 3. It can be seen that the short circuit current and open circuit voltage resulting from a direct lightning strike on a C.F.C. structure are extremely high at the terminals of unprotected cables and it will be shown in the next paragraph that solid state electronics, in general, will not survive these levels. This lecture will illustrate approaches in the design of the airframe and the system installation which will greatly reduce these values. It is interesting to note that within an aluminium structure, the short circuit current and the open circuit voltage is greatly reduced in comparison with those in a C.F.C. airframe. It is felt, however, that the practical limitations of electrical bonding in an aluminium airframe may have been inadequately allowed for in this analysis and experience (Ref. 10) has shown that these levels are low by approximately 10-20dB. One further point to notice is the relative levels resulting from the various major electromagnetic threat sources.

The upset damage threshold of various electronic technology has been assessed (Ref. 11). The conclusions from this work can be summarised by the diagram of Fig. 4. This diagram shows the order of magnitude of energy required to cause burn-out and upset in a variety of devices. Comparison of the energy limits of the devices and the likely energy deposited by the induced effects of lightning as shown in the previous paragraph, leaves no doubt about the potential hazards involved in the large useage of C.F.C. The trend illustrated in Fig. 4 shows that development in electronics is increasing the susceptibility both to damage and upset.

In addition to the susceptibility of the electrical and avionic systems of the aircraft it must be remembered that the intense current flowing in the airframe is a considerable threat to the safety of the fuel in integral fuel tanks within C.F.C. structures. This will be discussed in more detail later in the lecture, however, as an illustrative fact, it must be remembered that an optimum fuel/air mixture will be ignited by electrical sparks of as low as 0.2mJ in energy content. In other words 200mA flowing for 1 microsec in an arc generated by a voltage of 1KV or more will ignite the mixture. In a C.F.C. integral fuel tank this situation can easily arise unless care is taken with the structural and system design.

3. ELECTROMAGNETIC FIELDS RESULTING FROM LIGHTNING CURRENTS FLOWING IN THE STRUCTURE

The previous part of the lecture gave an insight into the extent of the threat. The way in which lightning attaches to aircraft will now be discussed and the resulting current distribution to be expected and how it arises will be described. The current distribution on the aircraft causes electromagnetic fields to arise inside the structure, the mechanisms which result in this field ingress are described and approximately quantified.

3.1 Lightning Attachment to Aircraft

In order to fully appreciate the fields resulting from the lightning currents flowing in the airframe, it is worthwhile examining the process of lightning attachment to the airframe.

As the aircraft approaches the vicinity of a thunder-cloud, the electric field in which the aircraft is immersed slowly increases. As the electric field increases the sharp edges of the aircraft will begin to discharge producing "streamering". In addition to streamering, the build-up of a leader advancing in steps towards the aircraft, usually from a cloud, causes further electric field build-up in a series of rapidly changing steps. Once the leader contacts the airframe at some point then the aircraft becomes part of a descending "leader" (or much less often, an ascending leader). When this leader reaches the ground or the small ascending leader channels from the ground a huge current will flow to equalise the potential difference between the two charge centres (e.g. earth and the cloud). This is the "return stroke" or lightning flash. The aircraft becomes part of that lightning channel. During the complete lightning event, which may consist of a number of restrikes following the initial return stroke, the aircraft will move some distance through the air. The lightning channel, if attached to a leading edge at A, as shown in Fig. 5, will "bend" back and will find attachment to an alternative point, (say B) further aft, a preferable path. This is the process by which the lightning sweeps back across an aircraft from the leading point attachment to the rear across the "swept stroke zone". Attachments at trailing edges merely stretch out and hang on, in general, for the entire lightning event. Considerations of the mechanisms of attachment to a moving vehicle led to the concept of "zoning" which is of more interest in the design of the direct effects of lightning protection which will not be covered in this lecture.

3.2 Lightning Current Flow In Aircraft Structures

Lightning is an erratic natural phenomena which produces currents whose variations in the time domain can not be exactly represented analytically. It is necessary therefore to make use of a function which nearly represents the current flow. Such a function was given in equation 2.1. This function will be used as the basis for the illustrative examples later in the lecture.

Prior to considering in detail the fields within a structure, it is important to understand the way in which lightning currents distribute themselves over the aircraft.

It has been described above that during a lightning strike the aircraft becomes part of the lightning channel. The situation for a nose to tail strike is illustrated in Fig. 6. The lightning channel can be represented (Ref. 12) as a transmission line as shown, with a characteristic impedance of approximately 400 Ohms. The aircraft can be considered to be a section of transmission line of different characteristic impedance (say 220 Ohms). This gives rise to resonances because of reflection at the transition from aircraft to lightning channel. A typical lightning event contains rates of change of electric and magnetic field which will excite resonating currents on the airframe. For a typical large transport aircraft of say, 50m long this resonance will be strongest at approximately 3MHz. The current flowing on the aircraft near the centre of the fuselage will be in the form of the lightning channel current with a damped sinusoid superimposed on that current as shown in Fig. 7. This damped sinusoid will have a sinusoidal, longitudinal current distribution with the maximum current centred between nose and tail.

The way in which lightning currents distribute over the airframe is controlled by the resistance, self and mutual inductance and capacitance of the various paths. This can be shown in a number of examples. If a cylinder has a high frequency current flowing along it, then the current density is equal at all points around its circumference as shown in Fig. 8(a). This is because the field lines produced by the curren flowing in the circular cylinder are a series of concentric circules. This results in all current paths in the cylindrical surface being cut by an equal flux density as a result of the current flow. The mutual inductance between any path of current and its neighbours is constant around the cylinder.

If a cylinder of elliptical cross-section is considered then it can be seen that the magnetic field lines which would try to form initially would be as shown in Fig. 8(b). Immediately, the normal component of magnetic field at the surface of the ellipse, near the edges would create circulating current in the conducting body. These circulating currents would produce their own field which would oppose the initiating field, thus tending to cancel it. It can be seen from Fig. 8(c) that these circulating currents would combine to form longitudinal current flow as shown. Such a current flow would enhance the driving current at the edges and reduce the total current in the middle as shown in fig. 8(c).

It can be seen that similar arguments can be made to gain an insight into the current distribution on any shape of conducting body. In general, however, it can be stated that current which is changing with time will distribute over the body such that the current density will be enhanced at smaller CONVEX (relative to the field source) radii of curvature and reduced at smaller CONCAVE (relative to the field source) radii of curvature. These principles are illustrated in Fig. 9 for a variety of situations.

The examples quoted are the simple cases of bodies or shells of uniform conductivity. In modern aircraft there is often a mix of materials, in particular, aluminium alloy and C.F.C. In this situation the distribution of current will change throughout the lightning pulse. The rapid changing leading edge (containing the high frequency components) will be distributed in the body in a manner dominated by the self and mutual inductance of the paths i.e. current concentration at regions of high radius of curvature. Later in the pulse, where rates of change are lower, the resistance of the various paths are the dominant factor. The effect of this complex situation was demonstrated in a recent experiment on a C.F.C. box structure with metal strips along all four corners.

The measurements of current in the structure at the two points shown are given in the frequency domain in Fig. 10(a). It can be seen that the majority of the total input current flows in the metal edges of the test box at high frequencies, this is governed by mutual inductance.

At lower frequencies the current actually reduces in the C.F.C. skin at the centre and increases in the metal edges. This is the result of purely resistive sharing. The situation can be compared with that in a metal box for which calculated results for identical measurement positions are shown in Fig. 10(b). In this case the current reduces at the edges with frequency and increases at the middle of the box. This demonstrates the change, with frequency, from inductively dominated to resistively dominated current paths.

3.3 The Penetration of Fields Into the Interior of Aircraft Arising from Lightning Currents Flowing on the Surface

The current distribution on the aircraft skin has been considered. It is this current distribution which produces electromagnetic fields within the aircraft which couple with the internal structure and systems and can produce voltages and currents which are of concern.

There are two mechanisms for the penetration of magnetic fields into the aircraft interior:-

(a) The diffusion of electromagnetic fields and current through conducting skins.

(b) The coupling of external electromagnetic fields into the interior via non-conducting apertures.

Each of these situations will be examined in detail and approaches to the reduction of the problem will be discussed later in the paper.

3.3.1 Diffusion Flux Penetration

This phenomena can be explained in terms of electromagnetic fields incident on finite conductors. Using Maxwell's Laws, it is possible to show that the electromagnetic fields penetrate the surface producing currrent flow within the material. In a finite conductor this current flow will dissipate energy in the conductor, this in turn will cause a reduing current flow through the conducting shell from the outside (the incident face) to the inside.

This effect is illustrated in Fig. 11. It can be seen that the fields and the current reduce through the thickness of the conductor exponentially. The current being given by:-

$$|I| = I_o e^{-x/\delta} \qquad \ldots\ldots (3.1)$$

The equations of electric and magnetic field are of the same form. However, the initial values of electric and magnetic field must be calculated on the basis of transmission and reflection of the incident wave at an impedance discontinuity between free-space and the conductor.

The constant "δ" is known as the "Skin Depth" and is the distance through the material at which the value of the field or current has reduced to 1/e of its initial value and is given by:-

$$\delta = \frac{1}{\sqrt{\pi f \mu \sigma}} \quad (m) \qquad \ldots\ldots (3.2)$$

It can be seen that the skin depth is inversely proportional to the square root of frequency and conductivity. This indicates that at high frequencies in good conductors the current and fields will decay rapidly through the material. A pulse current of field similar in nature to the lightning pulse at the surface of the conductor will therefore be attenuated by different amounts throughout the pulse. The fast leading edge (containing the high frequency components) will be strongly attenuated and the slower changing tail of the pulse will penetrate more readily.

A measure of the ability of a material or combination of materials to attenuate the diffusion of current or fields is given by a quantity known as "Surface Transfer Impedance". This is the ratio of EXTERNAL surface current density (or magnetic field strength at the surface of the conductor) to INTERNAL electric field strength, thus:-

$$\text{Surface Transfer Impedance } Z_T = \frac{Eint}{Jext} \quad (\text{Ohms}) \quad (3.2)$$

The fields and current-flow conditions described above are always described in terms of continuous wave (C.W.) phenomena and it is straight forward to appreciate the situation under these conditions. If the case of a pulse current applied to the conductor is considered, then the situation becomes a little more difficult to appreciate.

Consider the situation illustrated in Fig. 12. Assume a pulse current is applied longitudinally to the cylinder, instantaneously this current, changing with time, will produce circular field lines around the cyliner, both external to, and within the conductor of the cylindrical shell. These fields will be of increasing intensity, for a given current, deeper into the conducting shell, since $H \propto 1/r$. The self inductance of current paths closer to the inner surface of the cylinder will therefore have a higher self inductance. The rapidly changing parts (e.g. the leading edge) of a pulsed current flowing on the cylinder will therefore initially, preferentially flow on the external surface of the cylinder. The slower changes will flow throughout the material. This effect is illustrated in Fig. 12. The initial volume current distribution through the thickness of the shell wall is shown to have the majority of the current flowing on the outside surface at time t_1. As the input step changes to a steady value then the current distribution becomes constant throughout the shell wall as shown at time t_{final}. The total current in the material is of course constant for all time it is merely the distribution which is changing with time. The progression is shown at four increasing times. The difference in the self inductance of the current paths throughout the material thickness will be more marked for high conductivity materials (i.e. less series resistance). This produces the conductivity dependance of the "Skin Effect".

It is important to consider how this situation affects the behaviour of pulse current flow. If a unit step input of current is applied to cylinders of aluminium and C.F.C. of thickness h = 2m.m and diameter D = 2m and length 15m. The end to end voltage is shown in Fig. 13(a) and can be calculated (Ref. 13) by:-

$$V = I_L R \left\{ 1 + 2 \sum_{n=1}^{\infty} (-1)^n \exp \frac{-n^2 t}{\tau} \right\} \quad (V/m) \quad \ldots\ldots (3.3)$$

where the penetration time constant "τ" is given by:-

$$\tau = \frac{\mu_o h^2}{\pi^2 \rho} \quad (\text{secs}) \qquad \ldots\ldots (3.4)$$

and R is the resistance of the cylinder per unit length i.e.

$$R = \frac{\rho}{\pi} Dh \quad \text{(Ohms)} \quad \ldots\ldots (3.5)$$

It can be seen that the penetration time constant for aluminium is much greater than the rise time of the lightning current. This produces a reduced rate of rise, as predicted by the equation for skin effect and the explanation in terms of self inductance and therefore a reduced peak amplitude of current and voltage on the inside surface of an aluminium tube carrying lightning current.

It can be shown that the internal voltage as a result of an externally applied current of the form given in equation (2.1) is (Ref.14):-

$$(3.6) \quad V = 2I_L R \sum_{n=1}^{\infty} (-1)^{n-1} \left\{ \frac{\exp(-t/\tau_1) - \exp(-\frac{n^2 t}{\tau})}{(1 - \tau/n^2\tau_1)} - \frac{\exp(-t/\tau_2) - \exp(\frac{-n^2 t}{\tau})}{(1 - \tau/n^2\tau_2)} \right\}$$

The resultant voltage within the aluminium and C.F.C. cylindrical tubes illustrated in Fig. 13(a) when the current waveform of equation (2.1) is applied is shown in Fig. 13(b). It can be seen that the long penetration time of the current in the aluminium is extremely beneficial, producing an internal voltage peak of only 2.4V despite an external current peak of 200KA flowing. In contrast, the penetration time constant of C.F.C. of 2mm thick is much less than the rise time of the lightning current (see equation (3.4)). It can be seen there is therefore negligible attenuation of current and voltage between the internal and external surfaces. The voltage peak is 9.5KV.

It can be seen that the reduced conductivity of the C.F.C. has a dramatic effect on the diffusion flux coupling. The internal voltages resulting from this diffusion are a considerable threat to electronic systems contained within a C.F.C. vehicle, either as a direct result of possible voltage breakdown within the system or as a result of the extremely high currents which can be driven by this voltage.

3.3.2 Aperture Flux Penetration

It should be noticed that the cylinder size and wall thickness chosen for the illustrative example in 3.3.1 above is not dissimilar to that of a fighter aircraft fuselage. The voltages calculated for the aluminium case are not of particular concern, however, it is known from experience (Ref. 15) that voltages within aluminium skinned aircraft can be much higher and are often different in character, containing much faster rates of change of current than those calculations produced above.

The dominant mechanism of coupling of structural lightning currents with systems in all-aluminium aircraft is "Aperture Flux Coupling". This part of the lecture will consider the mechanism of aperture flux diffusion and arrive at some means by which it may be estimated for typical situations to be found in aerospace vehicles.

Initially, consider the current flow around a non-conducting aperture in an aircraft. A typical situation is shown in Fig. 14. The current "flow lines" have to divert around the aperture and tend to increase in density along the aperture edge, parallel to the current flow (cf. the edge of the ellipse). This diversion of current produces an impedance in the flow of current and thus a voltage is produced across the aperture. This voltage appears as an electric field in the aperture as shown. The inset of Fig.14 shows how the ingress of magnetic field occurs at the aperture edge. The cancellation of the magnetic field normal to the conducting surface can be thought to occur as shown. This cancellation cannot occur at the edge of the aperture, field lines therefore penetrate through the aperture to the interior.

In order to quantify the effects of the field ingress the approach is that described by Burrows (Ref. 16). The induced voltage in any circuit per metre of cable is given by:-

$$V = c\frac{dI}{dt} \quad V/m \qquad \ldots\ldots (3.7)$$

where I = instantaneous lightning current.

The constant of proportionality "c" of any circuit using the airframe as a return is the "fast flux transfer inductance" M_{TF} given by:-

$$M_{TF} = L'-M \quad (H/m) \qquad ..... (3.8)$$

M_{TF} can be calculated using a variety of 2-D field plotting or calculation techniques.

Typical M_{TF} contours are shown in Fig. 15. Using these illustrations either indiviudally or in combination with each other a reasonable estimate or the likely voltage to be induced on wiring can be obtained. All that is required is the M_{TF} from the most appropriate geometry and the rate of change of lightning current and the voltage per metre of wire exposed to the aperture can be calculated. If the aperture is longer than the wire then the length of the wire is used. If the wire is longer than the aperture then the aperture length is used.

In the case of apertures which are short in the direction of current flow a multiplicative enhancement factor is usually required. An aperture is considered short if the length, in the direction of the current flow, is less than the diameter of the body in which the slot arises. The enhancement factors for three different situations which can be used are shown in Fig. 16.

3.3.3 <u>The Combination of Aperture Flux and Diffusion Flux Penetration</u>

This situation arises when there is an area of material in an aircraft skin whose conductivity is lower than the surrounding skin material. For example, a panel of C.F.C. in an aluminium aircraft skin.

In situations such as these the voltage across the panel is calculated by:-

$$E = \frac{Js}{h} \rho \qquad V/m \qquad ..... (3.9)$$

where "E" is the electric field across the panel. (V/m) and "Js" is the surface current density (A/m)
and "ρ" is the resistivity of the material of the panel (Ω-m)
and "h" is the thickness of the panel (m)

The voltage induced in a wire running just across the back of a panel is given by:-

$$V = E \times l \quad (Volts) \qquad ..... (3.10)$$

where "l" is either the length of the wire or the length of the aperture as before.

If the voltage at some distance into the cavity is required then the voltage calculated at the rear face of the panel is merely scaled down in accordance with the M_{TF} curves shown earlier for the position required.

This approximate calculation assumes that the current distribution on the skin of the aircraft is not significantly perturbed by the presence of the lower conductivity panel. This is a reasonable assumption for well bonded panels of C.F.C. in an aluminium skin since the initial current distribution is inductively dominated as discussed earlier.

3.3.4 <u>Techniques for the Reduction of Ingress of Electromagnetic Fields Resulting from Lightning Currents</u>

It is clear from the discussions of 3.3.1 that the only method of reducing the effects of diffusion flux coupling through materials of poor conductivity is to increase the conductivity of the area in question. In general, this involves adding metal in some form, to the existing panel. A popular and weight efficient technique is to use aluminium foil. Whilst such thin foil (say 0.05mm thick) does not prevent diffusion of lightning current, the current flowing on the foil only develops a small voltage across it becuase of the excellent conductivity in comparison with, say C.F.C. For the foil to be effective it must be well bonded to the surrounding airframe. The bonding values to be achieved can be calculated using the approximate calculation described above (Section 3.3.3) for the short, aperture with resistive diffusion. The bonding should aim to be such that

the voltage induced by a particular bonding arrangement is not large compared to the allowed maximum. This can be achieved in two ways; reducing the aperture size (i.e. the bolt spacing), increasing the conductivity of the interfacing sealant. Instead of the addition of foil, which can have durability problems, other similar techniques can be used including, plasma coated metal and metallic mesh, however, particular attention must be paid to the bonding arrangements at the panel edges.

Increasing the shielding performance of an area of the aircraft skin is the most direct method of reducing the diffusion flux ingress into the interior of the aircraft. Another technique which has been used successfully in order to reduce the coupling between the lightning current and the systems is to add metal to structure (or retain some structural components in metal) which will carry the vast majority of the lightning pulse, thus diverting it away from the poorly screened area. In order for this technique to be successful it requires careful location of the metal and the system wiring in relationship with that metal. This will be covered more fully later in the lecture.

The reduction of the penetration of field into apertures can in some instances be achieved by the covering of the aperture by a gauze if the aperture is for the passage of air or liquid. Another useful method is the addition of a short conducting tube, bonded to the aircraft skin around the periphery of the aperture. This will behave as a waveguide below the cut-off frequency (Ref. 16) and provide sufficient attenuation of the field providing the length of the tube is at least three diameters. It must be carefully considered whether the aperture of concern is a threat from field ingress resulting from lightning currents which rarely have significant components of frequency above ~20MHz. Many of the intentional electromagnetic apertures in an aircraft fuselage, such as; radomes and canopies are not amenable to the reduction of field ingress, these problem areas must be treated in a different way and some techniques will be discussed later.

4. THE REDUCTION OF THE COUPLING OF THE PENETRATED ELECTROMAGNETIC FIELDS WITHIN THE AIRCRAFT

The structures of aerospace vehicles are designed for strength, aerodynamic shape and a long maintenance-free life. The electrical design of the airframe often takes a low priority in comparison with these other requirements. It is inevitable that despite careful design of the structure from an electrical point of view there will be significant ingress of electromagnetic fields in many areas of the aircraft. A lightning test (Ref. 10) on an all aluminium aircraft in which the fuselage of the aircraft was subjected to a simulated half scale lightning pulse of peak current 100KA and rate of rise of 20KA/microsec. produced damped sinusoidal voltages on equipment connector pins of up to 200V peak but more usually between 20V and 100V and double exponential type currents on a number of cable screens of up to 1000A. In the case of an airframe manufactured largely from C.F.C. this would increase significantly unless appropriate steps are taken.

4.1 Diffusion Flux Coupling to Systems

The process of diffusion of current and fields through materials of finite conductivity has already been described. The current which flows on the inner surface of the material as a result of the diffusion process develops a voltage along the inner surface, along a path parallel to the flow of current. This voltage is proportional to external current magnitude. Systems which have conductors (intentional or otherwise) whose direction has any component parallel to the direction of flow of current, will experience a voltage across any break in that conductor as illustrated in Fig. 17. If the conductor follows a complete loop then a current will flow or in the more usual case, current will flow and a voltage will be developed across any impedance in the path.

These voltages and currents can be a significant threat to electronic equipment, causing damage in semi-conductors and in extreme cases, voltage flash-over. In the case of C.F.C. integral fuel tanks, the various conductors in the fuel systems (e.g. pipes, fuel gauge wiring etc.) can be a fuel explosion risk of very high currents and voltages unless specific design measures are taken.

In order to highlight the particular problems of C.F.C. integral fuel tanks the case of a fuel pipe in such a tank is considered. The pipe may bridge a significant length of C.F.C. and be connected to structure by fuel couplings at both the root rib and the pylon rig (say) some distance out towards the tip. If lightning attaches to the wing then

the current flowing on the internal surfaces and structure will produce high voltages (in excess of 1KV) for a typical combat aircraft wing) which will drive very high currents (>15KA) down the fuel pipe. The flexible fuel couplings, whilst bonded to prevent potential differences through static charging, will not carry such large currents without sparking. The energy contained in the sparking is most certainly a grave fuel explosion risk. Similar hazards must be avoided with any wiring or metallic conduit system in C.F.C. integral fuel tanks.

4.2 Aperture Flux Coupling to Systems

The process of aperture flux penetration has been discussed previously and it was shown that at regions of the skin where there is no electrical conductivity the fields will penetrate the skin. These fields have magnitudes which are proportional to the instantaneous magnitude of the lightning currents in the structure. The fields which penetrate the structure link with the areas contained between system electrical conductors and the airframe. Since this coupling is in the form of a mutual inductance the voltages induced in the systems are proportional to the rate of change of the lightning current and the extent of the coupling varies with the geometry of the situation (i.e. the position of the conductor in relation to the M_{TP} contours).

It can be seen that the induced currents and voltages on the systems, resulting purely from aperture leakage of fields, are likely to contain much higher frequency components than those induced signals resulting from diffusion of flux. In practice, the resulting signals on system conductors consist of damped sinusoids of current and voltage, resulting from the excitation of airframe resonances and cable impedances dependant on termination loads. In the case of an aircraft containing a mix of metal and C.F.C. these signals will often be superimposed on a slowly changing double exponential.

4.3 The Protection of Systems Against Internal Fields Produced by Lightning Currents

The preivous sections have discussed the mechanisms by which the lightning currents on the surface result in electromagnetic fields within the vehicle. There are a variety of remedies which can be applied to a particular system in order to protect it from high induced voltages and currents as a result of these fields. Broadly speaking these can be divided into the following categories:-

(a) Cable routing

(b) Cable shielding

(c) System earthing and bonding

(d) Equipment protection

Many of the remedies outlined below are also good philosophies for protection of the systems against other electromagnetic hazards such as; N.E.M.P., high level R.F. transmitters etc.

4.3.1. Cable Routing

As described above many of the inherent geometrical features of an aircraft can provide significant reduction in the electromagnetic fields which couple with the system. In the case of an aircraft which is manufactured from C.F.C. and metal the majority of the current, particularly later in the pulse, will flow in the metal. The geometrical relationship between the airframe and the system cables and airframe components which are manufactured in metal is the key to a good cable routing policy. In an all metal aicraft, cable routing could often be optimised by inspection, however, the complexity of the electromagnetic behaviour of airframes containing materials of different conductivity results in a need to use computer based analytical techniques in order to have any confidence in the protection afforded to the system by a particular system layout. Nevertheless, it is still important to be able to make an initial attempt at cable layout by inspection.

Consider the cross-sections of the fuselages shown in Figs. 18(a) and 18(b). The suggested optimum wiring routes are as shown. The initial ruling is to keep the wiring close to metal, this will reduce the area between the cable and the airframe reference to a minimum, thus reducing the area available for coupling. The second goal is to place the wiring in concave corners (relative to the field source) of the metal structure. In the complete absence of metal in the fuselage it can be a weight efficient

solution to the protection problem to add metallic components of suitable shape, along which the cables can be run.

Figs. 18(c) and 18(d) shows a typical wing cross-section and the wiring positions shown are those recommended for low coupling with the lightning current. Once again the wiring is run close to the metal and in the concave corners. It should be remembered that whilst the leading edge of a wing is often an ideal shape in which to "hide" the wiring, it is often a moving flying surface, hence unuseable for the locating of wiring.

Consideration of the behaviour of fields in structures and the examples shown in Fig. 18 will lead very quickly to an intuitive ability in the location of wiring in an airframe by inspection. At best this will give the final solution to the cable routing, at worst it will provide a good starting point for optimisation by computer analysis.

4.3.2 Cable Shielding

Cable shielding is a means of providing broadband protection of signal cables from induced transient and continuous electromagnetic interference. The traditional means of cable shielding uses woven braid, this provides a flexible, electrically conducting screen over the cable carrying the required signal. This form of cable screening will provide both electrical and magnetic screening depending on the configuration of the screen connection to earth or the equipment case.

Simple rules can be followed which will result in a successful cable screening design. These are summarised below:-

(a) External cable screens must ALWAYS be connected to the equipment case at BOTH ends. The configuration will give electric AND magnetic field screening.

If the cable screen is connected to the equipment case at both ends then the total topological screened shell is complete, consisting of the equipment case at each end, and the cable screen between. A break in the continuity of the screen at any point will result in the open circuit voltage of the cable loop appearing across the break and being induced at the terminals of the equipment.

(b) External screen terminations must NEVER be taken through the connector into the equipment case otherwise the interference currents induced on the screen will be taken into the equipment case and negate any screening provided by the case.

(c) The external cable screen must not be used as a signal return unless the cable is feeding a narrow-band input (e.g. a radio receiver). If the input is broadband the electronic system is wide open to interference signals arising from screen currents impressed by airframe currents.

(d) The use of single wire connections (sometimes called pigtails) between the cable screen and the connector should be avoided. This type of connection is both inductive and highly coupled to the wires which are being screened. The screen currents are impeded from flowing and those currents which do flow induce interference in the wires which are being screened.

(e) Unscreened wires entering an equipment case must be filtered if entering the "clean area" (see later) otherwise, in a similar way to the problem of cable screen pigtails, the screening integrity will be breached.

In order to comply with all these requirements the general configuration of the screening of cables can be summarised by Fig. 19. In order to avoid using the screen as a signal return, screened, twisted pair cable can be used. Signals for which the dispersion of phase delay in twisted pair cables is a problem (e.g. video) then triaxial cable may be used in order to provide a coaxial transmission medium but aovid using the screen as a signal return.

4.3.3 System Earthing and Bonding

This is probably one of the most hotly debated subjects in the field of electromagnetic hazard protection. This lecture does

not claim to present a unique solution to the problem, however, a consistent philosophy is described which can be applied to the majority of system architectures.

First of all it is worthwhile considering the various reasons for earthing and bonding, namely; for safety reasons, to prevent electric shock hazard, to maintain minimum potential difference between different parts of the system, to maintain screening integrity, to enable fault detection and circuit breaking and finally to prevent potential differences arising from static charging.

In order to satisfy all these criteria at once the earthing and bonding of a system must be carefully planned.

The equipment case must be bonded to the airframe in order to prevent electric shock hazards and to enable circuit breaker operation in the event of a fault. It is preferable that this connection is made to the outside of the equipment case.

The internal zero volt reference of the equipment should be isolated from the airframe for all the frequencies consistent with the operation and noise rejection of the equipment. This can be achieved most effectively by using a D.C. to D.C. converter with isolation transformer and an internal T.R.U. for the A.C. power. An alternative arrangement for the D.C. power return is to use a filter. The bonding of internal zero volt reference to the inside of the equipment case will depend on the system configuration. It is advantageous in many instances to provide the internal zero volt reference from the chosen centre point of a single point, signal zero volt reference system. This ought to originate inside the equipment case of some centralised piece of equipment. This philosophy will protect the system from differences in potential at the two different sites of the equipments as a result of voltage drop in the airframe. If a signal zero volt reference line is taken into an equipment case then this line must have good low pass filtering.

Finally to re-iterate the guidance in the previous section (4.3.2) ALL cable screens must be terminated on the OUTSIDE of the equipment case.

In order to summarise these guidelines Fig. 20 shows a typical system arrangment and highlights the pertinent features. The arrangement shown is one particular situation, it must be worked out on a system basis which earthing arrangement should be used.

4.3.4 Equipment Protection

The final defense against a hostile electromagnetic environment is the filtering and transient, over-voltage protection which can be placed at the input (or output) to equipment. In recent years there has been great advances in the technology of filtering and over-voltage transient protection. Both these functions can now be obtained in the form of filter pins which can replace pins in many of the standard military connectors. There are however a number of disadvantages associated with the use of any form of filtering, namely; untestability, lowered reliability, limited low frequency performance and the danger of short circuit failure and latch-up.

The use of filters should always compliment the screening philosophy and as stated earlier unscreened cable entering the equipment case should be filtered in equipment which is required to survive in a modern environment. Filtering should always be achieved as close to the cable entry as possible, often a "noisy area" of the box is defined and screened from the rest of the box, within this volume all the filtering can be achieved. In addition all insensitive circuit functions such as relay operation, lamp illumination, transformer connection and opto-isolation can be carried out in the "noisy area" and any supplies required for such unsusceptible functions can be taken the incoming power prior to conversion thus saving on the capacity of the supply circuitry and the requirement for filtering. In the case of equipment for the aerospace industry weight, volume, reliability and testability are extremely important criteria therefore if circuit techniques can be found which will obviate the need for filtering and/or screening these should be used. In addition, it must be remembered that the frequency components of lightning are often too low to be protected aginst by filtering.

The balanced analogue or ditial line receiver is a circuit "building block" which can be used to reject common-mode interference, and provided good quality balanced transmission line is used for the interconnection to the outside world then the common-mode rejection can be quite high (>30dB). The common-mode voltage must be kept below circuit damage levels by either cable screening, system bonding or over-voltage protection.

4.3.5 Equipment Case Shielding

In some cases, for example, the equipment mounted high up in the cockpit, there may be a need to ensure that the shielding of the equipment is sufficient to ensure that the extremely high magnetic field strengths (40KA/m) will not upset or damage the equipment.

As an illustrative example an unprotected loop enclosing 100 squcms would have an open circuit voltage in the order of 500V induced in it. This would have to be taken care of by a moderate level of shielding in the box.

For the general case of equipment buried within the airframe, the major requirement for the shielding of the equipment case against lightning current, is in order to ensure that cable shield curents which are terminated on the equipment case do not cause unsafe field levels within the equipment. In general this is usually satisfied since the equipment case is made from cast aluminium alloy, and provided access covers are carefully designed for long term high frequency electrical bonding, the performance of equipment case shielding is adequate. There have been suggestions for the manufacture of composite equipment cases. In the event of a dramatic reduction in the conductivity of equipment case shells and therefore shielding performance the situation would have to be reviewed.

5. CONCLUSIONS

This lecture has described the phenomenon of lightning attachment to aircraft. The way in which lightning current distributes itself over the airframe has also been described and the mechanism for this explained. The coupling of the current and the associated electromagnetic fields with the systems has been treated in three distinct levels; the penetration of the fields into the interior of the aircraft, the coupling of these penetrated fields with the systems and finally voltages and currents which arrive at the equipment connectors. This three level approach to the description of the threat is followed by corresponding description of the techniques for protection at the three levels.

In summary, the protection afforded by the fuselage can be maximised by a good bonding strategy and the correct utilisation of the available metal.

The protection of the system is achieved by a correctly engineered earthing plicy for both the system references and the cable screens and appropriate cable routing.

The equipment protection is achieved by the application first of all, of a carefully thought out system architecture and secondly by the judicious use of filters and surge arrestors.

It is stated quite clearly that the optimisation of the lightning protection of an aircraft and its systems, for airframes constructed in a mixture of metal and C.F.C. is not possible without an ability to analyse the electromagnetic behaviour of the airframe and the systems contained within. This is a complicated analytical and numerical exercise requiring the use of large mainframe computers. The lecture does however give approximate methods for the analysis of a variety of situations and there is enough information to extend these methods to cover many different situations. This is left as a matter for further reading from the large list of references.

6. ACKNOWLEDGEMENTS

The author would first of all like to express his gratitude to British Aerospace for their support in the preparation of this lecture. Furthermore, thanks are due to Mr. C. P. Loller and Mr. C. C. R. Jones for their helpful suggestions during a number of discussions on the subjects of high frequency current distributions. Figures 15 and 16 have been reproduced with the kind permission of Culham Laboratories Oxford, England.

7. REFERENCES

1. "Screening and Shielding in Aircraft - The Balanced Approach", I. P. MacDiarmid, Proc. of an I.E.E. Colloquium on Screening and Shielding, Digest No. 1983/88, 22nd November, 1983.

2. "Blitstrom Parameter von Aufwarts Blitzen," K. Berger, Bull. S.E.V. 69 353-360.

3. "Lightning Parameters for Engineering Applications," R.B. Anderson and A. J. Eriksson, Discussion Paper for CIGRE Committee, 33 Roumania Colloquium: CSIR Special Report ELEK 170.

4. "Mil Std 1757A - Lightning Qualification Test Techniques for Aerospace Vehicles and Hardware", Dept. of Defence, Washington D.C. 20201 U.S.A., 17th June, 1980.

5. "Recommended Practice for Lightning Simulation and Testing Techniques for Aircraft", J. Phillpott, Report No. CLM-R-163, Culham Labs. 1977.

6. "Lightning Attachment Patterns & Flight Conditions Experienced by the NASA F106B Airplane; B. Fisher, A. Plumer; NASA, Langley Research Centre, Proc 8th Int. Conference on Lightning & Static Electricity, June, 1983, Fort Worth U.S.

7. "Electromagnetic Measurements of Lightning Attachment with Aircraft" P. L. Ruston, B. Kuhman, J. Reazer, J. Showalter, A. F. Wright Aero Lab, (Source as in Ref. 6).

8. "Designers' Guide to the Installation of Electronic Wiring and Equipment in Aircraft to Minimise Lightning Effects", B. J. C. Burrows, Report No. CLM-R-212, Culham Labs, 1981.

9. "Electromagnetic Coupling to Advanced Composite Aircraft with Application to Trade-off and Specification Determination", R. Wallenberg, E. Burt, G. Dike, Syracuse Research Corporation, AGARD Proc. No. 283, Electromagnetic Effects of (Carbon) Composite Materials upon Avionic Systems, June, 1980.

10. "Lightning Protection Design and Lightning Threat Flight Clearance of a Fly-by-wire Flight Control System for an Unstable Aircraft", P.A. Doggett and I. P. MacDiarmid, Proc. of the 8th International Aerospace and Ground Conference on Lightning and Static Electricity, DOT/FAA/CT-83/25, June 21-23, 1983 Fort Worth, Texas, U.S.A.

11. "In Depth Studies of Composite Aircraft Electromagnetic Performance", J. A. Birkin, AGARD Conference Proceedings No. 283, Electromagnetic Effects of (Carbon) Composite Materials upon Avionic Systems, 16-19 June, 1980, Lisbon, Portugal.

12. "Transmission Line Model for Assessing Hazards to Aircraft", P.F. Little and D. J. Churchman, CLSU Memo 104, May 1982, Culham Laboratories, Oxford, U.K.

13. "Lightning Protection of Aircraft", F.A. Fisher and J.A. Plumer, NASA REference Publication 1008, October 1977.

14. "Interim Report - Advanced Composite Aircraft Electromagnetic Design and Synthesis" R. Wallenberg et al., Report No. NAVAIR-518-1, April 1980.

15. See Ref. 10.

16. "Fields and Waves in Communication Electronics", S. Ramo, J. R. Whinnery and T. Van Duzer, Wiley, 1965.

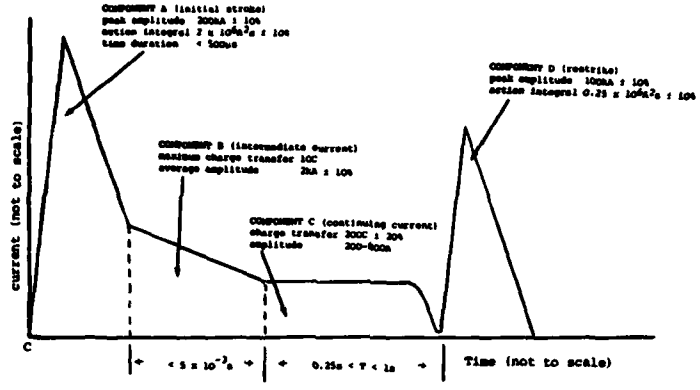

Fig. 1. Idealized current test waveform components for evaluation of group 1 effects.

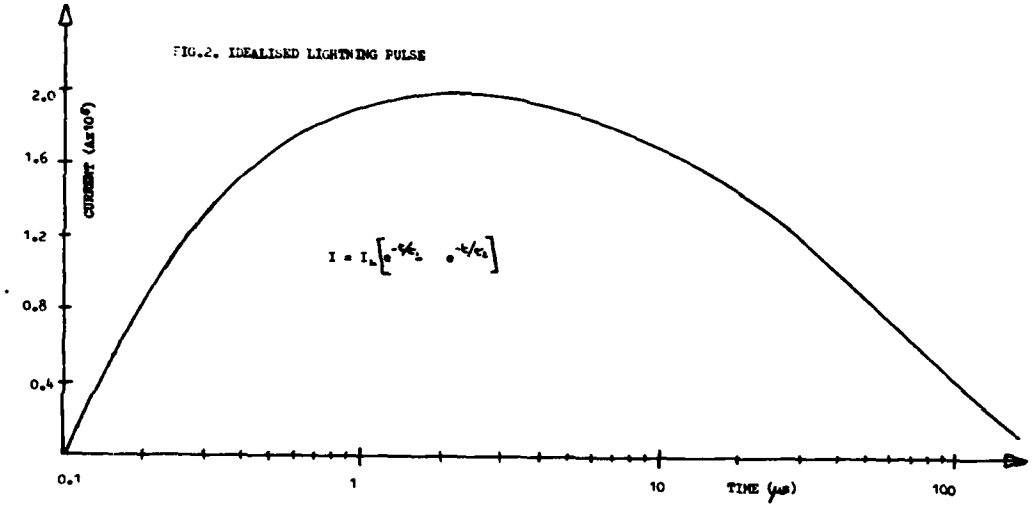

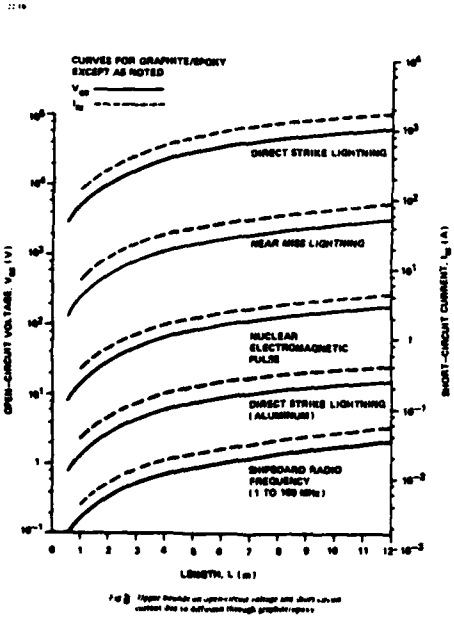

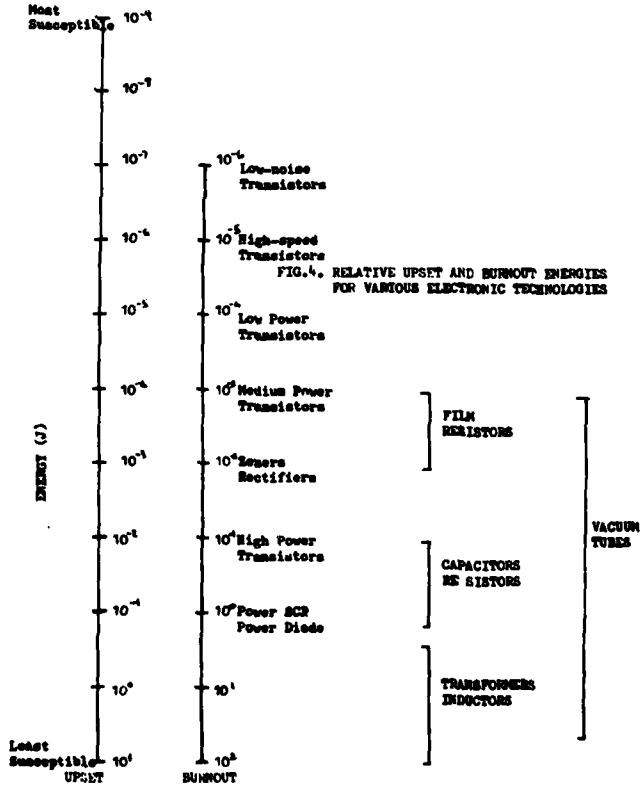

FIG.4. RELATIVE UPSET AND BURNOUT ENERGIES FOR VARIOUS ELECTRONIC TECHNOLOGIES

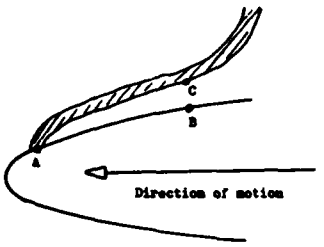

FIG.5. THE ILLUSTRATION OF THE SWEPT STROKE MECHANISM.

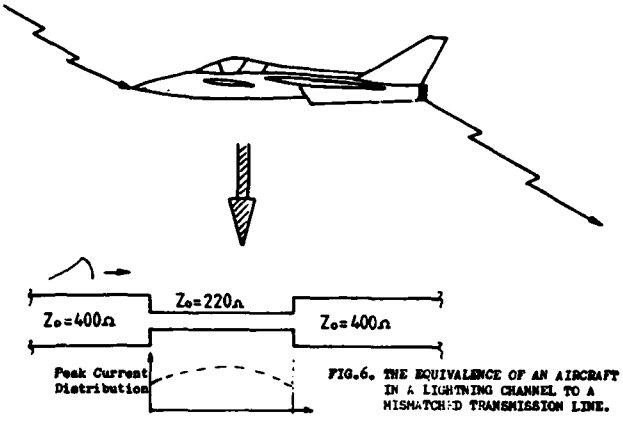

FIG.6. THE EQUIVALENCE OF AN AIRCRAFT IN A LIGHTNING CHANNEL TO A MISMATCHED TRANSMISSION LINE.

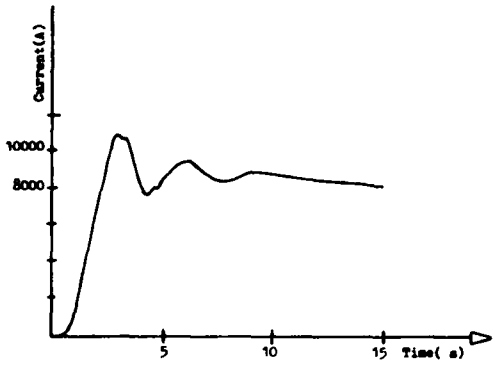

FIG.7. The Typical Lightning Current Waveform on an Aircraft

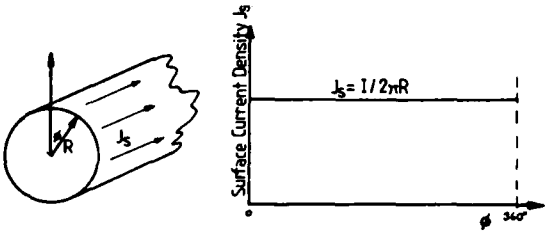

Fig.8(a). The Current Distribution Around a Circular Cylinder.

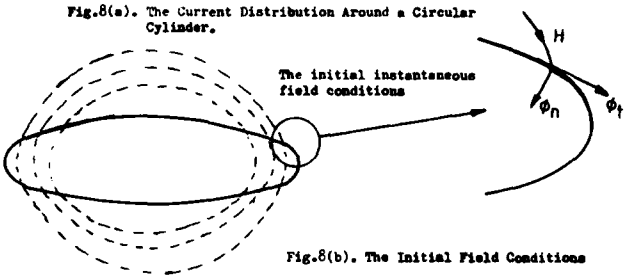

Fig.8(b). The Initial Field Conditions

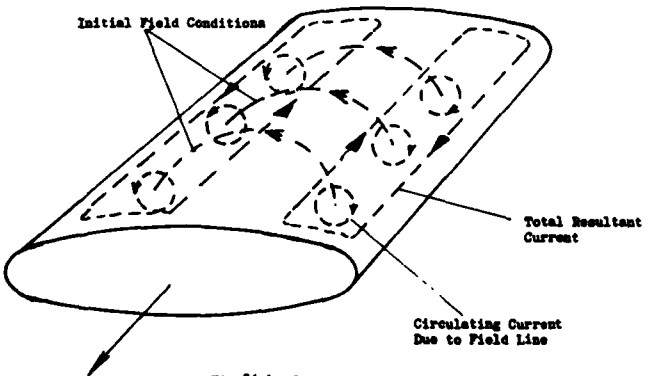

Fig.8(c). The Illustration of the Mechanism for the Concentration of Current at the Edges of an Ellipse.

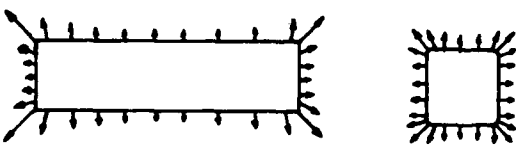

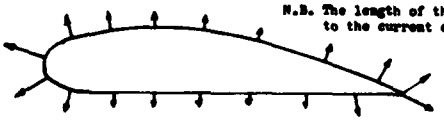

N.B. The length of the arrows is proportional to the current density.

Fig.9. A Variety of Current Distributions for Different Geometries

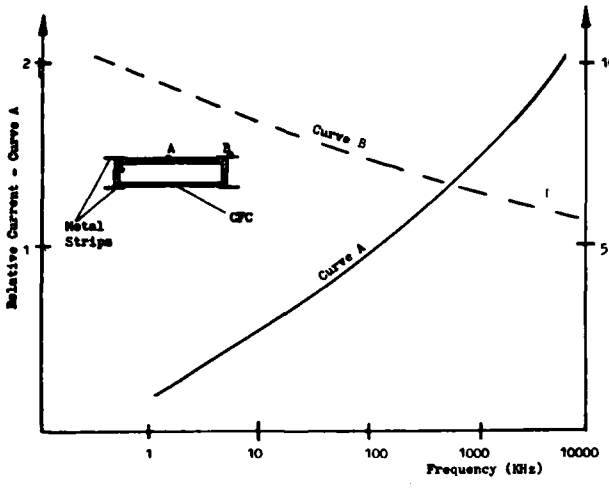

Fig.10(a) The Relative Currents in Metal and C.F.C. in the Test Box Shown.

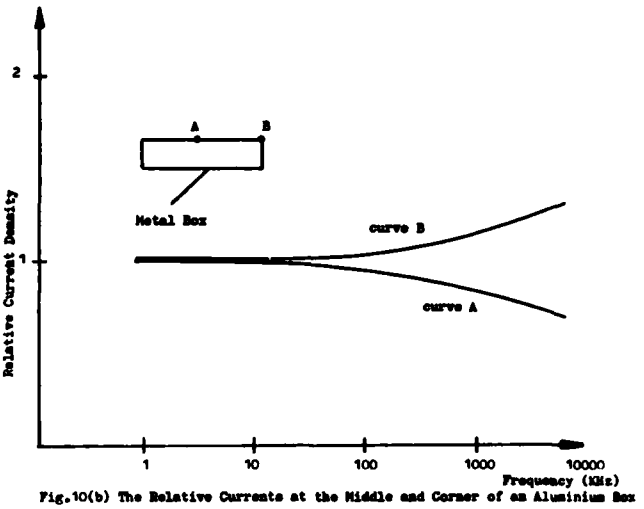

Fig.10(b) The Relative Currents at the Middle and Corner of an Aluminium Box

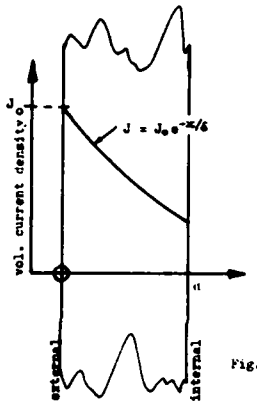

Fig.11. The Reducing Current Density Through Conducting Material.

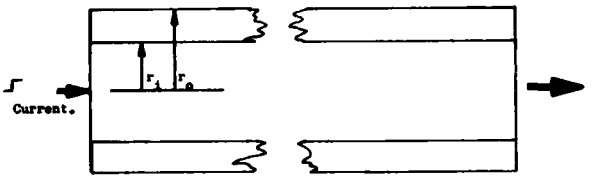

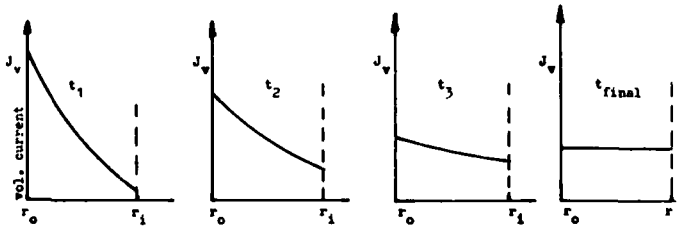

Fig.12. The Change of Distribution of Volume Current Density with Time Following a Step Input Current.

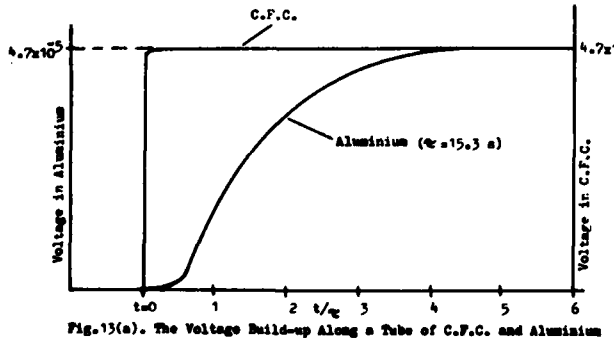

Fig.13(a). The Voltage Build-up Along a Tube of C.F.C. and Aluminium

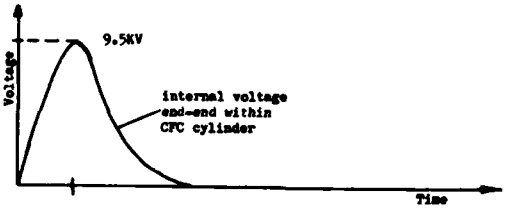

Fig.13(b). The Voltage within Both Aluminium and C.F.C. Cylinders During External Current Flow of the form given in Equation 2.1

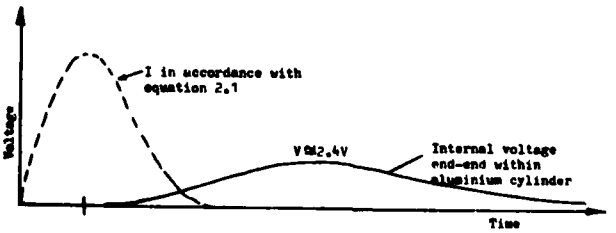

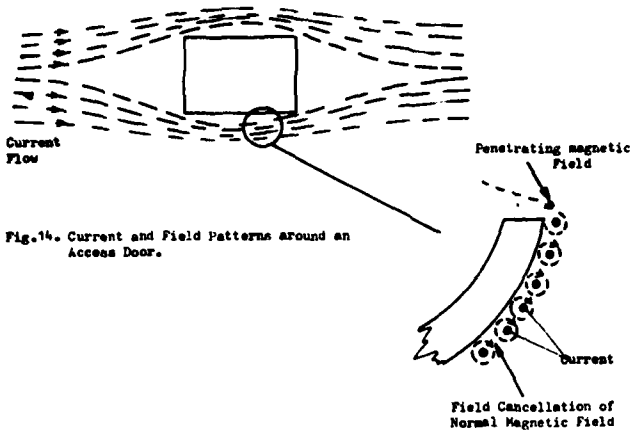

Fig.14. Current and Field Patterns around an Access Door.

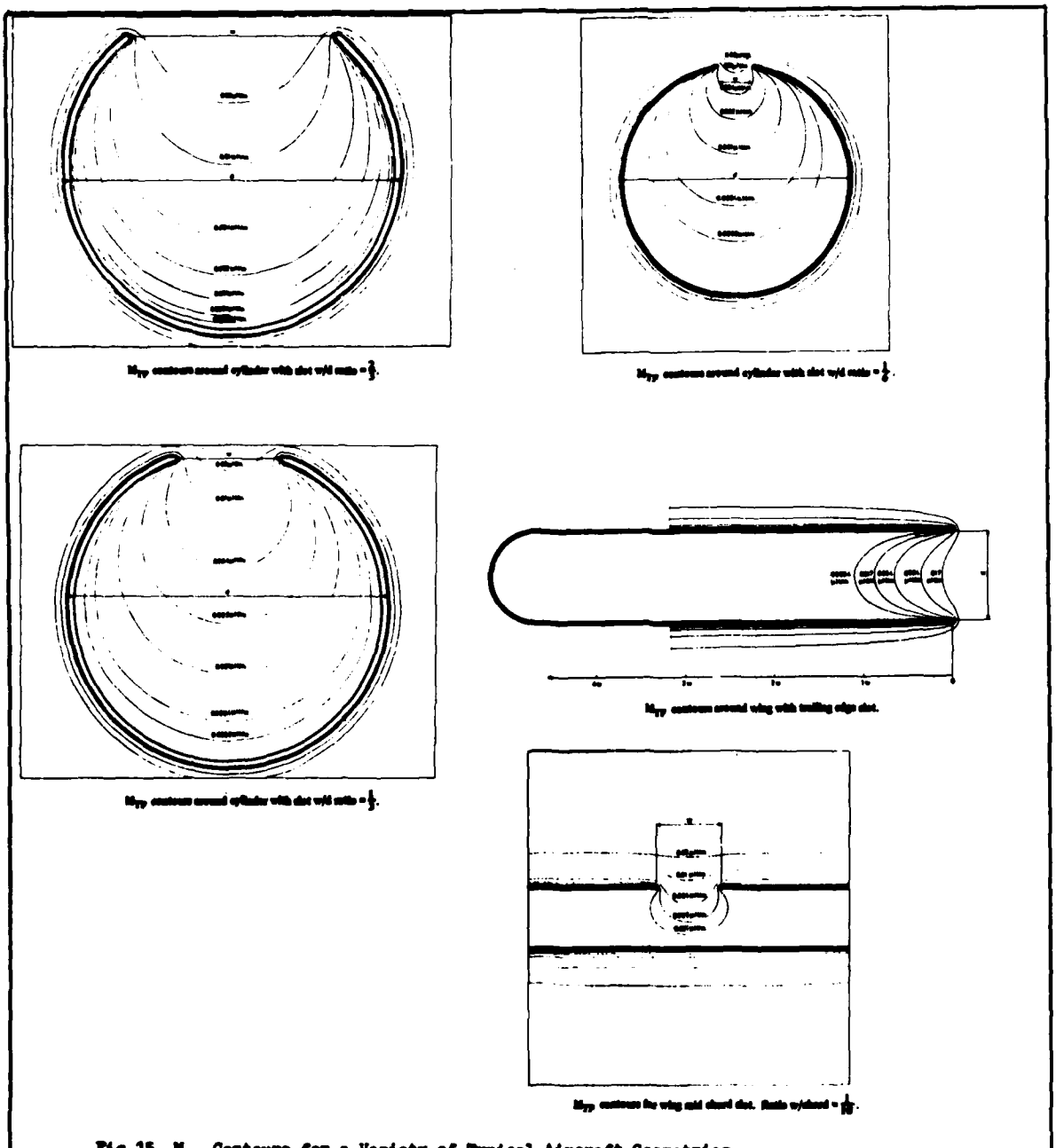

Fig.15. M_{yy} Contours for a Variety of Typical Aircraft Geometries.

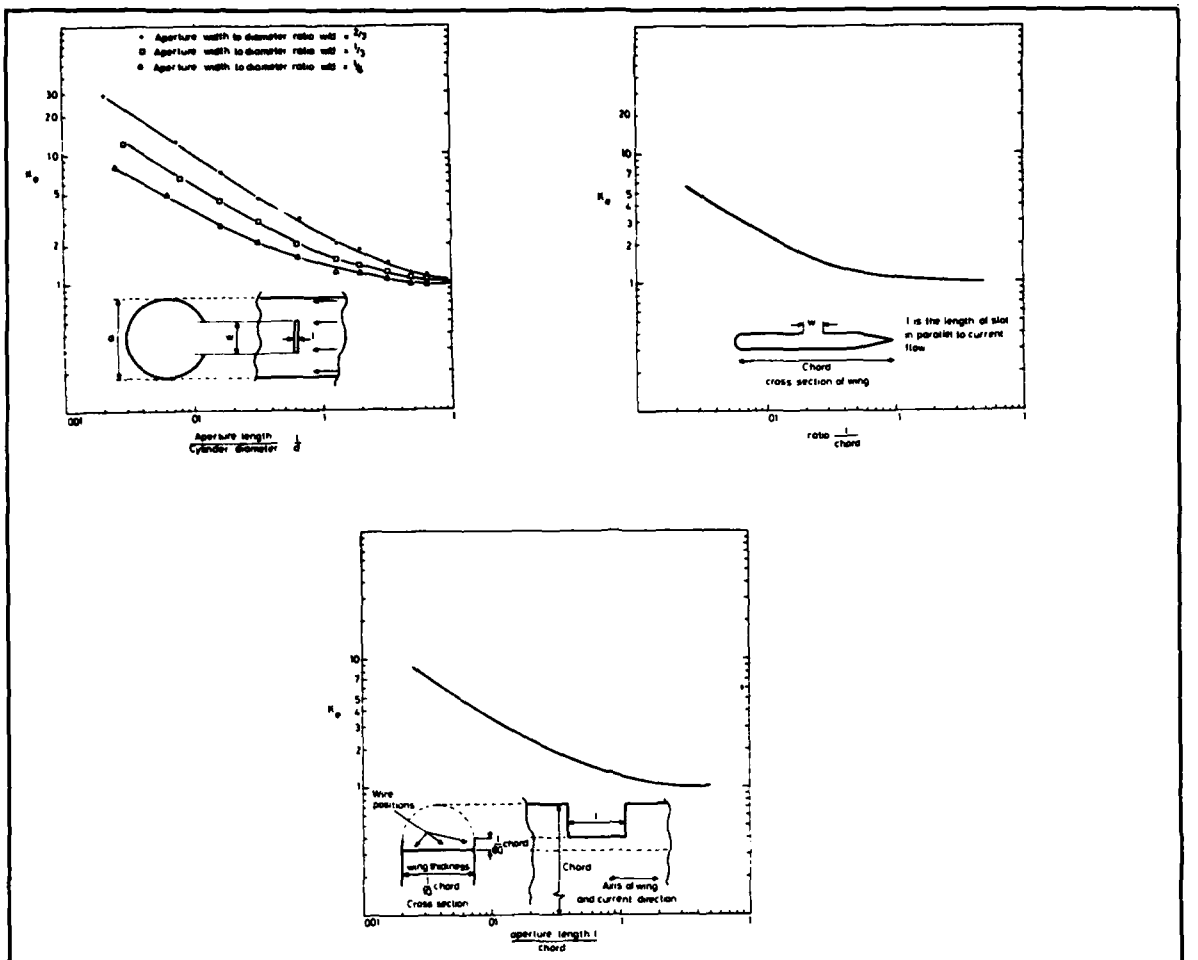

Fig.16. Various Geometries and the Associated Enhancement Factors.

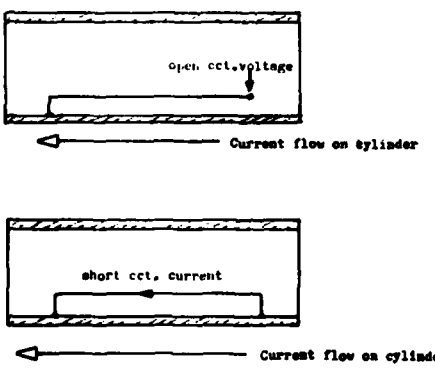

Fig.17 The Situation of Open Circuit Voltage Developed and Short Circuit Current Flow due to Diffusion Flux.

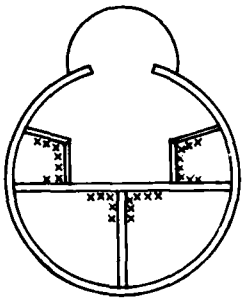

Fig.18(a)

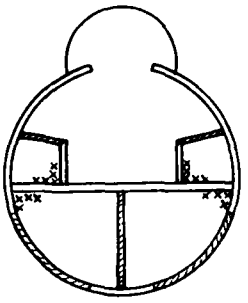

Fig.18(b)

C.F.C.

Metal

Fig.18(c)

Fig.18(d)

Fig.18. Illustrations of Preferred Cable Routings

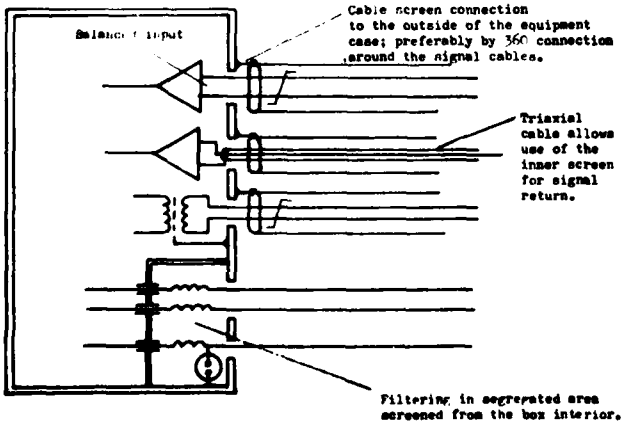

Fig.19. Typical Screening and Filtering Configurations.

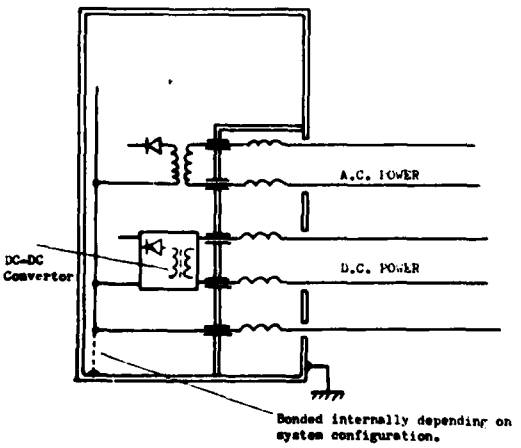

Fig.20. System Earthing and Bonding.

STATIC CHARGING EFFECTS ON AVIONIC SYSTEMS

Joseph E. Nanevicz
SRI International
333 Ravenswood Avenue
Menlo Park, California 94025

Summary

Static electrification of the airframe or its parts can often cause electromagnetic interference on aircraft or missile radio receiving and avionic systems. This paper reviews the causes and possible effects of this phenomenon. Sources of static electrification include frictional charging by precipitation particles, engine exhaust non-neutrality (at low altitudes), and exogenous electric fields (between oppositely charged cloud regions). The potential of a flight vehicle increases until a threshold is reached at which electrical discharges occur, generating electromagnetic noise that interferes with both avionics and communications. Noise-producing discharge mechanisms include: (1) corona-discharge breakdown of the air, (2) streamer discharges across insulating dielectric surfaces to the metal airframe, (3) sparks between inadvertently unbonded adjacent metal sections of the vehicle, and (4) the passage of charged particles past an antenna. Corona discharges and streamer discharges are discussed for both narrowband and broadband systems. The electromagnetic fields generated by discharges raise the local equivalent noise field above the atmospheric noise level, causing interference in narrowband radio receiving systems. Pulse discharges can be misinterpreted on broadband digital systems as operating signals. Aircraft charging parameters have been measured over time (after takeoff) and altitude for several aircraft types, including a jet fighter, a 707, a rocket, and a helicopter.

1.0 Introduction

1.1 General

The effects of electrostatic charging were observed when aircraft began operating under all weather conditions (1,2). It was found that when an aircraft was flown in precipitation, radio noise would often interfere with the operation of onboard communication and navigation systems, just when they were most needed. This relationship between electromagnetic interference ("static") and precipitation led to the name "precipitation static," or p-static. Careful study of the problem immediately after World War II indicated that the noise resulted from frictional charging occurring when precipitation particles struck the aircraft and deposited a charge on its surface (3). The charging, in turn, led to electrical discharges from the aircraft, which generated the noise that interfered with the communication and navigatio equipment.

Subsequent studies led to a better understanding of the various mechanisms involved in the charging and discharging processes, and techniques were developed to mitigate the undesirable effects of these processes. Today, conventional metal-skinned aircraft equipped with analog-type electronics can be made to operate successfully under all weather conditions.

1.2 Motivation for Continued Study of Static Charging

Although the problems of aircraft static charging have been recognized for at least 45 years and various techniques have been developed for their mitigation, there is need for continued study and development in this area. This is true largely because flight vehicles are continually evolving, so that many important details affecting charging, noise generation, and susceptibility are changing.

For example, in all-metal aircraft equipped with analog avionic systems, the primary concern was noise generated by corona discharges from the aircraft extremities coupling into communication and navigation systems via their receiving antennas, since the skin on such an aircraft is a good electromagnetic shield. The use of new materials such as dielectrics and composites changes the way in which charge is deposited on the aircraft and generally degrades its electromagnetic shielding. Thus, unless care is exercised, the electromagnetic noise levels on the interior of the new aircraft may be substantially higher than they were on conventional all-metal aircraft.

In addition, the original avionic systems were based on vacuum tube analog circuitry, which was quite immune to damage and catastrophic upset by electromagnetic noise pulses. The new systems, on the other hand, use digital avionics, which are far more susceptible to damage and upset. Also, momentary loss of avionic systems in the older generations of aircraft generally meant only a temporary inconvenience because the aircraft could be flown by the pilot during the period of outage. In future generations of aircraft, improved performance will be achieved through increased reliance on stability-augmentation devices -- possibly to the extent that the aircraft will be so unstable that the pilot will no longer be able to fly it without the avionic systems. Thus, a loss of a critical avionic system may jeopardize the entire aircraft.

Rockets and missiles are also subject to static charging. Since these vehicles are highly autonomous and depend on digital circuitry for their control, they are highly susceptible to the pulse interference typically generated by static charging.

Since protecting against static electrification implies cost and weight penalties, the designer needs accurate information about the processes and their effects to prevent overdesign or underdesign of the protection schemes. Accordingly, it is appropriate to refine of our knowledge in this area.

2.0 Static Electrification

The various ways that static electrification of a vehicle can occur are shown for an aircraft in Fig. 1. Fig. 1a illustrates frictional electrification; as uncharged precipitation particles strike the aircraft, they acquire a positive charge, leaving an equal and opposite (negative) charge on the aircraft and raising its potential (negatively) to tens or hundreds of thousands of volts (4,5). Charging occurs both on the metal structure of the aircraft and on dielectric surfaces such as the radome or windshield. Thus, dielectric surfaces can become charged with respect to the airframe (6-8). Engine charging (Fig. 1b) occurs when flight vehicles are operated at low altitudes (4,9). Processes not yet completely understood occur within the engine combustion chamber, causing a predominantly positive charge to be expelled with the engine exhaust. This imparts an equal and opposite (negative) charge to the aircraft, charging it to potentials of tens or hundreds of thousands of volts. Exogenous charging (Fig. 1c) occurs when the vehicle flies through an electric field, such as that existing between oppositely charged cloud regions. This field can cause discharges at the extremities of the vehicle.

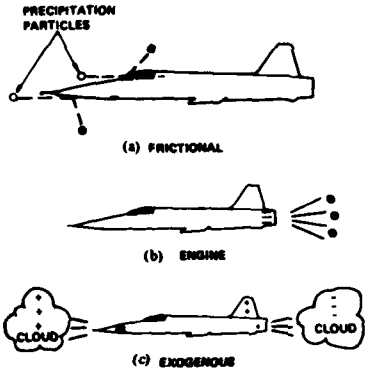

Fig. 1. Charging processes.

A typical record of precipitation charging at an altitude of 25,000 ft in cirrus clouds is shown in Fig. 2. The top trace shows the charging current arriving on an electrically isolated probe on the front of the aircraft. The total current arriving on the aircraft is proportional to the probe current. The middle trace shows the time history of the aircraft potential, which varies directly with charging current. The lower trace indicates that the current leaving an instrumented discharger mounted on the tip of the trailing edge of a wing follows the variations in aircraft potential. Note that negative charge arrives on the aircraft, the aircraft charges to a negative potential, and negative charge leaves the aircraft via the dischargers. During the period shown in Fig. 2, the peak aircraft voltage was 80 kV, and the maximum current leaving the instrumented discharger was roughly 45)A. These magnitudes are typical for flights through cirrus clouds. It is interesting to note that all of the parameters in Fig. 2 vary rapidly with time as the aircraft flies through different precipitation conditions within the cloud. In general, corona discharges occur within a few seconds of entry into a cloud.

A record of engine charging during the takeoff of a jet fighter aircraft is shown in Fig. 3. The wheels leave the ground at t = 0. At t = 0.5 s, the aircraft potential has reached -64 kV, and the discharger current is 13 μA. As the aircraft climbs, the airplane potential and discharger current gradually decrease. This decrease in engine charging during climb-out appears to be characteristic of all aircraft and also occurs on rockets (10). The changes in charging 5 s after takeoff (when discharger currents briefly increase by a factor of two or more) are associated with a power change evidenced by an abrupt 6 percent reduction in engine RPM. Such behavior associated with changes in throttle setting was also observed during flight tests on a 707 aircraft.

The aircraft potentials in Figs. 2 and 3 are of comparable magnitude, but the discharge current is somewhat less under engine-charging conditions. Precipitation-charging currents higher than those shown in Fig. 2 occur when the aircraft is flown in different cloud types -- for example, through frontal snow.

An interesting comparison of the electrostatic behavior of a large rocket and a large jet aircraft is shown in Fig. 4, which plots the potentials of a pair of large rockets during launch and a typical record of the potential of a 707 aircraft during takeoff. (On launch #1, the sky was clear; on launch #2, there were high-altitude clouds over the launch pad.) In the case of the 707, engine charging causes the potential to rise to 100 to 150 kV (depending on whether water injection or dry engine operation is being used) immediately after the wheels leave the ground. In the case of the rocket, the conductivity of the exhaust plume in contact with the ground holds the potential down until, at an altitude of 650 ft, contact is broken. Then the potential rises to hundreds of kV.

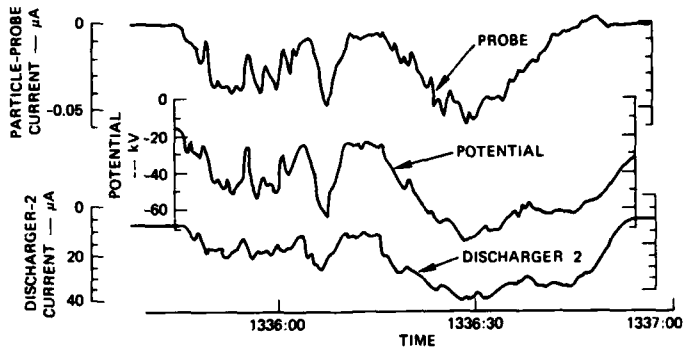

Fig. 2. Precipitation-charging of jet fighter aircraft in flight through cirrus cloud.

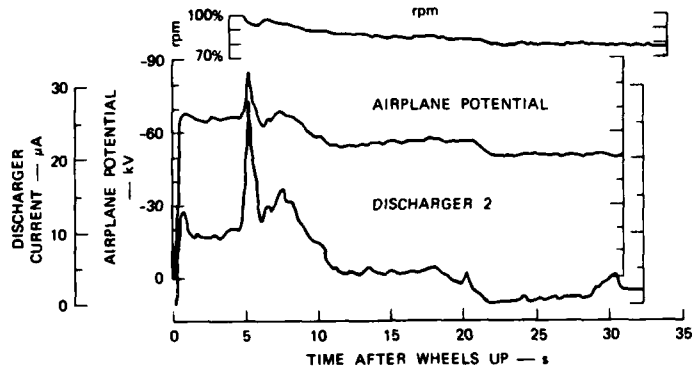

Fig. 3. Engine-charging during takeoff of jet fighter aircraft.

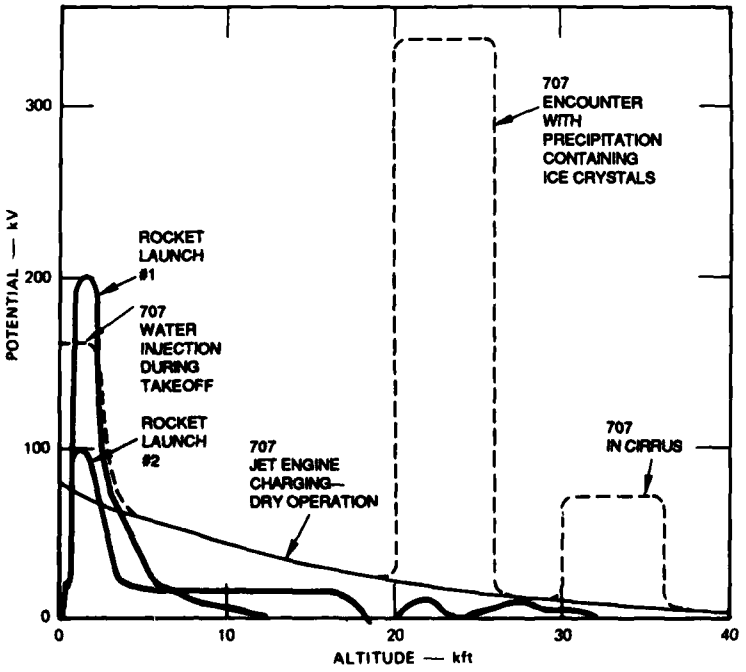

Fig. 4. Comparing potentials of 707 aircraft in flight and large rocket in launch.

As the 707 climbs, in clear weather, its potential gradually decreases monotonically to zero. If the 707 encounters precipitation, its potential rises to hundreds of kV (the precise value depends on the density and type of cloud). The potential of the rocket also decreases to zero as the rocket climbs. However, the rocket potential is only slightly affected by an encounter with precipitation. For example, on launch #2 at 20 kft altitude, rocket instrumentation showed that the frontal charging current was 8 $\mu A/ft^2$. (At this charging rate, the 707 potential would reach 150 kV). This insensitivity of rocket potential to charging undoubtedly stems from the high conductivity of the high temperature rocket plume. Similar behavior is observed on fighter aircraft equipped with afterburners. For example, flight tests showed that operating the afterburner on takeoff increased the engine charging, thereby increasing the aircraft potential (9). On the other hand, when the aircraft was at operational altitude in precipitation, the activation of the afterburners served to help discharge the aircraft and reduce its potential.

Typical precipitation-charging currents measured by SRI on a variety of flight vehicles are shown in Table I. Precipitation charging occurs only when the vehicle is operated in precipitation. The total charging current is directly proportional to speed and intercepting area and depends strongly on the particle concentration in the cloud. There is no marked change in charging processes during the transition to supersonic flight. Clouds containing ice crystals are much more effective in charging the aircraft than are clouds composed of liquid water.

Table I

Typical Precipitation Charging Currents Measured in Flight

Aircraft Type	Cloud Type	Total Charging Current (μA)
707	Cirrus	300-500
707	Frontal Snow	3000
Fighter (Mach 1.2)	Cirrus	500
DC-8	Frontal Snow	4000
Fighter	Ice Fog (Barely Visible)	30-50
Large Rocket	Stratus	300

Note: The vehicle virtually always acquired a negative charge.

Table II

Maximum Measured Engine-Charging Currents

Aircraft	Condition of Operation	Maximum Engine-Charging (μA)
Boeing 367-80 KC-135 Prototype	Dry	50
Boeing 707-138 Injection	Water	800
Boeing 707-138	Dry	175
Convair 880	Dry	75
Douglas DC-8 Injection	Water	300-400
Douglas DC-8	Dry	100
Fighter	Afterburner	45
Large Solid Rocket	--	55-100
Boeing 757*	Dry	0
Boeing 757* Cloud Particles	Ingesting	Slight

*Reported by C. King in reference 11.

Typical engine-charging currents measured by SRI are shown in Table II. The highest engine-charging current measured was 800 μA during the takeoff of a 707 with water-injection engine operation. With dry engine operation, the currents were in the range of 50 to 200 μA for a variety of fighter and transport aircraft, including a large rocket with solid rocket motors. Also shown are recent data obtained by King during tests of a Boeing 757, which indicate that virtually no engine charging (low aircraft potential) occurs when the aircraft is in a clear environment (10). Increased engine charging was observed during penetrations of water-droplet clouds during climb-out. Unfortunately, the aircraft instrumentation did not permit a determination of the magnitude of the engine-charging currents. King interprets these results to imply that the designers of modern engines carefully design the combustion chambers so that complete combustion occurs -- particularly in clear air. During flight through clouds, water vapor modifies the combustion and renders it less complete, so that engine charging is observed as it was with older engines, which were notorious for expelling a highly visible smoke plume on takeoff.

3.0 Interference Sources and Their Effects on Systems

3.1 General

The various interference sources that have been identified are shown in Fig. 5. When the entire airplane is charged, the electric fields at its extremities can become high enough to cause corona-discharge breakdown of the air (4,5).

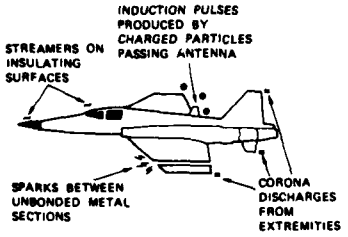

Fig. 5. Interference sources.

A second interference-generating process occurs on insulating dielectric surfaces, such as the windshield and radome, that become charged by impinging particles. The charge on these insulators is bound where it is deposited and cannot be discharged until sufficient electric charge has accumulated to produce a streamer (a spark-like discharge) across the dielectric surface to the metal airframe (6,7). In some cases, the streamering on a square inch of surface in a critical location is sufficient to seriously interfere with avionic systems.

A third source of interference is associated with sparking between inadvertently unbonded adjacent metal sections of the aircraft, illustrated in Fig. 5 by a break in the wing (12). Charging processes on the airframe can raise the potential of the inboard section with respect to the outboard section until sparking occurs across the gap.

Finally, slowly varying induction pulses can be produced in antennas by the passage of charged particles (6). This interference is of importance only at VLF or ELF and historically has not posed much of a problem to conventional communication and navigation equipment. However, the advent of systems operating at frequencies of the order of 10 kHz may require that induction noise be reconsidered.

3.2 Corona Discharges

3.2.1 Basic Processes

As charge accumulates on an aircraft, its potential will increase until a threshold is reached, above which corona discharge breakdown occurs in regions of high electric field at the aircraft extremities. At typical aircraft operating altitudes, this breakdown occurs not as a steady flow of current, but as a series of short bursts of current flow called Trichel pulses, whose time structure is such that they contain energy well into the radio-frequency spectrum (4,5). Fig. 6 shows an example of a pulse train produced by a corona discharge (40 μA, negative point) from the edge of a sheared aluminum sheet simulating the trailing edge of an airfoil. Since the 20 pulses shown carry away a total charge of $q_g = it = (40 \times 10^{-6})(500 \times 10^{-6}) = 20 \times 10^{-9}$ coulomb, the charge carried away per pulse is $q_p = 10^{-9}$ coulomb. Since a precipitation particle deposits roughly 10^{-11} coulomb of charge, each corona pulse removes the charge deposited by 100 precipitation particles. Since the capacitance of a large aircraft such as the 707 is 1000 pF, the charge carried away by a single corona pulse changes the aircraft potential by 1 V.

The time waveform of the current flowing in a typical corona pulse is shown in Fig. 7. It should be noted that the detailed pulse structure is affected by ambient pressure and discharge point tip radius. Decay and rise times are both inversely proportional to pressure. Amplitude increases with increasing tip radius.

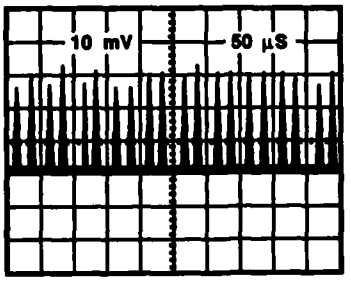

Fig. 6. Pulsed character of typical negative-point corona discharge from a sheared aluminum sheet (I_{dc} = 40 μA).

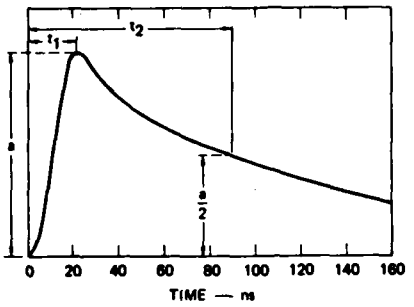

Fig. 7. Time structure of negative-point corona pulse; pressure = 200 mm/Hg.

3.2.2 Noise in Narrowband Systems

3.2.2.1 Spectral Measurements

Although data regarding corona pulse form and other characteristics provide insight into the corona discharge process, narrowband corona noise is most easily calculated using noise spectral data of the sort shown in Fig. 8 (4,5). The data in Fig. 8a present measured spectral characteristics as a function of operating altitude. The data were generated by inducing corona from a piece of sheared aluminum sheet mounted in a special coupling electrode structure housed in a vacuum bell jar. The discharge current kept constant as noise spectral measurements were made at ambient pressures ranging from sea level to 50,000 ft. It should be noted that the noise spectral density is higher at low frequencies, but it contains appreciable energy well into the HF band.

To predict noise levels under various changing conditions, it was necessary to measure absolute levels of corona noise as a function of corona current. This was done by installing a mock-up of a full-scale airfoil tip in a test fixture whose electrode structure was designed to duplicate the electrostatic and electromagnetic field structure in the vicinity of the tip in flight. The electromagnetic coupling ψ_L = E/V (a reciprocity relationship relating the electric field, E, observed at a reference point on the airfoil mock-up when a one volt signal is applied at the measurement terminals) was determined for the laboratory setup. Discharge current from the airfoil tip was varied from 6 to 250 μA, and measurements were made of spectral amplitude at a frequency f_o = 2 MHz. The spectral amplitude was divided by the mock-up coupling value, ψ_L, to yield the normalized source spectrum amplitude $|D(\omega)|$ shown in Fig. 8b. Essentially, Fig. 8b is a plot of the source spectrum amplitude per unit coupling and can be used to determine the absolute noise spectral density for any antenna/airframe system for which the coupling is known.

When the source characterization work leading to Fig. 8 was under way, aircraft used the VHF and UHF bands strictly for line-of-sight communication and navigational aids. These systems operated at received signal levels high enough that corona noise at these frequencies was not of concern. Accordingly, no effort was made to extend the corona spectrum studies above 14 MHz. This is unfortunate since satellite communication links operating at low received signal levels are planned for use on aircraft. Corona spectral data extending to VHF and UHF would be useful now to permit accurate assessment of the vulnerability of these communication links.

3.2.2.2 Coupling of Noise in Aircraft Systems

Frequently, corona noise sources on an aircraft are located in one place, and the affected antenna or system is located in another. Therefore, the coupling between the noise source and the victim system must be defined. This was done experimentally for two antenna locations on the 707 aircraft, as illustrated in Fig. 9 (4,5). The antennas used in the studies were a small tailcap and a flush belly antenna located in a fairing at the root of the wing. Coupling was measured between each of these antennas and the noise

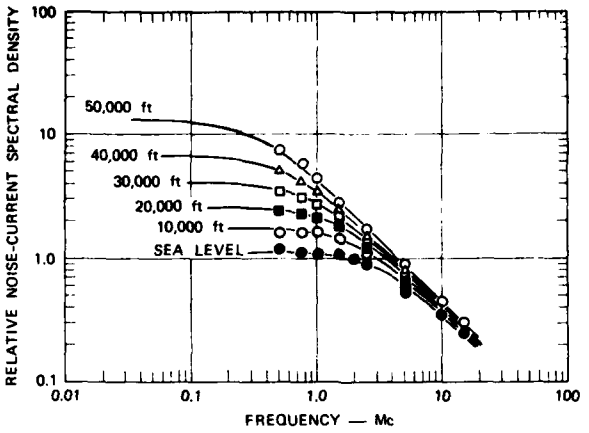

(a) NORMALIZED SPECTRUM SHOWING ALTITUDE EFFECTS

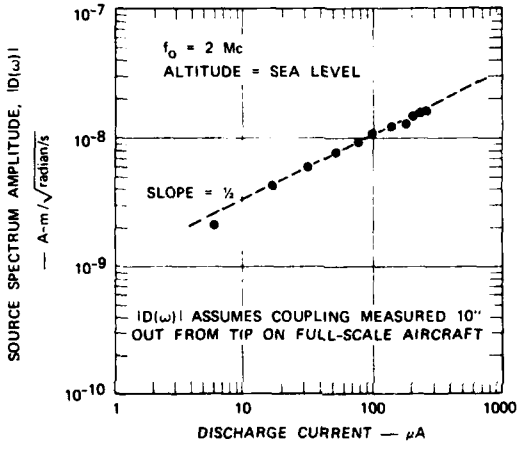

(b) RELATIONSHIP OF ABSOLUTE NOISE LEVEL TO DISCHARGE CURRENT

Fig. 8. Corona-noise-source spectrum characteristics.

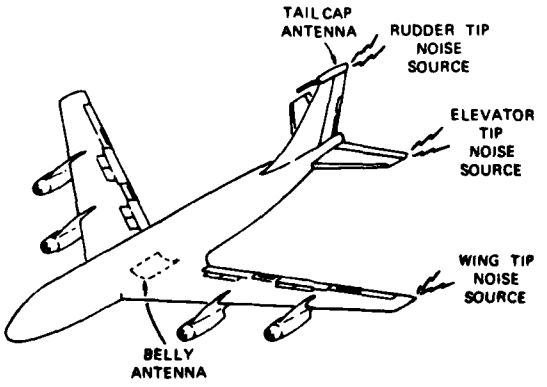

Fig. 9. Antenna and corona-noise-source locations for 707 coupling measurements.

source regions at each of the airfoil extremities. The results of the measurements are shown in Fig. 10. Coupling was measured using a 1/10 scale model of the 707 equipped with a receiver (operating at 10x the frequency of interest) that could be switched to one or the other of the two test antennas. A spark discharge between a pair of electrically isolated balls placed at an airfoil tip was used to provide RF excitation of the model.

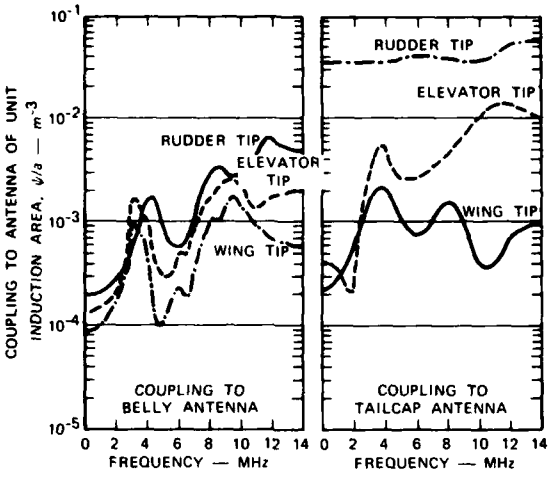

Fig. 10. Measured coupling factors for antennas on Boeing 707 prototype aircraft.

Although the coupling-measurement technique inevitably includes the test-antenna characteristics in the results, the form of the coupling as a function of frequency is not affected by the details of the test antenna, provided the antenna dimensions are small compared to a wavelength at the frequencies of interest. In this case, only the magnitude of the coupling function will be affected by a change in the antenna. Therefore, the data shown in Fig. 10 have been adjusted to represent the coupling to an antenna having unity induction area, a, in response to a low-frequency, veritically polarized signal.

The variation with frequency of the coupling to the various points is of considerable interest, since it shows the effect of the various electromagnetic resonances of the aircraft. For example, the peak in coupling between the belly antenna and the tips of the tail surfaces occurs at approximately 3 MHz. At this frequency, the path distance from a point just aft of the wings to a tip of one of the tail surfaces in one-quarter wavelength. The presence of the resonance peaks in the coupling function serves to emphasize that the pulses arriving at the antenna terminals will differ from the pulses generated by the corona discharges at the extremities in that they will be stretched out in time by aircraft resonances. It is also interesting to note that discharges from the rudder tip are strongly coupled to the tailcap antenna. Discharges from the fin will therefore generate the dominant corona noise signals in the tailcap.

The coupling data of Fig. 10 can be applied without restriction to aircraft of similar shape but different size. In general, the same resonances will occur on the scaled aircraft, but they will occur at the scaled frequency. The magnitude of the coupling must also be scaled with aircraft size (4,5).

3.2.2.3 Analytical Studies of Aircraft Noise Coupling

Actually, the data of Fig. 10 are the only coupling data presently available for conventional aircraft and have been scaled and applied to other aircraft with remarkably good results, even when the scaled aircraft were not very similar to the 707. Limited coupling studies have been carried out for a helicopter but have not been published (13). Additional coupling data covering a wider variety of aircraft configurations and antenna locations are badly needed. To investigate the feasibility of employing computer methods to determine the electromagnetic coupling between noise sources and antennas on aircraft, provisions were made to use an existing method-of-moments computer code (derived from reference 14) to calculate the coupling between the tailcap antenna and the wing-tip and elevator-tip regions of the 707 aircraft.

For the calculation, the 707 aircraft was approximated by the 0.5-m-diameter cylinders shown in Fig. 11. It is evident that such a model approximates only the grossest features of the aircraft. For example, the wings and empennage structures attach to the proper positions on the aircraft fuselage and are oriented at the correct angle to the fuselage, but the cylinder diameter is not properly scaled. In particular, no effort was made to scale the taper of the airfoils. The modeling was deliberately simple to restrict computer requirements to manageable levels (computer circa 1973). The restrictions on the modeling mean that although the gross currents on the aircraft may be accurately modeled, one should not expect accurate estimates of currents and fields near the tips of the airfoil extremities.

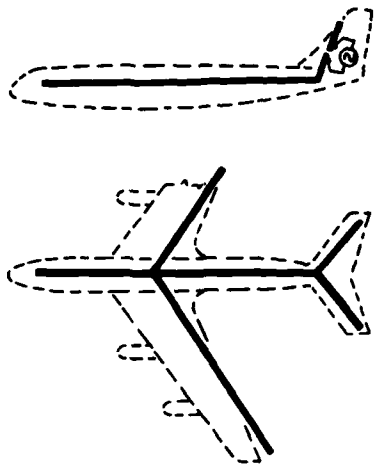

Fig. 11. Cylindrical element approximation to 707 aircraft for method-of-moments coupling calculation.

The way in which the tailcap antenna was modeled is also evident in Fig. 11. The top half of the vertical fin was considered to be isolated from the aircraft and driven by a 1-volt generator. Obviously, such an antenna is much larger than that actually used on the 707 aircraft, so the calculated coupling fields should be higher than the measured ones.

Calculations were made of the currents flowing on the various members and the fields in their vicinity as the result of the 1-volt excitation of the antenna. Of most interest here is the magnitude of the electric field in the vicinity of the airfoil tips. Calculations were made of the field intensity 0.5 m inboard from the "airfoil" tip and 0.01 m above the surface. The magnitude of this normalized field is, by definition, the magnitude of the coupling to this point, $\psi = E/V$, as discussed earlier. The results of the airfoil-tip field calculations are shown in Figure 12, along with experimentally measured data points from the corona coupling studies of reference 4. It should be noted that for both the wing-tip and the elevator-tip, the magnitudes of the coupling are in remarkably good agreement if one considers that no effort was made to accurately model the details of either the antenna or the airfoil tips.

To better show the degree to which the computation accurately predicted aircraft resonances, the magnitudes of the calculated couplings were adjusted in Fig. 13 to best fit the experimental data. In Fig. 13a, the calculated coupling curve duplicates the measured resonances with remarkable precision. Particularly significant is the coupling minimum at f = 2 MHz, predicted by the calculations. When the experimental data were first obtained in the work of reference 4, it was not clear whether the coupling minimum at f = 2 MHz should be considered to be real or should be construed as a bad data point. When the data were presented (Fig. 10), the minimum was treated as real. Rough computer calculations indicate that the coupling minimum is real.

In Fig. 13b, calculated and experimental data at low frequencies agree. Above about f = 3 MHz, this agreement gets worse. The magnitudes of the coupling variations also do not agree, and the frequencies of the maxima and minima disagree. Why the agreement is not better is not clear. Intuitively, one would expect the major resonances to be reproduced even with a model as crude as the one in Fig. 11. Unfortunately, lack of time and funds prevented variation of parameters, such as cylinder radius, in the calculations to investigate how the accuracy of computer output is affected by simplifications in the mathematical modeling of the vehicle. Such checks and experiments are essential to final judgments regarding the viability of the computer method -- particularly in light of the evolution of digital computers and computer modeling codes since 1973.

3.2.2.4 Predicted Aircraft Noise Levels

By combining data of the sort shown in Figures 8 and 10, it is possible to predict the corona discharge noise levels induced in the antennas of interest. Further, by making an analogy between the corona noise and signal levels that would be produced in the same antenna by a propagating electromagnetic wave, the corona-generated noise can be expressed as an equivalent noise field in the vicinity of the antenna. This was done for the case of the 707 aircraft. The results are shown in Fig. 14 with the results of flight test noise measurements (4,5). The two sets of data are in good agreement for both antennas.

The corona noise level in the tailcap antenna is substantially above the accepted value of nighttime atmospheric noise (15). Since the system designer can reduce the system input-noise figure to the atmo-

spheric noise level, it must be assumed that optimized systems are or will be operating at the atmospheric noise level. Thus, the tailcap corona noise severely degrades the performance of such a system. It should also be observed that 40 dB of noise reduction is required to reduce corona noise to the nighttime atmospheric noise level cited in reference 15. Even greater noise reduction is required to approach daytime atmospheric levels.

Although the belly antenna noise levels shown in Fig. 14 are comparable to the nighttime atmospheric noise at certain frequencies, it is important to note that a 350 μA charging current is typical of the charging conditions found in light cirrus and that currents up to 3 MA were measured in flight. Under these higher charging conditions, the noise levels will be 10 dB higher. Thus, at least 30 dB of noise reduction is required to reduce cornona noise to the nighttime atmospheric noise level at all frequencies.

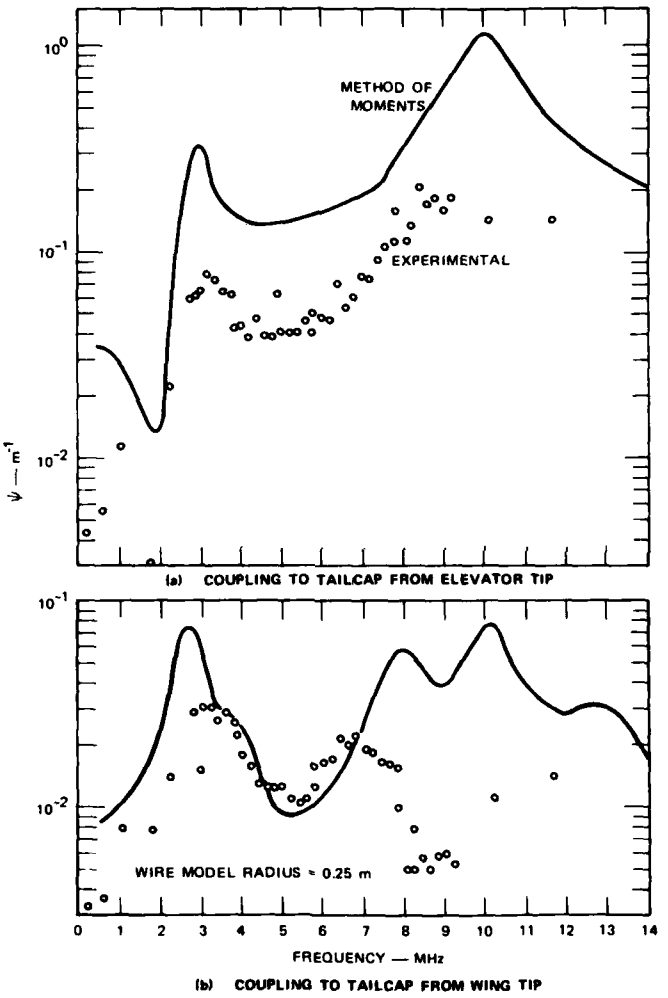

Fig. 12. Computed and experimental coupling data.

Because of the way in which charging current and noise coupling scale with aircraft size, corona noise problems are generally more severe on smaller aircraft (5,6).

3.2.2.5 Noise from Helicopter Blades

To investigate the problem of noise generated by discharges from helicopter rotor blades in the work of reference 13, a helicopter model (including an antenna mounted as indicated in Fig. 15) was assembled in the laboratory. Coupling between the rotor blade tips and the antenna was measured using a technique similar to that described in (4) and (5). Combining the coupling data with corona noise spectral curves from (4) and (5) and with streamer spectral curves (to be discussed later) yielded the equivalent noise fields of Fig. 16, for assumed discharge currents on the helicopter blades of 600 μA.

It is interesting to note from Fig. 16 that, below roughly 1 MHz, corona and streamer noise are comparable in magnitude. Above 1 MHz, the basic streamer source spectrum decreases so rapidly with increasing frequency that streamer noise becomes substantially lower than corona noise. Over most of the frequency range illustrated in Fig. 16, the noise from either source exceeds the nighttime atmospheric noise level, so that system performance can be improved by the elimination of both noise sources.

A comparison of Fig. 14 and Fig. 16 shows that the noise level predicted for the helicopter lies roughly halfway between the 707 tailcap and belly antenna noise curves.

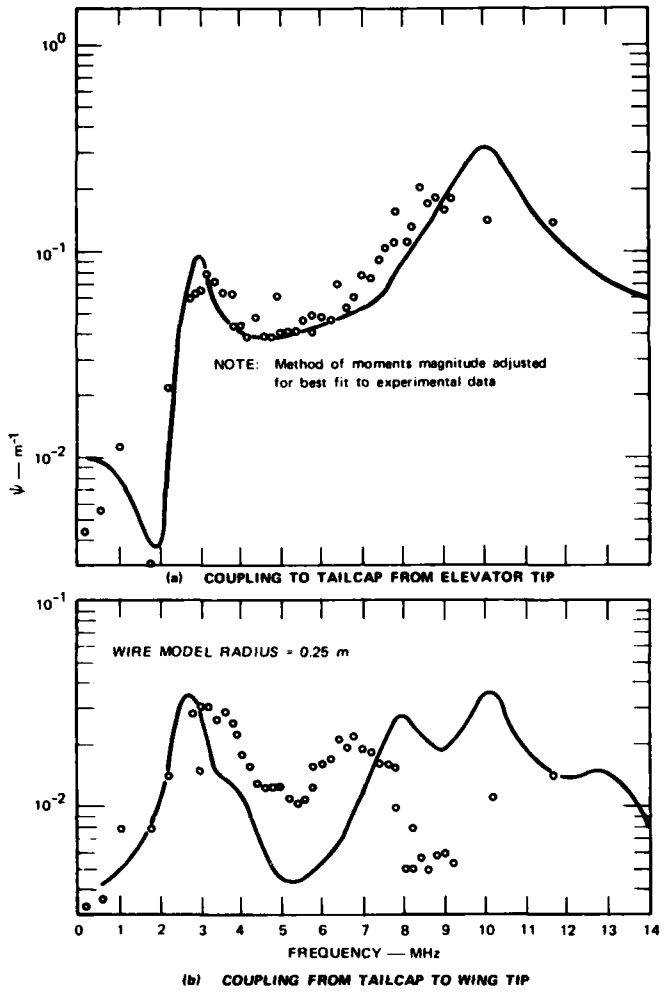

Fig. 13. Adjusted calculations compared to measured coupling data.

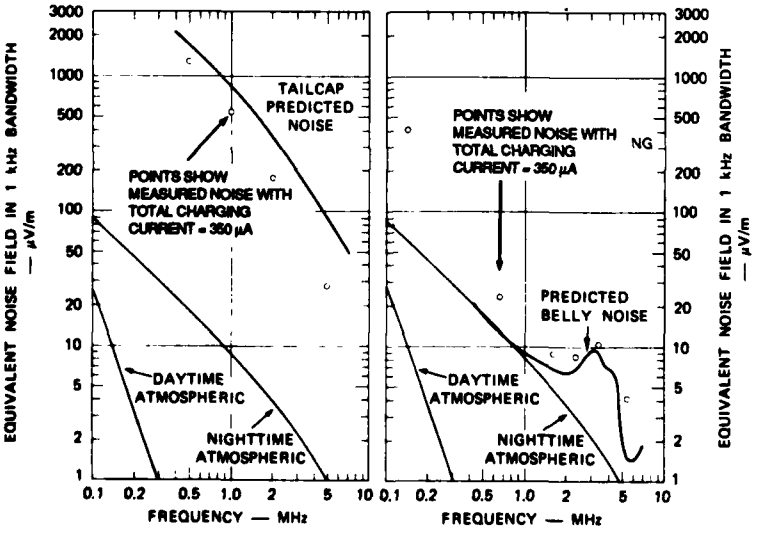

Fig. 14. Corona discharge noise in 707 antennas.

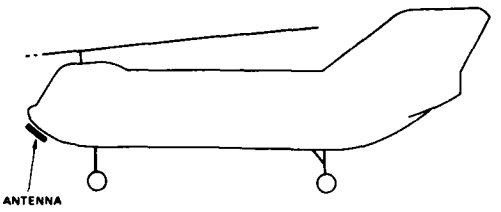

Fig. 15. Antenna location in helicopter noise study.

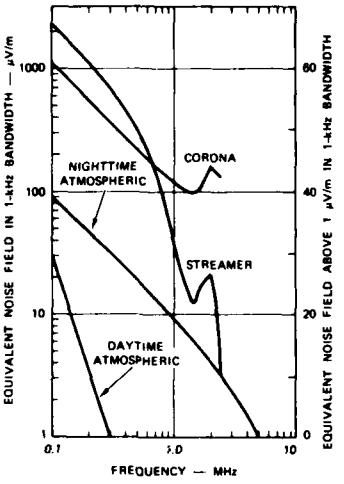

Fig. 16. Predicted noise at antenna location on helicopter due to discharges from rotor blades.

3.2.3 Noise in Broadband Systems

Most of the corona noise characterization discussed here was carried out when communication and navigation systems were the only avionics susceptible to precipitation-static interference. These systems incorporated narrowband receivers so that performance degradation by p-static could be characterized by considering only the magnitude of the noise spectrum at the antenna terminals. Wideband digital systems, on the other hand, are sensitive to individual noise pulses. To the author's knowledge, the only time careful consideration was given to the characterization of the received noise-pulse waveform in response to a corona discharge was in connection with an analysis by Vassiliadis of the effectiveness of noise-blanking systems in reducing corona-generated interference (16). In principle, the received pulse waveform can be determined by taking the inverse Fourier transform of the received noise spectrum. Unfortunately, the coupling measurement techniques used in (4) and (5) did not preserve phase, so that it was not possible to carry out such a calculation directly.

The need to characterize noise-pulse waveforms in connection with the study of the susceptibility of digital avionic systems was recognized by Vance, and modern techniques for accomplishing the required measurements are discussed in reference 17. Many appropriate analytical and computational tools for dealing with individual transient events have been developed by the nuclear EMP community and are summarized in reference 18.

3.3 Surface Streamer Discharges

3.3.1 General

Charge deposited on a dielectric surface generates a potential difference between the surface and the surrounding metal structures that is usually relieved by surface discharges or streamers originating on the rim and extending out onto the dielectric surface. This general problem was studied initially in the laboratory and in a set of flight tests by Tanner and Nanevicz (6,7). Tests were then carried out using sensors with clearly defined electromagnetic properties, but with an oscilloscope of limited capability by present standards (15 MHz bandwidth). Later, Oh conducted a set of laboratory experiments to study the properties of the surface streamer discharge (19). Unfortunately, Oh's choice of sensors makes electromagnetic analysis difficult. More recently, Taillet and his coworkers have been using well-defined modern instrumentations and well-designed sensors to study the physics of dielectric surface discharges in an effort to gain insight into the processes recurring in the lightning channel (20). Since their

principal interest has been the generation of fast, energetic processes typical of lightning propagation, they use a triggered spark-gap to initiate individual surface discharges that propagate and discharge most of the charge stored on the dielectric strip sample. Thus, their discharges are probably much more energetic and abrupt than those naturally occurring on aircraft, where initiation usually occurs from a sharp burr on a conductor adjacent to the charged dielectric. For, these reasons, we will concentrate here on the results of the flight tests of references 6 and 7, recognizing that it would be profitable to return to this area with modern instrumentation and concepts.

3.3.2 Surface Discharge Characterization

The instrumentation used to investigate streamering in the work of references 6 and 7 consisted of a special zone-plate probe, shown in schematic form in Fig. 17, mounted on a radome section that was built onto the nose of the aircraft. The probe was made of 2-inch-wide copper strips concentrically placed with a 0.25-inch spacing between adjacent strips. A thin plastic sheet was cemented over the surface of the strip.

This probe design was developed because coupling to a packet of charge moving radially is confined to the regions immediately above the gaps, with zero coupling above the copper strips, as suggested at the bottom of Fig. 17. Reference 7 shows that since the gap width is smaller than the length of the propagating discharge packet, the current induced in the zone-plate probe terminals is identical to the current flowing in the streamer discharge as it passes over one of the gaps. Thus, as the plastic covering the probe becomes charged and discharges occur from the metal rim surrounding the probe, the progress of the discharge can be observed as it passes over succeeding gaps. The terminating point of a discharge can be estimated, for instance, by determining the number of gaps that a discharge plasma cell has crossed. The shape of the discharge cell and the velocity of propagation can be determined from the shapes and durations of the individual pulses.

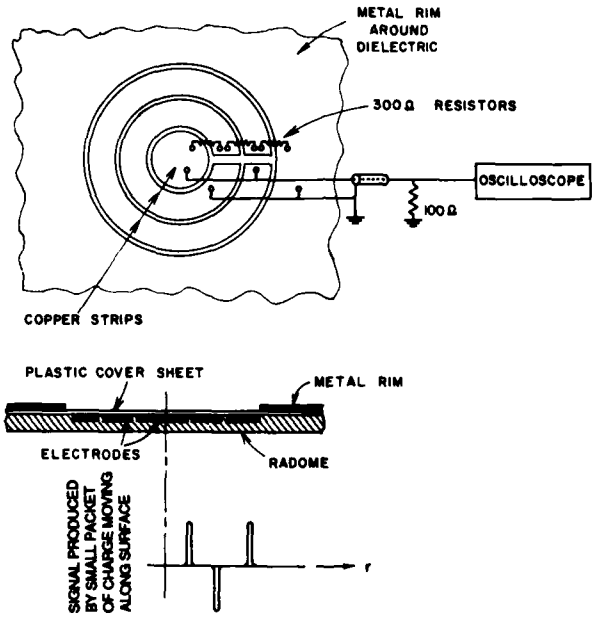

Fig. 17. Schematic drawing of zone-plate probe for flight investigation of surface streamer discharges.

Details of the actual zone-plate probe and the manner of mounting it for the flight tests are shown in Fig. 8a. The electrodes have been deformed to conform to the shape of the radome section on which the probe is mounted. Also, notches have been etched into the copper electrode strips to provide better adhesion between the plastic cover sheet and the radome proper. Electromagnetically, however, the probes of Figs. 17 and 18a are identical. Insight into the region charged by precipitation particles in flight can be gained from Fig. 18b, which shows the erosion observed on the conductive paint used to coat an adjacent radome section. It is apparent that only a small fraction of the radome near the nose becomes charged.

Samples of the oscillograms obtained from the zone-plate probe are shown in Fig. 19. The first positive pulse in an oscillogram is produced as the charge packet crosses the gap nearest the metal rim, and the succeeding pulses, alternately negative and positive, are produced by the crossing of succeeding gaps.

Positive polarity of the first pulse indicates that the discharge may be considered to consist of a packet of positive charge breaking away from a point on the metal rim and moving to some region on the dielectric sheet.

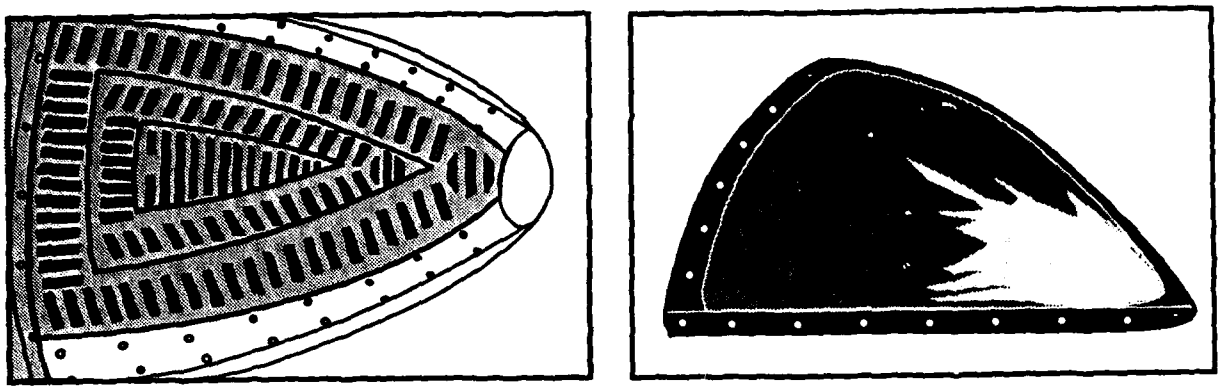

a) Surface discharge probe on aircraft.

b) Erosion of radome coating by impinging precipitation particles.

Fig. 18. Sensor used for flight measurement of dielectric surface discharges.

The spatial extent of the propagating plasma cell was inferred from the oscillograms in which more than one pulse occurred. Fig. 19d and Fig. 19e indicate that the second pulse began before the amplitude of the first pulse reached zero. This means that the leading edge of the packet reached the second gap while the trailing edge of the packet was still over the first gap. Thus, the length of the plasma cell appears to be at least three inches.

The velocity of propagation of the discharge was determined from the length of time required for the leading edge of the packet to travel from the first gap to the second gap in the probe. The average time interval between the leading edges of the two pulses on the oscillograms was found to be 0.4 μs. Since the gaps were two inches apart, the velocity of propagation is 1.27×10^7 cm/s.

It was found that the current pulses on the oscillograms, which represent the current flowing at the point s_1 above one of the gaps, could be approximated by an equation of the form

$$I(s_1, t) = I_{max} e^{-\alpha t} u(t) \tag{1}$$

The spatial distribution of charge in the charge packet is also of exponential form and may be written $q(s) = q_{max} e^{-\alpha s/v}$. Since the velocity of propagation, v, of the discharge is known, it is possible to generalize Equation 1 and write for the current at any point, s, along the path of the discharge

$$I(s, t) = I_{max} e^{-\alpha(t - \frac{s}{v})} u(t - \frac{s}{v}) \tag{2}$$

where $u(t - t_o)$ is the unit step occurring at time $t = t_o$.

Since, as is indicated in Fig. 19, there was considerable variation in both I_{max} and α, average values for both of these quantities were determined by reading a large number of oscillograms. The average values found were

$$\overline{I_{max}} = 0.01025 \text{ A}$$

$$\bar{a} = 7 \times 10^6 \text{ s}^{-1}$$

and the equation of the average discharge current pulse is, therefore,

$$I(s_1, t) = 0.01025\, e^{-7 \times 10^6 t} \tag{3}$$

When the results of the flight tests were being reviewed in reference 7, certain comments and speculations were made. They are repeated here because they still appear relevant:

> Some comment is appropriate concerning the properties of streamer discharges as revealed in these investigations. As stated, the discharges produce electrical effects equivalent to those which would be produced by packets of positive charge, approximately three inches long with exponential density distributions, which move from the discharge point on the metal rim to a region on the plastic surface, with a speed of 1.27×10^7 centimeters per second. It is evident after brief consideration that such a physical situation is impossible. The mobility of positive ions or even electrons is much too low to achieve the velocities corresponding to the velocity of the "charge packet" under the existing field conditions. The "charge packet" appears in actuality to be a cell of plasma which breaks away from the discharge point and propagates as a wave toward the negatively charged dielectric. At the leading edge of the cell an ionizing avalanche process occurs similar to that which occurs in positive point corona. Free electrons produced in the avalanche move to the rear of the cell under the action of the field, and there disappear by recombination. The apparent speed of packet motion is the speed at which the ionizing avalanche propagates (7).

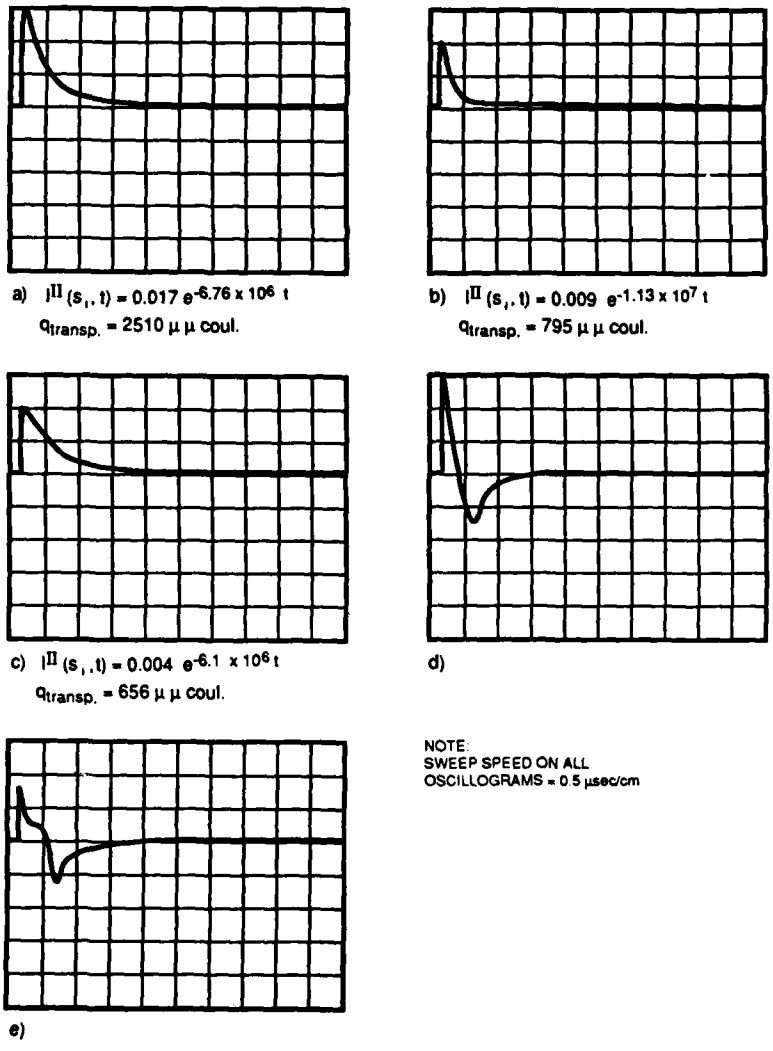

Fig. 19. Pulses induced in zone-plate probe by streamer discharges.

3.3.3 Noise in Broadband Systems

Frequently in aircraft designs, one finds an electrical conductor located immediately below a dielectric surface on which surface discharges can occur. This physical arrangement was set up in the laboratory in the work of reference 7, and measurements were made of the coupling between the wire and the dielectric surface discharge region. This coupling information was used, together with the streamer discharge characteristics discussed in Section 3.3.2 above, to predict the waveform characteristics of the current pulse induced in such a wire. The results of this calculation are shown in Fig. 20. The three waveforms indicate the effect of varying streamer discharge length, ℓ, from 1 to 4 inches. If the wire is terminated in an impedance of 1000 Ω, for example, the current pulses of Fig. 20 will generate voltage pulses from 0.3 to 0.5 V. This pulse amplitude is sufficient to upset a variety of circuits. Accordingly, cables associated with digital systems should not be routed under dielectrics located on aircraft frontal surfaces.

3.3.4 Noise in Narrowband Systems

To investigate the effects of streamer discharge noise on narrowband systems such as radio receivers, it is convenient to express the source function in terms of a noise-frequency spectrum. It was recognized that the pulse waveform of the signal produced by a streamer discharge depends on the geometry of the region where it occurs. Accordingly, streamer-noise-source spectrum calculations were carried out for several arrangements of the dielectric region as shown in Fig. 21a for the case of unity coupling ($\psi = 1\ m^{-1}$) and a charging current to the dieletric region of $I_{dc} = 1\ \mu A$. (To apply the data to other charging and coupling conditions, it should be kept in mind that the noise spectral density varies directly with the coupling factor ψ and as $\sqrt{I_{dc}}$.) In spite of the differences in the selected physical arrangements considered in Fig. 21, the three spectra are almost identical in the frequency range considered. Thus, a precise definition of the streamer geometry is not required to obtain a valid estimate of the noise spectrum. To apply these results to the case of an antenna wire on the back of a dielectric, it is merely necessary to recall that, for this case, the coupling function is $\psi = 3\ m^{-1}$ (Fig. 20).

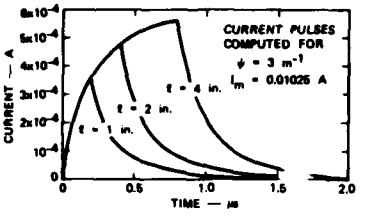

Fig. 20. Typical current pulses induced by streamer discharges.

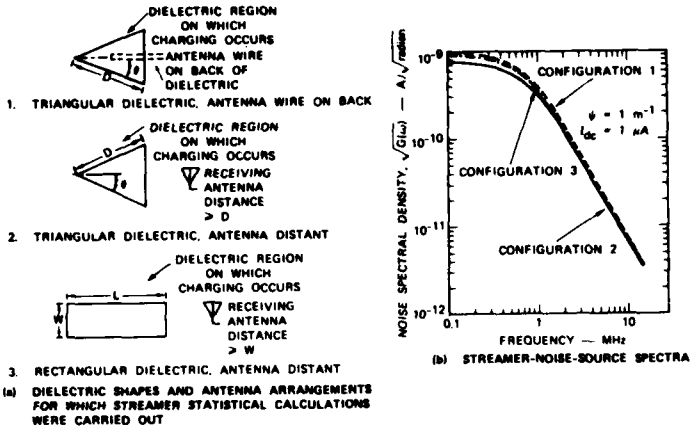

Fig. 21. Normalized streamer-noise-source spectra for several physical configurations of the dielectric region.

To apply the results to another configuration, it is necessary to know the coupling between the source region and the antenna in question. Fig. 22 shows the results of measurements made to determine the coupling between three typical antenna locations on the fuselage of an aircraft and the surface of a radome located on the nose. It should be noted that the coupling data have been normalized to unity antenna induction area ($a = 1$). The magnitude of the coupling function ψ can be determined by multiplying the values in Fig. 22 by the actual induction area of the antenna in question.

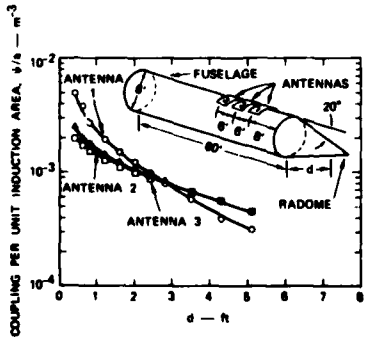

Fig. 22. Noise-coupling to sources along radome.

3.4 Spark Discharges

Spark discharges involve processes capable of generating high-amplitude, fast-risetime pulses containing energy extending from the LF through the VHF range. Operational experience with this noise source has generally involved instances in which various electrical conductors become unbonded in subtle ways. Examples of three such instances on operational aircraft are shown in Fig. 23 (21).

In the example of Fig. 23a, an aircraft began to experience p-static that affected VHF omnidirectional range (VOR) navigation and VHF communications. Minute cracks were found in the lightning diverter strips on the nose radome due to weathering of the thin aluminum foil. Charge deposited on the radome surface by precipitation had flowed to the isolated portion of the diverter strip and accumulated until the voltage across the gap became high enough to initiate a spark. Since each spark discharged the isolated strip completely, considerable charge was transferred, and the spark was an extremely energetic noise source. The dimensions of the diverter strips, furthermore, were such that, at VHF, they were a large fraction of a wavelength long. Thus, at VHF, a defective diverter system degenerated into an efficient antenna system driven by a spark noise source.

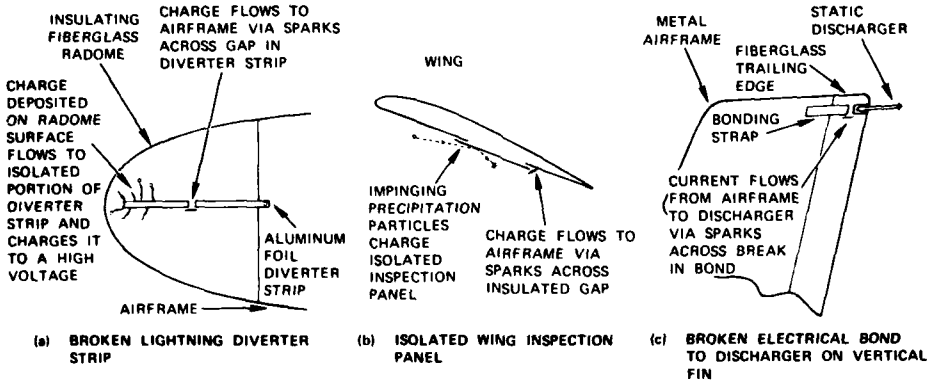

Fig. 23. Examples of sparking-noise sources on operational aircraft (after Moore).

In the example of Fig. 23b, an aircraft experienced p-static on its radios of sufficient severity to threaten to ground the aircraft as unsafe for long-range flight. Ultimately, an outboard wing inspection panel was discovered to have been repainted during a previous inspection; when it was reinstalled on the aircraft, the mounting screws had not penetrated the paint, thereby creating an isolated section. Precipitation charging raised the isolated panel to a high potential with respect to the airframe, so that sparking occurred across the insulating gap. Thus the insulated panel was, in effect, an electric dipole antenna driven by a spark noise source.

The example of Fig. 23c occurred early in the application of ortho-decoupled dischargers to jet transports. Two airlines flying DC-8 aircraft reported serious p-static on discharger-equipped aircraft. The design of the DC-8 vertical fin is such that a bonding strap was used to bridge the metal main structure of the forward part of the fin and the dischargers mounted on the insulating plastic trailing edge. The electrical bond was found to be so damaged that current flowing from the airframe to the discharger produced sparks across the gap in the discharger bonding system, resulting in excessive interference.

Perhaps the most significant implication of Fig. 23 is that minor inadvertant departures from the design configuration can ultimately be responsible for generating sparking noise. Patience and a high degree of attention to detail are necessary to track down noise sources on an operational aircraft.

4.0 CONCLUSIONS

Static charging of airplanes as the result of flight through precipitation or of engine-charging processes causes electrical discharges on the aircraft. Narrowband radio receiving equipment is affected because these discharges generate electromagnetic interference that raises the local equivalent noise field to levels above the atmospheric noise level. Radio performance can be improved by reducing the precipitation-static noise levels to the atmospheric level.

Broadband digital systems can also be affected because the discharges occur as a series of pulses that can be misinterpreted as system operating signals.

Great care must be taken to ensure the electrical bonding of adjacent metallic sections and adequate draining of charge from insulating dielectrics on the frontal surfaces of aircraft.

REFERENCES

1. H. G. Hucke, "Precipitation Static Interference," Proc. IRE, Vol. 27, May 1939.
2. R. C. Ayers and J. O. Jarrard, "Aircraft Precipitation Static Investigation," Contract W33-106 SC-70, Trans-World Airlines Inc., 1944.
3. R. Gunn et al., "Army-Navy Precipitation Static Project," Proc. IRE, Vol. 34, 1946.
4. R. L. Tanner and J. E. Nanevicz, "Precipitation Charging and Corona-Generated Interference in Aircraft," Technical Report 73, Contract AF19(604)-3458, Stanford Research Institute, Menlo Park, California, 1961.
5. ---, "An Analysis of Corona-Generated Interference in Aircraft," Proc. IEEE, Vol. 52, January 1964.
6. ---, "Radio Noise Generated on Aircraft Surfaces," Final Report, Contract AF33(616)-2761, Stanford Research Institute, Menlo Park, California, 1956.
7. J. E. Nanevicz, "A Study of Precipitation Static Noise Generation in Aircraft Canopy Antennas," Technical Report 62, Contract AF33(604)-1296, Stanford Research Institute, Menlo Park, California, 1957.
8. J. E. Nanevicz and E. F. Vance, "Studies of Supersonic Vehicle Electrification," Lightning and Static Electricity Conference, Air Force Avionics Laboratory, Wright-Patterson AFB, Ohio, 1970.
9. J. E. Nanevicz, "Flight-Test Studies of Static Electrification on a Supersonic Aircraft," 1975 Conference on Lightning and Static Electricity at Culham Laboratory, England, Royal Aeronautical Society, England, 1975.
10. ---, "Results of Titan III Flight Electrostatic Experiments," Lightning and Static Electricity Conference Papers, 12-15 December 1972, Las Vegas, Nevada, AFAL, AFSC, WPAFB, Ohio, Contract AFAL-TR-72-325.
11. C. H. King, "P-Static Flight Evaluation of a Large Jet Aircraft," Proceedings of the Eighth International Aerospace and Ground Conference on Lightning and Static Electricity, Report Number DOTT/FAA/CT-83/25, Federal Aviation Administration Technial Center, Atlantic City Airport, New Jersey, June 1983.
12. J. E. Nanevicz, E. F. Vance, R. L. Tanner, and G. R. Hilbers, "Development and testing of techniques for Precipitation Static Interference Reduction," Final Report, Contract AF33(616)-6561, Stanford Research Institute, Menlo Park, California, 1962.
13. J. E. Nanevicz and D. G. Douglas, SRI International, "Supporting Laboratory Studies for the Development of Rotor-Blade Treatments to Minimize Electrostatically Generated Noise on the HLH Helicopter," 1974, Final Report SRI Project 2868, Contract DAAJ01-71-C-0840, p. 40.
14. D. C. Kuo and B. J. Strait, "Improved Programs for Analysis of Radiation and Scaterring by Configurations of Arbitrarily Bent Thin Wires," AFCRL-72-0051, Contract F19628-68C-0180, Project 5635, Scientific Report 15, Department of Electrical and Computer Engineering, Syracuse University, Syracuse, New York, January 1972.
15. Reference Data for Engineers, Fourth Edition, International Telephone and Telegraph Corporation, New York, 1956.
16. A. Vassiliadis, "A Study of Corona Discharge Noise in Aircraft Antennas," Technical Report 70, SRI Project 2494, Contract AF19(604)-3458, Stanford Research Institute, Menlo Park, California, 1960.
17. E. F. Vance, "Techniques for the Study of Noise Generation and Coupling," Lightning and Static Electricity Coverence Papers, AFAL-TR-72-325, Air Force Avionics Laboratory, Wright-Patterson AFB, Ohio, December 1972.
18. K.S.H. Lee, ed., "EMP Interaction: Principles, Techniques and Reference Data, EMP Interaction 2-1, Final Report, Contract F29601-76-C-0149, Dikewood Industries, Inc., Albuquerque, New Mexico, December 1980.
19. Luis Oh, G. C. Huang, R. Goldman et al., "Natural and Induced Electrical Effects on Integrated Antennas and Circuits at Frequencies to 10 GHz," Technical Report June 28,1968-April 30, 1969, Contract F33615-68-C-1720, The Boeing Company, Seattle, Washington.
20. S. Larigaldie, "High Current Surface Discharge Propagation Analysis--Application to the Lightning Leader," Tenth International Aerospace and Ground Conference on Lightning and Static Electricity, 10-13 June 1985, Paris, France.

ALLEVIATION/TESTING TECHNIQUES FOR AIRCRAFT CHARGING

J. E. Nanevicz
Deputy Director, Electromagnetic Sciences Laboratory
SRI International
333 Ravenswood Avenue
Menlo Park, California 94025

Summary

In general, it is productive to consider electromagnetic interference control problems, and the alleviation of precipitation static, in terms of the source, the coupling process, and the victim system.

Since the radio interference of concern stems from noise-producing discharges resulting from aircraft charging, it is tempting to try to eliminate the ultimate source of the problem by eliminating the aircraft charging itself. Unfortunately, it has not been possible to devise workable schemes for the elimination of charging. Accordingly, noise reduction schemes to eliminate the source have been confined principally to the elimination of surface streamer discharges on electrically-insulating frontal surfaces. This can be achieved by coating the surfaces with electrically-conductive material to allow the charging current to flow off the surface as rapidly as it arrives, without generating noise. Another technique for eliminating surface streamer noise at the source is simply to relocate the offending insulating materials (i.e., antenna-insulating materials) to the aft of the aircraft where they will not be struck by precipitation particles, or to install particle deflectors upstream of the dielectric surface.

Similarly, the source of noise generated by sparking between sections of the metal structure can be eliminated by electrical bonding of all portions of the structure.

Successful techniques for the control of corona discharge noise involve forcing the discharge to occur from special discharging devices installed at high field regions on the aircraft where corona discharges are likely to occur naturally. The dischargers are designed both to reduce the corona source intensity and to decouple the discharge source from the airframe. Practical dischargers are capable of reducing corona discharge noise by as much as 60 dB.

Techniques demonstrated by laboratory and flight tests to be successful in controlling precipitation-charging interference are described.

Special instrumentation and testing techniques for the development and implementation of alleviation schemes are discussed.

1.0 Introduction

As indicated in the previous paper, static charging of flight vehicles results in electrical discharge processes that can adversely affect the functioning of avionic systems. The previous paper discussed the noise generating processes and ways to quantify their effects. This paper will concentrate on techniques for the alleviation of the effects of charging. We will also discuss the design and use of special devices that permit the testing of flight vehicles and their components in flight and on the ground.

In developing alleviation techniques, it is productive to consider the generic manner in which electromagnetic interference is generated and coupled into electronic systems. Fig. 1 shows the problem in three separate stages: a source of interference exists on the aircraft and excites the various coupling paths, which transfer the interference to the victim system or circuits. The alleviation process can be applied at any one or all of these stages. One can concentrate on eliminating of the noise source, minimizing the coupling between the source and the victim, or rendering the victim system inherently immune to interference. In the case of static charging effects, the approaches to alleviation techniques have included each of these basic areas with varying degrees of success. The problem of alleviation will be considered here in light of these general concepts.

2.0 Elimination of Charging

As soon as it was demonstrated that precipitation static was caused by frictional charging of the aircraft or parts of the aircraft, workers immediately recognized that the source of Fig. 1 could be eliminated if a means could be developed to eliminate or reduce the charging itself. It was argued that a coating could be developed to "match" the properties of the impinging ice crystals so that no charge transfer would occur on impact. This was pursued substantially in the work reported by Gunn (1). Unfortunately, the charge separation occurring when two bodies are brought into contact and then separated depends upon the properties of the contacting surfaces and not upon the underlying bulk materials. Thus a coating that reduced charging substantially when first applied to an aircraft had its desirable properties destroyed when the leading edges of the wings were wiped down with a cloth having traces of oil. Also, the static charging properties of ice varied substantially with temperature, so that a coating satisfactory at one temperature would be ineffective at another temperature. More recently, the general problem of prediction and control of frictional electrification was reviewed by Inculet who observed that:

> Under rigidly controlled conditions (in a hard vacuum using freshly cleared samples), the present status of knowledge of electron transfer between materials of different work functions permits the prediction of the polarity of the static electrification. The magnitude of the charge transfer which remains on the surface after separation is still far from being predictable. Engineering applications involving electrification can only be based on experimental results of a sufficiently large number of tests as well as on the proven ability to maintain or reproduce the surface and ambient conditions under which the original experiments were carried (2).

Another reason not to pursue charging-control coatings is that they would have no effect on engine charging. Thus, even if a successful coating could be developed, other alleviation techniques would have to be developed for engine charging. In light of these difficulties, it was decided to pursue alleviation techniques that did not depend on controlling the charging process.

In subsequent programs, measurements have been made of important charging parameters, such as the charge transferred to the aircraft by an individual precipitation particle, the total charging current to an aircraft as a function of cloud type, the way in which charging current varies with aircraft size, and the location of current discharge from an aircraft (3-7). These measurements were directed at quantifying the noise problem and understanding the discharge processes involved, not at attempting to control the charging.

3.0 Alleviation of Corona Discharge Noise

3.1 General

As indicated in the previous section, it is not possible to eliminate the charging of the aircraft leading to the corona discharges at the aircraft extremities. Thus, it is not feasible to eliminate the corona source in Fig. 1. Instead, it is necessary to focus on ways to reduce the strength of the corona source or to reduce the coupling between the source and the victim. In general, the most successful techniques employ both approaches.

It is important to observe that the properties of the static electric fields around an electrically conducting body are such that the highest fields occur at the extremities -- the airfoil tips on a conventional aircraft. Thus, corona discharges will occur from the regions of the airfoil tips under conditions of precipitation or engine charging. That corona discharges tended to occur in a few localized regions on the aircraft indicated that the discharge current normally experienced in flight could be forced to leave via specially designed dischargers installed in these same regions. If the dischargers were designed to control source intensity and noise coupling, corona noise could be substantially reduced.

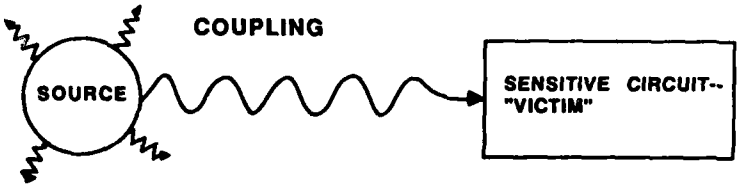

Fig. 1. Generation and coupling of electromagnetic interference.

3.2 Decoupled Dischargers

3.2.1 Passive

To devise a discharger intended to take advantage of every facet of noise control, corona noise generation and its coupling into antenna systems were considered in light of a reciprocity theorem that can be derived in much the same manner as the familiar Lorentz reciprocity theorem (3,4,8). The coupling theorem states that

$$I(\omega) = \frac{1}{V(\omega)} \int_T \underline{E}(\underline{x},\omega) \cdot \underline{J}(x,\omega)dv \qquad (1)$$

Equation 1 may be interpreted as follows: if the space and time distribution of the current density ($\underline{J}$) produced by the disturbance are known, and if the field ($\underline{E}$) in the region (T) produced by a voltage ($\overline{V}$) applied to the antenna terminals can be determined, then it is possible to compute the short-circuit current (I) induced in the antenna terminals. (Essentially, the coupling theorem states that the noise current generated in a receiving antenna by a discharge is proportional to the RF field that would exist at the location of the discharge if the antenna were used for transmitting).

Applying the coupling theorem to the problem of discharging an aircraft, we may consider $\underline{J}$ to be the discharge current. The coupling theorem then suggests several ways in which the noise content of the antenna current (I) can be reduced or eliminated:

- By letting the noise content of $\underline{J}$ approach zero
- By letting the ratio E/V approach zero (reducing the coupling)
- By letting $\underline{J}$ be perpendicular to $\underline{E}$ (reducing the coupling).

It should be noted that, perversely, the regions of high dc field, such as the airfoil extremities where the corona discharges occur and where the dischargers must be located, also correspond to regions of high RF coupling fields. For example, consider the field in a small region about the trailing edge of a wing (Fig. 2a). It is evident that the field configuration, either RF or static, is determined by the shape of the conductor forming the field boundary. To develop a decoupled discharger, therefore, it is necessary to devise a scheme for causing a difference between the two fields. In particular, we would like to have a high dc field imposed upon the discharge point and at the same time to have the RF field at the point equal to zero.

How this was done in the development of the flush-mounted, decoupled discharger is evident from Fig. 2b, which shows a cross section of the trailing edge of an airfoil surface in which the rear-most portion is electrically isolated from the remainder of the surface. It is evident that there are two lines along the conductor on which the field is zero and a considerable region over which the field is very small. If a discharge could be made to occur at the point of zero field, no noise would be coupled into the receiving system. For a discharge to occur at the point of zero field, however, the isolated section must be maintained at the same dc potential as the remainder of the aircraft. The requirements that the trailing edge be isolated at RF and directly connected at dc can be very closely approximated by connecting the trailing edge to the airframe through a very high resistance. If the value of the connecting resistance is high compared to the capacitive reactance between the isolated trailing edge and the remainder of the airfoil, the RF field will remain essentially as depicted in Fig. 2b. The dc field in the immediate vicinity of the trailing edge will be of the form indicated in Fig. 3c, which differs only slightly from that illustrated in Fig. 2a. Fortunately, the dc current through the connecting resistance is small, so that the voltage drop is not significant except at a very high discharging rates.

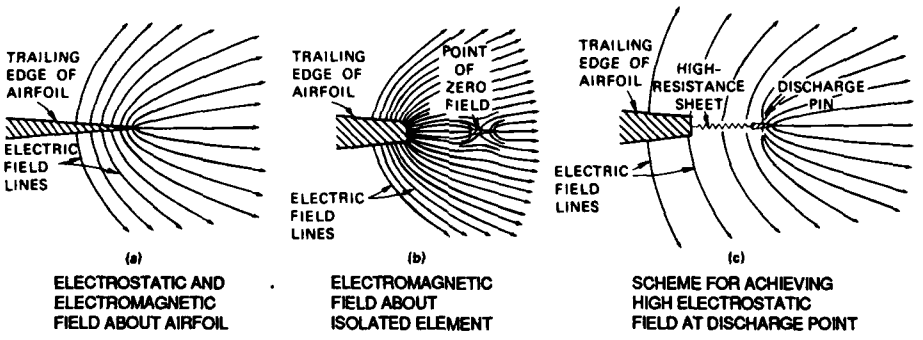

Fig. 2. Illustrating decoupled discharger evolution.

A practical flush-mounted discharger, employed in a series of flight tests in 1957-59 on the Boeing 707 prototype (4,9,10), embodying the techniques just discussed is illustrated in Fig. 3. Observe that the discharge is forced to occur in the region of minimum reciprocal field due to installation of low-threshold needles in this region. Since the discharge occurs from the points of the needles, the discharge current flows at approximately right angles to the reciprocal field lines. The discharge is thus orthogonally decoupled as well as being decoupled by virtue of the minimum in the reciprocal field. Finally, if very sharp points are used, the amplitudes of the individual current pulses are small, yielding a reduced noise content in the discharge current. In the practical design, then, all three of the noise-reduction methods are employed, although the majority of the noise reduction results from the decoupling techniques.

Although tests of the flush dischargers were encouraging, it was found that they had a high corona threshold potential. Furthermore, because it is an integral part of the airfoil trailing edge, the flush-mounted discharger is expensive to install on a retrofit basis. Consequently, another design was considered -- particularly for retrofit.

Production versions of the retrofit decoupled dischargers that were finally developed are shown in Fig. 4. Although two physically different dischargers are shown, they are identical in principle and differ only in that Type A (shown in the lower part of the figure) is designed to mount at the trailing edges of airfoils parallel to the widestream, and Type B (shown in the upper part of the figure) is designed to mount on the outboard tips of airfoils at right angles to the airstream. Essentially, the discharger consists of a rod of high-resistance material with a tungsten discharge point located at the point of minimum coupling near the end of the rod. The aft end of the rod is hemispherically rounded and coated with a dielectric to prevent coronas from occurring at the tip where the coupling is relatively high. The rod fits into a metallic socket on the mounting base that protrudes aft of the trailing edge and serves as a lightning diverter, tending to protect the trailing edge from direct lightning strikes.

Type-B dischargers are required on the outboard portions of the airfoils. The vortices generated in these regions produce localized pressure reductions that reduce the corona threshold sufficiently so that discharges can occur from sections of relatively large radius. The type-B dischargers produce a column of space charge along the wing tip, which reduces the dc field in this region and prevents discharges from the wing tip itself.

Because of its relatively simple geometry, the theoretical decoupling of the Type-A discharger can be calculated. For rods such as those illustrated in the lower part of Fig. 4, the calculation indicated that, with a total rod resistance of 20 MΩ noise at a frequency of 500 kHz should be reduced by 55.6 dB (the noise reduction increases 20 dB per octave with increasing frequency). The noise reduction afforded by the dischargers as determined from flight test data obtained on the instrumented Boeing 707 prototype was at least 50 dB. Laboratory measurements indicate that 60-dB noise reductions are obtainable in practice (10).

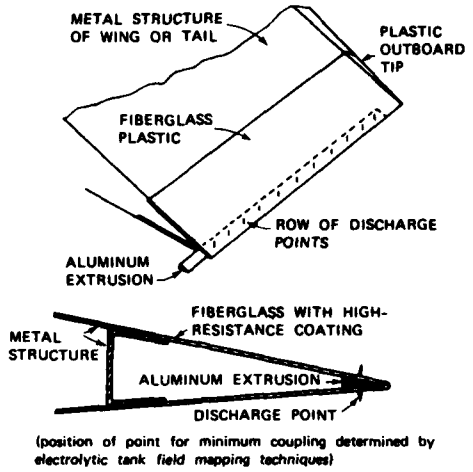

Fig. 3. Construction of flush-mounted decoupled discharger.

Fig. 4. Production models of type -A and type -B ortho-decoupled dischargers.

3.2.2 Active

An active discharger capable of maintaining zero aircraft potential, based on the principles of Fig. 2 and physically resembling the passive discharger of Fig. 3, was developed and tested (11,12). The physical arrangement of the active discharging element is shown in Fig. 5. A metal bar located in the plane of the wing was mounted roughly 6 inches aft of the trailing edge, parallel to the edge. Dielectric support struts provided mechanical support for the bar and kept it electrically insulated from the rest of the airframe. Sharp tungsten pins were mounted at one-inch intervals along the null-field line on the bar. Electrical connection to the high-voltage supply was made via a 1-MΩ resistor. This value of resistance is sufficiently high that the RF field structure about the bar is unaltered, but is sufficiently low that the rated discharger current of 3 mA produces voltage drop of only 10% of rated power-supply output. The high-voltage supply was a special unit developed at SRI and could be controlled over the range -60 to 0 to + 60 kV. It's two voltage multiplier strings used controlled SCR's instead of diodes.

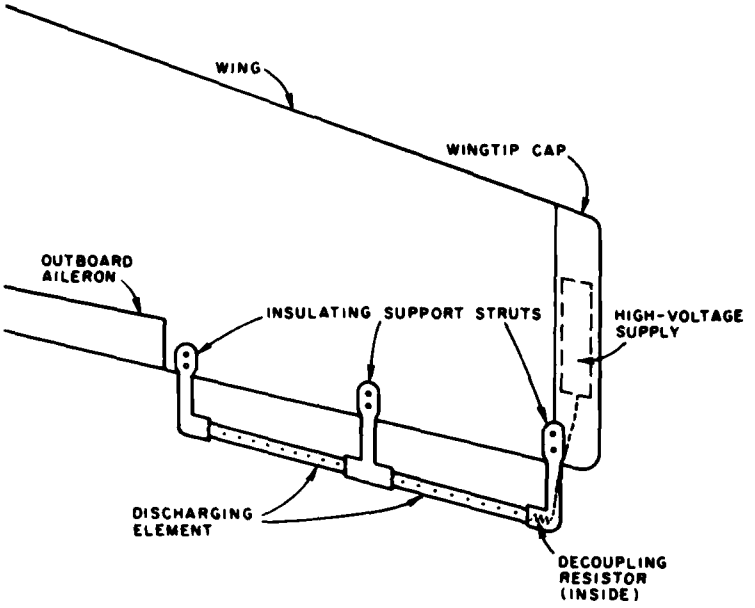

Fig. 5. Discharging-element arrangement.

The control system for maintaining the aircraft potential at zero consisted of a field meter to detect the aircraft potential, a polarity and amplitude controller (to control the polarity and amplitude of a high-voltage bias supply), the high-voltage bias supply whose output voltage and polarity were electronically controllable, and discharger elements that produced a decoupled corona current (I_d) to oppose the natural charging current (I_c). A simplified block diagram of the system is shown in Fig. 6, where the airframe is represented by a capacitor of capacitance C_a, that is charged to a potential (V_a) by the natural charging current (I_c). The discharge current (I_d) flows off the discharge element through a resistance (R_d) which depends on the bias voltage, the altitude, and the air speed. This resistance is therefore neither constant nor linear. The discharge current (I_d) is determined primarily by the bias supply voltage, but the airframe potential also affects this current if the airframe is charged to significant potentials. To permit a simplified, linearized analysis, however, the effect of airframe potential on discharge current can be neglected.

Thus, assuming linear system performance, the current transfer function will be of the form

$$\frac{I_d}{I_c} = \frac{1}{1 + sC_a R_d/G} \qquad (2)$$

where G is the combined transfer function of the field meter, controllers, and high-voltage unit. Further simplifying assumptions were made regarding the circuits in the field meter, controller, and high-voltage units, and calculations were made to determine system response. These calculations indicated that the maximum steady-state charging currents that can be handled by the system with gains in the stable range are 300 to 400 μA, if the aircraft potential is to remain below 1000 V. On jet transports, the maximum potential that can be tolerated may be 5 to 10 times as great, however, so that charging currents in the mA range can be handled on such aircraft. This general behavior was observed in the flight tests of the system on a Boeing 707 aircraft (12).

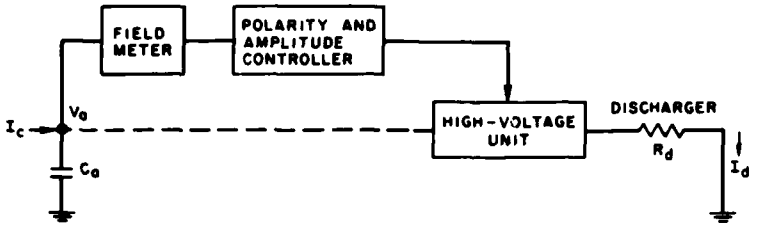

Fig. 6. Block diagram of control system.

3.3 Other Discharger Designs

In connection with the development of the decoupled discharger at SRI, other discharger configurations were conceived, and their performance was predicted in light of the coupling theorem of Equation 1. The results of laboratory measurements to verify the analyses are shown in Fig. 7. It is evident from the figure that the AN/ASA-3 is a highly successful design for noise reduction. Unfortunately, the wick cannot survive the aerodynamic environment typical of jet aircraft, and the remaining designs in Fig. 7 do not perform as well as the decoupled discharger in Fig. 7E. In the discussion of discharger designs in reference 9, it was observed that a significant portion of the noise reduction afforded by a wick follows from the pulse-amplitude-limiting action of the high resistance and low capacitance of the individual fibers at the ends of the wicks. On a new wick, most of the fibers are slightly conducting so that they can sustain discharges. The effective capacitance of the fiber is so low, however, that only a small amount of charge can accumulate on the fiber before the threshold field is reached at the surface. The charge transferred in one corona pulse is therefore quite small, and the result is that the noise content of the discharge (J) is relatively low.

Since the publication of reference 9, activity has been substantial in the development of carbon fibers for use in carbon-composite structural materials. These fibers are inherently conductive, so that no problem with loss of fiber conductivity with time exists as it did with the AN/ASA-3 materials. Accordingly, manufacturers have begun providing dischargers that employ a bundle of carbon fibers encased in a plastic matrix to yield a hard, rod-shaped discharger.

Feeling that a metal discharging element should lead to a longer discharging lifetime, other manufacturers have embedded a number of small metallic particles in a high-resistance matrix. Thus, each particle is electromagnetically isolated from its neighbors and discharges independently of them. If the metal particle is made sufficiently small, the charge it can store before discharging will be less than the charge transfer in a corona pulse from a burr on an airfoil trailing edge ($\approx 10^{-9}$ coulomb, as shown in the previous paper). If we consider an individual metal particle to be a sphere, the electric field (E) at its surface is given by

$$E = \frac{q}{4 \pi \varepsilon_o r^2} \qquad (3)$$

where q = charge on particle, r = particle radius, and ε_o is the dielectric constant. Since electrical breakdown of air at sea level occurs when $E = 3 \times 10^6$ V/m, we can solve Equation 3 for the radius at which the charge on the sphere is $q = 10^{-9}$ coulomb when $E = 3 \times 10^6$ V/m. The radius for this condition is r = 1.7 mm. Thus, if the metal particles are made, for instance, less then 1 mm in effective diameter, a substantial reduction in the charge transferred per discharge can be achieved with a concomitant reduction in noise. Conceptually, such a discharger design can be considered to be equivalent to replacing the fine wire of Fig. 7H with a number of such wires 1 mm or less in length.

4.0 Alleviation of Surface Streamer Discharger

4.1 General

Although the word "alleviation" is used in the title of this section, successful techniques for the control of streamer-generated interference generally involve the elimination of the dischargers on critical surfaces. In general, streamer noise control is conceptually simple and straightforward. Problems most frequently rise because design and production engineers are not sensitive to the degree to which attention must be paid to details if noise problems are to be avoided.

4.2 Preventing Charge Deposit

Since streamer noise is generated only when charging occurs on dielectric surfaces, it is reasonable to devise techniques to avoid the deposit of charge on critical surfaces. In general, this involves locating the surface in such a way that it is not struck by precipitation particles. For example, ADF sense antennas are generally located roughly midway between nose and tail on the fuselage to achieve 0° tilt angle (13). Although the antenna generally includes a dielectric cover capable of storing charge, these antenna installations have been free of corona discharge problems -- essentially because there is no particle impact this far back on the fuselage.

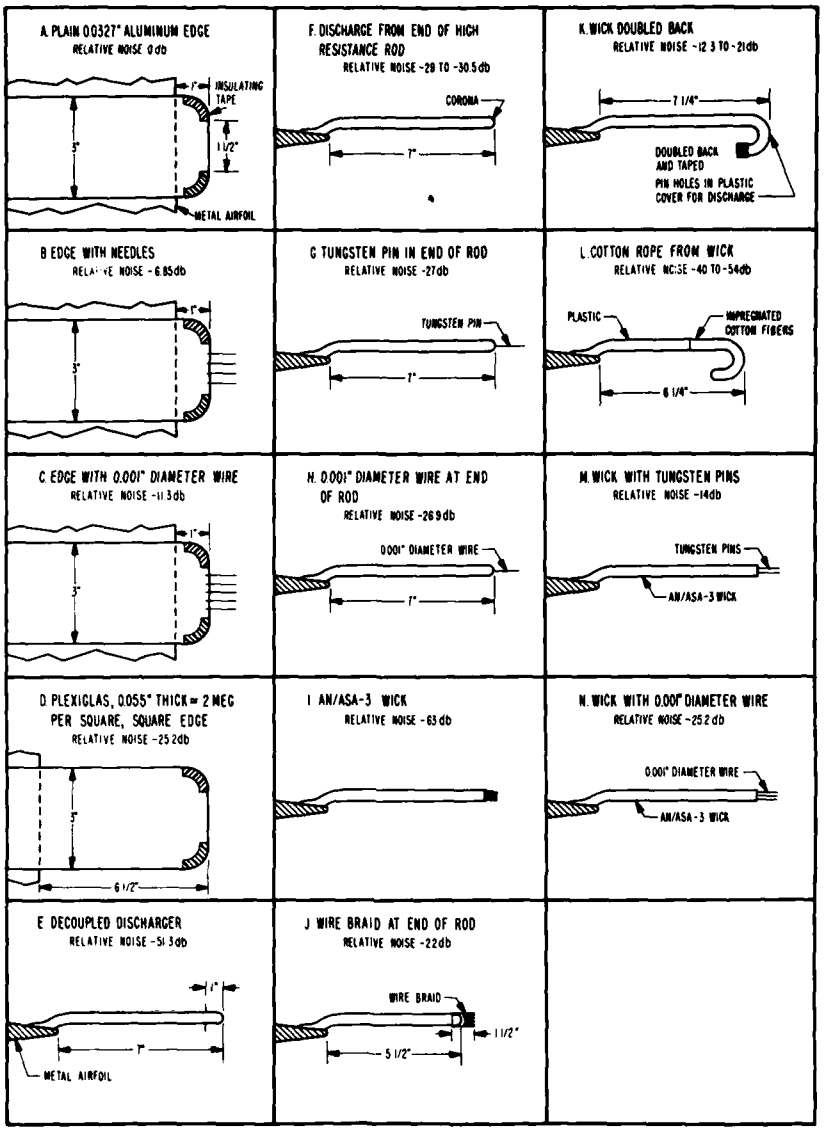

Fig. 7. Results of measurements of noise generated when given current is discharged from a proposed discharger. Noise levels are expressed relative to the noise generated when the same current is discharged from the edge of a 0.0327-inch-thick aluminum sheet simulating the trailing edge of an airfoil.

Whenever possible, critical dielectric surfaces should be located far aft on the fuselage and designed to be flush with the mold lines of the aircraft. Blade antennas that must protrude from the aircraft surface can be designed with a metal leading edge to provide a drain path for the arriving charge. Insulators at the base of the antenna should be made thinner than the "shadow zone" (region next to the skin where the particle density is zero) to keep the insulators from charging. In the case of a small dielectric region, such as the base insulator of an antenna, that must be located near the the nose of an aircraft, it is often possible to install a small particle shield or deflector upstream of the dielectric to shield it from impinging particles.

4.3 Avoidance of Dielectric Frontal Surfaces

Frequently, dielectric materials are installed in what turn out to be critical regions on the frontal surfaces of aircraft when no justification exists for this choice of material. Often, the dielectric was chosen for its low cost, ease of fabrication, or some other property, by an engineer or production supervisor knowledgeable in his specialty, but unaware of the likely consequences of his material choice. For example, the author was involved in tracking down the interference source that caused the ADF system on a

particular aircraft fleet to malfunction consistently under modest charging conditions. The problem was obviously related to precipitation charging, but even flight testing in which candidate offending surfaces were treated did not locate the source. Finally, ground testing with an artificial charging device (discussed later in Section 6.2.1) traced the problem to an aerodynamic plug in the front end of a hollow "towel-rail" antenna bar running along the fuselage. The designer of the antenna had intended that the plug be made of aluminum, but the manufacturer replaced it with dielectric, which was more desirable for mechanical reasons and which he knew wouldn't appreciably change the receiving characteristics of the antenna. After the whole assembly had been painted, it was impossible even for the designer to detect the substitution of materials. Charging of this 1-inch-diameter plug generated sufficient streamer noise in the antenna on which it was mounted to disable the ADF system. Replacing the plastic plug with a metal one cleared up the noise problem in this fleet of aircraft.

This example illustrates a problem frequently encountered in tracking down sources of malfunction similar to that described above. The designer of the antenna was questioned regarding the materials used in antenna fabrication. (The antenna design incorporated sophisticated features such as metal shields on the stand-off masts to prevent streamers). He indicated that all leading-edge surfaces were made of metal. However, it was not until the aerodynamic plug was exposed to charging by a directed stream of lycopodium powder that the change of materials used in making the plug was discovered. Accordingly, it is necessary for the troubleshooter to have available a means for simulating dielectric charging. In the case discussed here, lycopodium powder spray provided a nonconfrontive way to verify the assertion that "all leading edge surfaces on the antenna were made of metal."

4.4 Provisions for Discharging Dielectric Surfaces

Increasingly, dielectrics are being specified for use on frontal surfaces of aircraft. When this is the c. e, it is possible to coat their outer surface with electrically conducting material to drain away charge as rapidly as it arrives. If the dielectric is only a structural member, such as a wing leading edge, the conductivity of the coating can be as high as is convenient. Flame-sprayed coatings that apply a substantial thickness of metal have been used in these applications.

Other dielectric frontal surfaces, such as radomes, must be transparent to RF radiation, but their optical properties are unimportant. These surfaces can be coated with a layer of high-resistance conductive paint. Appropriate paints are usually made of a mixture of carbon black and graphite added to a paint vehicle such as lacquer or epoxy. Carbon material to approximately 45% by weight must be added to the paint vehicle to render it conductive. Analysis of the fields generated by current flow through the conductive layer (15) indicates that surface resistivities as high as roughly 1000 MΩ/square provide enough conductivity to avoid surface electrical breakdown, even under high precipitation-charging conditions. Thus, it is possible to provide adequate static discharging without causing appreciable attenuation of the radar signal.

Optical surfaces, such as windshields, must also be located on frontal surfaces. These can be rendered conductive by coating them with a thin optically transparent film of a material such as stannous oxide. Unfortunately, these films are fragile and are abraded by the impinging precipitation particles. The durability of the conducting layer on a glass windshield can be improved substantially by baking the glass after the layer is applied. Unfortunately, polycarbonate windshields cannot be baked and so no satisfactory technique exists at present for controlling charge build up on their surfaces.

5.0 Alleviation of Sparking Problems

Strictly speaking, since the occurrence of sparking implies that adjacent metallic conductors are not electrically bonded, sparking problems should not be encountered on aircraft, where proper bonding is an important design consideration. That sparking problems do occur, in spite of deliberate precautions, indicates that the bonding problems capable of causing difficulties are of a minor nature and extremely subtle. Indeed, the solution is trivially simple -- bond the adjacent parts. The difficulty lies in locating and identifying the culprits.

Usually, a minor deviation from the intended design or assembly is responsible and can be repaired in a matter of minutes. Unfortunately, hours or months may be spent tracking down the problem, unless the proper equipment for simulating charging happens to be available. In essence, sparking is not alleviated. It is prevented by proper bonding arrangements, and it is eliminated by correcting lapses in electrical bonding. It should be observed that to control the sparking resulting from static charging, the bond does not have to be a low impedance one as for lightning. A bond resistance of tens or hundreds of kilohms is adequate to handle most static charging currents.

6.0 Testing Techniques

6.1 General

The engineer working on problems associated with aircraft charging frequently needs to carry out tests and simulations quite unlike those employed by specialists in other facets of electromagnetic interference control. Some of these tests can be carried out with a simple current meter and a few pieces of copper tape. Other tests require provisions to apply charge to dielectric surfaces. Some of the testing techniques that have been developed by workers concerned with aircraft charging will be presented together with way. they can be applied.

6.2 Ground Testing

6.2.1. Simulation of Surface Charging

Often it is important to duplicate on the ground the charging an aircraft experiences in flight. Such a simulation is important in proof-testing a design prior to flight. It is also useful in tracking down problems on an operational aircraft. For example, in the work of reference 14, simulation enabled a design change hidden by layers of paint to be detected quickly.

A field technique developed by SRI for this purpose is shown in Fig. 8. A portable sandblaster filled with lycopodium powder is used to spray surfaces of interest with the powder to produce frictional charging closely simulating that observed in flight. Lycopodium powder was chosen because it flows readily, charges most surfaces, is biodegradable, is non abrasive so that it doesn't have to be scrupulously cleaned out of machinery, and is not overly expensive. Depending on where the tests are conducted, humidity is often substantially higher than in a high-altitude ice crystal cloud. To dry out the test surface, it is effective to clean it with a cloth saturated in pure grain alcohol. Nondenatured alcohol is best because it does not leave a film.

The facility developed at SRI for the proof-testing of new systems is shown in Fig. 9. The test chamber is a folded wind-tunnel device that houses the test vehicle nose section at the inlet end. Lycopodium powder is blown onto the frontal area of the test object with a high- pressure (100 psi) gun to simulate the charging environment encountered during flight. After charging, the spent powder is ducted through the tunnel onto a series of wet filter pads that trap the powder and prevent it from exhausting into the ambient air. Thus, charging testing can be continued for substantial periods of time without discomfort either to the residents of the laboratory or its neighbors. The system includes provisions for monitoring the charging and for observing the functioning of critical circuits within the test object. Although not shown in Fig. 9, a small portable radio receiver is useful for indicating the occurrence of streamers. If the room is darkened, the discharges can be seen.

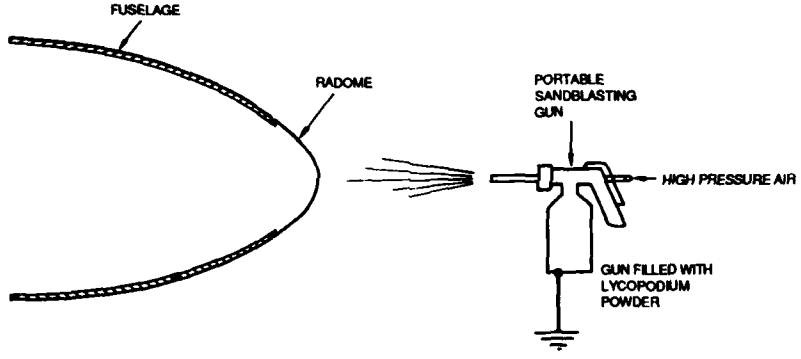

Fig. 8. Technique developed by SRI for in-field simulation of surface charging.

An alternative charging techniques, that does not depend on particulates for its operation, has been developed by Taillet and his coworkers at ONERA (16), based on a method first prepared by Whewell, Bright, and Makin (17) following previous work by Marks, Baretto, and Chu (18). The device is shown in schematic form in Fig. 10. In this device, low-mobility charged microparticles of ice, obtained by condensation and freezing of water vapor in humid air expanding in a supersonic nozzle, and driven by fluid friction in the jet, are used as charge carriers. This principle is applied to direct charges on an insulating surface. The microparticles of ice sublime after leaving the supersonic region of the jet. This simulation method is, therefore, clean in the sense that the local properties (surface resistance and breakdown voltage) are not modified when the charge injector is operating. This device is marketed under the trade name INJECO.

Workers at SRI were attracted to the INJECO device because of its cleanliness and ease of use. In initial tests with thin dielectrics backed with metal or with paints on metal, it was easy to obtain surface discharges. However, when such a device was tested on thick dielectrics or unbacked radomes, streamers could not be generated. It was conjectured that the ice microparticles had largely sublimed before they reached the surface, so that they were repelled by the fields generated by the charge accumulating on the test surface. (It should be noted that the external field per unit deposited charge is higher on an isolated dielectric surface then it is on one backed by a grounded conducting sheet.) Thus, although the accumulated surface charge was high enough to prevent further charging, it was not high enough to support surface streamers. When the opportunity arises, further investigation will be made into the charging properties of the INJECO device or isolated dielectric sheets. In the meantime, the existing lycopodium powder facility is used for such tests.

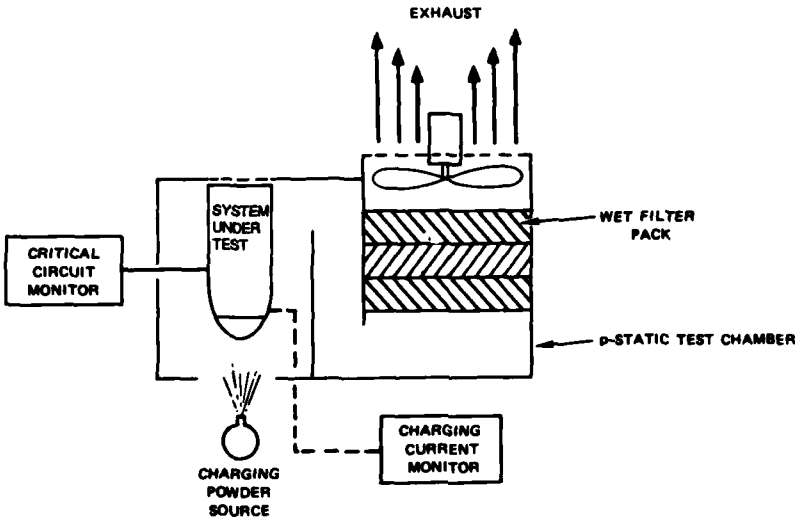

Fig. 9. Test vehicle installed in p-static test facility.

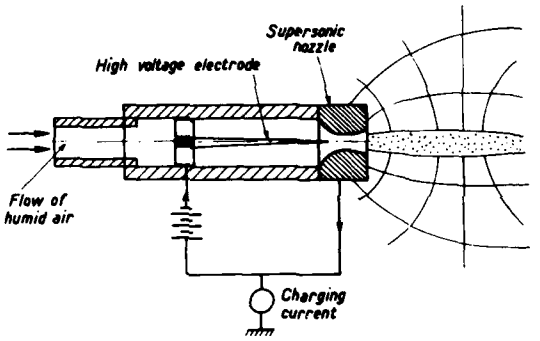

Fig. 10. Diagram of the INJECO device (reference 16).

6.2.2 Surface Resistivity Measurement

Often in working with dielectric surfaces, it is necessary to determine their surface resistivity. A device such as that illustrated in Fig. 11 is convenient for this purpose. In operation, the steel wool pads are pressed against the surface whose resistance is to be measured. The spacing and diameter of the tubing shown are such that the ohmmeter reads half the resitivity, in ohms per square, of the surface being tested. The device is an analog of a TEM transmission line, and transmission line theory can be used to d vise other electrode configurations to accomplish the measurement. For example, for the arrangemen. shown in Fig. 11, the calibration is valid provided there are no conductors, such as the rim of the transparency, closer than a few distances (D) from either of the electrodes. A coaxial electrode arrangement is also possible, and, since current flow is confined entirely to the inside of the outer electrode, resistance measurements can be made as close as desired to other electrical conductors. One design for a coaxial probe used at SRI is shown in Fig. 12. The dimensions of the coaxial probe were chosen so that the conductivity (in ohms/square) of any surface could be determined by multiplying the measured resistance by 4. To obtain uniform surface contact over the entire probe, soft conducting vinyl pads were applied to the brass contact pads of the probe. These pads had side-to-side resistances of less than 1 Ω.

The simple surface resitivity sensors shown in Figs. 11 and 12 cannot be used if the surface to be tested is covered with paint. Taillet and his coworkers at ONERA have considered this problem and have devised a system, sold commercially as CORAS, that is based on ac measurement so that it can function even in the presence of a thin insulating film over the surface to be tested (19). The system employs a specially designed head with multiple concentric electrodes that include guard rings and sleeves surrounding the measuring electrodes. The accompanying electronics processing unit includes several synchronous detectors to permit phase-sensitive measurements. The sophistication and complexity of the CORAS instrumentation is such that it would not be reasonable to attempt to assemble it from available laboratory equipment.

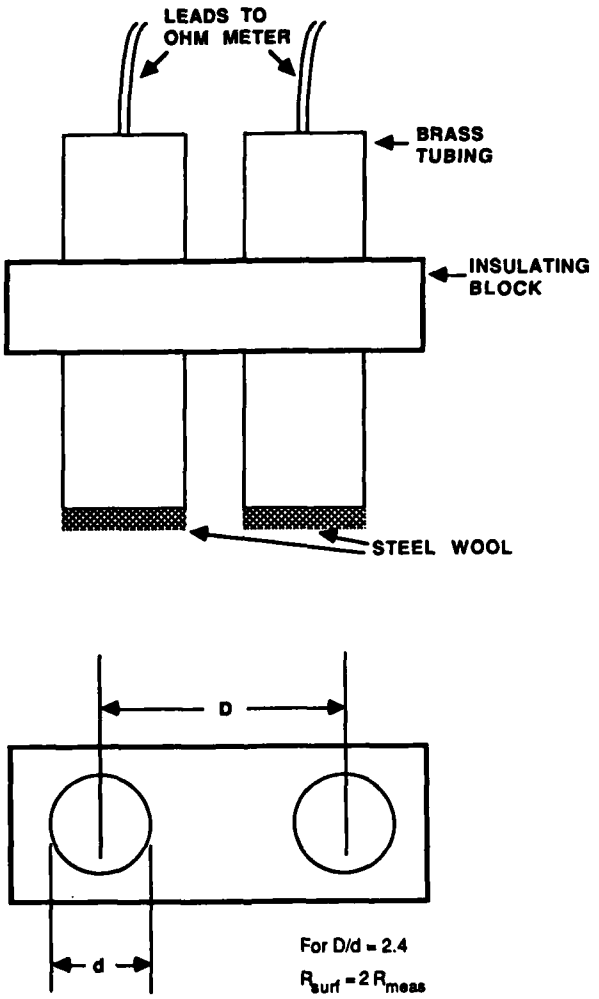

Fig. 11. Device for measuring surface resistivity.

6.2.3 Electrical Bonding Measurements

Although the concept of measuring bonding seems trivially simple at first glance (particularly since bonds for electrostatic purposes are adequate if they have a resistance of 10^5 Ω or less), practical considerations, such as the existence of paint over the surfaces to be tested, can greatly complicate the problem. If the surfaces are unpainted, the device of Fig. 11 can be bridged across the joint between a dielectric panel and the surrounding structure to verify continuity. Again, if the surfaces are unpainted, an ohmmeter can be used to verify continuity between various conductors and the frame of the aircraft.

For tests on painted surfaces, the CORAS system developed by Taillet and his coworkers can be used to verify bonding adequacy (19). In the "bonding" mode of operation, an electrode in contact with the insulating paint layer is used to inject an audio frequency current through the layer into the metallic piece. (The other terminal of the generator is connected to the airframe). A high-impedance sensing device measures, through the same paint layer, the ac voltage of the piece. If this voltage is not negligible with respect to the forcing electrode voltage, the bond is not acceptable.

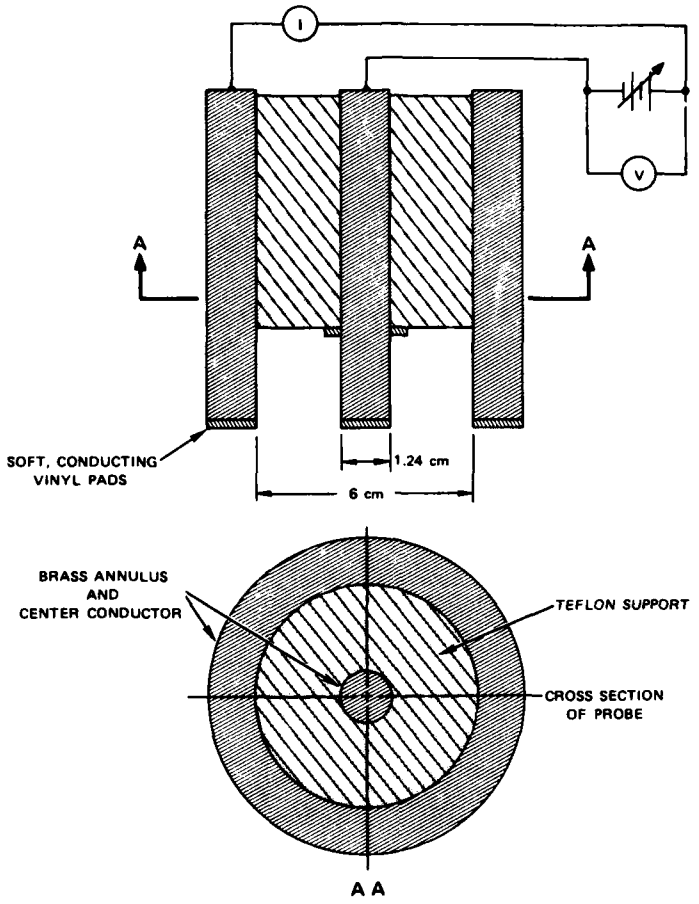

Fig. 12. Coaxial conductivity probe used to measure surface resistivity.

6.2.4 Corona Discharge Tests

Frequently, it is important to assess the vulnerability of a vehicle to corona discharge in flight. For example, before the first model is flown in charging conditions, it is reassuring to know that it has been exposed to and functioned properly under the anticipated discharging levels. This is often the first time the vehicle systems have been assembled in their entirety. Alternatively, it may be that a vehicle has been experiencing difficulty and that the source has not been identified. A test can be carried out using the setup shown in Fig. 13 in an area as free as possible of clutter, to simulate free flight conditions. Ideally, the vehicle could be mounted on a stand to minimize ground effects. To simulate actual flight conditions, no electrical connections should be made except for a connection to ground through a high-resistance carbon fiber wire that provides the necessary RF isolation and does not significantly alter the electrical field distribution around the vehicle. Communication should be via fiber-optics links; internal power can be provided by batteries or by a hydraulic generator, fed via nonconducting hydraulic hoses. Thus, as far as radio frequency noise is concerned, the vehicle should be completely isolated (electrically), as it would be in flight.

Corona current is drawn from the wings and fins by high-voltage "field bowls". These field bowls can be made of wood covered with high-resistance paint. Due to the high surface resistivity, good RF isolation is achieved, and, thus, the RF coupling to the wings and fins is the same when the vehicle is in flight. The high voltage applied to the field bowls produces the same dc fields at the vehicle extremeties as may be expected to occur under actual flight conditions. The field bowls used at the wings consist of a V-shaped structure, placed about 12 cm from the rear wing edge. For the fins, a flat plate can be used to draw current simultaneously from all the fins.

A safety resistor, indicated in the figure, of roughly 35 MΩ is used to limit current in the event of a short circuit. The high-voltage line is usually split three ways and connected to the two wing bowls and the flat fin collector. These connections consist of a distributed high-resistance wire to provide RF isolation. Three current meters can be used to monitor the current drawn by each wing and the fins. To achieve the proper ratio of current from wings and fins, the distance of each field bowl from the vehicle extremities is varied, while the high voltage is kept constant.

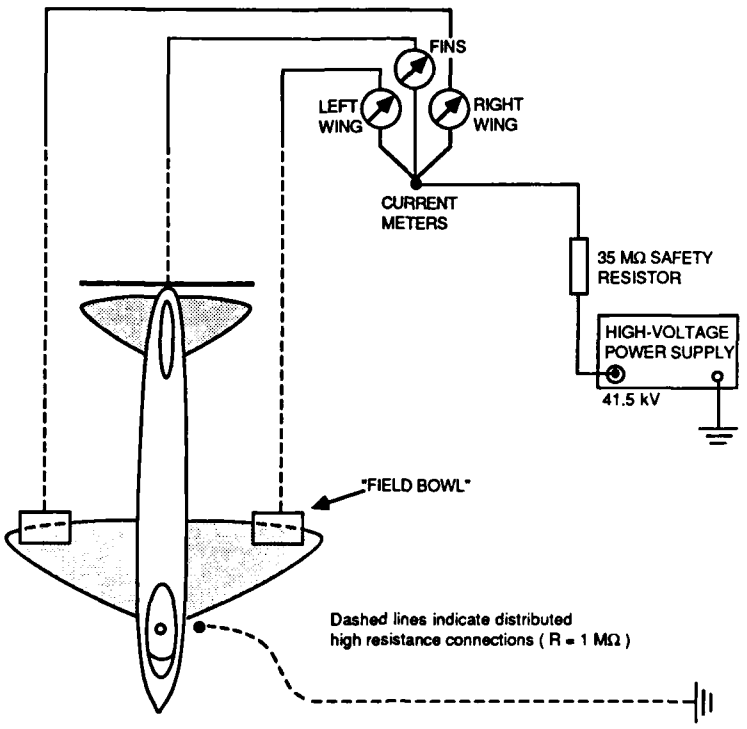

Fig. 13. Schematic of test setup for studying corona discharge noise effects.

6.3 Flight tracking

6.3.1 Ambient Charging

In conducting tests to study p-static noise elimination, it is generally necessary to specify the charging levels to which the test vehicle was exposed. This can be accomplished by installing an electrically isolated metal patch on a frontal surface, as suggested in Fig. 14. The installation can be surprisingly primitive and still yield perfectly acceptable results. For example, as shown in the figure, it is possible to simply apply insulating tape to the airfoil leading edge, place a thin metal sheet on top, and hold the sheet in place with tape around the edges. A wire connected to the sensor plate can be fished through an existing nearby screw hole. Tape applied over the wire keeps it from whipping and breaking in flight. Tests yielding valuable insights has been conducted by SRI, using installations no more elegant than the one shown in Fig. 14.

6.3.2 Charging of Dielectric Region

Frequently, it is necessary to determine the charging rate of a dielectric surface on an aircraft without unduly modifying its properties. This can be accomplished by installing a ring around the exterior periphery of the surface, as shown in Fig. 15. A dc ammeter can be used to measure the charging current. If it is of interest to detect the occurrence of discharges on the dielectric, an oscilloscope or other pulse-detection system can be capacitively coupled to the foil ring without affecting its current-measuring characteristics.

6.3.3 Discharge Current

The current being discharged from the airplane is a parameter of great interest. A simple scheme used to measure discharge current in flight is shown in Fig. 16. A decoupled discharger is modified by scraping away a band of high-resistance paint at the attachment end of the discharger to produce an insulating band. A piece of wire is attached to the resistive paint aft of the insulating band. The wire is brought to the interior through a convenient hole in the airfoil. (Generally, it is possible to remove one of a series of screws attaching an end cap or cover plate for the duration of the test and to use the hole to conduct the wire).

6.3.4 Aircraft Potential

Another parameter of great interest is the aircraft potential during periods of charging, since the potential is sensitive to engine charging as well as to frictional charging resulting from particle impact. If the airplane is operating in a field-free environment (typical in high-altitude clouds -- cirrus, etc. -- away from thunderstorm cells), the measurement of the electrostatic field at a single location on the aircraft is sufficient to define the potential. (The relationship between the field and the potential can be established by laboratory modeling measurements of the sort described in reference 20).

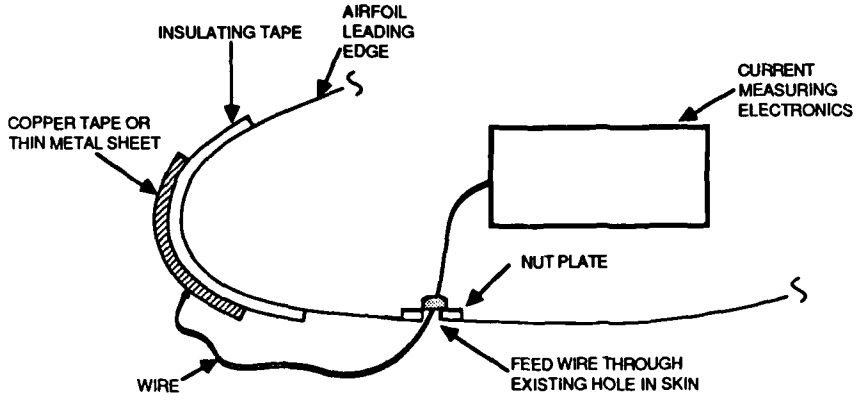

Fig. 14. Scheme for measuring current deposited on an aircraft forward surface.

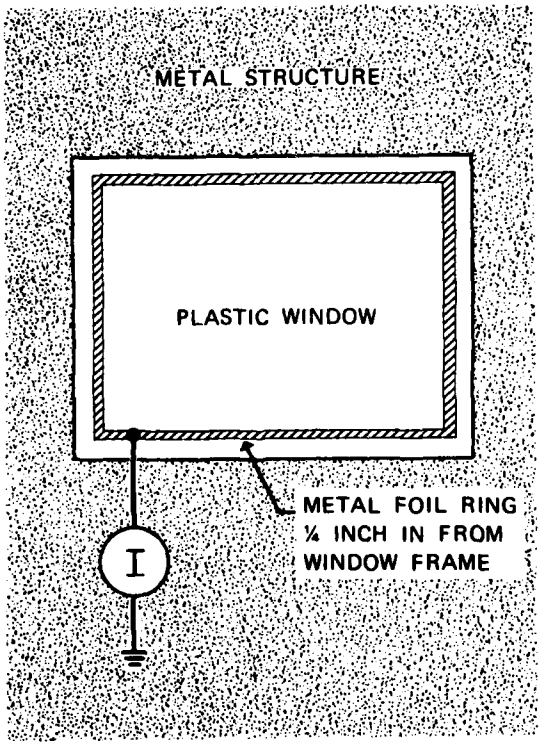

Fig. 15. Technique for measuring charging current to plastic region.

cirrus, etc. -- away from thunderstorm cells), the measurement of the electrostatic field at a single location on the aircraft is sufficient to define the potential. (The relationship between the field and the potential can be established by laboratory modeling measurements of the sort described in reference 20).

Although the field can, in principle, be measured anywhere on the aircraft, modeling is greatly simplified if the field is measured in a region of large radius of curvature, such as the belly of the airplane. This is also practical: to sample the external field, the field sensor has to penetrate to the outside of the skin (i.e., a hole has to be cut in the skin). Generally, on the belly of the aircraft, a nonloadbearing access hatch or cover plate can be found in which the sensor can be mounted without affecting the structural integrity of the aircraft.

The field meters used for this purpose at SRI have been of the rotating vane sensor type. These are extremely rugged and are straightforward to build, install, and calibrate.

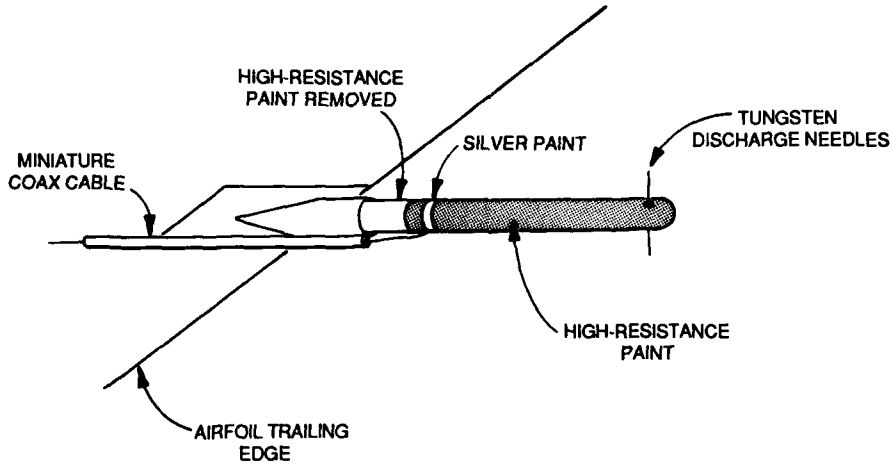

Fig. 16. Modification of existing ortho-decoupled discharger to measure discharge current.

7.0 Conclusions

The processes of aircraft electrification and consequent noise generation are now understood in substantial detail, and effective techniques for interference avoidance and control have been developed. These techniques have been described in this paper, and, if conscientiously applied, should permit satisfactory operation of flight vehicles under conditions of static electrification.

Unfortunately, in practice, small inadvertent deviations from good practice or relatively trivial shortcomings in design detail can often completely negate an otherwise excellent static interference control program. The troubleshooter in these cases is faced with the need to identify the source of the problem and to take steps to correct it. Measurement techniques to help in this regard are available and have been discussed here.

Perhaps the most important ingredient in this area of electromagnetic interference control is the realization that it can be successful. No black magic is involved, the sources of interference have been identified, and practical methods for their control have been developed. However, great care and attention to their application are essential.

REFERENCES

1. Ross Runn et al., "Army-Navy Precipitation Static Project," Proc. IRE, Vol. 34 (1946).

2. Ion I. Inculet, "Processes in Frictional Electrification" Lightning and Static Electricity Conference Papers, 12-15 December 1972, AFAL-TR-72-325, Air Force Avionics Laboratory, Wright-Patterson AFB, OH (1972).

3. R. L. Tanner and J. E. Nanevicz, "Radio Noise Generated on Aircraft Surfaces," Final Report, Contract AF 33(616)-2761, Stanford Research Institute, Menlo Park, CA (1956).

4. R. L. Tanner and J. E. Nanevicz, "Precipitation Charging and Corona-Generated Interference in Aircraft," Tech. Rep. 73, Contract AF 19(604)-3458, Stanford Research Institute, Menlo Park, CA (1961).

5. J. E. Nanevicz and E. F. Vance, "Studies of Supersonic Vehicle Electrification," Lightning and Static Electricity Conference, Air Force Avionics Laboratory, Wright-Patterson AFB, OH (1970).

6. J. E. Nanevicz, "Flight-Test Studies of Static Electrification on a Supersonic Aircraft," 1975 Conference on Lightning and Static Electricity at Culham Laboratory, England, the Royal Aeronautical Society, England (1975).

7. J. E. Nanevicz, "Results of Titan III Flight Electrostatic Experiments," Lightning and Static Electricity Conference Papers, 12-15 December 1972, Las Vegas, NV, AFAL, AFSC, WPAFB, Ohio, Contract AFAL-TR-72-325 (1972).

8. R. L. Tanner and J. E. Nanevicz, "An Analysis of Corona-Generated Interference in Aircraft," Proc. IEEE, Vol. 52 (January 1964).

9. J. E. Nanevicz and R. L. Tanner, Stanford Research Institute, "Some Techniques for the Elimination of Corona Discharge Noise in Aircraft Antennas," Proc. IEEE, Vol. 52 (January 1964).

10. J. E. Nanevicz et al., Stanford Research Institute, "Development and Testing of Techniques for Precipitation Static Interference Reduction," Final Report, Contract AF 33(16)-6561 (1962).

11. J.E. Nanevicz et al., Stanford Research Institute, "Experimental Development of Dynamic Static Discharger System for Large Jet Aircraft," Contract AFAl-TR-67-313, SRI Project 6129 (1967).

12. J. E. Nanevicz and G. R. Hilbers, Stanford Research Institute, "Flight Test Evaluation of an Active Discharger System," Interim Technical Report 1 (Phase II), Contract F33615-68-C-1359, SRI Project 7104 (1970).

13. J. V. N. Granger and J. T. Balljahn, "Aircraft Antennas" Proc. IRE, Vol. 43, No. 5, pp. 533-550 (May 1955).

14. J. E. Nanevicz, Stanford Research Institute, "Investigation of Static Noise Problems on the HS-125 Aircraft," Final Report, Contract P.O. S-16724, SRI Project 674 (1976).

15. J. E. Nanevicz, SRI International, "Advanced Materials and Concepts for the Development of Antistatic Coatings for Aircraft Transparencies," Final Report, Contract F33615-72-C-2113, SRI Project 2393 (1973).

16. J. Taillet, "Aircraft Static Charging Testing" Atmospheric Electricity - Aircraft Interaction, AGARD-LS-100 7 Rue Ancalla, 92200 Nevilly Sur Seine, France.

17. B. R. Whewell et al., "The Application of Charged Aerosol to the Discharge of Static from Aircraft," 1st Int. Conf. on Static Electricity, Vienna, Austria (1970).

18. A. Marks et al., "Charged Aerosol Energy Converter," AIAA Journal, Vol. 2, No. 1, p. 45-51 (1964).

19. J. Taillet et al., "Instrumentation for Testing Aircraft Antistatic Protection," International Aerospace Conference on Lightning and Static Electricity, 23-25 March 1982, Published by Public Relations Section Culham Laboratory, Abingdon Oxon, England (1982).

20. J. E. Nanevicz and E. F. Vance, "Corona Threshold Determination by Three-Stage Physical Modelling of Aircraft" 10th International Aerospace and Ground Conference on Lightning and Static Electricity, Paris, 10-13 June 1985. Published by Les Editions de Physique, Avenue de Hoggar, Zone Industrielle de Courtaboeuf, B.P. 112, 91944 Las Vlis Cedex, France.

Shielding Against EMP Induced Currents and Voltages, EMP Simulation and Testing and EMP Coupling to Cables

Richard J. Sturm

head of electronics, EMP and shock effects branch
in Federal Armed Forces Science Agency for NBC-Protection,
Humboldtstr., POB 1320, 3042 Munster
Fed. Rep. Germany

Summary

The frequency domain transmission line equations for an uniform transmission line are presented on the bases of an equivalent circuit description of the interaction problem of a transmission line with an incident field. Source terms are included in a convenient formulation. The general solutions are presented and interpreted for special cases which are typical for conditions in airborne systems. The resonance behaviour of cables is discussed and compared to frequency independent excitation. Typical forms of excitations are discussed in frequency and in time domain. The excitation conditions interior of an airborne system are discussed briefly. The physical phenomena of shielding are described. The parameters transfer impedance and transfer admittance are introduced and interpreted in terms of electrical and geometrical shield properties. Methods for cable tests are discussed and compared among one another.

Preface

Since the publication of the monograph "Coupling to Shielded Cables" by E.F. Vance /1/ and the report on "EMP Interaction 2 - 1" by K.S.H. Lee (ed.) /2/ coupling to cables has become a classic problem. Although further development in particular on multiconductor cables seems to be desirable, /1/ and /2/ can be considered standards. In this lecture we will closely stick to the notation of Vance /1/. This enables the reader to continue studies without changing the notation.

1. Introduction

With regard to the impact of an EMP-field incident on an airborne system the cables and antennas are prominent collectors of electromagnetic energy. Their prominence is at least to some degree due to the fact that cables usually are connected to inputs (points of entry) of electronic (sub-) systems. So cables guide the transients to the components which are likely to be damaged. It is since worthwhile to study their interaction with EMP like fields or with fields which result from the scattering of the incident field with the outer shell of the object.

From an interaction point of view cables in airborne systems can be considered slim circular cylinders which are mounted closely and in many cases parallel to a metallic surface. (In case that no reference plane is present there is usually an other cable or conductor which can act as return path for the current. However this must then be treated by a different model). In this lecture we shall confine ourselves to cylinders parallel to a metallic surface as return path. Together with the metal surface, cables of cylindrical shape form systems which are well understood, at least for the frequency region we are concerned with ($0 < f < 100$ MHz). Th transmission line model has proved to predict successfully the response to electromagnetic fields with enough accuracy even in extrem cases. The most important limitation is that the wavelength of the highest frequency under consideration should be less than 10 times the height of the cylinder above ground plane. This is almost automatically fulfilled in airborne systems. The model looses its meaning when the cable length is comparable to h. This also is no serious limitation.

2. The model

Fig. 1 represents the geometry of the transmission line model. Together with the conductivity of the cylinder and of the metal plane (and the electrical properties of the medium) the geometric parameters a (radius of the cylinder) and h (height above ground) define the model. In addition to that the resonances of the system are roughly defined by the length of the cables between the terminals and by the impedances Z_1 and Z_2 (fig. 2).

The equivalent transmission line circuit (including internal sources, which will be defined later) is given in fig. 3. It shows an element of the total line, dz in length. The series impedance per unit length is given by $Z = R + j\omega L$, the shunt admittance by $Y = G + j\omega C$. R, L, G and C are the series resistance and inductance and the shunt admittance of the medium and the capacitance per unit length. Besides the fact that a source term is included, this is the classical transmission line formulation. The characteristic impedance is given by

$$Z_0 = \sqrt{(R + j\omega L) / (G + j\omega C)}$$

the propagation constant is

$$\gamma = \sqrt{(R + j\omega L)(G + j\omega C)}$$

For a lossless line Z_0 and γ are reduced to simple expressions:

$$Z_0 = \sqrt{L/C}\,; \gamma = i\omega L C$$

The reflection conditions at the ends of the line (fig. 2) are defined by the reflection factors

$$\rho_1 = \frac{Z_1 - Z_0}{Z_1 + Z_0} \quad \text{and} \quad \rho_2 = \frac{Z_2 - Z_0}{Z_1 + Z_0}$$

It is possible to express Z_0 and γ in terms of geometrical quantities and properties of the medium. For the geometry described in fig. 1 we get

$$Z_0 = \frac{1}{2\pi}\sqrt{\frac{\mu}{\varepsilon}} \cdot \log \frac{2h}{a} \qquad (h >> a)$$

The parameters μ, ε are the permeability and permittivity respectively of the medium between wire and ground plane. For lossless lines we get

$\gamma \approx j\omega/c$ with c velocity of light, $\omega = 2\pi f$; f frequency

3. Excitation by an incident field

It can be shown that die driving source which originates from an incident field can be approximated by a series voltage source as given in fig. 3. The source term per unit length depends only on E_z that is the component of the E field vector which is parallel to the axis of the cylinder. When using this very convenient approximation the other source terms which are not shown here must be taken into account by series voltage sources in the terminations. (we will not make use of that in this lecture but it is obvious that vertical field components will induce currents in the vertical oriented conductors at the terminals of the line).

E_z is the field which would exist at the position of the cylinder if the cylinder were absent.

For harmonically varying signals the following differential equations can be derived from fig. 3.

$$\frac{dV}{dz} = E_z - I \cdot Z$$

$$\frac{dI}{dz} = - V \cdot Y$$

By decoupling I and V the following second order differential equations are obtained

$$(1) \quad \frac{d^2V}{dz^2} - \gamma^2 V = \frac{dE_z}{dz}$$

$$(2) \quad \frac{d^2I}{dz^2} - \gamma^2 I = - YE_z$$

The solution of (1) and (2) is given by

$$(3) \quad I(z) = [K_1 + P(z)]\, e^{-\gamma z} + [K_2 + Q(z)]\, e^{\gamma z}$$

$$(4) \quad V(z) = Z_0 \left([K_1 + P(z)]\, e^{-\gamma z} - [K_2 + Q(z)]\, e^{\gamma z} \right.$$

$$(5) \text{ where } \quad P(z) = \frac{1}{2Z_0} \int_{z_1}^{z} e^{\gamma v} E_z \, dv$$

and

$$(6) \qquad Q(z) = \frac{1}{2Z_0} \int_{z}^{z_2} e^{-\gamma v} E_z \, dv$$

The constants K_1 and K_2 depend on the reflection factors ρ_1 and ρ_2 and on the length $l = z_2 - z_1$

$$(7) \quad K_1 = \rho_1 e^{\gamma z_1} \frac{\rho_2 P(z_2) e^{-\gamma z_2} - Q(z_1) e^{\gamma z_2}}{e^{\gamma (z_2 - z_1)} - \rho_1 \rho_2 e^{-\gamma (z_2 - z_1)}}$$

$$(8)\quad K_2 = \rho_2\, e^{-\gamma z_2} \frac{\rho_1\, Q(z_1)\, e^{\gamma z_1} - P(z_2)\, e^{-\gamma z_1}}{e^{\gamma (z_2 - z_1)} - \rho_1 \rho_2\, e^{-\gamma (z_2 - z_1)}}$$

The resonance frequencies.

Supposing the cylinder in our model is a cable shield which is short circuited at both ends, then $\rho_1 = \rho_2 = -1$. The denomirator of K_1 and K_2 are reduced to $2\, j \sin \beta l$ ($\gamma = \beta = j\omega/c$)

The poles of K_1 and K_2 are at $\omega l/c = n\pi$. (n = 0, 1, 2...) and consequently the resonance frequencies are given by

$$(9)\quad f_{res} = \frac{n \cdot c}{2l}$$

Excitation under special conditions

At frequencies much below the first resonance the expression for the current is reduced to

$$(10)\quad I(z_1) = I(z_2) = \frac{2E_z}{Z_0}\, h$$

independent of frequency.

Since the resonances of cables shorter than 1,5 m are above 100 MHz, they are outside of the frequency spectrum of EMP and no significant excitation of resonances should occur.

Even for longer cables, where the resonance frequencies coinside with areas of higher spectral density of the field, the resonances are not excited under all circumstances. The nulls of the nominator can cancel the poles under certain conditions, eg. for normal incidence of a plane wave. In time domain this means again that the time history of the current equals that of E_z.

Fig. 4 through 6 show a number of time histories of measured bulk currents induced by double exponential fields on shielded cables.

4. The excitation of cables which are part of a cabling system

The fields within an airplane or a missile are usually completely different from the incident EMP-field. When penetrating through an aperture the fields are more or less a replica of those at the outer surface of the structure which is a superposition of the incident and the scattered field. The ratio of the two portions vary from place to place. Nevertheless the scattered field always plays an important role and the ringing of the outer structure strongly affects the excitation of the interior cabling. This means that in general the resonances of the exterior surface will appear in the spectra of the currents induced on interior cables.

Dependent on the coupling conditions (as was pointed out earlier) resonances of the structure can domirate the individual resonances of the cables (see fig. 7).

But this is not the whole truth. The penetrating field excites a great number of modes in the interior, as there are

(.) cavity excitation
(..) currents on individual cables
(...) currents on conducting loops, rods etc.

Most of the modes are strongly coupled and since only little energy is reflected back through the aperture into the exterior space the interior system has time enough to distribute the energy among the subsystems, even to those components which are not directly illuminated by the penetrating field. The eigenstates of such a system depend on a great number of eigenstates of the subsystems. Only occasionally pure single cable resonances are observed. Typical for systems are narrow spaced resonances as shown in fig. 8 and 9.

It can be seen from Eq. (10) that the parameter h plays an important role in coupling. (Roughly speaking the maximum induced current is given by Eq. (10)). To minimize h is therefore a cheap and useful method to decrease coupling.

5. Shielded cables

The circular cylinders which are the basic elements of our model have not yet been specified. In this chapter we assume that the cylinders are the outer surface of a shielded cable no matter what the shield is. We shall limit the discussion on tubular and braided shields.

General considerations and definitions

The shield currents (and voltages) are those described in the preceding sections. In this sections we are interested in the currents and voltages on the interior conductors inside of the shield. The shield current density and the charge density are considered to be the driving source of the interior currents and voltages. If the shield were perfect the internal conductors should not be affected by the external electromagnetic environmert at all. However since the field diffuses through the shield (tube) and since moreover shields can contain apertures the shielding efficiency is limited. Again we describe the influence of the external environment on interior lines by distributed sources along the line. (Fig. 10 and 11)

We assume that the influence of the sheath current density is represented by a series distributed voltage source per unit length

$$E_z(z) = Z_T \cdot I_0(z)$$

The influence of the exterior surface charge density is described in an analogous way by a distributed shunt current source per unit length

$$J(z) = - Y_T \; V_0(z)$$

note: the voltage $V_0(z)$ is directly related to the exterior surface charge density.

We call Z_T the *transfer impedance* and Y_T the *transfer admittance*. Z_T and Y_T describe the shielding property of the cable sheath. It is now straight forward to set up an equivalent curcuit. This was done in fig. 11.

The corresponding differential equations are

$$(11) \quad \frac{dV}{dz} + ZI = E_z(z)$$

$$(12) \quad \frac{dI}{dz} + YV = J(z)$$

The general solution would imply the solution of the external problem and the internal one. Since we are dealing with "good" cable shields we assume that E_z and $J(z)$ are only dependent on the external environment. Moreover for simplicity we want to get the low frequency approximation only. This implies that the wavelength is long in comparison with the cable length l. Consequently the currents and voltages do not strongly depend on z. In this approximation the currents I_1 and I_2 which flow through the termination 1 and 2 (see fig. 10) are given by

$$(13) \quad I_1 \approx I_0 Z_T \frac{1}{Z_1+Z_2} + V_0 Y_T \ell \frac{Z_2}{Z_1+Z_2}$$

$$(14) \quad I_2 \approx I_0 Z_T \ell \frac{1}{Z_1+Z_2} - V_0 Y_T \ell \frac{Z_1}{Z_1+Z_2}$$

The voltages across the terminations are

$$V_1 \approx - I_1 Z_1$$

$$V_2 \approx I_2 Z_2$$

If the cable shields are short circuited at the ends and if the distance to ground plan is small we have a low impedance system. We then expect that even for a strong current I_0 the corresponding voltage V_0 will be small (low frequencies, no cable resonances). Then mainly the first term of (13) and (14) will contribute.

This is no longer true when the cable shield is open ended at one or both terminals. Then Y_T and V_0 grow drastically and the contribution of the second term in (13) and (14) can supersede that of the first term.

6. Interpretation of transfer impedance and transfer admittance

1. Tubular shields

Coupling through a completely closed thin walled shield is possible by diffusion only. The expression for Z_T was derived by Schelkunoff

$$Z_T^{tub} = \frac{1}{2\pi a \sigma T} \frac{(1+j)\, T/\delta}{\sinh (1+j)T/\delta}$$

with

- a radius of the shield
- T wall thickness
- σ conductivity of the shield
- δ skin depth given by $\sqrt{\pi f \mu \sigma}$
- $\mu_0 = 4\pi \cdot 10^{-7}$ Vs/Am
- $\mu = \mu_0 \cdot \mu_r$
- μ_r relative permeability of the shield material

2. Braided shields

Two ways of coupling are important. The external circumferential magnetic field associated with the current on the shield penetrates through the aperture as shown in fig. 12. It changes the magnetic flux in the internal circuit and this results in an induced series voltage (transfer impedance). The electric flux can also penetrate through the aperture. It induces a surface charge on the inner conductor (transfer admittance; see fig. 13). The source of the exterior electric field is the surface charge. (If the external system is described as a transmission line system, the surface charge parameter is usually replaced by the voltage of the exterior system). Since we (hopefully) are dealing with low impedance systems the transfer impedance is of higher practical relevance than the transfer admittance. In fig. 14 the typical characteristic of transfer impedance versus frequency is shown (note that Z_T of a braided shield also includes a term similar to Z_T^{tub}).

7. Cable testing

The aim of cable testing is normally to simulate currents and voltages on lines or on the cable shield which are similar to those which one would expect in case of an EMP. If the test is part of an acceptance test, usually standardized pulse shapes are used. In this lecture we confine ourselves to the principles. The technical solution will be discussed elsewhere. Two ranges of application and three kinds of coupling with quite a number of modifications are in common use.

The method can be applied to inject currents

1. on interior lines or directly to the pins of plugs at the inputs of electronic equipment

   or

2. on the external sheath of shielded cables

The coupling is either

galvanic, or
capacitive, or
inductive
or a combination thereof.

Fig. 15 shows a set up for injection on pins or on interior lines. The current is coupled directly by galvanic or by capacitiv coupling. The network indicated in fig. 15 can have several functions. The dominant functions are pulse shaping and current limitation. The first aspect is self explaining, the second needs some explanation. In many cases it is advisable to limit the current. If a break through occurs behind one or more pins, the input impedance can drop to extremely low values. When using a low impedance generator the input current can go up to unrealistic values which cannot occur under real conditions.

If EMP coupling to a cable is the source of the transient the current is limited by the characteristic impedance of the transmission line system which consists either of the cable and the ground plane or of the interior line and the sheat. This limiting effect can be taken into account by using a current limiting resistor.

Fig. 16 and 17 show the basic experimental arrangements with capacitive and inductive coupling. Capacitive coupling devices predominantly generate a surface charge on the shield (or a voltage). The currents and voltages induced on the exterior system are aproximalety given by Eq. (13) and (14). Note that the currents induced in this case are directed to the coupling device as indicated in fig. 16. The capacitive coupling device acts as a current source.

An inductive coupling device works like a series voltage source. The current vectors are indicated in fig. 17. As is easily seen from fig. 16 and 17 the symmetries of the induced currents are reversed. One of the concequences is that different excitation modes are excited dependent on the coupling mechanisme.

Practical aspects

Direct current injection measurements seem to be very easy at least at the first glance. Nevertheless a lot of things can go wrong and they often do go wrong. For this reason some rules are listed to help the learner to start in the right direction.

rule 1. The most realistic response of a system is achieved when the current is injected on the original cable with the original electronic equipments connected to both terminals, every thing grounded and mounted in the correct way. Nevertheless the coupling device changes the system properties to some degree e.g. high Q resonances are usually damped.

rule 2. In many cases only one (electronic) unit is under test whereas another (auxillary) unit is needed for control purposes or to perform a working program during the test. In this case the original cable is usually replaced by a test set up which includes a decoupling device which decouples the equipment under test from the one which is not under test with respect to the injected transient.

The decoupling unit should have a number of properties.

a. it must assure that the auxillary equipment is not damaged

b. it must allow the signal (or power) to pass without inadequate attenuation.

c. it's input impedance (seen from the side where the injection is done) must not be lower than the input impedance of the component under test. When using a filter or a combination of filters and surge arrestors, or any other unspecified device, make sure that no large capacitance and no spark gap is directly connected to the tested conductor. By such an element, the cable is short circuited at one end and most of the current will flow through this connection to ground.

rule 3. If a special test set up is used, make sure that the high frequency response is adequate. Use a metal plane as reference plane and as return path of the current. The height of the cable above this plane should somehow reflect the real height. This system shows a transmission line behaviour similar to that of a real cable above metallic ground.

rule 4. Make sure that the injected current corresponds to the desired signal. Make current measurements at various points of the cable in particular when working at high frequencies and with fast rising pulses.

rule 5. When doing injection into pins, don't be surprised if the current or the voltage look strange. (in most cases a ringing will be observed) This results in many cases from the complex input impedance at the pins. In this case use in a first step a resistor as the load of the generator. The resistance should be close the characteristic impedance of the transmission line. Check if the current through the resistor is close to the desired signal.

rule 6. Although the interpretation of currents/voltages at pins is difficult, observe at least in critical cases how the peak voltage at the pin changes, when the output voltage of the generator is increased. An almost constant or slowly growing input voltage indicates a nonlinear characteristic or a simple break through. This observation is very important for the interpretation of the test results.

rule 7. Make sure that the working voltage on the lines or at the pins does not damage the generator. Use a capacitor and/or a varistor in case of a.c. power to avoid undesirable interaction with the generator.

This list includes only the general aspects. Special problems require special solution. The possible pitfalls are numerous, it is important to be aware of that.

8. Conclusion

With respect to coupling of electromagnetic fields, cables represent a class of objects. They are well understood as long as isolated individuals are considered. A system of interconnected cables usually shows a collectiv behaviour which is difficult to predict. Cable testing is a powerful tool to examine the EMP response of electronic units. It is more appropriate than the field test when details are of special interest. Its application requires a deep understanding of the system or the systems in which the tested unit is going to be installed.

References

/1/ E.F. Vance
Coupling to Shielded Cables; Wiley and sons, New York 1978

/2/ Lee, K.S.H. (ed)
EMP Interaction; Report AFWL-TR-80-402 (unclassified); Dec 1980

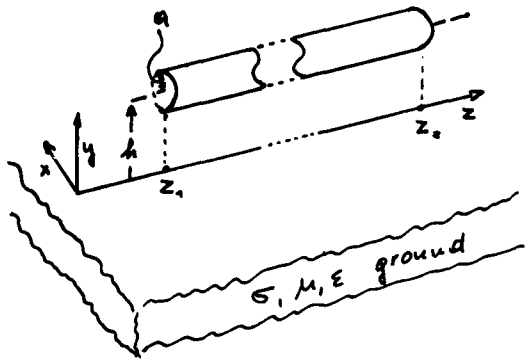

Fig. 1 The transmission line model used in this lecture

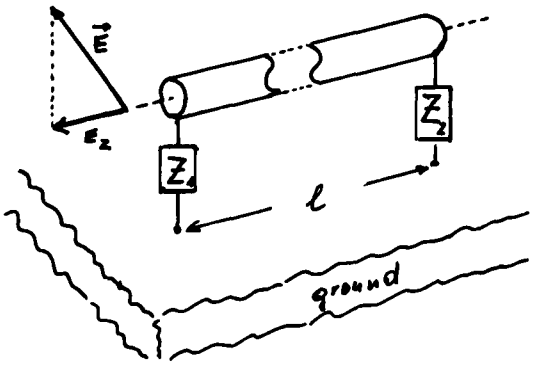

Fig. 2 The parameters which define the resonances and the coupling to a transmission line

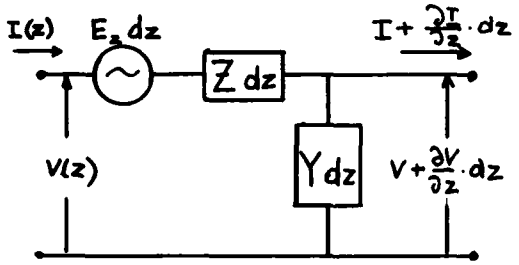

Fig. 3 Equivalent circuit of a transmission line

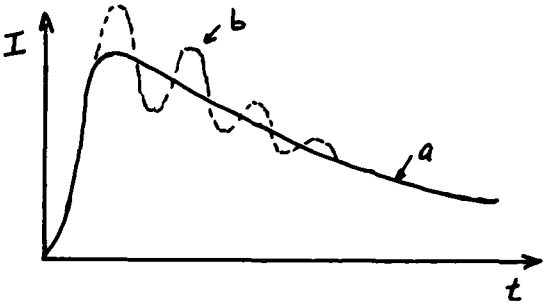

Fig. 4 Typical response of a cable
a. below resonance
b. when first resonance is excited

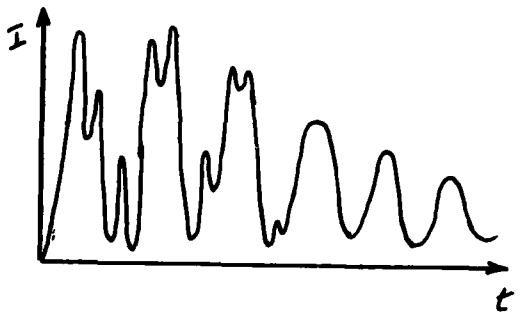

Fig. 5 The most common mode of excitation with strong ringing and some frequency independent portion

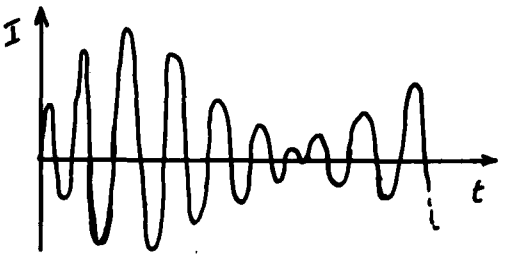

Fig. 6 Excitation which predominantly results from coupling to other cables

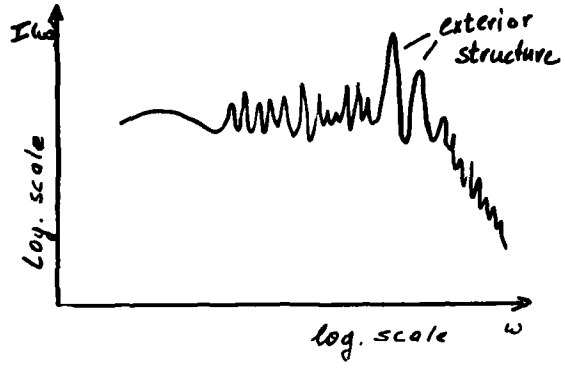

Fig. 7 Typical Fourierspectrum of current if the exterior structure shows a resonance (which in most cases is lower in frequency than the individual resonances of the cables). The resonance of the structure shows up (at the same position) on many cables.

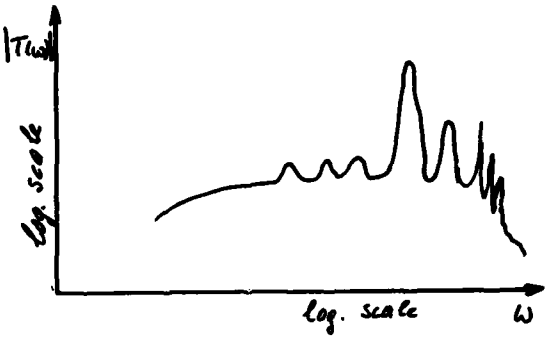

Fig. 8 Typical transfer function of interior cables. The resonances of the exterior structure are dominant in many cases.

Fig. 9 Another typ of frequently observed transfer functions

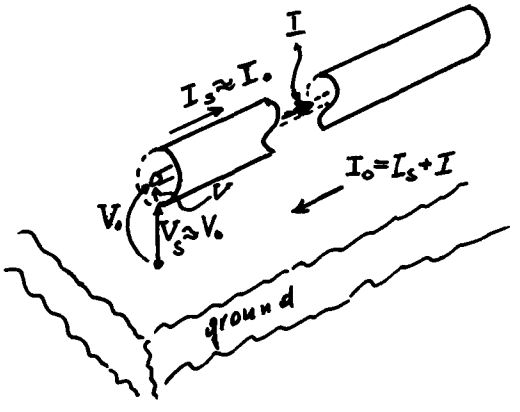

Fig. 10 Voltages and currents on a shielded cable (approximation are valid only for "good" shields)

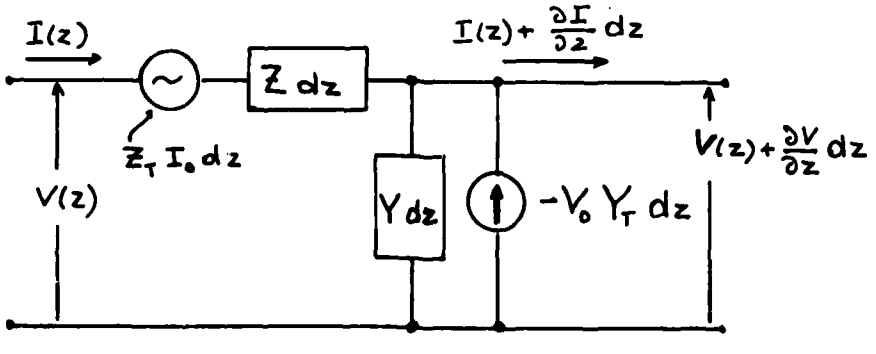

Fig. 11 Equivalent circuit for the internal circuit of a shielded cable

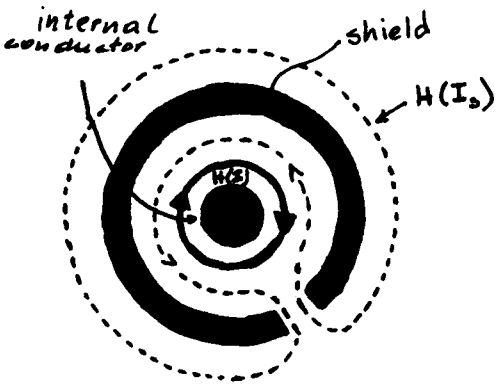

Fig. 12 Magnetic flux penetrating through an aperture

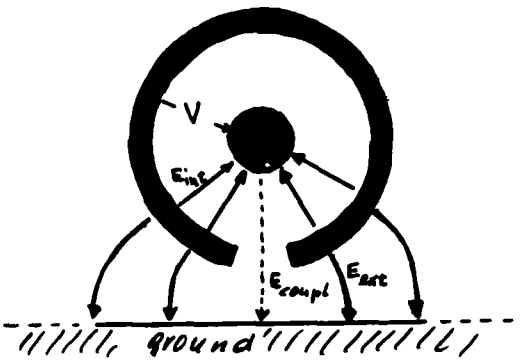

Fig. 13 Electric flux penetrating through an aperture

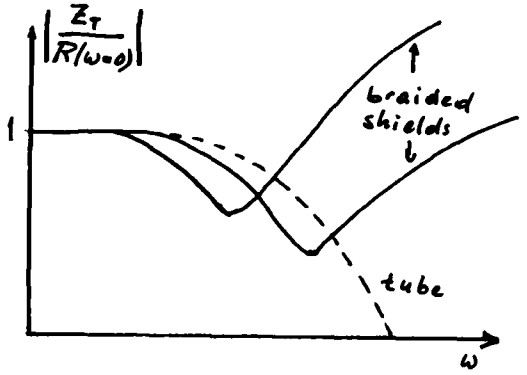

Fig. 14 Typical transfer impedance curve of a braided shield versus frequency

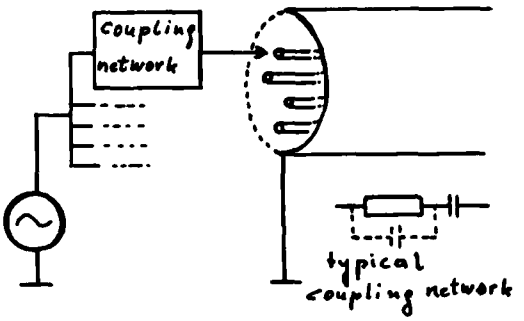

Fig. 15 Current injection on internal lines

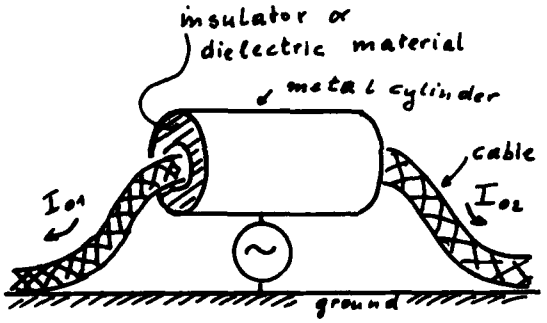

Fig. 16 Capacitive coupling to shielded cables (principle)

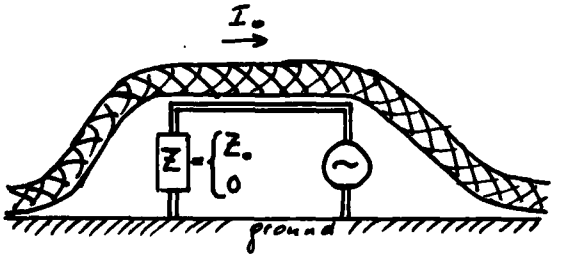

Fig. 17 Inductive coupling to shielded cables (principle)

Balanced EMP-Shielding of C^3-facilities

P.A.A. Sevat
FEL-TNO
P.O. Box 96864
2509 JG THE HAGUE
The Netherlands

Summary

If a large and complex system with sensitive equipment, like a C^3-facility, has to be protected against EMP it can have advantage to shield the system as a whole and not to provide all parts and subsystems separately with shields and limiters.

In this case the shield of the room or building in which the system (equipment with cabling) is installed, has to be designed in relation to the threat, the requirements (to avoid upset, malfunction or damage) and the sensitivity of the system.

In this paper the keys are given to make a choice of the type and thickness of the material needed to construct a tailored and cost-effective EMP-shield.

1. Introduction

Experience has learned that in many cases the equipment itself is sufficiently shielded by its own metal cabinet. The effects upon the equipment are mostly caused by the induced transients on the cables connected to the equipment.

The equipment can be protected against these transients by shielding the cables and providing limiters at the points where the cables are connected to the equipment.

Sometimes the interconnecting cabling can be so complex and extensive, for instance in the case of large computers with auxiliary equipment, that shielding of all conductors or installing limiters on the multi-wire in- and outputs of the subsystems is expensive, unpractical and probably even impossible. In such cases shielding of the room or building can be the best way of protecting the equipment. This has the advantage that unhardened, off the shelf equipment with its interconnecting cabling can be installed in it and easily replaced by other and later perhaps more sensitive systems. In this case only the cables entering and leaving the shielded room or building have to be provided with limiters.

For the design of a tailored shield, it is necessary to know the effects of the threat (the EMP environment) upon the system installed in a shielded enclosure. These effects have to be calculated. In general an accurate calculation of all the combined effects of EMP upon a complex facility is not possible. However, it will be shown that with a conservative approach and the application of safety-margins a reasonably reliable design of a shielding enclosure can be made.

2. The EMP-environment

It is assumed that the incident field is a plane wave. Reflections to the ground or other conducting surfaces in the neighbourhood are not taken into account.

The time dependence of the EMP of an exo-atmospheric burst can be formulated, e.g. for the magnetic component, by a double exponential expression

$$H_o(t) = H_c(e^{-\alpha t} - e^{-\beta t}) \qquad (1)$$

For more complicated wave shapes, like those of the endo-atmospheric EMP, more exponentials are needed. The spectrum of Eq (1) is

$$H_o(\omega) = H_c \left(\frac{1}{\alpha + j\omega} - \frac{1}{\beta + j\omega} \right) \qquad (2)$$

3. Some characteristics of a shield

In this paper only solid shell shields are considered. The calculation of the type and thickness of the shielding material is based upon the assumption that the shield is a continuous, conducting shell. The effects of interruptions in the flat walls caused by doors, ventilation openings, etc. and by cable penetrations cannot be decreased by applying better or thicker shielding material than designed for the solid shell.
The imperfections themselves must be properly treated.

The attenuation of a shield is frequency dependent.
At the higher frequencies, e.g. $f > 1$ MHz, the attenuation of a solid shell is very high. The contribution of these frequencies to the total field inside the enclosure is very low.

The dimensions of the enclosures are mostly small compared to the wavelength of the lower frequencies. Therefore the incident field can be considered as a quasi-static field and the electric and magnetic component of the field can be considered separately.

The attenuation of magnetic fields at low frequencies is very poor. Electric fields on the contrary are very much attenuated [1], [2].
Because the electric component of the field is much more attenuated than the magnetic component the attention will be focused on the magnetic field H.

A magnetic field couples very efficiently with loops. The induced voltage in loops is related to the first derivitive of this field.

$$U_1(t) = \mu A \frac{dH(t)}{dt} \qquad (3)$$

$\mu = \mu_o \mu_r$

A = area of the loop

For the calculation of the effects the field $H_i(t)$ inside the enclosure must be known.

4. The inside field $H_i(t)$

For the calculation of the inside field $H_i(t)$ the transfer functions derived by Kaden for quasi-static fields can be used [3].

$$T_H(\omega) = \frac{H_i(\omega)}{H_o(\omega)} \qquad (4)$$

For $H_o(\omega)$ Eq. (2) can be used.
The transfer functions $T_H(\omega)$ for three basic shapes are given in table 1.
By inverse fourier transformation $H_i(t)$ can be calculated [2], [3].

The shielding enclosure can roughly be approximated by one of three basic shapes, see table 1. A large room with a relatively small height can be replaced by two parallel plates, a long enclosure with a square cross-section by a cylindrical shell and a cubical enclosure by a spherical shell.

The time dependence of $H_i(t)$ can also be formulated by a double exponential expression. Compared to Eq. (1) the factor H_c is lower and the time constants α and β are usually a few orders of magnitude smaller. This means that the rise and fall time of $H_i(t)$ are much larger than those of the outside field $H_o(t)$.
The lower ΔH_o together with a larger Δt in Eq. (3) result in a double effect upon the induced voltages in loops. Shielding of the EMP is a very effective measure.

With $H_i(t)$ the effects upon the system can be calculated. It gives a direct relation between the threat and the effects upon the equipment.
Moreover the concept of safety margins can be used.

5. The effects of $H_i(t)$

As discussed earlier the cables of the system act as antennae and form loops.
The ratio of the induced peak voltage in a loop without and with shielding can be expressed in decibels.

$$S_{EMP} = 20 \log \frac{U_o}{U_i} \text{ dB} \qquad (5)$$

With this definition the shielding effect for EMP can be expressed in only one single figure [4].

In practice the rise time of $H_i(t)$, defined as the time between 10% and 90% of $H_{i,pk}$ is $t_r > 1$ µs. Therefore Eq. (3) can be used for large loops.

In fig. 1 the peak voltage per square metre in a loop in the centre of a sphere with radius r = 1m is plotted versus the thickness of four different types of shielding material [4].
In the calculations the EMP of the exo-atmospheric burst of STANAG 4145 is used for $H_o(t)$. With the transfer functions $T_H(\omega)$ of table 1 and inverse fourier transformation $H_i(t)$ is calculated. $U_{1,pk}$ is derived from Eq. (3).

In ref. [2] and [4] it is shown that if the parameter C >3 the $U_{1,pk}$ is inversely proportional to the radius r.

$$C = \frac{r}{3\mu_r d} \qquad \text{for spheres} \qquad (6)$$

$$C = \frac{r}{2\mu_r d} \qquad \text{for two plates and cylinders} \qquad (7)$$

If in Eq. (7) C>3, fig. 1 can also be used for two plates and cylinders. For r see table 1.

The last step is the comparison of the output voltage of the expected loops with the different threshold levels of the equipment.

6. Threshold levels of sensitive equipment

Three different threshold levels can be distinguished, namely for upset, malfunction and damage. For upset and malfunction mostly the peak voltage determines the effect, for damage (burn-out) also the time behaviour of the waveform is important.
Currents entering the shielded room by cable penetrations are left out of consideration here.

If the voltage threshold levels of the equipment are not known and cannot be established the following rough, but conservative rules of thumb can be used.
Upset of sensitive, small signal circuits (e.g. in data processing equipment) can be expected from a few tenths of volts and damage from a few tens of volts (a factor 100 difference).
Because of the transfer attenuation between the cable connectors and the sensitive circuits inside the equipment, the threshold levels at the cable connectors are generally higher than the above mentioned voltage levels.

When damage (burn-out) can be expected it is advisable to calculate the energy at the input of the sensitive component and to compare this value with the corresponding energy threshold level.

Besides the inside field $H_i(t)$ caused by the EMP it should be kept in mind that the equipment with its interconnecting cabling should be capable of tolerating the inside interference level generated by the equipment inside the shielded room.

Some manufacturers of data processing systems (e.g. computers) guarantee that their system with interconnecting cabling is capable of tolerating radio frequency interference levels with a peak field-strenght up to about 10 V/m.
In this case it would not be cost-effective to design a shield with an inside magnetic peak field-strength $H_{i,pk}$ which is smaller than a reasonable safety-margin (say 20 dB) below the corresponding interference peak fieldstrength of 26 mA/m.

7. Procedure for the design of a shield

Briefly summarized the procedure is as follows.
- The first step is to determine which equipment has to fulfil its mission at all events.
- The next step is to localize the critical, sensitive circuits in this equipment.
- Observe the coupling between these circuits and the external connections of the equipment and make an estimation of the concerning threshold levels at the cable connectors.
- Apply a suitable safety margin to these levels.
- Devide by the maximum area of the loops expected in the cabling to the cable connectors.
- Multiply by the distance or radius r of the corresponding basic shape replacing the room or building to be shielded.
- Read from fig. 1 the thickness needed for the material of your choice.

8. Example

In a room with length 10 m, width 10 m and height 5 m Data Processing Equipment (DPE) will be installed. It is critical equipment that has to perform its mission without any interruption.

The threat is the EMP of an exo-atmospheric burst (H_{pk} = 133 A/m, t_r = 5 ns and t_h = 200 ns).

The induced peak voltage per square metre in electrically small loops without shielding the room is

$$U_{1,pk} \approx \mu \frac{0.8\, H_{o,pk}}{t_r} = 27 \text{ kV/m}^2$$

The logic levels inside the DPE are in the order of a few volts. It is obvious that the equipment must be protected against EMP.

The next step is to replace the room for instance by a sphere with corresponding volume.

$$V = 10 \times 10 \times 5 \text{ m}^3 = \frac{4\pi r^3}{3}$$

The radius r of the sphere is 4.92 m.

Assume the threshold levels for upset the DPE are 0.1 V. Apply a safety margin of 20 dB. If no attenuation exists in the transmission between the cable connectors and the critical sensitive circuits inside the equipment, the maximum allowable peak voltage at the cable connectors is 0.01 V.

The maximum possible area of a loop in the room is 10 x 10 = 100 m^2. Of course loops in the cabling should be avoided or the area should be kept to a minimum. Correction for the larger area of the loop gives a value of 10^{-4} V/m^2.

Multiplying by r for correction of the larger radius of the enclosure results in a maximum allowable value of about 5 x 10^{-4} V/m^2.

From fig. 1 it can be read that the necessary thickness of steel is about 0.4 mm, copper 0.7 mm and aluminium 1 mm.

This is a rather conservative approach, because it is assumed that the output voltage of the loop is the same as the induced voltage (high impedance termination by the DPE).

Calculate parameter C of the sphere. Steel has the lowest value.

$$C = \frac{r}{3\mu_r d} = \frac{4.92}{3 \times 200 \times 0.4 \times 10^{-3}} = 20.5$$

Because C > 3 the extrapolation for the larger radius was correct and the following equations may be used [4].

$$H_{i,pk} \approx \frac{A}{B^2 C} \qquad (8)$$

$$t_r \approx 0.2\, B^2 \qquad (9)$$

in which A = 3.7 x 10^{-5} A/m/Hz and $B^2 = d^2 \mu \sigma$

For steel plate with d = 0.4 mm is B^2 = 9.9 x 10^{-4}

The $H_{i,pk} \approx$ 1.8 mA/m and $t_r \approx$ 200 µs.

With these figures and Eq. (3) the induced peak voltage per square metre inside the steel plated enclosure can be calculated: $U_{1,pk} \approx 9$ µV/m^2.

With the definition given in paragraph 5 and Eq. (5) the EMP shielding effect of the solid shell, steel plated enclosure is 190 dB. This value will be degraded by imperfections in the shield, see next paragraph.

The peak fieldstrength $H_{i,pk}$ = 1.8 mA/m is about 23 dB below the 26 mA/m interference level of paragraph 6, where upset from internal generated interference can be expected. This provides a reasonable safety margin. The protection against EMP is balanced against the upset level caused by internal RFI.

9. Imperfections in the shield

Once the type and thickness of the shielding material has been chosen the attention should be focused on the imperfections in the shield.

During the construction special attention should be paid on a continuous electrical contact between the plates to compose a solid shell [5].

Then the interruptions in the flat walls caused by doors, ventilation openings, etc. should be constructed so that they do not degrade the shielding effect of the solid shell. Imperfections in these constructions cannot be compensated by thicker or better shielding material of the solid shell.

Local degradations of the shield can be discovered by wellknown CW fieldstrength measurements. Measurements in the time domain with EMP-simulators have shown that imperfections in the shield produce large, oscillating transients, both E and H fields, with a short rise time in front of and separated from the normal wave shape of $H_i(t)$ [5].
They are easily overlooked with CW measurements.
These transient fields have important consequences for the induced responses on cables.

To gain maximum profit of the shield, the other techniques for protection, such as grounding, bonding, treatment of cable penetrations, etc. should also be applied.

10. Other factors influencing thickness

In practice it has advantage to use thicker material than needed for EMP protection. Sometimes 3 mm steel plate is used because it can better be welded.
Another reason to use thicker material is to have some spare thickness if corrosion can be expected. To avoid corrosion as much as possible a rather expensive coating is used.

Another method to solve the problem of corrosion is to use a type of stainless steel, e.g. Cor Ten A steel. The lower EMP shielding effect (see striped curve in fig. 1) can be tried to compensate by a larger thickness, e.g. 3 mm.
In this case $U_{1,pk} \approx 3$ mV/m^2.
This material is more expensive than for instance steel 37-2, however a special coating is not needed and as a consequence the coating cannot be damaged by welding.

11. Conclusions

It has been shown that even with simple calculations an assessment of the shielding effect against EMP can be made.

It appears that in many cases sufficient shielding can be obtained with relatively thin material.

In practice it may be that the thickness of the shield is more determined by structural considerations than by EMP considerations.

References

[1] P.A.A. Sevat, "A method for calculating the shielding effect of solid shell enclosures against EMP", 1st EMC Symposium, Montreux, May 1975.

[2] P.A.A. Sevat, "Methods for calculating the shielding effect of solid shell enclosures against EMP", Physics Laboratory TNO, Report IR 1981-27, May 1981.

[3] H. Kaden, "Wirbelströme und Schirmung in der Nachrichtentechnik, 1959, Springer Verlag (book).

[4] EMP Engineering Practices Handbook, NATO File No. 1460-2, Oct. 1977, Appendix E.

[5] P.A.A. Sevat, "Experimental verification of some EMP shielding predictions", Proc. NATO DRG Seminar on EMP Vulnerability of Military Systems, Vol. 2, NR. April 1980.

Shape nr	transfer function $T_H(\omega) = \frac{H_i(\omega)}{H_o(\omega)}$
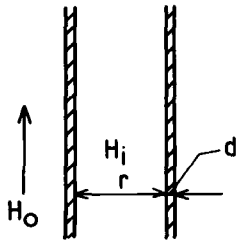 1	$\frac{1}{\cosh \gamma d + \frac{1}{2} k \sinh \gamma d}$
cylinder with axial field H_o	see shape nr. 1
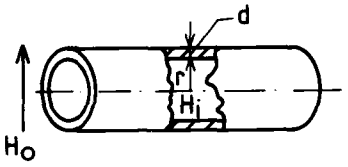 2	$\frac{1}{\cosh \gamma d + \frac{1}{2} (k + \frac{1}{k}) \sinh \gamma d}$
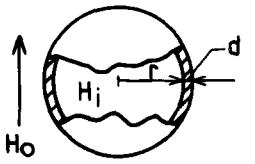 3	$\frac{1}{\cosh \gamma d + \frac{1}{3} (k + \frac{2}{k}) \sinh \gamma d}$

$$\gamma = \sqrt{j\omega\mu\sigma} \qquad k = \frac{\gamma r}{\mu_r}$$

Table 1 The transfer function of two parallel plates, a cylindrical shell and a spherical shell.

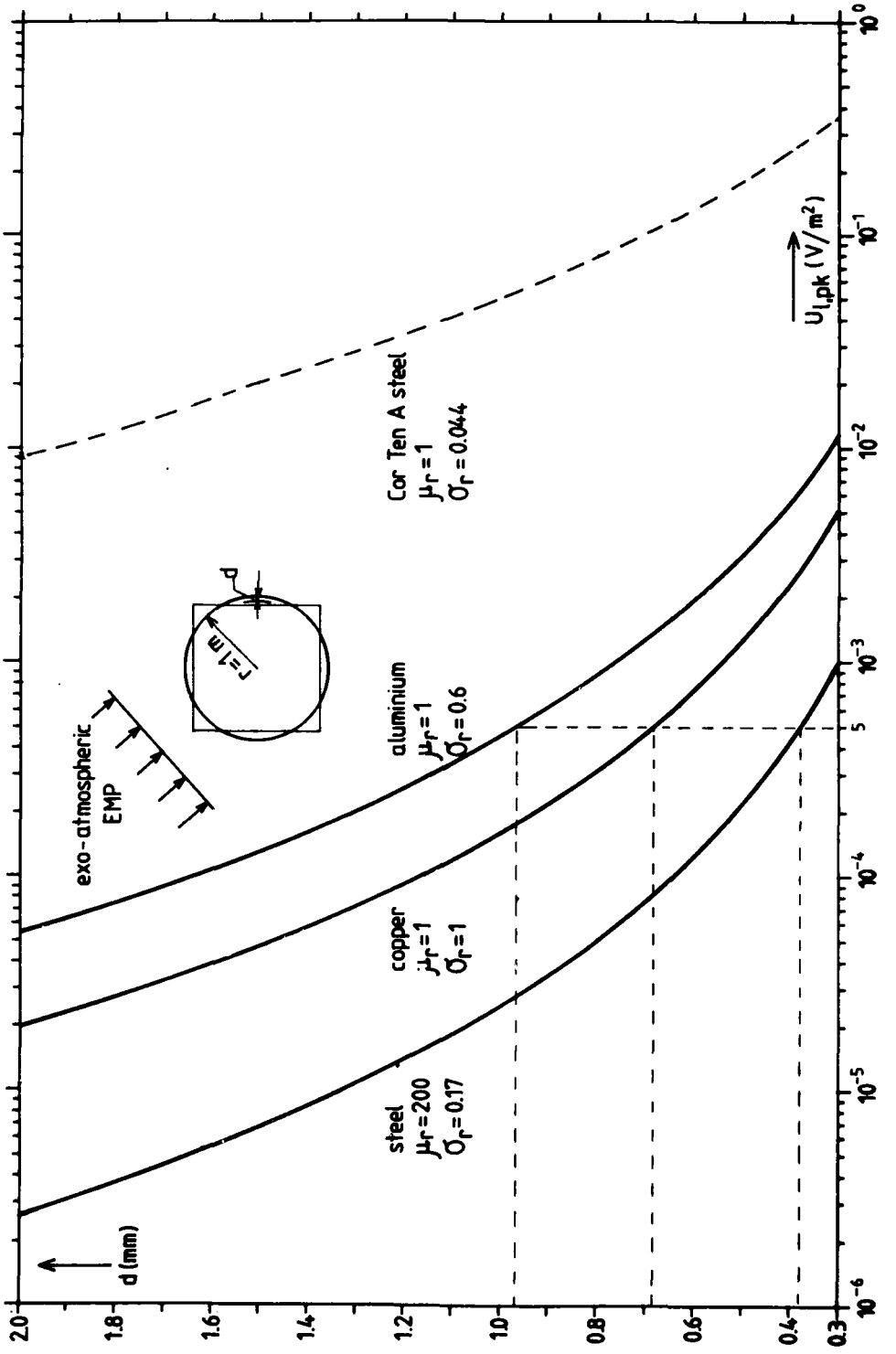

Fig. 1 Induced peak voltage per square metre in a loop in the centre of a sphere with radius r = 1m and wall thickness d = 0.3 to 2 mm.
For C>3 the $U_{i,pk}$ is inversely proportional to r

INDUCING LARGE CURRENTS INTO CABLES

by
P.A.A. Sevat
FEL-TNO
P.O.Box 96864
2509 JG The Hague
The Netherlands

SUMMARY

EMP and Lightning can induce large currents into long cables. For the purpose of testing or verification protection measures, simulation of the induced currents is necessary. Current injection of common mode bulk currents appears to be a very useful method. The most realistic way is indirect coupling, without interrupting the normal operation of the equipment. Two methods of inductive coupling are described.

1. INTRODUCTION

Modern electric and electronic systems are equipped with many vulnerable components, like IC's, micro processors, etc. Even relatively small peak voltages and peak currents can cause upset and damage in these equipment.

The phenomena that cause electrical overstress (EOS) are EMP, Lightning, ESD, Inductive Switching, HERO, etc.

In this paper the attention will be focused on EMP, because of the extensive influence upon large cable systems, while the other phenomena are concentrated in smaller areas, or are localized at equipment level.

The effects of EMP are mainly caused by the cables which act as antennae and deliver the collected energy to the connected equipment. Long cables collect much energy.

Command, Control and Communication (C^3) Systems, Air Trafic Control Centres, Missile Launching Systems, etc., are mostly connected to long cables. These objects are often equipped with critical and vulnerable systems and have to meet specified EMP requirements. For verification of these requirements it is suggested to expose the object to a radiated threat-level EMP environment and to observe the effects in the system [1]. This has the advantage that defects in a shielded enclosure can be discovered and realistic transients in the local cabling can be induced. However, it is not possible to expose the cables connecting the object to the outside world over the whole length, because of the limited area over which the field of an EMP simulator is radiated.

One of the possibilities to overcome this problem is to inject currents onto cables at places where they enter or leave the object under test. These currents should be representative of the transients induced by the EMP. This means that large currents should be induced with the same waveform and in the same way as those of the EMP.

In this paper the advantages and disadvantages of the different types of current injection will be discussed and an example will be given of a method to induce large currents into cables.

2. CURRENT WAVEFORM

The magnitude and shape of the current induced by the EMP into cables is dependent on many factors. The cables can be buried in the ground, laid upon the ground or suspended above the ground. They can be situated close together in a bundle or separated from each other. They can be installed in conduits or not.

The geography of a cable with respect to the incident EMP can be very complicated. Different parts of the cable can have different angles with respect to the direction of incidence. At places of discontinuities in the transmission way the energy is reflected, e.g. at the entry-plate of a shielded building or at sharp bends in the cables.

The induced currents reradiate energy and between cables in a bundle cross-coupling causes complex situations.

Experience has learned that the measured transients upon cables mostly have a waveform of an exponentially damped sinusoid with a rise time considerably larger than that of the EMP. The frequency of the oscillations is related to the different possibilities of resonance of the cable. The damping is dependent on the attenuation of the transmission way, for buried cables the characteristics of the soil.

The peak magnitude of the current is limited to a maximum value. Increasing the length of the cable to more than a certain value, say 100 m, does not increase the peak magnitude of the current very much.

The measured currents are common mode (CM) bulk currents, i.e. the total current of a wire bundle, or the total current of the shield and the inner conductors of a shielded cable. The most realistic way of current injection is inducing (indirect injection) of CM bulk currents into cables or wire bundles.

Representative magnitudes and waveforms of the current to be injected can be determined either through theoretical predictions or extrapolation of low level measurements.

2.1 Analysis

The calculation of the currents expected upon long cables connecting a large and complex system to the outside world is mostly very complicated. The geographic lay-out of the cables can be tried to replace by models. These models are approximations of the real situation. The accuracy of the results are highly dependent on assumptions, the applied simplifications and the parameters supposed, such as the characteristics of the soil in cases of buried cables and the termination at the cable ends.

Also the reflections of the EMP on conducting surfaces in the neighbourhood are influencing the results. Not always all facts are known, such as hidden grounding places of cable shields. Therefore a high accuracy of the calculations cannot be expected.

2.2 Measurements

Measurement of currents induced into long cables by exposing them by a radiated field from a low-level EMP simulator is possible in a limited geographical area. Extrapolation to larger lengths of the cables, to other directions of incidence and polarization and to the time history of a real EMP, introduce again an amount of uncertainties. Extrapolation processes normaly assume a linear relationship between the pulse excitation and the induced response.

It can be concluded that for large and complex electronic systems it is not possible to predict the currents in long cables with sufficient accuracy only be calculations or only by EMP-simulation. Both methods are necessary and have to complete and support each other.

3. CURRENT INJECTION

In stead of exposing long cables to a threat-level simulated EMP it can be tried to simulate the effects of the EMP in the cable. This can be done by current injection.

Current injection can be used for threat-level testing, for example to determine damage thresholds or to carry out a degree of overtest to ensure credibility of protection measures. An overtest of 20 dB for instance has the advantage of removing some of the uncertainty involved in the prediction or scaling process.

Currents can be injected at different levels of the system, e.g. into cables outside the object, at the cable entrance of a building, at a junction box somewhere in the system and at the connectors of the equipment. At the equipment site less energy from the source is needed, however the desired current waveform and magnitude are difficult to predict.

The equipment is mostly connected to more than one cable or conductor, such as cables for the power, signal, remote control, antennae, etc. The incoming currents can have different magnitude, shape, polarity and phase. The combination of all currents ultimately defines the effects in the equipment. It is important to keep this in mind.

As noted previously current injection can be performed at different system levels. The most realistic way is current injection simultaneously into more than one cable at places where the cables are entering the object.

Current injection can be performed in a direct and an indirect way.

3.1 Direct injection

Currents can be injected directly into the pins of a cable connector or junction box. An advantage is that less energy is needed from the injection source than with indirect coupling methods. For instance the current in the inner conductors of a shielded cable have a lower magnitude than the current in the cable shield. Also the rise time is longer, since the high frequencies are more attenuated.

An important disadvantage is the interruption of the normal cable function if the cable must be disconnected to have access to the inner conductors. Without power, upset of the equipment cannot be observed. Parallel injection is sometimes possible, however care should be taken not to influence the performance of the equipment. On the other side the more loosely the source is coupled to the system, the more energy from the source is required.

Pulse shaping and termination conditions (internal impedance of the source) should be representative for the disconnected part of the system. By injecting currents into only one or a few wires of a multi-conductor bundle, cross-coupling effects are neglected.

Another way of direct injection is more promising, namely injection of current into the shield of shielded cables [2]. The return path is limiting the possibilities, e.g. the soil for buried cables. With help of conductors parallel to the cable, transmission lines can be formed. This mehod can only be used for shielded cables. The shield must be accessible somewhere and be grounded at the other side. Sometimes it is possible to use the inner and outer shield of a double shielded cable as transmission line.

3.2 Indirect injection

For indirect injection methods, transformers and capacitance pipes can be used for respectively inductive and capacitive coupling with the cable. One of the main advantages of indirect injection is, that CM bulk currents can be injected into cables, just as they are induced by the EMP and measured during low-level EMP-simulations. Moreover, the system can be leaved in its original configuration without disconnecting the cables and

thus without disturbing the normal operation.

To inject currents a voltage source is needed. Mostly a capacitor is charged to a high voltage and then discharged somewhere, somehow into the cable system. Injection with a simple exponential pulse from a capacitor allows the cabling to act as a pulse forming network and as a transmission path to the system inputs. The geometry of the cable system will shape the waveform. This greatly simplifies the design of the driving pulse source.

With sources of enough energy the quality of the feed-throughs in shields (entry-plate) can be tested up to threat level, also the shielding effect of cables, the action of limiters and protection devices in the vault, the performance of the connected equipment and the grounding of the entry-plate.

For testing equipment or devices connected to shielded cables a large representative current into a considerable length of the cable shield is needed, since the coupling between the shield and inner conductors is dependent on the length of the cable. In cases where the shield current is strongly attenuated during propagation, e.g. with buried cables, the injection should be distributed over a large length of the cable.

3.3 Inductive coupling

A study of the two coupling methods of indirect injection shows that inductive coupling has important advantages over capacitive coupling. A capacitively-coupled system, consisting of a tube placed over the cable, becomes efficient with a coupler capacitance for instance of 100 pF at frequencies above 20 MHz. These frequencies are poorly represented in the spectrum of the cable current induced by the EMP.

At present new core materials for transformers greatly increase the efficiency of inductive coupling. A toroidal core can be split and clamped around the cable without disturbing the system. The cable forms the single-turn secondary of the transformer. This current transformer is by nature a voltage injector. The current is the result of the applied voltage and the impedance offered by the cable under test. Therefore the cable impedance will first be studied.

4. CABLE IMPEDANCE

In Holland nearly all cables are buried in the ground. Only in mobile military communication centres the cables are laid upon the ground. Therefore the attention will be concentrated to buried cables, though the same approximations can be applied to other cable configurations.

The cables are buried at a depth of about 60 cm. As a first approximation the soil around the cable is assumed to be homogeneous. The spectrum of the EMP contains frequencies from very low to more than 100 MHz. A part of the incident field is reflected at the ground and another part is penetrating into the ground. The cable forms a transmission line with its environment. For the early-time part of the cable response (the high frequencies) the cable system can be considered at best as a transmission line.

Two types of cable are of interest, namely cables with and without outer insulation. In the calculations they are replaced by insulated or bare, cylindrical, thin wall conductors. Their behaviour in the ground, driven by a voltage injector, will be discussed both, in the time and in the frequency domain.

4.1 Impedance in the frequency domain

Assume a signal cable (PTT) with 300 wire pairs is buried in the ground. The cable is shielded and covered with a polyethylene jacket. The shield forms a natural coaxial geometry with the soil as return path. The plastic jacket is the dielectric between the

two conductors.

The characteristic impedance of the transmission line formed by the cable and the soil can be approximated with

$$Z_0 \approx \left(\frac{j\omega L + Z_s}{j\omega C}\right)^{1/2} \tag{1}$$

with corresponding propagation factor

$$\gamma = [j\omega C(j\omega L + Z_s)]^{1/2} = \alpha + j\beta \tag{2}$$

$$L = \frac{\mu_0}{2\pi} \ln \frac{r_i}{r_s} \tag{3}$$

$$C = \frac{2\pi\epsilon}{\ln \frac{r_i}{r_s}} \tag{4}$$

$$Z_s \approx \frac{1}{4\sigma\delta^2} + j \frac{1}{\pi\sigma\delta^2} \ln \frac{1.4}{\gamma_0 r_i} \tag{5}$$

r_s is radius shield
r_i is outside radius insulating jacket
ϵ is insulation permittivity
δ is skin depth in the soil
γ_0 is Euler's constant (1.78)
σ is soil conductivity

C and L are respectively the capacitance and inductance per unit length associated with the insulating gap, Z_s is the impedance per unit length of the return path through the soil [2].

In fig. 1 $|Z_0|$ and α are shown versus frequency for a cable with a shield diameter of 5.8 cm, insulation thickness of 5.5 mm, relative permittivity of the insulation ϵ_r = 2.6 and a conductivity of the soil $\sigma = 10^{-2}$ S/m.

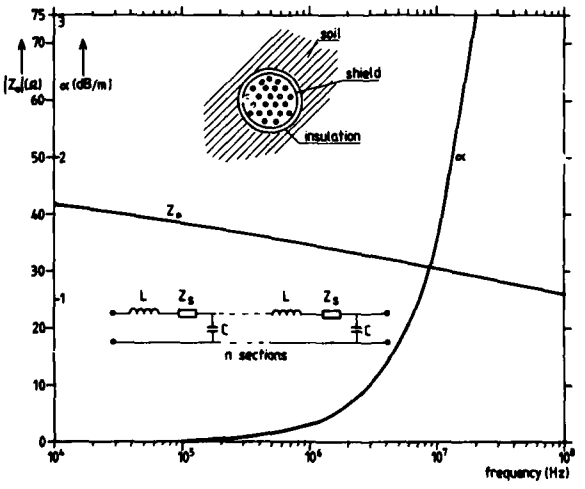

Fig. 1 Cable characteristics for a 58 mm diameter cable in soil

It appears that the impedance $|Z_0|$ is only little dependent on frequency and has a mean value of about 35 Ω. The attenuation at frequencies above 1 MHz is increasing very rapidly. Therefore these frequencies will not propagate very far along the cable since they are dissipated by the soil. As a result the rise time will increase while propagating along the cable (see fig. 10). This limitation is not severe for solid shell shielded cables since these frequencies are not penetrating the shield very well.

4.2 Impedance in the time domain

Assume a power cable is buried in the ground. Consider the cable as a slender biconical transmission line buried in a homogeneous medium. Suppose the cable has a limited length of 160 m and is driven at its centre by a step function voltage injector, see fig. 2. The cable can be devided in 1 m sections and their inductance, capacitance and resistance per unit length can be calculated. With the parameters of these sections an equivalent transmission line can be constructed, see fig. 3.

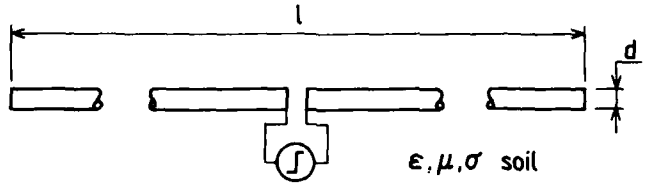

Fig. 2 Biconical transmission line buried in soil

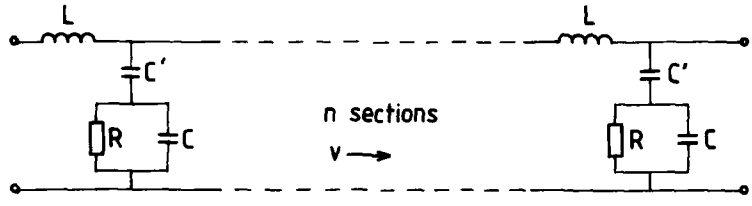

Fig. 3 Equivalent circuit biconical transmission line

Now the impedance of the biconical transmission line, as seen by the driving source, can be calculated. Therefor the sections are approximated by bicones, see fig. 4. At early times the half-cone angle θ_{hc} is larger than at later times, since the length of the concerning bicone is shorter.

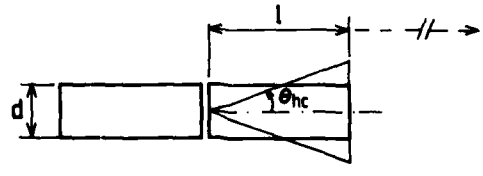

Fig. 4 Approach of a section by a bicone

The characteristic impedance of a bicone is

$$Z_0 = \frac{120}{\sqrt{\varepsilon_r}} \ln \cot. \frac{\theta_{hc}}{2} \tag{6}$$

The wave velocity in the earth medium is

$$v = \frac{1}{(\mu_0 \varepsilon_s)^{1/2}} \tag{7}$$

$\varepsilon_s = \varepsilon_0 . \varepsilon_r$. ε_r is the relative permittivity of the soil. For an $\varepsilon_r = 20$ is the transit time per unit length $\tau_s = 1/v = 15$ ns/m.
The parameters of the sections can be calculated from

$$L = \tau_s Z_0 \tag{8}$$

$$C = \frac{\tau_s}{Z_0} \tag{9}$$

$$R = \frac{\varepsilon_s}{\sigma_s C} \tag{10}$$

σ_s is the conductivity of the soil. C' is the same as C in (4).
The impedance versus time as seen from the driving point into the equivalent transmission line can be calculated [3].

Fig. 5 shows the result for a cable with the same characteristics as in paragraph 4.1. The early-time impedance for a step function excitation is rather large. After 50 ns it is decreased to about 65 Ω and then approaches a late time value of about 38 Ω.

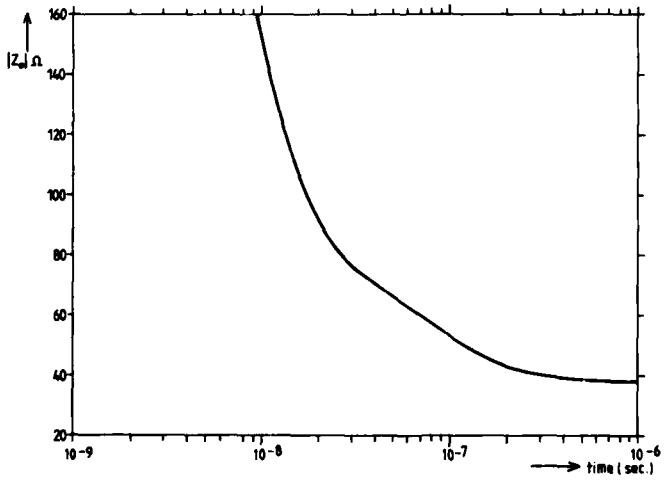

Fig. 5 Impedance versus time of biconical transmission line in fig. 2

The same calculation can be carried out for a cable without insulation. In this case capacitor C' in fig. 3 can be replaced by a short circuit. Since C' >> C, only little difference is noticeable.

Also with the parameters of the method used in paragraph 4.1 an equivalent transmission line can be constructed. In this model all sections have the same parameters (Z_s in series with L, see fig. 1). Fig. 6 shows the results. In theory the impedance

should be half that of the bicone transmission line. For early times (t < 20 ns) this is in agreement with the calculations; for late times they should have to be the same.

It can be concluded that excitation with very short rise times is not very significant.

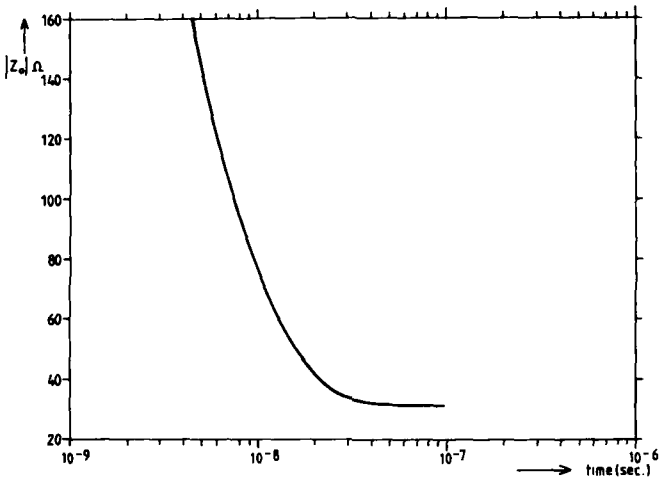

Fig. 6 Impedance versus time of coaxial transmission line in fig. 1

5. TRANSFORMER COUPLED CURRENT DRIVER

5.1 Design

For the design of an inductive coupled current driver the following considerations have been used.

The impedance at the terminals of the voltage injector is dependent on time. For a first approach assume an average value of 50 Ω. In a later analysis the complex values of the impedance are used. For test purposes a peak current of 2 kA is desired. This requires a driving voltage of 100 kV.

As source for general investigations a current with double exponential waveform is chosen. This shape can easily be obtained by a capacitor discharge into a resistor. It has a continuous and flat spectrum without zeros or poles. It is a fair simulation of the pulse shape induced by the EMP into buried cables. Based upon the calculations of paragraph 4.2 a minimum rise time of 30 ns is chosen, corresponding to a bandwidth of 12 MHz. To limit the costs, weight and volume of the transformer an e-fold time of 500 ns is accepted. From $\tau = R.C = 500$ ns and $R = 50$ Ω the capacitor should have a value C = 10 nF.

In fig. 7 an equivalent circuit is given. All parameters are transfered to the secondary of the transformer. L_s and C_s are the stray inductance and stray capacitor

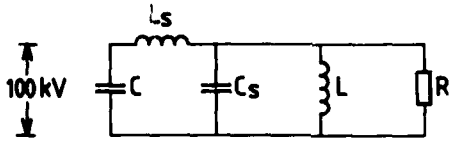

Fig. 7 Equivalent circuit, generator, transformer, load (L_s = 200 nH, C_s = 100 pF)

of the transformer, L the magnetizing inductance. The pulse generator, transformer and load form an RLC circuit. For critical damping L should be

$$L = 4R^2C = 100\ \mu H \tag{11}$$

It can be shown that the voltage-time product of the output voltage U = f(t) across R determines the change of flux in the core of the transformer. Neglecting the rise time

$$\int_0^\infty U_{pk} \exp - t/\tau\ dt = \Delta B \cdot A_c \tag{12}$$

ΔB is the change of induction and A_c is the effective cross sectional area of the core. For U_{pk} = 100 kV and τ = 500 ns the product $\Delta B.A_c = 5x10^{-2}$ Vs.

To limit the core area A_c and thus the associated volume and weight of the transformer, a core material is needed with a large change of induction without saturation. Also a high permeability at high frequencies (12 MHz) is needed. Since a few years new amorphous metallic glass materials are developed that combines a large pulse permeability with high saturation properties and low losses. This material is made in very thin tape and from this, tape wound cores are fabricated.

A suitable choice is Silectron (3% Silicon, balance iron), although some of the low core loss properties is sacrificed for a high flux density and to limit the costs [4]. The thickness of the tape is 0.05 mm, so that hundreds of layers form the core. This material has a saturation inductance of 1.8 T. To further reduce weight and volume the core is dc biased into "negative" induction. With a ΔB = 2T the total effective cross area of the core is 250 cm^2. This area can be subdivided in a number of smaller areas.

The permeability of the material is dependent on frequency and therefore also the magnetizing inductance L, see (11)

$$L \sim \frac{\mu n^2 A_c}{l} \tag{13}$$

n is the turn ratio, l the magnetic path length in the core, μ_r = 2500 at 20 kHz and 0.1 T.
A_c and l determine the core dimensions; l is dictated by the largest cable diameter, here 10 cm.
Also the air gap between the two halves of the core should be taken into account. All this ultimately led to a turn ratio n = 3.
Assuming a stray inductance L_s = 200 nH, it can be concluded that $L >> L_s$, even at 12 MHz, thus the voltage division during the early time, fast rising part of the waveform is small and the output voltage will approach 100 kV/3 = 33.3 kV. To achieve 100 kV output voltage three transformers in series are needed.

The choice of three transformers is also based upon considerations of ease of handling in a field environment (weight and volume) and upon the insulation required to sustain the applied electrical stress.

Each transformer has its own pulse generator. They are powered, triggered and operated from a central control console. The power and trigger units are designed for six transformers. The system is built in transportable containers of standard size (3 m).

The power supply, trigger unit, pulse generators and remote controle are rather conventional and therefore not described here. The design and construction of the transformers on the contrary are very unique and made by Physics International, San Leandro, CA.

5.2 Performance

The following results were measured with three transformers clamped close together around an aluminium cylinder with diameter d = 10 cm. Both sides of the cylinder extended about 10 cm out of the transformers and were terminated in 25 Ω, see fig. 8. The pulse generators were charged to 100 kV.

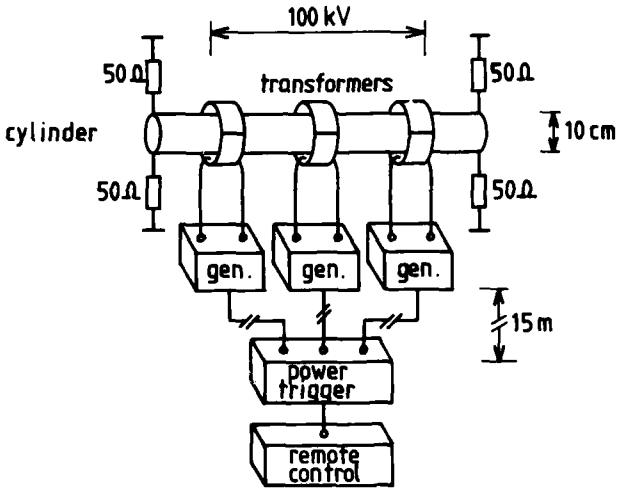

Fig. 8 Schematic diagram, transformer coupled current driver

Fig. 9 shows the current measured in the cylinder. The waveform is approximately double exponential. A small pre-pulse and some oscillation can be observed.
The peak current is about 2 kA, the rise time 30 ns, the e-fold time 500 ns and the first cross-over time 1.2 μs.

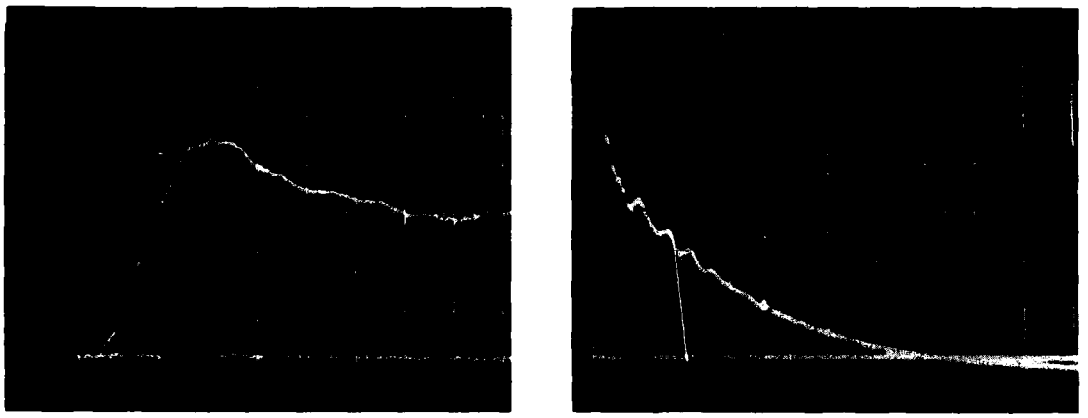

Fig. 9 Current measured in cylinder of fig. 8
(vert. 470 A/div., hor. 20 and 200 ns/div.)

The jitter is less than 5 ns, the pulse repetition rate at 100 kV is about 1 per minute and the output voltage can be adjusted between 10 and 100 kV. The weight is 46 kg per transformer.

The total energy stored in the capacitors is 150 J. The energy dissipated in resistor R = 50 Ω in fig. 7 is about 75 J. The efficiency of the generator-transformer combinations is approximately 50%. By using another core material, e.g. *Supermendur*, this can perhaps be improved.

The previous results were measured with a resistive load R = 50 Ω. As discussed in paragraph 4.1 the impedance of a buried cable has complex values. It is interesting to know the current in the cable of the examples in paragraph 4.1 and 4.2.

As a first approach the step-function voltage of the two models is replaced by a voltage with the same waveform as shown in fig. 9, and a peak value of 100 kV. The internal impedance of the source is neglected.

Fig. 10 shows the current at the injection point and at a distance of 10 m from that point, solid and dotted line respectively, calculated with the method of paragraph 4.1.

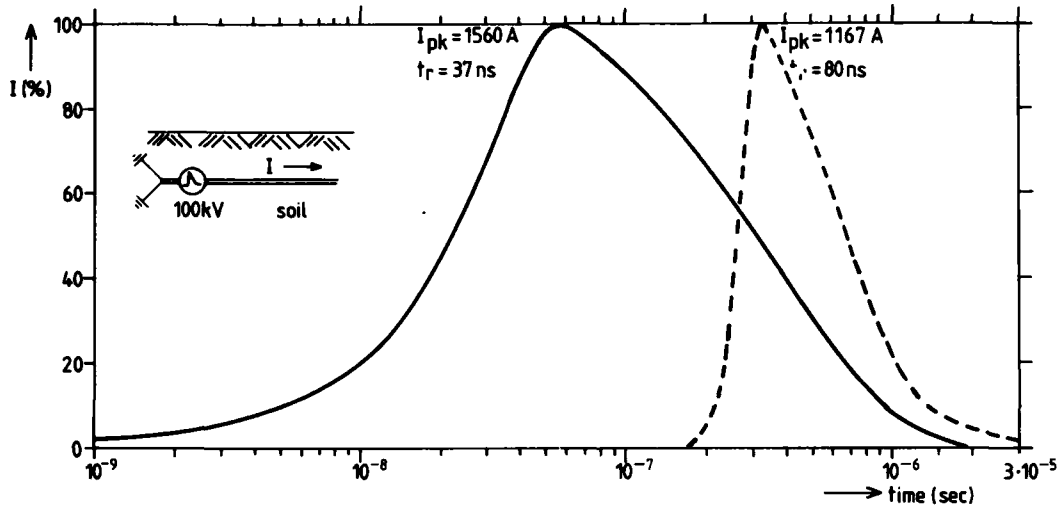

Fig. 10 Cable current in coaxial transmission line, fig. 1. At injection point solid line, 10 m from injection point dotted line.

Fig. 11 shows the same, calculated with the method of paragraph 4.2 (injection voltage 50 kV, current in one direction).

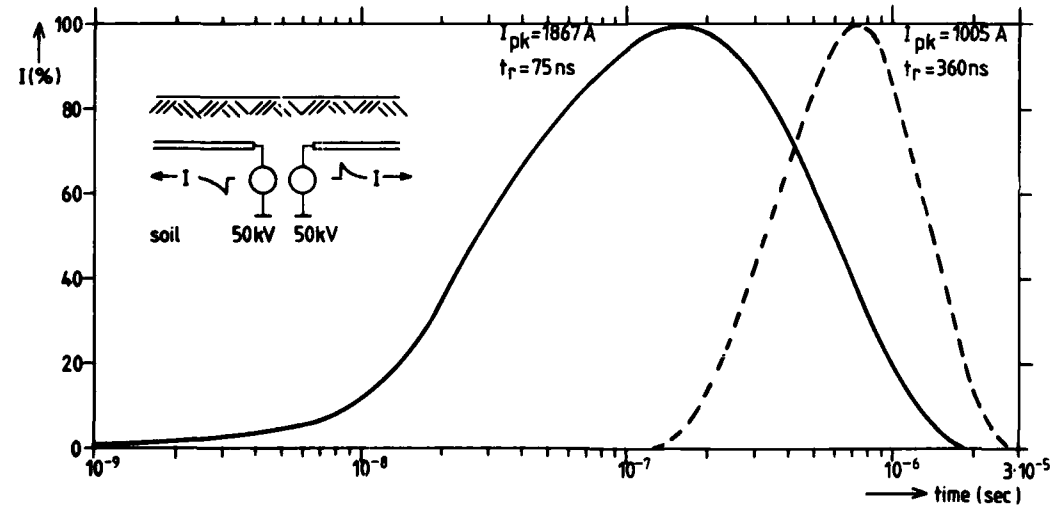

Fig. 11 Cable current in biconical transmission line, fig. 2. At injection point solid line, 10 m from injection point dotted line.

The results of the two methods are not in agreement, perhaps because no ε for the soil is used in the first model. Fig. 11 shows more attenuation at high frequencies. However, in both methods it is obvious that the propagation losses are high and the increase in rise time is considerable during propagation.

5.3 Applications

One to three transformers can be clamped on one cable, close together or separated at a maximum distance of 15 m. The trigger time can be adjusted by the length of the trigger cable.

The three transformers can also simultaneously be clamped on different cables of a system, e.g. power, signal and antenna cable. It is also possible to clamp one transformer on more than one cable. The output voltage of each transformer can be adjusted between 3.33 and 33.3 kV and with three transformers between 10 and 100 kV.

Special safety precautions should be taken in avoiding shock hazards to operating personel. Large voltage gradients will be caused in the ground.

The transformer coupled current driver is a local injector of a high voltage. The induced low voltages by the EMP however, are distributed over the whole length of cable. This can have consequences for buried shielded cables, since the propagation in earth is very poor and the surface transfer impedance Z_T of the cable is defined in Ω/m. To induce more energy into the inner conductors of shielded cables, loop coupled current drivers can be used.

6. LOOP COUPLED CURRENT DRIVER

When it is desirable to couple energy into cables spread over a large length of the cable, large area loops can be used as an inductive coupling method. The loops are laid on the ground over cables buried in the earth. The loops, when energized from the pulse generators will magnetically couple current onto buried cables. For this purpose the 50 J pulse generators are replaced by 500 J pulse generators and the transformers by large area loops, see fig. 12.

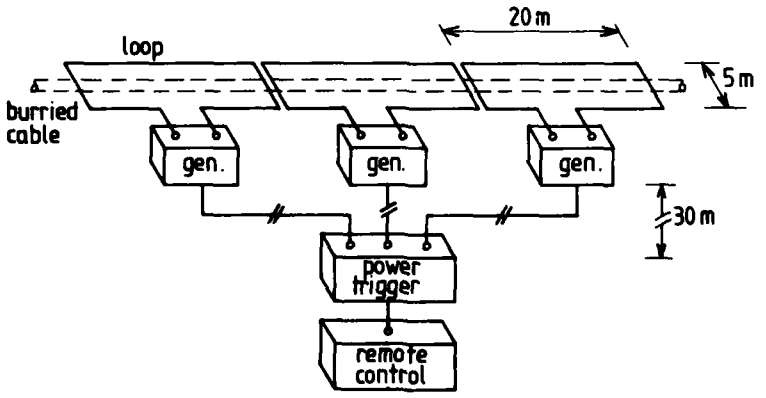

Fig. 12 Schematic diagram, loop coupled current driver

6.1 Design

The capacitor in the three pulse generators has a capacitance of 0.1 μF. The charge voltage can be adjusted from 10 kV to 100 kV. The available energy of each generator is 50 to 500 J.

In the example of fig. 12 the loops have an area A = 100 m^2 and a corresponding inductance L = 60 µH. The capacitors are shunted by a resistor R = 280 Ω. Fig. 13 shows the equivalent RCL circuit of the generator-loop combination. This circuit is underdamped. It produces an exponentially damped oscillatory waveform with frequency f = 65 kHz. The first peak has a value of 4 kA. The damping factor α is 23 x 10^3. The measured values are in good agreement with the calculations, see fig. 14.

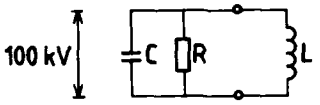

Fig. 13 Equivalent circuit of generator with loop

Fig. 14 Measured loop current in fig. 13 (vert. 1000 A/div., hor. 5 µs/div.)

The burial depth of the cable is about 60 cm. The skin depth in the earth is at 65 kHz respectively 20 or 62 m for a conductivity of the soil σ = 10^{-2} and 10^{-3} S/m. Thus the cable is buried at a depth small compared to skin depth and the magnetic field from the loop is not significantly attenuated.

Of course also other dimensions of the loops with other ringing frequencies are possible. In this case the total length of the coupling mechanism is 3 x 20 = 60 m. The time of triggering can be changed by adjusting the length of the trigger cables. The loops are made from the insulated centre conductor of a special high voltage cable.

6.2 Applications

The three loop/generator combinations can be installed in series and parallel. In parallel the current is induced, in this case, over a length of 20 m with a magnitude √3 larger than in series.

Sometimes an insulated cable buried in the ground is connected to earth by ground rods at each side of the length under consideration. Then the cable forms a loop with the soil as return path. The current distribution in the earth and the inductance and resistance of the return path determine the efficiency of the coupling between the two loops.

In cases where an insulated cable is not connected to earth at certain intervals, energy can be coupled into buried cables by dumping a large current in the soil parallel to the cable between two ground rods, see fig. 15.

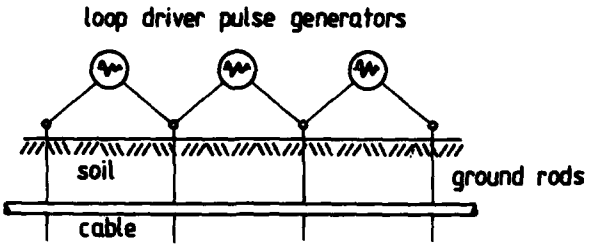

Fig. 15 Dumping large currents in the soil

7. CONCLUSIONS

- The most realistic way of simulating the large currents in long cables induced by the EMP, is indirect injection of common mode bulk currents.

- Indirect injection of currents into cables can be concentrated at a local point or distributed over a large length of cable.

- A transformer coupled current driver can be constructed, consisting of a 100 kV voltage injector with a double exponential waveform. Rise time and e-fold time are 30 ns and 500 ns respectively. This system is based on indirect local injection.

- With additional pulse generators this system can also be used to drive large area loops. The loops are laid on the ground over cables buried in the earth. By magnetically coupling, currents into cables can be induced, distributed over a large length.

8. ACKNOWLEDGEMENT

Ir. C.D. de Haan performed the computer programming. Mr. H. Aslin from Physics International was responsible for the electrical and mechanical design of the transformer- and loop coupled current drivers.

9. LITERATURE

[1] NATO-SHAPE document 2202.2.4/SHORC/P-84, Procedures and methods for the verification and acceptance of common funded EMP protected facilities, installations and equipment, March 1984.

[2] A.L. Whitson, Engineering Techniques for Electromagnetic Pulse Hardness Testing, AD-786722, September 1974, SRI, CA.

[3] H. Aslin, Physics International, San Leandro, CA, Private communication.

[4] TC-101C, Tape Wound Cores, Arnold, Palo Alto, CA.

EMP INTERACTION WITH AIRCRAFT AND MISSILES: A DESCRIPTION OF AVAILABLE COUPLING, PENETRATION, AND PROPAGATION ANALYSIS TOOLS

F.M. Tesche

LuTech, Inc.
3742 Mt. Diablo Blvd.
Lafayette, CA 94549
USA

ABSTRACT

This paper presents a discussion of a number of simple modeling concepts useful for conducting an analysis of the response of airborne systems to a transient electromagnetic field excitation, such as an electromagnetic pulse (EMP). Using electromagnetic topology concepts, the system may be decomposed into separate parts, each of which may be analyzed independently, and the results later combined to permit estimates of the system-level response.

I. INTRODUCTION

Determining the behavior of an airborne system, such as a missile or aircraft, to an external electrical disturbance continues to be a problem of pressing interest. Such excitation routinely occurs in the form of lightning discharges in the vicinity of the system, but could also be in the form of nuclear EMP in the event of a nuclear detonation. The main interest in these cases is that the normal functioning of the airborne system not be degraded by this external electrical stress.

Due to the mechanical and electrical complexity of these systems, it is virtually impossible to determine the system's response analytically. Frequently, system-level tests of the system are required to ascertain if the system is "hard" to the specified environment.

There are instances, however, where calculations play an important role in determining estimates of the system response. During the design phase of the system, preliminary response estimates aid the designers in determining what, if any, electrical protection should be provided in the system. In addition, calculations are frequently useful in interpreting the experimental results. Often it is necessary to extrapolate measurements made in a low-level electromagnetic environment to a higher level which is more representative of the actual "threat" to the system.

In a companion paper [1], a structured approach for treating a complex electrical system has been discussed. This involves defining one or more shielding layers or "barriers" in the system, and then identifying the points where electromagnetic (EM) energy can penetrate into the system. This results in the system topological shielding diagram. In addition, the important propagation paths within the system are identified in the form of an interaction sequence diagram. Using this concept, the EM interaction process can be divided into several different parts: coupling, penetration and propagation.

Studies of the EM coupling phenomenon involve the determination of the induced currents and charges on the surface of any of the barriers or shields in the system. For example, if the system were an aircraft, external EM fields would induce currents and charges on the aircraft surface and a knowledge of the behavior of these quantities is necessary to determine subsequent responses within the system. Because this interaction is occurring in the external regions of the system, it is usually referred to as the "external coupling" problem. For a system having more than one electromagnetic barrier, there can also be an "internal coupling" problem which relates to the determination of the currents and charges on the internal topological shielding surfaces arising from external sources.

The penetration portion of the EM interaction process is the determination of how the induced currents and charges on the outside of a barrier penetrate into the interior. This may occur through conducting or "hard-wire" penetrations, apertures, or by diffusion. Generally, the conducting penetrations provide the largest penetration into the system.

Once the EM energy has penetrated into a barrier, it is able to propagate within the enclosure and arrive at the next topological barrier where the interaction process begins anew. This EM propagation can occur in the form of transmission line propagation, where waves are guided along electrical conductors, or by the EM radiation process.

In each of the areas of coupling, penetration and propagation, there are a number of simple calculational models which can be used to estimate the EM response of a wide variety of systems. These are all discussed in detail in references [2] and [3]. In this paper, those calculational models most applicable to airborne systems are reviewed. Section II discusses several external interaction models useful for estimating the behavior of external currents and charges on missiles or aircraft. Section III treats several penetration models, and the area of propagation is reviewed in Section IV. Finally, Section V presents some concluding remarks.

II. EXTERNAL INTERACTION

As previously mentioned, the first step in conducting an analysis of the response of an aircraft or missile to an external EM excitation is to determine the behavior of the induced currents and charges on the exterior of the system. As noted in figure 1, this is essentially a classical EM scattering problem, in which the incident electromagnetic field, $\bar{E}^{inc}$, induces a body current in such a way that the scattered field produced by this current, $\bar{E}^{sca}$, will satisfy the boundary condition on the body

$$\hat{n} \times (\bar{E}^{inc} + \bar{E}^{sca}) = 0. \tag{1}$$

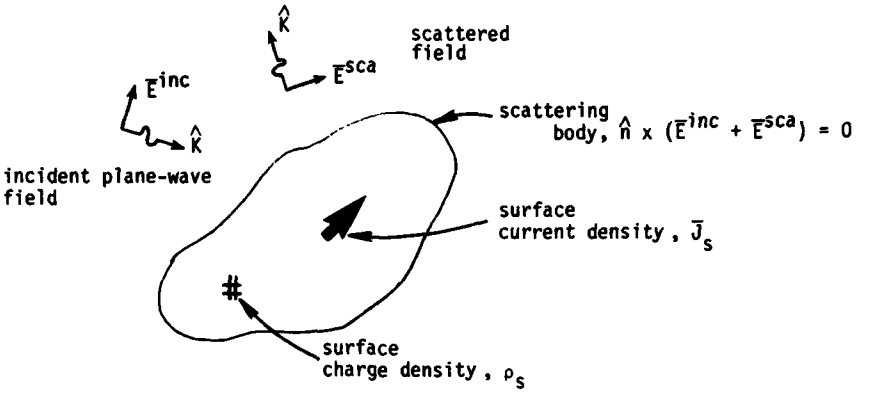

Figure 1. Geometry of external scattering problem.

For a time harmonic incident field having an angular frequency ω, the surface current, density $\bar{J}_s$, may be described by the electric field integral equation of the form (References [4] and [5]):

$$\hat{n} \times \bar{E}^{inc}(\bar{r}) = \frac{1}{2\pi j\omega\epsilon_0} \hat{n} \times \int_s \left\{ -\omega^2 \mu_0 \epsilon_0 \bar{J}_s(\bar{r}')\phi + [\nabla' \cdot \bar{J}_s(\bar{r}')] \nabla'\phi \right\} ds' \tag{2}$$

where both $\bar{r}$ and $\bar{r}'$ lie on the body surface which is denoted by s. The term ϕ is the scalar free space Green's function and is given by

$$\phi = \frac{e^{jk|\bar{r}-\bar{r}'|}}{|\bar{r}-\bar{r}'|} \tag{3}$$

Frequently, the surface charge density is required in the solution of the interaction problem. This is because an aperture or other opening in the surface can be excited not only by the surface current, but by the surface charge. This quantity is related to the surface current through the continuity equation

$$\nabla_s \cdot J_s = -\rho_s/\epsilon_0 \tag{4}$$

Because the current in equation 2 occurs within the integral sign, it is impossible to write an explicit expression for the solution. A common method for obtaining a solution is to use the method of moments, as discussed in reference [6]. This approach involves expanding the unknown current in n suitable basis functions having unknown coefficients. This expansion is inserted in equation 2 and the equation is then multiplied by n suitable testing functions and the results integrated over the body to obtain a set of $n \times n$ linear equations for the unknown current coefficients. In applying this process to equation 2 it must be kept in mind that the unknown current and the incident tangential electric field are two dimensional vectors on defined on the surface of the scatterer. Thus, the numerical scheme used for obtaining the solution must take this fact into account.

Applying the moment method to equation 2 yields a matrix equation for the current of the form

$$[\bar{V}_i] = [\bar{\bar{Z}}_B] [\bar{I}_B] \tag{5}$$

Note that because of the vector nature of the incident field and the body current, the individual elements of the above equation are actually two dimensional. Thus, this equation is a matrix equation of order n involving vectors and a matrix of order 2, and is commonly referred to as a supermatrix equation. In equation 5 $[\bar{V}_i]$ is a two dimensional n-vector which represents the incident tangential electric field on the body, and $[\bar{I}_B]$ is the surface current n-vector. The term $[\bar{\bar{Z}}_B]$ is referred to as the system impedance matrix and is a matrix operator which is dependent only on the body shape, the nature of the basis and testing functions, and the frequency.

The solution for the body current can be effected by a matrix inversion of equation 5, and is expressed as

$$[\bar{I}_B] = [\bar{\bar{Z}}_B]^{-1} [\bar{V}_i]. \tag{6}$$

The inversion of the $[\bar{\bar{z}}_B]$ matrix is usually performed numerically, and once the body current is known, the scattered field also may be computed, if desired. For the EMP problem, however, only the local current and charge are the desired quantities.

One possible solution for the body current defined in equation 2 has been described in a paper by Rao, et. al. [7]. This solution involves the use of the moment method and involves representing the scattering body as a series of connected plates, as shown in figure 2. Details of this numerical solution approach are well documented in their paper, and will not be repeated here.

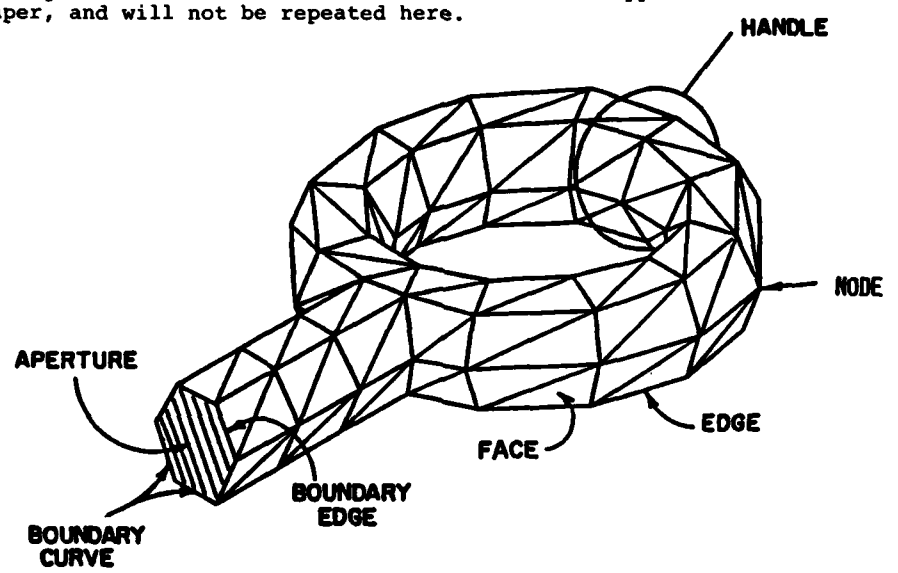

Figure 2. Example of arbitrary scatterer treated by EFIE. (From reference [8].)

Associated with reference [7] is a general purpose computer code, called EFIE, [8]. This is a code which computes the current distribution and scattered fields from an arbitrary, electrically thick body and can be used for computing the EM field induced body currents. This code was originally written for a mainframe computer, but recent investigations using the code as a tool have employed an IBM-PC computer with no difficulties. As an example of calculated current densities on a simple missile-like body using the EFIE code, figure 3 presents contour plots of the z directed and the ϕ directed surface currents on a fat cylinder of length L=10 meters and radius a = 1 meter. This body was illuminated broadside by an incident field having its electric field vector in the direction of the cylinder, and with a frequency of 15 MHz, which corresponds to the cylinder length being a half wavelength. Note that even at this low frequency, the effects of shadowing are apparent in the current.

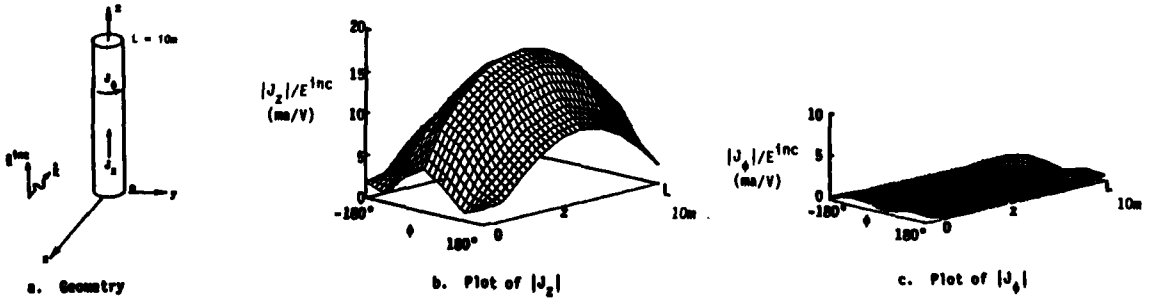

a. Geometry b. Plot of $|J_z|$ c. Plot of $|J_\phi|$

Figure 3. Plot of surface current density magnitude on cylinder of L = 10m for f = 15 MHz.

This approach for solving the external interaction problem is a general one, and results in very accurate solutions. However, the computational requirements of computer time and storage can become excessive for many problems of practical interest. Consequently, there is a need for an approximate solution for the induced body current which can be obtained more simply. This has resulted in the so called "stick model" in which the scattering body is represented by a set of intersecting conductors on which the current flows in only one direction [2]. Figure 4 shows a stick model for an aircraft. Obviously this modeling approach is applicable only for those cases where the scattering body looks roughly like one or more cylindrical elements.

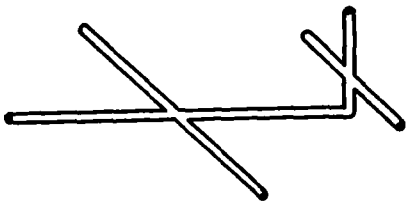

Figure 4. Stick model of an aircraft.

The stick model represents the EM field induced current on each stick in the form

$$I(x) = I_0(x) + C_1 \sinh \gamma x + C_2 \cosh \gamma x \qquad (7)$$

where x is the distance along the stick, $\gamma = j\omega/c$, and C_1 and C_2 are unknown constants which must be evaluated. The quantity I_0 denotes the current induced on an infinite wire by an incident plane wave whose magnetic vector is perpendicular to the wire, and is expressed as

$$I_0(x) = \frac{-4\pi E^{inc}}{\gamma Z_0 \Omega \sin\theta} e^{\gamma x \cos\theta} \qquad (8)$$

in which $\Omega = 2 \ln$ [stick length/stick radius], γ is the propagation vector of the incident field, Z_0 is the characteristic impedance of free space, E^{inc} is the incident electric field strength, and θ is the angle between the propagation vector of the incident field and the negative unit vector along the stick.

For each stick in the model of the scatterer, there is an expression of the form of equation 7 for the stick current. The two unknown constants for each stick must be determined by enforcing the boundary conditions that the current vanish at all free ends of the sticks, and that currents and potentials at all stick junctions be equal. This results in a matrix equation for these unknown constants, and once this is solved, the body current may be easily determined.

One difficulty in this approach is that the effect of radiation loss is not taken into account in the solution. Thus, the natural resonant frequencies of the stick model lie along the $j\omega$ axis in the complex frequency plane and this gives rise to infinite currents at these frequencies. Actually, these natural frequencies lie slightly off the $j\omega$ axis, by an amount which is related to the Q of the scatterer at each resonance. Reference [2] discusses how this Q may be estimated from the stick model solution, and how the resulting expression for the current can be modified to take into account this radiation damping.

As an example of typical results obtained using the stick model, consider figure 5 which shows a comparison of a computed stick model response for current on an aircraft model with experimental stick model measurements, and numerical calculations using a body of revolution integral equation solution technique. As may be seen, the agreement between these data is good.

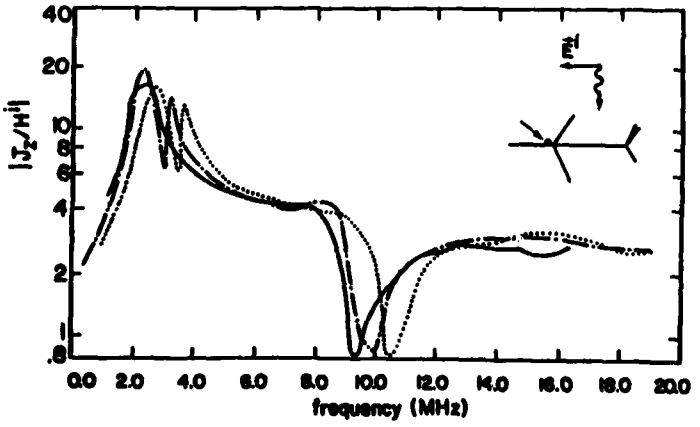

Figure 5. Current density on the topside of fuselage of an aircraft. —— scaled stick model experimental data; —·— stick model numerical data; •••• body of revolution code. (From [2])

Additional techniques exist for the solution of the external coupling problem. Perhaps one of the most popular is the finite difference approach which involves solving the time-dependent, Maxwell equations in differential form by gridding space and time in an appropriate manner, and then time-stepping through the solution. This is a powerful technique, especially for cases involving nonlinearities in the system response, or for

spatially complex systems. Alternate approaches for determining the external response involve the use of high frequency ray optics, eigenfunction expansions, and lumped parameter modeling. In the present paper, however, we will not explore these techniques, due to space limitations.

III. PENETRATION MODELS

Once the current and charge are determined on the surface of the electromagnetic barrier, it is possible to estimate the penetration of the EM energy into the system through the use of various penetration models. As previously noted, these penetrations can occur in the form of conducting wires, apertures, and field diffusion. Several of these models will be discussed in this section.

A. Conducting Penetrations

There are two basic conducting penetration types, as illustrated in figure 6. The first is a simple conductor penetrating the shield, as shown in figure 6a. The conductor could be a power line or other signal line, designed to deliberately carry electrical signals from one point to another in the system. In addition, it could be a non-electrical, but conducting, penetration such as a hydraulic line or a mechanical control cable. This class of penetrations can be further subdivided into conductors which can be directly connected to the barrier (such as the hydraulic lines), and those which cannot (the power or signal lines).

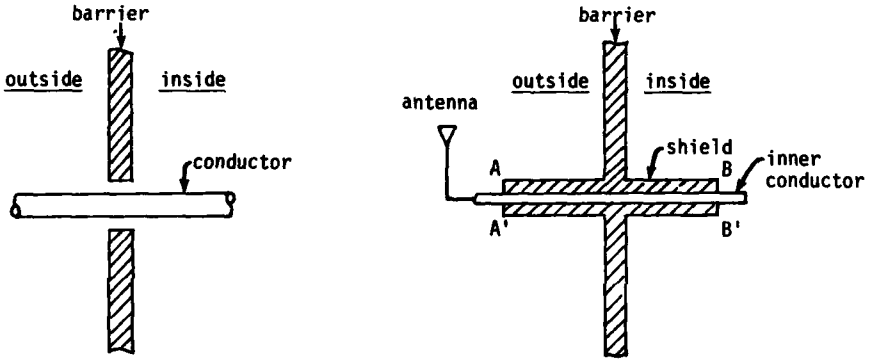

a. Simple conducting penetration b. Shielded conducting penetration

Figure 6. Two generic types of conducting penetrations.

The second type of penetration is a shielded penetration which is shown in figure 6b, and is commonly found in signal cables passing into the system. Note that in this case, the surface of the electromagnetic barrier extends over the inner conductor both in the outside and the inside regions. Generally, the end of the cable denoted as A-A' is connected to an antenna or an electromagnetic transducer, and this creates a signal which propagates down the line and arrives at a point B-B' inside the system. In order to analyze this latter class of penetrations, it is necessary to first have suitable models for determining the antenna response as seen by the line at A-A'. Once that is determined, the appropriate propagation models to be discussed in Section IV can be used to determine the response at B-B'.

1. Antenna Excitation Models

Antennas and antenna-like structures are frequently found on aerospace systems. By virtue of their designed function, "deliberate" antennas are found in the communications subsystems which serve to transmit voice or digital data, or in the navagational subsystem.

There are several different types of antennas for aircraft, and figure 7 illustrates a few of these. By virtue of their design, some antennas are more susceptible to EMP excitation than are others. An antenna may be viewed as a simple matching transformer which transforms the impedance of the final stage of a transmitter or receiver to the impedance of free space, so as to maximize the efficiency of energy transmission.

Because electromagnetic radiation is possible over a wide range of frequencies, as illustrated in Table 1, there are many different designs for antennas. Those antennas designed to operate in the HF band, such as the tail cap antenna or the wing-tip antenna, occur in a band where the EMP signal has a strong spectral content, and have the potential of responding strongly to an EMP. Higher frequency microwave antennas, however, are not as strongly affected by the EMP.

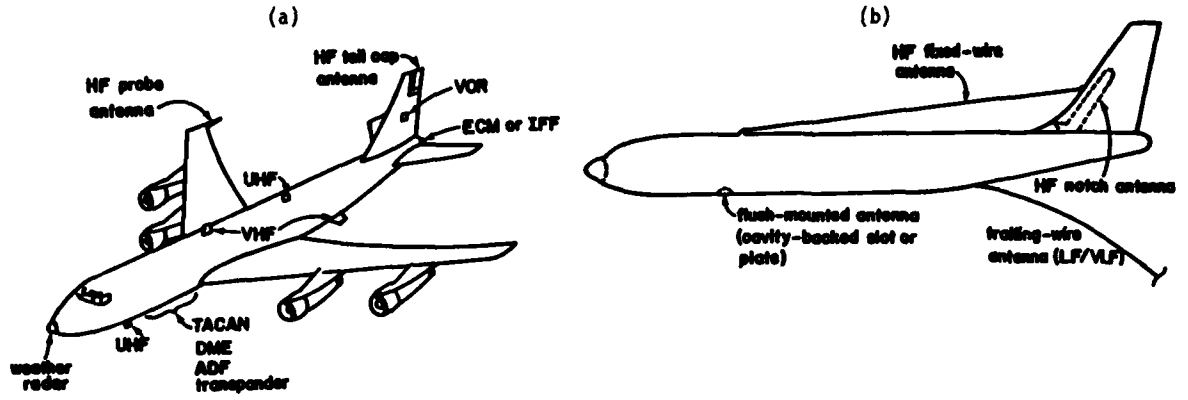

Figure 7. (a) Some antennas on aircraft; (b) wire antennas and flush-mounted antennas.

Table 1

FREQUENCY BANDS

Band Number	Frequency Range	Metric Subdivision		Frequency Nomenclature
4	3- 30 kc	Myriometric waves	VLF	Very-low frequency
5	30- 300 kc	Kilometric waves	LF	Low frequency
6	300- 3,000 kc	Hectometric waves	MF	Medium frequency
7	3,000- 30,000 kc	Decametric waves	HF	High frequency
8	30- 300 mc	Metric waves	VHF	Very-high frequency
9	300- 3,000 mc	Decimetric waves	UHF	Ultra-high frequency
10	3,000- 30,000 mc	Centimetric waves	SHF	Super-high frequency
11	30,000- 300,000 mc	Millimetric waves	EHF	Extremely-high frequency
12	300,000-3,000,000 mc	Decimillimetric waves	---	---

In performing an assessment of a system, all energy gathering antennas should be examined for possible adverse effects. To do this, a simple Thevenin equivalent circuit as shown in figure 8 is developed to represent the open circuit voltage and the antenna input impedance as seen at the terminals of the antenna. These electrical quantities are then used to excite the transmission line to compute the response at point B-B' of Figure 6b.

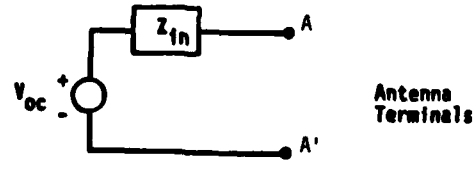

Figure 8. Thevenin equivalent circuit for an antenna at terminals A-A'.

a. Electrically Small Antennas

For monopole type antennas, which are electrically small compared to the wavelengths contained in the EMP signal, it is possible to develop a relatively simple expression for the EMP excitation [2]. Figure 9 shows the geometry for this antenna, which could represent a typical blade antenna on an aircraft. As discussed in [2] the open circuit Thevenin voltage for this class of antennas can be represented through an equivalent electrical height as:

$$V_{oc}(\omega) = h_e E_n(\omega) \qquad (9)$$

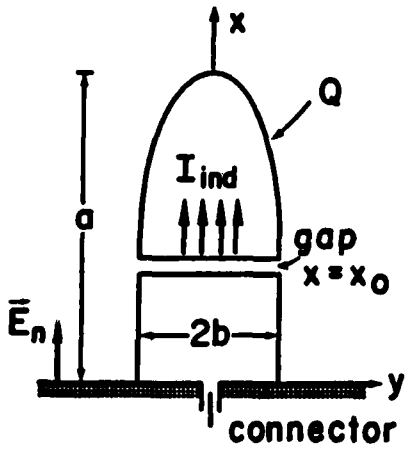

Figure 9. Illustration of a generic monopole antenna.

where E_n is the total electric field normal to the ground plane in the vicinity of the antenna. Note that this is proportional to the surface charge density on the antenna ground plane, and is determined using the external coupling models previously described. The input impedance of this antenna is expressed as:

$$Z_{in}(\omega) \approx \frac{1}{j\omega C_a} \qquad (10)$$

where C_a is the effective capacitance of the antenna, which may be easily calculated or measured. The effective height, h_e, is expressed as:

$$h_e = \frac{\varepsilon_o A_{eq}}{C_a} = \frac{\varepsilon_o}{C_a} \frac{\pi a b m}{(1-m)} \frac{(1-x_o^2/a^2)}{K(m)-E(m)} \qquad (11)$$

where $m = (1 - b^2/a^2)$, and K(m) and E(m) are the complete elliptical integrals.

At times, such simple looking blade antennas can be deceptive, due to complicated internal impedance matching circuitry. For example, figure 10a shows a real UHF communications antenna with the internal structure indicated. Figure 10b presents the equivalent electrical circuit as seen at the antenna terminals. Note that the admittance element Y_a and the current source I_{ind} are directly related to the open circuit voltage and external impedance through a Thevenin to Norton transformation. The resulting input impedance and effective height of this antenna are illustrated in figure 11. Note that in the 0 to 100 MHz frequency range where the EMP spectral content is the greatest, the equivalent height of this antenna is small, indicating that this small antenna is not highly excited by EMP.

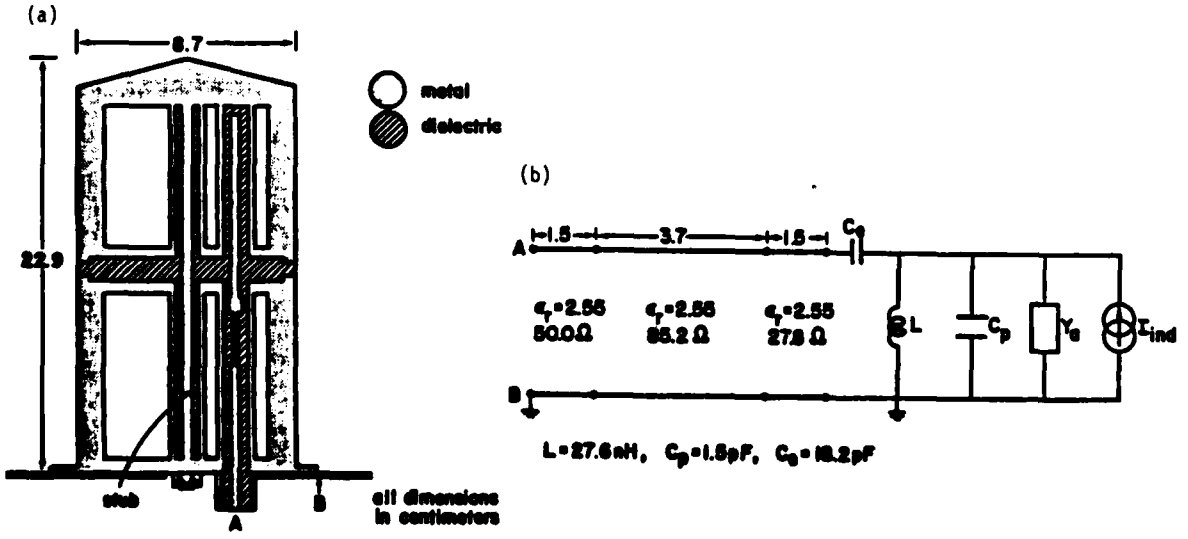

Figure 10. Schematic diagram and equivalent circuit of a UHF Communication Antenna. [2]

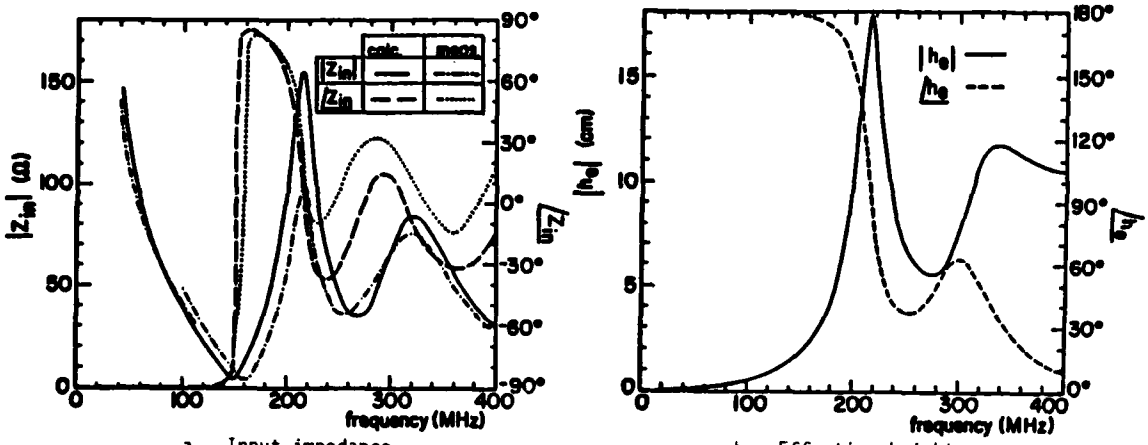

a. Input impedance b. Effective height

Figure 11. Input impedance (a) and effective height (b) of the UHF Communication Antenna of Figure 9.

Due to the diversity of this class of antennas, it difficult to give one simple equation which is valid for all electrically small antennas. However, the concept discussed above of developing an input capacitance and an equivalent height is generally valid for all such antennas. Details of the analysis, however, need to be worked out on a case-by-case basis for the individual antennas found in the airborne system.

b. Resonant Antennas

For antennas whose size is on the order of the wavelengths contained in the EMP portion of the spectrum, a different modeling approach for the EMP response has been developed. This applies to antennas having characteristic linear dimensions on the order of a meter or great as, such as the HF antennas described previously.

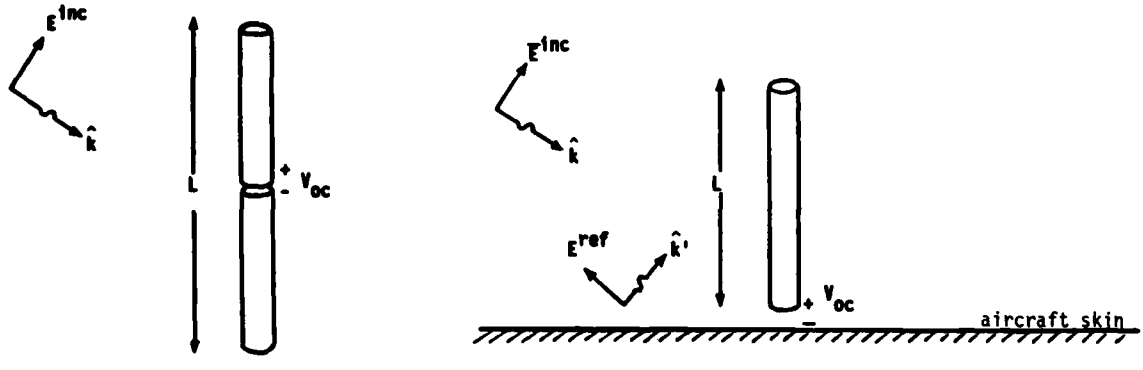

a. Isolated dipole b. Monopole antenna

Figure 12. Simplified models for resonant antennas.

Figure 12 shows two simple models used for estimating the EMP-induced open circuit voltage for a wide variety of practical antennas. Using analysis concepts developed from the Singularity Expansion Method (SEM) [2], [9], simple expressions for the frequency domain short circuit current and input admittance at a point x on the dipole can be written as

$$I_{sc}(s,x) = \sum_{\alpha} \frac{s\beta_{\alpha} n_{\alpha}^{(s)} M_{\alpha}(x)}{s_{\alpha}(s_{\alpha} - s_{\alpha})} \qquad (12)$$

and

$$Y_{in}(s,x) = \sum_{\alpha} \frac{s\beta_{\alpha} n_{\alpha}^{(a)} M_{\alpha}(x)}{s_{\alpha}(s_{\alpha} - s_{\alpha})} \qquad (13)$$

In these expressions, the following terms are defined:

$s = j\omega$ = complex frequency
$\alpha = \pm 1 \rightarrow \pm\infty$ = summation index
$s_{\alpha} = j\omega\pi c/L$ = natural frequencies
$M_{\alpha}(x) = \sin(\alpha\pi x/L)$ = natural modes

$\beta_{\alpha} = \frac{4\pi c}{Z_0 L \Omega}$ = normalization constant (independent of α)

$\Omega = 2\ln(L/a)$ = antenna factor

$\eta_\alpha^{(a)} = V_o \sin(\alpha\pi x/L)$

$$\eta_\alpha^{(s)} = \frac{E_o \sin\theta_i \; cs_\alpha}{j(s^2 \cos^2\theta_i - s_\alpha^2)} \quad 1 - (-1)^\alpha \; e^{\frac{sL}{c}\cos\theta_i}$$

The term $\eta_\alpha^{(s)}$ is referred to as a coupling coefficient for the coupling problem, and $\eta_\alpha^{(a)}$ is the corresponding coupling coefficient for the driven antenna problem, providing the input impedance.

Once these Norton equivalent circuit elements have been defined, the Thevenin equivalent voltage at the antenna's terminals may be defined as:

$$V_{oc}(s) = I_{sc}(s)/Y_{in}(s) \qquad (14)$$

and the input impedance as:

$$Z_{in}(s) = 1/Y_{in}(s) \qquad (15)$$

To illustrate a typical response of an antenna to EMP, consider the case of a center-fed dipole antenna of the type shown in figure 12a having a total length of 10 meters, and a radius of 1 cm. This antenna is assumed to be excited by the canonical EMP waveform described in reference [2] with an angle of incidence of 90 degrees. The application of the above expressions to the calculation of the input admittance and the short circuit current spectrum provide the results shown in figure 13. Note that the input admittance varies with frequency in a manner similar to that of a transmission line. The time domain response for the short circuit current is obtained by taking the inverse Fourier transform of the data in figure 13b, and this is shown in figure 14. Note that the peak current is on the order of 500 amps with a rise time of about 0.03 microseconds. The equivalent Thevenin quantities can be calculated from these Norton equivalent circuit parameters, if desired.

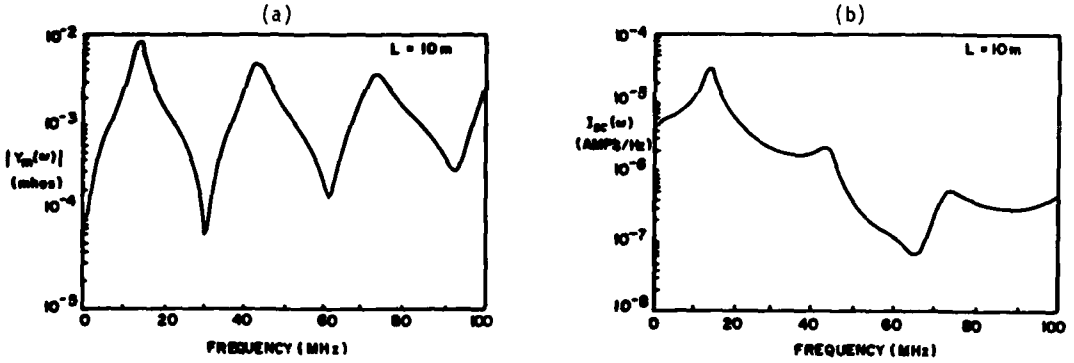

Figure 13. Input admittance (a) and short circuit current spectrum (b) of a center-fed dipole antenna or radius a = .01 m, length L = 10 m, and angle of incidence = 90°.

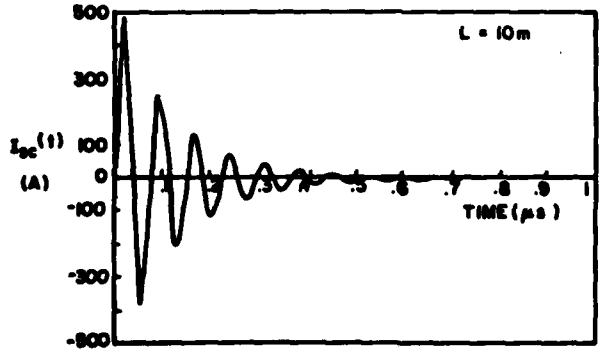

Figure 14. EMP-induced short circuit current at center of dipole antenna.

Note that in the definition of the coupling coefficient $n_\alpha^{(s)}$, the electric field tangential to the antenna is required. If the antenna in question is located far from an aircraft or missile surface, this field is simply the incident field. However, if the antenna is located near the scattering body, it is the total (i.e., the incident plus the body-scattered field) which must be used. This scattered field can be computed using the solution to the body current from equation 2.

c. Microwave Antennas

The final antenna category to be discussed in relation to the EMP response of aircraft and missiles is the microwave antenna. A commonly used antenna feeding mechanism is through the use of a waveguide which transmits energy from the antenna to the receiver or transmitter. Fortunately, from an EMP protection standpoint, this type of system is self-protecting, since the waveguide naturally attenuates all energy at frequencies below a cutoff frequency given by $f_c = c/2a$, where c is the speed of light and a is the largest cross sectional dimension of the waveguide. For a waveguide having a 5cm width, the corresponding cutoff frequency is around 3 GHz, well above the EMP spectrum. Since the attenuation of energy below cutoff occurs exponentially as a function of distance down the guide, EMP excitation of waveguide-fed antennas seldom pose a problem to the system.

2. Ungroundable Conducting Penetrations

Penetrations of this type are shown in figure 6a and encompass power and unshielded signal cables in the system. EM energy in the exterior of the system can induce currents and charges on the line as it penetrates the system, and often the propagation of these quantities can be modeled using a TEM transmission line model as shown in figure 15a. Here, it is assumed that there is a suitable reference ground plane to permit the use of a uniform transmission line. The effect of the line passing through the barrier in an unhardened manner is accounted for by using a lumped capacitance in the line at the point of penetration.

At high frequencies, this capacitance can affect the line response significantly, but not at the lower frequencies. Because it is not possible to simply ground the conductor at the penetration point, it is common to use a line filter at this point whose operating characteristics permit the passage of the desired signals on the line, but shunt off the unwanted EMP signals. One possible filter design is illustrated in figure 15b. Knowing the values of the individual filter components, as well as the wire penetration capacitance allows an estimation of the protection provided by the filter. This latter quantity is a function of the wire and penetration hole diameters and must be determined from a solution of a simple electrostatics problem.

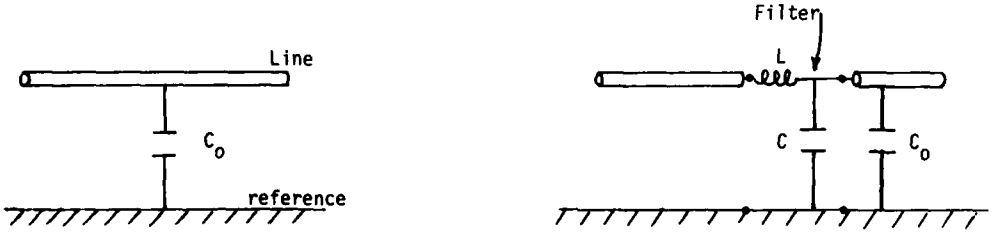

a. Unmodified conducting penetration

b. Protected conducting penetration

Figure 15. Ungroundable conducting penetration (a) and hardened version (b).

3. Groundable Conducting Penetrations

These types of penetrations are much easier to treat, since the line may be shorted directly to the topological barrier on the outside of the system. Generally, such a short is not perfect, and there is small resistance and inductance in the bond. Figure 16 presents an equivalent circuit for this case. Generally, determining the appropriate values for these lumped circuit values is a difficult task, and it is often possible to measure these values in the laboratory.

B. Aperture Penetration Models

A significant amount of past work has been conducted into the determination of the penetration of EMP energy into apertures. Generally, apertures are electrically small compared with the EMP pulse, implying that low frequency models of the aperture penetration are applicable. Reference [2] summarizes many of the aperture modeling techniques which are useful for performing an assessment of a system illuminated by EMP.

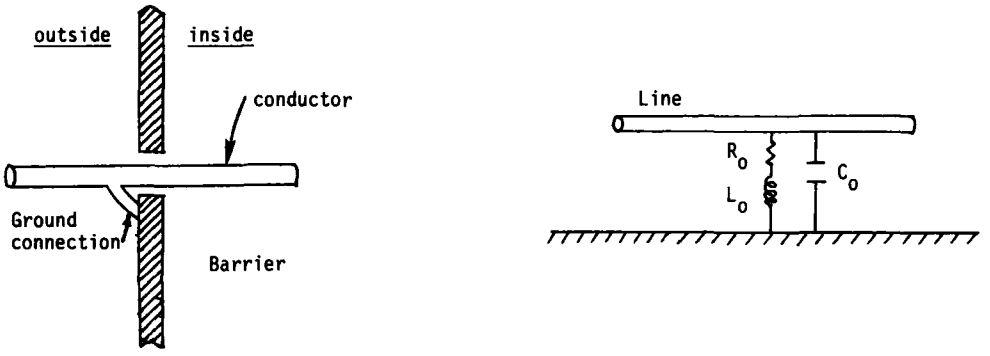

a. Grounded conducting penetration

b. Equivalent circuit

Figure 16. Equivalent circuit for a bonded, penetrating conductor.

Consider a simple aperture in the skin of a shielded enclosure as shown in figure 17. The incident field induces surface currents and charges on the exterior of the system and in the vicinity of an aperture, these distributions are perturbed from that normally occurring on the surface. This perturbation of the surface currents and charges causes magnetic and electric fields to penetrate through the aperture and enter into the shielded region, as illustrated in figure 17a.

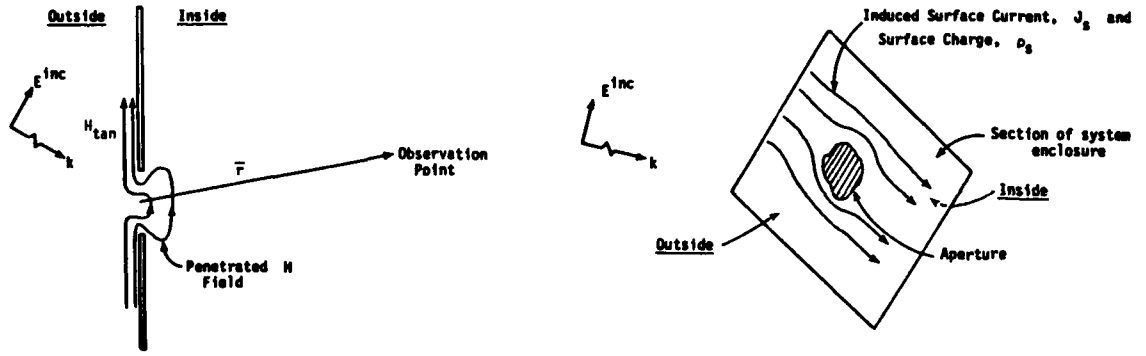

a. Perspective view

b. Cross Sectional view

Figure 17. Aperture located in a conducting plane.

As originally described by Bethe and discussed in [2], the effective penetration of the fields through the aperture can be described through effective dipole moments located at the aperture location, with the aperture short circuited as shown in figure 18. These equivalent electric and magnetic dipoles can in turn be related to the short circuit current and charge which exists over the aperture on the outside region when the aperture is filled in and is illuminated by EMP.

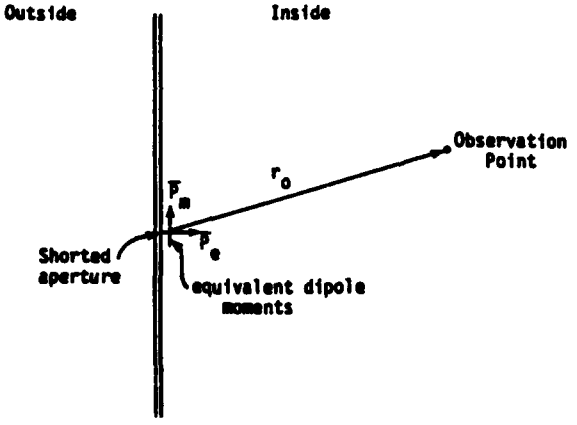

Figure 18. Representation of aperture penetration by equivalent electric and magnetic dipole moments.

In this manner, the electric and magnetic fields at point r inside the shield can be expressed in the frequency domain as

$$\vec{E}^d(\vec{r},s) = -\frac{1}{\varepsilon}\ \nabla \times [\vec{p}_a(s) \times \nabla G(\vec{r},s)] + s\mu\, \vec{m}_a(s) \times \nabla G(\vec{r},s) \qquad (16)$$

and

$$\vec{H}^d(\vec{r},s) = -s\, \vec{p}_a(s) \times \nabla G(\vec{r},s) - \nabla \times [\vec{m}_a(s) \times \nabla G(\vec{r},s)] \qquad (17)$$

where the parameter s is the generalized complex frequency variable and $G(r,s) = e^{-\gamma r}/(4\pi r)$ is the free space scalar Greens function. In the time domain, these expressions become:

$$\vec{E}^d(\vec{r},t) = \frac{1}{4\pi\varepsilon} \nabla \times \left[\frac{1}{r^2} P_a(t)\vec{T}_z \times \vec{T}_r\right] - \frac{\mu}{4\pi}\ \frac{1}{r^2}\, \dot{\vec{m}}_a(t) \times \vec{T}_r \qquad (18)$$

and

$$\vec{H}^d(\vec{r},t) = \frac{1}{4\pi}\frac{1}{r^2}\, \dot{p}_a(t)\vec{T}_z \times \vec{T}_r + \frac{1}{4\pi} \nabla \times \left[\frac{1}{r^2}\, \vec{m}_a(t) \times \vec{T}_r\right] \qquad (19)$$

In the above expressions, the symbols $\bar{p}_a$ and $\bar{m}_a$ represent the equivalent electric and magnetic dipole moments respectiveiy, and are given by the expressions:

$$\bar{p}_a = 2\varepsilon\, \bar{\bar{\alpha}}_e \cdot \bar{E}_{sc} \qquad (20)$$

and

$$\bar{m}_a = -2\, \bar{\bar{\alpha}}_m \cdot \bar{H}_{sc} \qquad (21)$$

where $\bar{E}_{sc}$ is the normal electric field and $\bar{H}_{sc}$ is the tangential magnetic field over the aperture, with the aperture short circuited.

In these last relations, the parameters $\bar{\bar{\alpha}}_e$ and $\bar{\bar{\alpha}}_m$ are referred to as the electrical and magnetic polarizabilities of the aperture, and are functions of only the aperture size and shape and are not dependent on the incident field. Note that the polarizabilities are actually tensor quantities, but with the proper choice of a coordinate system, these quantities may be simplified to have only one component for the $\bar{\bar{\alpha}}_e$ and two components for $\bar{\bar{\alpha}}_m$.

For apertures having very simple shapes, these polarizabilities may be calculated analytically. For more complicated shapes, numerical procedures must be used in order to determine the values. In Reference [2] various polarizabilities are presented. Table 2 presents the analytically derived polarizabilities for elliptical apertures. Figures 19 through 22 present the electrical and magnetic polarizabilities for more complex aperture shapes.

Table 2

APERTURE POLARIZABILITIES [2]

Shape	$\alpha_{e,zz}$	$\alpha_{m,xx}$	$\alpha_{m,yy}$
Circle (d = Diameter)	$\frac{1}{12} d^3$	$\frac{1}{6} d^3$	$\frac{1}{6} d^3$
Ellipse*	$\frac{\pi}{24} \frac{w^2 \ell}{E(m)}$	$\frac{\pi}{24} \frac{\ell^3 m}{K(m) - E(m)}$	$\frac{\pi}{24} \frac{\ell^3 m}{(\ell/w)^2 E(m) - K(m)}$
Narrow Ellipse ($w \gg \ell$)	$\frac{\pi}{24} w^2 \ell$	$\frac{\pi}{24} \frac{\ell^3}{\ln(4\ell/w) - 1}$	$\frac{\pi}{24} w^2 \ell$
Narrow Slit ($w \gg \ell$)	$\frac{\pi}{16} w^2 \ell$	$\frac{\pi}{24} \frac{\ell^3}{\ln(4\ell/w) - 1}$	$\frac{\pi}{16} w^2 \ell$

*Ellipse eccentricity $e = 1 - (w/\ell)^2$.

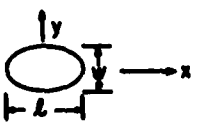

K and E are the complete elliptic integrals of the first and second kind, $m = e^2$.

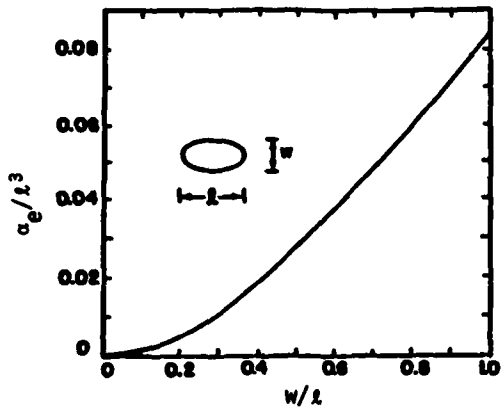

Figure 19. Normalized electric (imaged) polarizability of an elliptical aperture. [2]

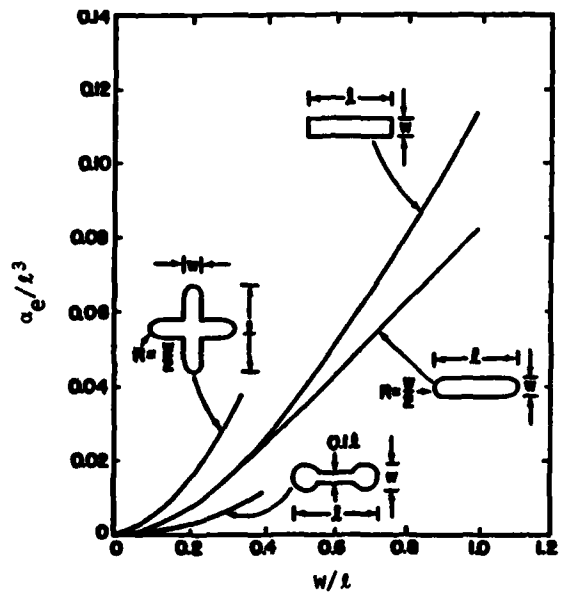

Figure 20. Normalized electric (imaged) polarizabilities for four aperture shapes. [2]

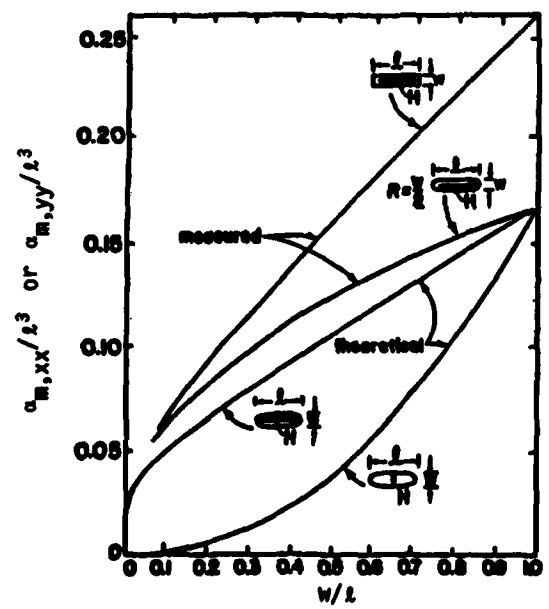

Figure 21. Normalized magnetic (imaged) polarizabilities for elliptical, rectangular, and rounded rectangular apertures. [2]

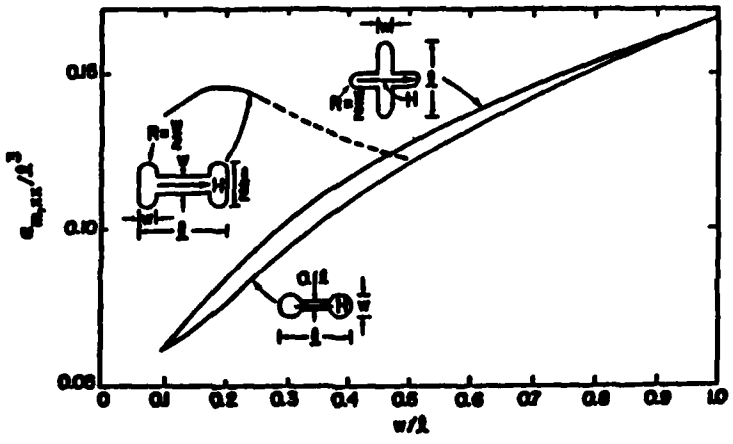

Figure 22. Normalized magnetic (imaged) polarizabilities for three aperture shapes. [2]

In addition to simple apertures as discussed above, it is possible to have apertures in the form of slits around doors or other hatch closures as shown in figure 23. The penetration of EMP fields through these apertures may also be described in terms of equivalent dipole moments, and the pertinent aperture polarizabilities are expressed in [2] as indicated in Table 3.

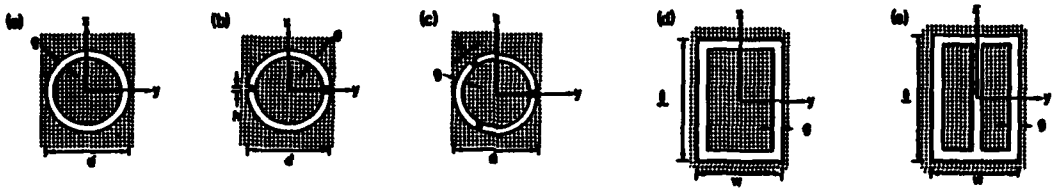

Figure 23. Hatch apertures.

Table 3

POLARIZABILITIES OF HATCH APERTURES [2]

Aperture	α_e	$\alpha_{m,xx}$	$\alpha_{m,yy}$
Fig. 23a	$\frac{\pi^2}{32}\frac{d^3}{\ln(16\,d/g)-2}$	$\frac{\pi^2}{4}\frac{d^3}{\ln(16\,d/g)-2}$	$\frac{\pi^2}{4}\frac{d^3}{\ln(16\,d/g)-2}$
Fig. 23b	$\frac{\pi^2 d^3}{16\Omega}\frac{s^2\mu\epsilon}{s^2\mu\epsilon + 128h/(\pi\Omega dg^2)}$	$\frac{\pi^2 d^3}{8\Omega}\left[1-\frac{8/\pi^2}{1+\Omega g^2/(8\pi dh)}\right]$	$\frac{\pi^2}{16}\frac{d^3}{\ln(16\,d/g)-2}$
Fig. 23c	$\frac{\pi^2 d^3}{16\Omega}\frac{s^2\mu\epsilon}{s^2\mu\epsilon + 192h/(\pi\Omega dg^2)}$	$\frac{\pi^2 d^3}{8\Omega}\left[1-\frac{27/(4\pi^2)}{1+9\Omega g^2/(64\pi dh)}\right]$	$\frac{\pi^2 d^3}{8\Omega}\left[1-\frac{27/(4\pi^2)}{1+9\Omega g^2/(64\pi dh)}\right]$
Fig. 23d	$\frac{\pi}{4}\frac{\ell^2 w}{(1+\ell/w)\ln[4(\ell+w)/g]}$	$\frac{\pi}{12}\frac{\ell^3[1+3(w/\ell)]}{\ln[4(\ell+w)/g]}$	$\frac{\pi}{12}\frac{w^3[1+3(\ell/w)]}{\ln[4(\ell+w)/g]}$
Fig. 23e	$\frac{\pi}{4}\frac{\ell^2 w}{(1+\ell/2)\ln[4(\ell+w)/g]}$	$\frac{\pi}{24}\frac{\ell^3[8/3+7(w/\ell)+2(w/\ell)^2]}{\ln[4(\ell+w)/g]}$	$\frac{\pi}{12}\frac{w^3[1+3(\ell/w)]}{\ln[4(\ell+w)/g]}$

NOTE: $\Omega = 2[\ln(16d/g) - 2]$

At times, the apertures in the hatches and doors of figure 23 are filled with a conducting material in the form of a seal or gasket, for the express purpose of eliminating the EMP penetration. Mathematical models for the effect of such gaskets have been developed, and Table 4 from [2] summarizes resulting aperture polarizabilities. Note that these quantities are frequency dependent.

Table 4

POLARIZABILITIES OF GASKET-SEALED HATCH APERTURES [2]

Aperture	$\alpha_e(s)$	$\alpha_{m,xx}(s)$	$\alpha_{m,yy}(s)$
Fig. 23a	$\frac{\pi^2 s\varepsilon}{16} \frac{d^4}{2G_c + sC_c}$	$\frac{\pi^2}{4} \cdot \frac{2}{1/L_c + sG_c}$	$\frac{\pi^2}{4\mu} \cdot \frac{2}{1/L_c + sG_c}$
Fig. 23b	$\frac{\pi^2 s\varepsilon}{16} \cdot \frac{d^4}{2G_c + sC_c + 2/sL_h}$		$\frac{\pi^2}{4\mu} \cdot \frac{d^2}{1/L_c + sG_c}$
Fig. 23c	$\frac{\pi^2 s\varepsilon}{16} \cdot \frac{d^4}{2G_c + sC_c + 3/sL_h}$		
Fig. 23d	$\frac{s\varepsilon \ell^2 w^2}{G + sC}$	$\frac{1}{1 + sL_x G_x} \alpha_{m,xx}(0)$	$\frac{1}{1 + sL_y G_y} \alpha_{m,yy}(0)$
Fig. 23e	$\frac{s\varepsilon \ell^2 w^2}{G + sC}$	$\frac{1}{1 + s(L_x + L_a)G'_x} \alpha_{m,xx}(0)$	$\frac{1}{1 + sL_y G_y} \alpha_{m,yy}(0)$

Notes: (i) Δ = gasket thickness; σ = gasket conductivity.

(ii) The static polarizabilities $\alpha_{m,xx}(0)$ and $\alpha_{m,yy}(0)$ in the table entries are those of the corresponding hatch aperture without gasket found in Table 8.

(iii) Constants: $G = 2\sigma\Delta(\ell+w)/g$; $C = 2\varepsilon\Omega(\ell+w)/\pi$; $\Omega_x = 2\ell n[4(\ell+w)/g]$; $L = \mu\pi\ell(1+2w/\ell)/8\Omega$; $L_y = \mu\pi w(1+2\ell/w)/8\Omega$; $G_x = \sigma\Delta\ell/g$; $G'_x = G_x/(1+w/3\ell)$; $L_a = (\pi\mu\ell/24\Omega)w^2/\ell^2$; $G_y = \sigma\Delta w/g$; $G_c = \pi\sigma\Delta d/2g$; $L_c = \mu d/[4\ell n(16d/g)-8]$; $L_h = \mu\pi g^2/(64h)$; $C_c = 2\varepsilon d[\ell n(16d/g)-2]$.

C. Diffusion Penetration Models

The final and usually least important EMP penetration mechanism is that of field diffusion into a shielded region. Electromagnetic field diffusion comes about because the electrical conductivity of the shield surrounding the system is not infinite. At low frequencies for which the wall thickness is less than the electrical penetration depth (skin depth), the diffusion mechanism is known to be an effective means for penetration by the magnetic field, while penetration by the electrical field is negligibly small. At higher frequencies where the wall thickness is larger than the skin depth, most of the incident magnetic field is shielded due to reflections at the surface, and attenuation losses in the wall. Hence, this phenomenon deals mainly with low frequency (late-time) magnetic fields.

An example of this effect is shown in figure 24 where a volume is enclosed by a thin shell of thickness Δ having electrical parameters σ and μ. An incident EMP falls on the body, and some of this pulse is able to penetrate into the interior.

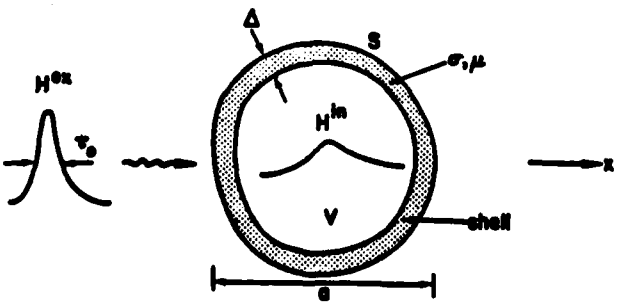

Figure 24. Geometry of shield for magnetic field attenuation.

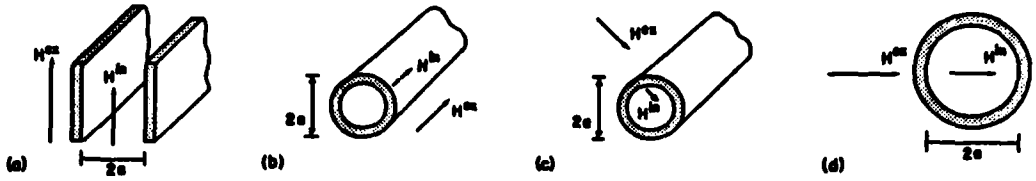

Figure 25. Several magnetic field shielding geometries: a) parallel plates, b) cylinder excited by longitudinal field, c) cylinder excited by transverse field, d) sphere.

As in the case of the aperture penetration models, it is possible to develop some simple expressions for the penetrated fields for the canonical bodies shown in figure 25. Reference [2] defines a transfer function for the magnetic fields T_m as:

$$T_m(s) = \frac{H^{in}(s)}{H^{ex}(s)} = \frac{\text{magnetic field inside cavity}}{\text{magnetic field incident on the cavity}} \qquad (22)$$

For an assumed uniform incident magnetic field, the frequency dependent transfer functions for the shield geometries shown in figure 25a are given as

$$T_p(p) = \frac{1}{\cosh p + kp \sinh p} \qquad (23)$$

for the parallel plate geometry of figure 25a

$$T_c(p) = \frac{1}{\cosh p + \frac{1}{2} kp \sinh p} \qquad (24)$$

for the cylindrical shell having longitudinal excitation as in figure 25b

$$T_c^{(t)}(p) = \frac{1}{\cosh p + \frac{1}{2}\left(kp + \frac{1}{kp}\right) \sinh p} \qquad (25)$$

for the cylinder with transverse excitation as in figure 25c, and

$$T_s(p) = \frac{1}{\cosh p + \frac{1}{3}\left(kp + \frac{2}{kp}\right) \sinh p} \qquad (26)$$

for the spherical shell shown in figure 25d. In these expressions, s is the complex angular frequency and:

$$k = \frac{\mu_o a}{\mu \Delta} \qquad p = s\tau_d \qquad \tau_d = \mu\sigma\Delta^2 \qquad (27)$$

For a non-ferrous shield, such as aluminum, figure 26 shows the frequency dependent transfer function in magnitude and phase for the canonical bodies. Given a particular body geometry, the K factor in equations 23 to 26 may be calculated and used to define ξ in figure 26, depending on the body type. As may be noted from the figure, the low frequency attenuation of the field approaches zero.

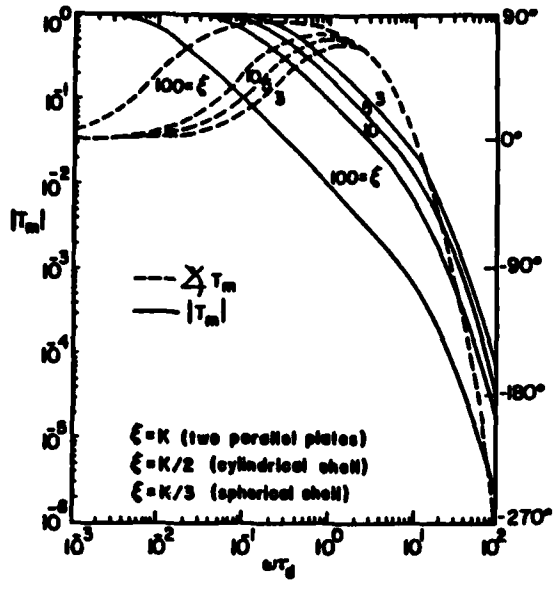

Figure 26. Magnitude and phase of frequency domain magnetic field transfer function for a non-magnetic shield. ($\tau_d = \mu\sigma\Delta^2$), $k = a/\Delta$)

For electrically thin shields, where the skin depth $\delta << \Delta$, it is possible to simplify the shield transfer functions:

$$T_p(s) = \frac{1}{1 + s\mu_0\sigma\Delta a} \tag{28}$$

$$T_c^{(t)}(s) = T_c^{(\ell)}(s) = \frac{1}{1 + s\mu_0\sigma\Delta a/2} \tag{29}$$

$$T_s(s) = \frac{1}{1 + s\mu_0\sigma\Delta a/3} \tag{30}$$

It is important to be able to compute the time history of the internal magnetic field, given the transient behavior of the incident field. One approach is to use purely numerical methods for determining the frequency domain spectrum of the internal field. An alternate approach is to develop an approximate expression, based on the assumption that the incident magnetic field is a delta function in time as:

$$H^{ex}(t,x) = H_0\delta(t-x/c) \tag{31}$$

where H_0 is the time integral of the incident magnetic field. That this is a useful approximation is due to the fact that the diffusion process tends to blur out the fine details of the incident field, since its time variation is much slower than that of the incident field.

With this approximation to the incident field, the inverse Laplace transform of the internal H field can be approximated as:

$$H^{in}(t) = \frac{2H_0}{\sqrt{\pi\xi\tau_d}}\sqrt{\frac{\tau_d}{t}}\, e^{-\tau_d/(4t)}, \text{ for } t/\tau_d \le 0.1 \tag{32}$$

for early times, and by:

$$H^{in}(t) = \frac{H_0}{\xi\tau_d}\left[e^{-\xi^{-1}t/\tau_d} - 2e^{-\pi^2 t/\tau_d} + 2e^{-4\pi^2 t/\tau_d}\right], \text{ for } t/\tau_d \ge 0.1 \tag{33}$$

for late times. Figure 27 presents the normalized internal magnetic field as a function of normalized time for several different values of the parameter ξ .

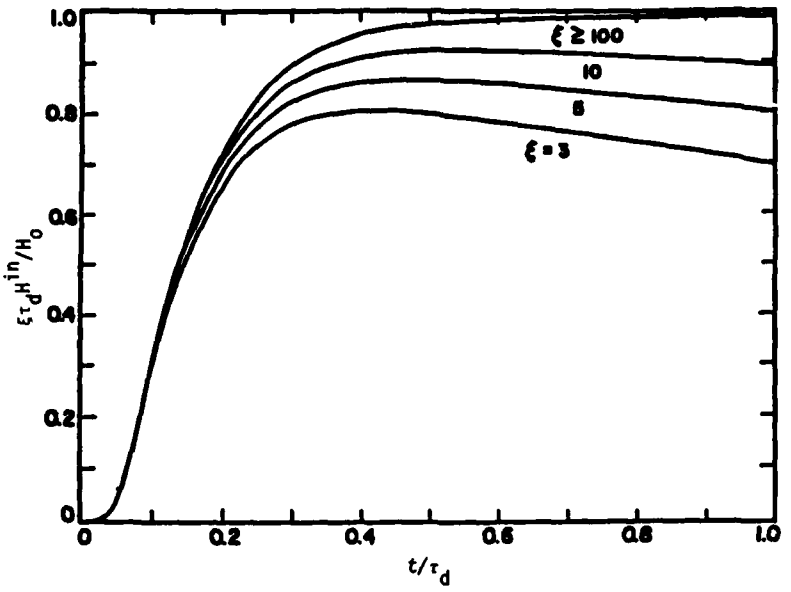

Figure 27. Time domain variation of the normalized penetrated EMP magnetic field within a shielded enclosure. ($\tau_d = \mu\sigma\Delta^2$)

IV. PROPAGATION MODELS

Often, the determination of the electric and magnetic fields inside of a shielded region does not provide the final system response used in a system assessment. These internal fields usually couple to internal conductors, and the EM energy is then propagated to other points within the system. In order to describe this propagation effect, conventional transmission line theory may be applied to a multiconductor transmission line model of the internal conductors. Figure 28 shows a general multiconductor transmission line model consisting of N conductors plus a reference conductor which may be excited by either an incident electromagnetic field, or by a set of lumped voltage and current sources.

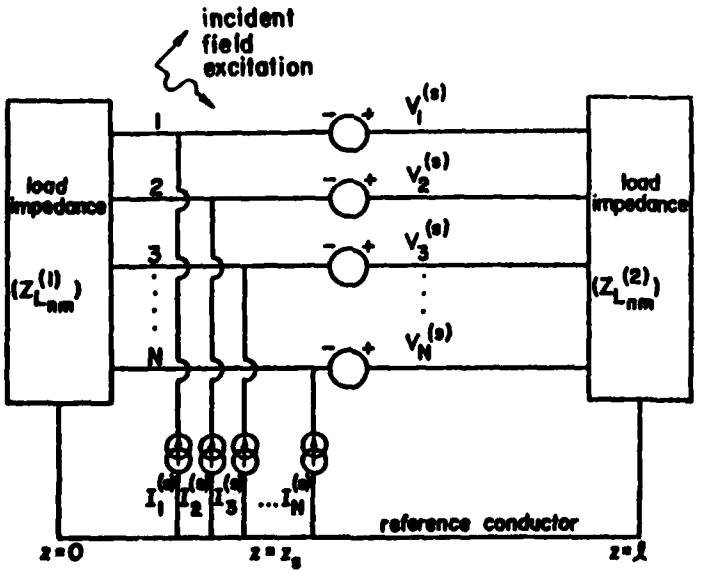

Figure 28. Single section of multiconductor transmission line excited by lumped sources, or by an incident electromagnetic field.

The solution for voltages and currents on this line has been thoroughly discussed by a number of authors, including [10], [11], and [12]. It is possible to obtain a solution at a particular frequency using the time harmonic analysis detailed in reference [10], or a direct transient solution using the time-marching calculations in reference [11]. For the present paper, no detailed discussion of these various

calculational approaches will be presented. It should be noted that the case of a single wire transmission line is simply the limiting case of a multiconductor line where N = 1 and this case is treated in detail in reference [13].

From the details of these analyses, it is apparent that there are a number of important physical parameters which define the electrical behavior of a general multiconductor transmission line. These are listed as follows:

$\bar{\bar{C}}$ = Capacitive coefficient matrix relating charges and voltages on all wires in the transmission line.

$\bar{\bar{L}}$ = Inductance matrix relating current and magnetic flux for all wires.

$\bar{\bar{R}}$ = Resistance matrix for losses along the transmission line.

$\bar{\bar{G}}$ = Conductance matrix for possible dielectric losses.

ℓ = Physical length of the line.

$\bar{\bar{Z}}_L$ = Generalized impedance termination matrix at ends of line.

$\bar{V}'_s$ = Distributed voltage sources exciting the line.

$\bar{I}'_s$ = Distributed current sources exciting the line.

For a simple, single wire line, all of these vector and matrix quantities become scalars, making the resulting analysis much simpler.

The response of the transmission line depends on all of the above parameters. However, for low frequencies (such that the line length is less than $\lambda/4$) the transmission line appears to be more like a simple lumped circuit. For example, at low frequencies the single line version of the line in figure 28 appears like that in figure 29a. For even lower frequencies, the equivalent circuit approaches that of figure 29b which is that of a lumped, low frequency circuit.

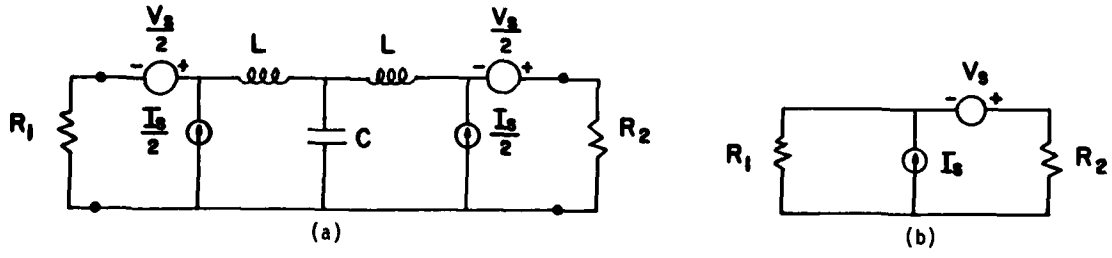

Figure 29. Representation of short single wire transmission line with loads (a) and equivalent circuit of line and loads, neglecting line effects (b).

There are many different methods for solving the telegrapher's equations which describe the behavior of the voltage and current on the multiconductor line. One common approach is to divide the transmission line into a number of sections which are small compared with a wavelength, and then represent each section by a lumped parameter circuit similar to that in figure 29a. This is described briefly in reference [2]. The resulting network is then solved, either in the time domain or in the frequency domain, using a large circuit analysis code such as TRAFFIC or NET2. This method is particularly useful for transmission lines having parameters which vary with position along the line, but due to the large amount of input data required, as well as computer memory requirements, its use is usually restricted to rather small problems.

Another method for solving the telegrapher's equations involves a direct time-stepping solution of the differential equations. This is discussed in references [11] and [14], where the voltage and the current at each point on the line is determined in terms of independently propagating voltage and current modes on the multiconductor line. These modes are excited by the sources on the line, and are coupled together at the line ends or line discontinuities. Their propagation velocities are, in general, all different, implying that after a few reflections back and forth on the line, a very large number of modal amplitudes are needed to represent the solution. Kajfez [15] has studied this approach and indicates that it is useful for early time responses only, due to the progressively larger number of modes that must be tracked as time increases.

A frequency domain solution is also possible for the multiconductor transmission line equations. There are a number of authors who have discussed this approach, each with minor variations of some of the details of the solution techniques. A summary of this frequency domain approach is presented in reference [2].

The basic concept for this analysis is to define forward and reverse propagating voltage and/or current waves on the line at a single frequency, and relate their

amplitudes to the sources and reflection coefficients at the loads. This method is somewhat similar to the time domain modal analysis, but yields an analytic expression for the load voltages and currents at a single frequency. Transient results may be obtained by Fourier inversion, a process that requires a large number of frequency domain calculations be made.

Although these solution techniques have been discussed in the context of a single section section of multiconductor line, it is possible to consider more complex cable geometries involving cascaded multiconductor lines [10], or even general multiconductor transmission line networks [16], [17].

As a practical example of the use of these propagation models, consider the problem discussed in reference [2] which involves the aperture excitation of a conductor as shown in figure 30a. A simple transmission line model shown in figure 29c may be used for the analysis. Here, the wire is assumed to be represented by a transmission line model having distributed inductance and capacitance. The effect of the aperture is to induce an additional lumped inductance and capacitance in the line at the aperture location, as well as a lumped voltage and current source. The relationship of these to the aperture polarizabilities is given in reference [2].

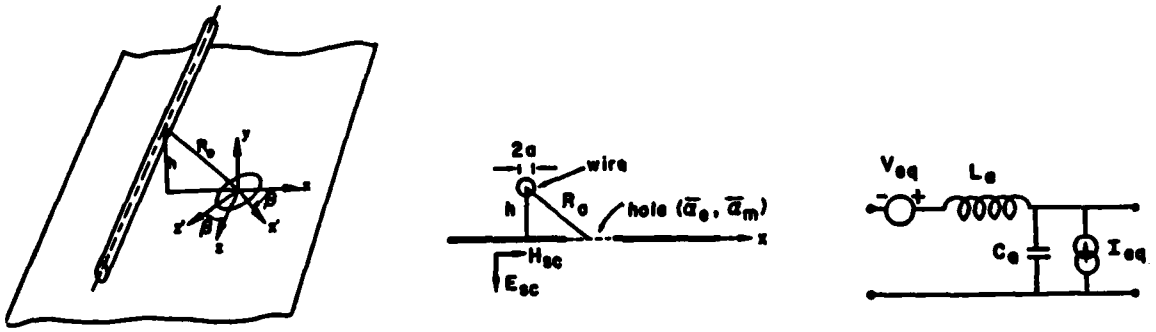

a. Perspective view b. Cross-sectional view c. Equivalent circuit

Figure 30. Aperture coupling to nearby conductor.

Usually the correction of the line inductance and capacitance is insignificant, so that only the lumped excitation sources need to be considered in estimating the line response. Once these sources are determined, the transmission line coupling methods described in the above may be utilized to infer the induced line current and voltage.

V. CONCLUDING REMARKS

This paper has attempted to provide an overview of some useful analysis techniques for estimating the EMP response of aircraft and missiles. Obviously, this topic is a large one, and it is not possible to provide a comprehensive review of all of the possible models and techniques in such a short paper. Nevertheless, the material reviewed here has been used by the author for a number of years for conducting such analyses, and has been found to provide a reasonably complete set of "tools" for problems commonly encountered in the EMP area.

In using these and other analytical approaches for EMP modeling of systems, it should be remembered that the calculated results are usually only approximate, since the actual system is much more complicated than the simple models used in the analysis. The true utility of such analysis tools lies in using them in conjunction with experiments performed on the actual system.

VI. REFERENCES

1. Tesche, F.M., "Introduction to Concepts of Electromagnetic Topology as Applied to EMP Interaction with Systems", Companion paper in this publication, May, 1986.

2. EMP INTERACTION: PRINCIPLES, TECHNIQUES AND REFERENCE DATA, K.S.H. Lee, Editor, Air Force Weapons Laboratory, AFWL-TR-80-402, Kirtland AFB, 1980.

3. Joint Special Issue on the Nuclear Electromagnetic Pulse, IEEE Trans. EMC, Vol. EMC-20, No. 1, February 1978.

4. Felsen, L.B., TRANSIENT ELECTROMAGNETIC FIELDS, Springer-Verlag, New York, 1976.

5. Van Bladel, J., ELECTROMAGNETIC FIELDS, McGraw-Hill, New York, 1964.

6. Harrington, R.F., FIELD COMPUTATION BY MOMENT METHODS, McMillan, New York, 1968.

7. Rao, S.M., D.R. Wilton and A.W. Glisson, "Electromagnetic Scattering by Surfaces of Arbitrary Shape, IEEE TRANS AP, Vol.AP-30, No.2, May 1982, pp. 409-418.

8. Wilton, A.W. Glisson, and S.M. Rao, "Handbook for EFIE - A Computer Code for Electromagnetic Scattering Problems Involving Arbitrary Shaped Conducting Surfaces", available from the authors, University of Mississippi, 1982.

9. Tesche, F.M., "On the Analysis of Scattering and Antenna Problems Using the Singularity Expansion Technique, IEEE TRANS. AP, Vol. AP-21, pp. 53-62, January, 1973.

10. Paul, C.R., "On Uniform Multimode Transmission Lines", IEEE TRANS. MTT., Vol. MTT-21, pp. 556-558, August, 1973.

11. Gibson, G.A., "Wave Propagation and Reflection on Multiconductor Transmission Lines with Inhomogenious Dielectrics", M.S. Thesis, University of Mississippi, May, 1978.

12. Frankel, S., MULTICONDUCTOR TRANSMISSION LINE ANALYSIS, Artech House, Dedham, Mass. 1978.

13. Smith, A.A., Jr., COUPLING OF EXTERNAL ELECTROMAGNETIC FIELDS TO TRANSMISSION LINES, John Wilely, New York, 1977.

14. Agrawal, A.K., et. al., "Time Domain Analysis of Multiconductor Transmission Lines with Branches in Inhomogenious Media, AFWL EMP INTERACTION NOTES, February, 1978.

15. Kajfez, D., Private Communication, University of Mississippi, Oxford, MS.

16. Baum, C.E., T.K. Liu, and F.M. Tesche, "On the General Analysis of Multiconductor Transmission Line Networks," AFWL EMP INTERACTION NOTES, Note 350, November, 1978.

17. Baum, C.E., T.K. Liu, F.M. Tesche, and S.K. Chang, "Numerical Results for Multiconductor Transmission Lines," AFWL EMP INTERACTION NOTES, Note 322, September, 1977.

MEASUREMENT TECHNIQUES FOR TRANSIENT ELECTROMAGNETICS

Carl E. Baum
Air Force Weapons Laboratory
Kirtland AFB, New Mexico 87117-6008

ABSTRACT

For over two decades now this author with some colleaques has developed various sensors for measuring transient (or broadband) electromaqnetic parameters, includinq electromaqnetic fields, current, voltaqe, etc. (especially emphasizinq the time derivatives). These have been optimized in terms of bandwidth consistent with sensitivity and physical size. Besides for the case of measurements in benign media (such as free space), some of these sensors are designed for measurements in nonlinear media which may also include sources; such sensors are appropriate for nuclear source regions and near lightninq arcs. Besides the sensors themselves this paper addresses some of the principles of topology and symmetry for installing these sensors in experimental configurations.

I. The literature on this subject is quite large now. The interested reader is referred to three review papers:

Baum, C. E., E. L. Breen, J. C. Giles, J. P. O'Neill, and G. D. Sower, Sensors for Electromaqnetic Pulse Measurements Both Inside and Away from Nuclear Source Regions, Sensor and Simulation Note 239, January 1978, IEEE Trans. Antennas and Propagation, January 1978, pp. 22-35, and IEEE Trans. EMC, February 1978, pp. 22-35.

Baum, C. E., Sensors for Measurement of Intense Electromaqnetic Pulses, Sensor and Simulation Note 271, June 1981, and Proc. 3rd IEEE International Pulsed Power Conference, Albuquerque, NM, June 1981, pp. 179-185.

Baum, C. E., E. L. Breen, F. L. Pitts, G. D. Sower, and M. E. Thomas, The Measurement of Lightninq Environmental Parameters Related to Interaction with Electronic Systems, Sensor and Simulation Note 274, May 1982, and IEEE Transactions on Electromaqnetic Compatibility, May 1982, pp. 123-137.

Recently I have combined this into a chapter for a forthcominq book

Baum, C. E., Measurement Techniques for Transient Electromagnetics, in L. H. Leussen and J. E. Thompson (eds.), Advanced Electrical and Optical Diagnostics, Martinus Nijhoff, The Hague.

This book chapter is quite lengthy and contains over a hundred references. Unfortunately it could not be reproduced here.

SELECTIVE BIBLIOGRAPHY

This bibliography with Abstracts has been prepared to support AGARD Lecture Series No. 144 by the Scientific and Technical Information Branch of the US National Aeronautics and Space Administration, Washington, D.C., in consultation with the Lecture Series Director, A. W. Biggs, University of Alabama, Huntsville, Alabama.

PRINT 07/4/1-113 TERMINAL=66

UTTL: International Symposium on Electromagnetic Compatibility, 21st, San Diego, Calif., October 9-11, 1979, Proceedings Symposium sponsored by the Institute of Electrical and Electronics Engineers. New York, Institute of Electrical and Electronics Engineers, Inc., 1979. 469 p (For individual items see A81-14252 to A81-14294)

ABS: Subjects discussed include electromagnetic pulse, electromagnetic shielding, modeling, lightning, components, advanced composites electromagnetic characteristics, electromagnetic compatibility design, and spectrum compatibility. Other subjects are: electromagnetic environments, coupling, analysis, communications, spectrum management, regulations, instrumentation, and measurements. 79/00/00 81A14251

UTTL: International Symposium on Electromagnetic Compatibility, 24th, Santa Clara, CA, September 8-10, 1982, Proceedings Symposium sponsored by the Institute of Electrical and Electronics Engineers. New York, Institute of Electrical and Electronics Engineers, Inc., 1982, 520 p.

ABS: The incorporation of electromagnetic compatibility (EMC), and the prevention of electromagnetic interference (EMI) in the design of electronic devices are considered in individual contributions. Topics covered include EMC regulation, spectrum management, equipment shielding, system analysis and modeling, computer-systems EMC, measurement techniques, composite materials in EMC design, personnel electrostatic discharge, EMC testing, electromagnetic environments, and coupling and shielding analysis. Discussion is also presented on EMI design, industrial and commercial EMC, lightning and electromagnetic pulses (including aircraft-design problems), and naval EMC applications. No individual items are abstracted in this volume 82/00/00 84A15384

UTTL: International Symposium on Electromagnetic Compatibility, 25th, Arlington, VA, August 23-25, 1983, Symposium Record Symposium sponsored by the Institute of Electrical and Electronics Engineers. New York, Institute of Electrical and Electronics Engineers, Inc., 1983, 610 p. For individual items see A85-26677 to A85-26687.

ABS: Subjects related to electromagnetic compatibility (EMC) analysis are discussed, taking into account forcing terms of line equations for externally excited transmission lines, E-fields over ground, electromagnetic near fields as a function of electrical size, a program for experimental verification of EMC analysis models, random susceptability of an IC 7400 TTL NAND gate, and a comparison of IEMCAP and SEMCAP. Other topics explored are concerned with EMC measurements, spectrum management, the electromagnetic pulse (EMP), a Navy EMC program, measurement systems, filters, EMC design, electromagnetic vulnerability (EMV) assessment of weapon systems, FCC rules and regulations, shielding, and electromagnetic interference (EMI) in communication systems. Attention is also given to nonsinusoidal functions in radar and communications, transients/electrostatic discharge, open field testing, cables and connectors, interference effects of induced and conducted earth current at dc and ELF, test cells, and cable coupling. 83/00/00 85A26676

UTTL: EXEMPT programmers manual CORP: BDM Corp., Albuquerque, N. Mex.

ABS: EXEMPT is a computer program which functions as an executive routine that interfaces with computer program models describing electromagnetic pulse EMP coupling to aircraft subsystems. As it now exists, EXEMPT is a modification of an earlier version which was difficult to use and which could be used only with B-1 aircraft subsystem models. It was necessary to modify that version to produce a code which would be more user oriented and which could interface with computer program models of EMP coupling to other aircraft subsystems. These modifications have been accomplished, and this report documents the result.

RPT#: AD-A066807 AD-E200261 BMA/A-77-098-TR-R2 AFWL-TR-77-206 79/01/00 79N25282

UTTL: Federal Aviation Administration - Georgia Institute of Technology Workshop on Grounding and Lightning Protection CORP: Georgia Inst. of Tech., Atlanta. Workshop held at Atlanta, 2-4 May 1978

ABS: A state-of-art review and background research reveals a number of opinions as to the preferred techniques of grounding of electronic equipment and systems. These techniques become important when protection must be provided for transients induced by lightning, electromagnetic pulses and other sources.

RPT#: AD-A058797 FAA-RD-78-83 78/05/00 79N12332

UTTL: Screening of monitoring and control subsystem equipment for hardness testing. Volume 1B: Recommendations for testing, EMP CORP: Ammann and Whitney, New York.
ABS: The document presents the results of a Criticality Analysis and Equipment Screening of the Monitoring and Control (M/C) Subsystems for the PAR Site. Lists of critical M/C items and equipment characteristics are presented for purposes of test/analysis evaluation.
RPT#: AD-748060 PAR-A/W-94-VOL-1B 72/06/00 73N12161

UTTL: Protection instructions, EMP/RFI protection information USAEDH hardness program EMP, SAFEGUARD ground facilities grand Forks, volume 1 CORP: Black and Veatch Consulting Engineers, Kansas City, Mo.
ABS: Protection instructions covering techniques applicable to the protection of tactical ground facilities from the effects of electromagnetic pulse (EMP) resulting from a nuclear explosion, and from radio frequency interference (RFI) generated by plant equipment or by external sources are presented. The protection instructions are based on the most recent authoritative data on EMP/RFI environment.
RPT#: AD-A007911 HNDDSP-72-145-ED-R-VOL-1 74/12/00 75N17080

UTTL: Structures protection CORP: General Electric Co., Pittsfield, Mass. In its Lightning Protect. of Aircraft p 185-252 (SEE N78-11024 02-03)
ABS: Materials of which an aircraft is made and the methods used to hold these materials together forming the aircraft structure were studied as factors important in protecting a modern aircraft from hazardous natural environments. Since all-metal aircraft are being replaced by aircraft constructed partly of fiber reinforced plastics with desirable light weight and high strength properties but with poor electrical conductivity, the danger of lightning strikes has become more serious. Lightning effects on metal structures were reviewed and design protection was discussed. The expected lightning effects on nonmetallic materials such as fiberglass and advanced composites were also reviewed. 77/10/00 78N11031

UTTL: West Europe report: Science and technology CORP: Joint Publications Research Service, Arlington, Va.
RPT#: JPRS-WST-84-032 84/09/25 85N29095

UTTL: The EMP interaction with a missile and plume: A comparison of theory and experiment
AUTH: A/AIKELE, M. H.; B/STRIBLING, D. R. PAA: A/(Lutech, Inc., Berkeley, Calif.) CORP: Science Applications, Inc., Colorado Springs, Colo. In APL JANNAF 13th Plume Technol. Meeting, Vol. 1 p 419-429 (SEE N82-31412 22-20)
ABS: To better understand the EMP response of missiles with conducting exhaust plumes, the antenna characteristics of a small-scale rocket motor were both measured and calculated theoretically. Instrumentation was developed to measure a predictable electrical response of the motor-plume system, the input admittance. These data were then compared with those calculated theoretically by existing plume chemistry and antenna coupling codes. Results show that when the plume is sufficiently conductive in the chamber and afterburning regions the instrumentation could detect changes in the input admittance that the calculations did not predict. The reason for this appears to be incorrect modeling of capacitative coupling, especially between the nozzle and plume at the exit plane. 82/04/00 82N31439

UTTL: A technology plan for electromagnetic characteristics of advanced composites
AUTH: A/ALLEN, J.; B/GAJDA, W.; C/GRIFFIN, D.; D/HARRINGTON, R. F.; E/HEINTZ, R.; F/JOY, E. B.; G/LYON, J.; H/WALKER, W. PAA: A/(South Fla. Univ.); B/(Notre Dame Univ.); C/(Adelaide Univ.); E/(Rochester Inst. of Technol.); F/(Georgia Inst. of Technol.); G/(Mich. Univ., Ann Arbor); H/(Rochester Inst. of Technol.) CORP: Syracuse Univ., N. Y.
ABS: The report presents a program for the development of the fundamental technology for the assessment of the electromagnetic compatibility (EMC) effects of the use of advanced composite materials in aircraft. A survey of the electromagnetic impact of the use of advanced composite materials in aircraft is given. Electromagnetic hazards (lightning, nuclear blast EMP, precipitation static and radar) are described and related to the shielding performance of advanced composite materials. In addition the effects of composite materials on antenna performance is discussed. The measurement of basic electrical properties and the definition and measurement of shielding effectiveness is treated in detail. Finally and most importantly, future study tasks are defined which aim to develop electromagnetic environment analysis capability for existing and future aircraft systems using advanced composite materials.
RPT#: AD-A030507 RADC-TR-76-206 RIT-EE-76-101 76/07/00 77N17175

UTTL: A 100-kA direct drive EMP pulser
AUTH: A/ALLEN, J. E. CORP: GTE Sylvania, Inc., Needham Heights, Mass. CSS: (Communication Systems Div.)
ABS: A pulser is described which was built to directly drive 100 kA into a Minuteman silo closure seal. The pulser has a 50-kV charge voltage, a 10-nanosecond rise time and a 50 microsecond fall time. Physical features and performance characteristics are described along with a summary of its successful operation in pulsing the silo cover.
RPT#: PEM-39 75/07/00 76N27482

UTTL: Lightning effects on aircraft and compcsites. Literature study on lightning strikes and protection
AUTH: A/ALM, A. CORP: Research Inst. of National Defence, Stockholm (Sweden). CSS: (Huvudavdelning 2.)
ABS: The frequency and different types of lightning strike on different parts of aircraft and several ways of protection against direct and indirect lightning effects were reviewed. Fiber composites, lightning damage and testing of lightning protection for modern aircraft material are studied by means of simulation techniques. Unshielded composite materials are damaged by lightning. With a correctly shaped lightning shield damage can be prevented.
RPT#: FOA-C-20388-F9 80/11/00 82N10024

UTTL: Lightning effect on aircraft electronics
AUTH: A/ANDERSON, R. V. PAA: A/(U.S. Navy, Naval Research Laboratory, Washington, DC) American Institute of Aeronautics and Astronautics, Aerospace Sciences Meeting, 22nd, Reno, NV, Jan. 9-12, 1984. 6 p.
ABS: Three trends in aircraft practice are shown to affect the possible importance of lightning activity on the safety and effectiveness of aircraft operations. It is shown that current directions in electronics utilization, electronics technology, and aircraft structural design all tend to exacerbate the lightning problem. Three mechanisms are described through which lightning strike energy is coupled to electronic systems; and the third, the (relatively) low frequency magnetic field produced by the passage of a discharge current, is described as relatively underappreciated. There is a brief discussion of lightning hazard definitions with suggestions for further study, and the paper concludes with an overview of strategies with which to address the perceived threat.
RPT#: AIAA PAPER 84-0465 84/01/00 84A18108

UTTL: Induced currents on two dimensional electromagnetic planar structures
AUTH: A/BALTA, J. A. R.; B/ADLER, R. W. CORP: Naval Postgraduate School, Monterey, Calif.
ABS: Electromagnetic pulse has become a possible threat to nearly all sophisticated military systems. The crossed dipole receiving antenna has been used as a representative model to approximate electromagnatic pulse effects on aircraft. A very basic way to approximate an aircraft structure is by a two-dimensional cross. The paper is an application of the Piecewise-Sinusoidal Reaction Matching Technique (PSRMT) to find the current density distribution in a two-dimensional cross illuminated by a monochromatic plane wave. Other two-dimensional structures are solved previous to the cross structure in order to gain insight and to validate this approach with respect to previous solution techniques.
RPT#: AD-A005733 NPS-52AB74124 74/12/00 75N29339

UTTL: Three-fluid MHD model of the current sheath in a Z pinch
AUTH: A/BAZDENKOV, S. V.; B/VIKHREV, V. V. PAA: B/(Akademiia Nauk SSSR, Institut Atomnoi Energii, Moscow, USSR) Fizika Plazmy, vol. 1, May-June 1975, p. 451-457. In Russian.
ABS: The formation and motion of a current sheath in a high-power pulsed discharge (Z pinch) are examined. A one-dimensional nonsteady-state problem concerning a discharge in deuterium is solved numerically in a three-fluid MHD approximation taking into account gas ionization and the initiation of neutral-atom motion. It is shown that after removal of the sheath, a sufficiently large quantity of nonionized gas remains near an isolated wall and that a secondary rupture may subsequently occur in this gas. It is found that a moving current sheath has a binary structure: the usual current 'piston' and a current sheet at the shock front. 75/06/00 75A43661

UTTL: Three-fluid MHD model for the current shell in a Z pinch
AUTH: A/BAZDENKOV, S. V.; B/VIKHREV, V. V. PAA: B/(Akademiia Nauk SSSR, Institut Atomnoi Energii, Moscow, USSR) (Fizika Plazmy, vol. 1, May-June 1975, p. 451-457.) Soviet Journal of Plasma Physics, vol. 1, May-June 1975, p. 250-253. Translation.
ABS: (For abstract see issue 22, p. 3325, Accession no. A75-43661) 75/06/00 76A27037

UTTL: Digital system upset. The effects of simulated lightning-induced transients on a general-purpose microprocessor
AUTH: A/BELCASTRO, C. M. CORP: National Aeronautics and Space Administration. Langley Research Center, Hampton, Va.
ABS: Flight critical computer based control systems designed for advanced aircraft must exhibit ultrareliable performance in lightning charged environments. Digital system upset can occur as a result of lightning induced electrical transients, and a methodology was developed to test specific digital systems for upset susceptibility. Initial upset data indicates that there are several distinct upset modes and that the occurrence of upset is related to the relative synchronization of the transieht input with the processing sate of the digital system. A large upset test data base will aid in the formulation and verification of analytical upset reliability modeling techniques which are being developed.
RPT#: NASA-TM-84652 NAS 1.15:84652 83/04/00 83N24212

UTTL: Digital system upset: The effects of simulated lightning-induced transients on a general purpose microprocessor
AUTH: A/BELCASTRO, C. M. CORP: National Aeronautics and Space Administration. Langley Research Center, Hampton, Va. In FAA Eighth Intern. Aerospace and Ground Conf. on Lightning and Static Elec. 12 p (SEE N83-31163 19-47)
ABS: Flight-critical computer-based control systems designed for advanced aircraft must exhibit ultrareliable performance in lightning-charged environments. Digital system upset can occur as a result of lightning-induced electrical transients, and a methodology was developed to test specific digital systems for upset susceptibility. Initial upset data indicates that there are several distinct upset modes and that the occurrence of upset is related to the relative synchronization of the transient input with the processing state of the digital system. A large upset test data base will aid in the formulation and verification of analytical upset reliability modeling techniques which are being developed. 83/06/00 83N31233

UTTL: EMP in the ionosphere: Rocket test 152-133
AUTH: A/BENTON, C. U.; B/WAKEFIELD, R. L.; C/NIPER, E. D.; D/SCHELLENBAUM, R. L. CORP: Los Alamos Scientific Lab., N. Mex.
ABS: The third in a series of rocket EMP experiments was conducted 30 October 1971 during the Barbizon exercise. The flight test of new instrumentation was primarily for the observation of the propagation characteristics of EMP-type signals at altitudes between 100 and 280 km. Two ground-based EMP simulators with close-in sensors, two ground-based ionosondes, a C-135 aircraft, and a 9-in. Nike-Tomahawk rocket were used to conduct the experiment. Development of instrumentation for this experiment, data from the experiment, and experiment planning are discussed.
RPT#: LA-4947 72/09/00 73N17521

UTTL: Lightning and composite materials
AUTH: A/BETEILLE, J.; B/WEBER, R. PAA: B/(SocieteNationale Industrielle Aerospatiale, Paris, France) IN: International Council of the Aeronautical Sciences, Congress, 14th, Toulouse, France, September 9-14, 1984, Proceedings. Volume 1 (A84-44926 22-01). New York, American Institute of Aeronautics and Astronautics, 1984, p. 203-209.
ABS: Recent investigations carried out to examine the effects of lightning on composite materials in aerospace applications are summarized. The materials studied consisted of conducting carbon fiber composites and nonconducting fiber glass/epoxy and aramid/epoxy composites. The effects of lightning strokes were examined in the arc attachment zone, swept stroke zones and in transfer zones in the case of the carbon fiber materials. Indirect effects on components within the aircraft walls made of the composites include sparking, insulation breakdown and equipment damage. Protection measures investigated covered keeping the currents continuous, spread out and on the outside of the structure, and the addition of hang-on metal sheets in high strike probability zones. Indirect effects could be ameliorated by cladding wiring in metal foil and installing surge protectors on sensitive devices. Design features and test configurations for examining the effectiveness of the techniques are outlined. 84/00/00 84A44950

UTTL: Charge and current density distributions on moderately thick transmitting crossed-monopole antennas
AUTH: A/BEYATTE, W. E.; B/BURTON, R. W. CORP: Naval Postgraduate School, Monterey, Calif.
ABS: Charge and current density distributions in the vicinity of the cross junction of several configurations of electrically long, moderately thick, crossed-monopole antennas with an intersecting angle of 45 degrees were measured. The recorded data was compared with a monopole antenna with the same

dimensions as the vertical segment of the crossed monopole. Junction conditions such that there would be a maximum current/minimum charge and minimum current/maximum charge on the vertical monopole were investigated.

RPT#: AD-A035818 NPS-62ZN76121 76/12/00 77N25420

UTTL: The prediction of lightning-induced voltages on metallic and composite aircraft

AUTH: A/BIRKEN, J. CORP: Naval Air Systems Command, Washington, D. C. In Tenn. Univ. Space Inst. Proc. of the 2nd Ann. Workshop on Meteorol. and Environ. Inputs to Aviation Systems p 153-177 (SEE N79-17413 08-47)

ABS: Various government agencies have put forth effort to enable the prediction of what lightning current will do to aircraft avionic systems. Ongoing and future efforts of predicting avionic voltages and currents caused by electromagnetic fields external to the aircraft are illustrated. The Intrasystem Analysis Program (IAP) was put to use to predict lightning-induced voltages on avionic systems. Presently funded programs are investigating the modification nonmetallic composite materials will cause to the metallic IAP program predictions. The various factors involved in designing prediction techniques are discussed. 78/03/00 79N17422

UTTL: Composite material aircraft electromagnetic properties and design guidelines

AUTH: A/BIRKEN, J. A.; B/DUFF, W. G.; C/PFLUG, D. R.; D/WALLENBERG, R. A. CORP: Atlantic Research Corp., Alexandria, Va.

ABS: This document collects and primarily summarizes aircraft advanced composite material electromagnetic properties, and secondarily, summarizes composite material mechanical, thermal, environmental, fabrication properties noting their ramifications on electromagnetic performance. It, then, overviews the electromagnetic sub-disciplines of threats, external to internal aircraft coupling, component and subsystems susceptibility protective methods as well as test and evaluation of small sample to total aircraft composite material electromagnetic performance. The sub-disciplines constitute a partioned set of independent variables which allow the reader to locate his area of interest in one section of the book. The sub-discipline are then combined to perform total aircraft electromagnetic system performance noting the protective methods, advantages and penalties.

RPT#: AD-A124016 81/10/00 83N25795

UTTL: Composites - Their electrical and electromagnetic impact

AUTH: A/BLAKE, C. L. PAA: A/(USAF, Aeronautical Systems Div., Wright-Patterson AFB, Ohio) In: International Symposium on Electromagnetic Compatibility, Washington, D.C., July 13-15, 1976, Record. (A77-31751 13-33) New York, Institute of Electrical and Electronics Engineers, Inc., 1976, p. 170-173.

ABS: The use of composite materials, of boron, graphite, Kevlar or glass fiber, on aircraft is increasing greatly, the decisions being made on the potential savings in weight and cost afforded by their substitution for metals. The decisions for composite application must be based on the total aircraft system impact, considering such factors as the electrical and electromagnetic impact of composites. Attention is focused on six general areas relative to electrical and electromagnetic characteristics, which must be considered when applying composites to an aircraft. These areas include lightning, shielding, antennas, electrical systems, static electricity, and radar cross section. 76/00/00 77A31762

UTTL: Electrical/electromagnetic concerns associated with advanced composite materials in aerospace systems

AUTH: A/BLAKE, C. L.; B/CORBIN, J. C., JR. PAA: B/(USAF, Aeronautical Systems Div., Wright-Patterson AFB, OH) In: Materials 1980; Proceedings of the Twelfth National Technical Conference, Seattle, WA, October 7-9, 1980. (A81-43601 20-23) Azusa, CA, Society for the Advancement of Material and Process Engineering, 1980, p. 449-460. USAF-sponsored research.

ABS: It is pointed out that an increasing use of composites instead of metal in aircraft structures can lead to substantial changes in the electromagnetic characteristics of the aircraft. Largely taken-for-granted features of the all-metal aircraft, such as readily available 'common ground' return paths for signal and power, and a low impedance, high conductivity outer skin for carrying direct lightning strike currents, will have to be reexamined. A new technology data base will have to be established if design changes have to be made to assure safe and satisfactory aircraft operation. In connection with the considered development, an assessment study was requested by Air Force Headquarters. The primary objective of the assessment was to determine the status of advanced composite material development in areas associated with possible electrical/electromagnetic (E/EM) impacts to aerospace systems. Attention is given to the conduct of the study, the scope of the study, implementation studies, design capability, design data, and E/EM concerns.

80/00/00 81A43630

UTTL: Aircraft lightning vulnerability testing
AUTH: A/BOGGESS, R. L. PAA: A/(USAF, Directorate of Avionics Engineering, Wright-Patterson AFB, Ohio)
In: NAECON '77; Proceedings of the National Aerospace and Electronics Conference, Dayton, Ohio, May 17-19, 1977. (A78-15551 04-33) New York, Institute of Electrical and Electronics Engineers, Inc., 1977, p. 282-285.
ABS: Flight critical fly-by-wire systems, solid state electronics, and an increased use of composite materials tend to increase the vulnerability of modern aircraft to lightning field effects. Lightning is transient, random and destructive. Therefore, laboratory testing is required to determine vulnerability levels. Laboratory testing provides design criteria data now, and improved circuit modeling can provide even better data. One such improvement is suggested and an example is given. 77/00/00 78A15585

UTTL: System safety program plan
AUTH: A/BONHAM, A. J. CORP: Edgerton, Germeshausen and Grier, Inc., Albuquerque, N. Mex.
ABS: This document, System Safety Program Plan, is the implementing document covering the safety aspects of performing an EMP Test on the A7E aircraft in the HPD (Horizontally Polarized Dipole), VPD (Vertically Polarized Dipole), and NWEF hangar facilities at Kirtland AFB, New Mexico.
RPT#: AD-A104557 AG-1446 DNA-5467F 80/08/08 82N11354

UTTL: Nuclear pulse. I - Awakening to the chaos factor
AUTH: A/BROAD, W. J. Science, vol. 212, May 29, 1981, p. 1009-1012.
ABS: The discovery of the significance of the high-voltage wave termed electromagnetic pulse (EMP), which occurs following the high-altitude detonation of a nuclear device, is discussed. The disruptions to the street lights, burglar alarms and circuit breakers of Hawaii caused by the detonation of a nuclear device 248 mi above Johnson Island in the Pacific in July, 1962 are described and attributed to the Compton electrons produced by the impact of gamma rays from the nuclear explosion on air in the upper atmosphere. It is pointed out, however, that at the time of the explosion, most communications systems were based on vacuum tube and electromechanical technology, which is about 10,000,000 times harder against EMP than integrated solid-state circuitry, and thus the threat posed by EMP to the power grid and communications capabilities was not apparent. Efforts undertaken to harden discrete (missile) and communications systems against EMP are outlined for the example of the Safeguard ABM system, and difficulties are pointed out. Soviet awareness of EMP is considered, and the discovery of vacuum tubes on board the state-of-the-art Foxbat MiG interceptor flown into Japan is noted as a possible indicator of this awareness. It is concluded that the problem of EMP will increase in significance as semiconductor electronics proliferates. 81/05/29 81A35991

UTTL: Nuclear pulse. III - Playing a wild card
AUTH: A/BROAD, W. J. Science, vol. 212, June 12, 1981, p. 1248-1251.
ABS: Implications of the phenomenon of electromagnetic pulse (EMP), a high-voltage by-product of nuclear explosions in space which could render useless unprotected communications equipment and power grids over a wide area, for the feasibility of conducting a limited nuclear war by the United States are discussed. Arguments on the one hand that the effects of EMP demand direct investigation and should be protected against by the hardening of U.S. military communications are summarized and contrasted with those on the other hand which assert that the presence of EMP, as well as other exotic nuclear effects, would, despite any attempts at hardening, make it impossible to maintain the precision of command and control necessary for a limited nuclear action against Soviet military targets. Uncertainties about Soviet intentions in regard to the use of EMP as a weapon are also pointed out. 81/06/12 81A35872

UTTL: EMP simulators for missiles and airplanes
AUTH: A/BUMGARDNER, M. K.; B/DREGER, M. A.; C/GILES, J. C. ; D/ROSS, G. F. CORP: Edgerton, Germeshausen and Grier, Inc., Albuquerque, N. Mex.
ABS: The manual is intended as a guide to EMP (electromagnetic pulse) Simulator selection. Descriptions of EMP Simulators were collected from a large number of documents and up-dated. Detailed technical discussions of 16 operating simulators are given along with cost and schedule information. Cost estimates for the construction of various types of simulators are also provided. Technical and financial information is summarized in table form for quick reference. A general discussion of the EM criterion pulse and EMP simulation is included as an aid for evaluating simulator performance.
RPT#: AD-780236 EG/G-AL-1026 74/02/04 74N30601

UTTL: The behavior of CFRP panels in metal aircraft during simulated lightning strokes
AUTH: A/BURROWS, B. J. C.; B/HANSON, A. W. CORP: United Kingdom Atomic Energy Authority, Abingdon (England). In AGARD Electromagnetic Effects of (Carbon) Composite Mater. Upon Avionics Systems 7 p (SEE N81-16144 07-24)
ABS: The current flow-pattern in a CFRP panel and the surrounding metal skin changes significantly during a current pulse simulating a lightning stroke. Measurements of the current distribution changes are made and compared with a theoretical treatment. The effects of different lay-ups of CFRP and different methods of mounting the panel are described. Observations are made of the influence of thin metal foils used to cover the outer surface on the screening provided by CFRP panels to simulated lightning current pulses. Screening by complex panels consisting of an aluminum honeycomb sandwiched between two CFRP skins is compared with these results. The direct damage suffered by both types of panels is also described, and their behavior analyzed theoretically. 80/10/00 81N16161

UTTL: New structures made of composite materials for high performance combat aircraft
AUTH: A/CORREGE, G. CORP: Departement Structures B. E. Aerospatiale, Toulouse (France). In AGARD Fighter Aircraft Design 18 p (SEE N78-30099 21-05)
ABS: Composite materials utilized in aircraft construction are described. Other areas of study are the following: (1) Types of composite structures utilized; (2) Materials; (3) Principles of local reinforcement; and (4) Protection against lightning strike. 78/06/00 78N30114

UTTL: Circumvention for electromagnetic pulse.
AUTH: A/COX, J. W., JR. PAA: A/(Rockwell International Corp., Electronics Group, Anaheim, Calif.) In: International Electromagnetic Compatibility Symposium, New York, N.Y., June 20-22, 1973, Record. (A73-41785 22-07) New York, Institute of Electrical and Electronics Engineers, Inc., 1973, p. 30-38.
ABS: Circumvention is a design concept for the EMP environment that has been applied with success in work sponsored by the U.S. Air Force on the Minuteman ICBM weapon system. The concept could be used with any complex system having certain unique operational characteristics. This paper presents the approach that was used to develop active circuitry in conjunction with passive shielding to meet the EMP design requirements. It explores the environmental and operational characteristics that made circumvention desirable. Analysis and tests verify that the new hardware has met its requirements and is compatible with the overall system. 73/00/00 73A41786

UTTL: Detection of sparks in fuel system tests
AUTH: A/CROUCH, K. E. PAA: A/(Lightning Technologies, Inc., Pittsfield, MA) IN: International Aerospace Conference on Lightning and Static Electricity, Oxford, England, March 23-25, 1982, Proceedings. Volume 1 (A84-18508 06-01). Abingdon, Oxon, England, Culham Laboratory, 1982, p. D16-1 to D16-6.
ABS: Two alternative methods for detecting sparks during lightning tests of fuel system components, i.e., the photographic technique and the fuel-air mixture technique, are examined. In the photographic method, a major problem is the lack of a distance (spark to lens) requirement. If the camera were removed far enough or if many lossy mirrors were used, the light from a small spark would be lost. Although the fuel-air mixture method also has its drawbacks, the technical problems associated with this method are fewer than with the photographic technique. It is pointed out that several recent developments, such as the use of structural adhesive bonding, the use of fuels with lower flash points, and an industry-wide rejection of fuel tank inerting, make it imperative that a new reliable and accurate method of detecting sparks in a fuel system during simulated lightning tests be developed. 82/00/00 84A18536

UTTL: The singularity expansion method applied to perdendicular crossed wires over an imperfect ground plane, a Sommerfeld integral formulation
AUTH: A/CROW, T. T.; B/KUO, J. C.; C/TAYLOR, C. D. CORP: Mississippi State Univ., Mississippi State.
ABS: The singularity expansion method (SEM) has been applied to determine natural resonances of a horizontal wire and perpendicular crossed wires oriented over an imperfect ground plane. In order to account for the imperfect conductivity of the ground, the Sommerfeld formulation is used and a theoretical-numerical solution obtained. Sample results are presented for both the frequency domain and the SEM solutions.
RPT#: AD-A089741 AFOSR-80-0749TR 80/01/00 81N11302

UTTL: Scale modeling for the PATRIOT electromagnetic pulse test
AUTH: A/CUNEO, A. A., JR.; B/LOFTUS, J. J. CORP: Harry Diamond Labs., Adelphi, Md.
ABS: Experimental electromagnetic coupling studies were made of a scale model of the PATRIOT air defense system as part of the evaluation of this system's ability to survive exposure to an electromagnetic pulse (EMP). This exercise was primarily concerned with providing basic information this is either too costly and time consuming or impossible to obtain in a full-scale field operation. This basic information consists of the answers to such questions as these: how the external receptor currents change with variations of the incident field's azimuthal and elevation angles as well as polarization, what the effect of cable routing is on EMP coupling, and how critical the system grounding is to EMP protection.
RPT#: AD-A107480 HDL-TM-81-16 81/05/00 82N26363

UTTL: SHIVA electromagnetic implosion X-ray source
AUTH: A/DEGNAN, J. H.; B/CLARK, M. C.; C/KIUTTU, J. F.; D/MCCLENAHAN, C. R.; E/BAKER, W. L. CORP: Air Force Weapons Lab., Kirtland AFB, N. Mex.
ABS: The generation of pulsed high-energy density plasmas by electromagnetic implosion of cylindrical foils (i.e., imploding liners or hollow Z-pinches) has been investigated experimentally and theoretically at the Air Force Weapons Laboratory. The experimental studies involve discharging a 1.3 microsecond, 1.1 megajoule capacitor bank through 7 cm radius, 2 cm tall, 3 to 30 mg cylindrical foil liners. Typical discharge parameters are 7 to 12 MA peak current and 1-1.5 microsecond current rise time. Current and voltage waveforms indicate strong coupling of the load to the capacitor bank, and analysis of the waveforms indicates good implosion of the current sheath. Optical and magnetic probe measurements are consistent with 1 to 2 cm thickness of the imploding plasma shell and with final implosion velocities. Comparison of electrical, magnetic, and radiation data with one dimensional magnetohydrodynamic and two dimensional magnetohydrodynamic calculations is presented. The prospects for improving the performance with the present energy source and scaling to larger energy sources are briefly discussed.
RPT#: AD-A061884 AD-E200170 78/05/00 79N19870

UTTL: Description of the Space Test Program P78-2 spacecraft and payloads
AUTH: A/DURRETT, J. C.; B/STEVENS, J. R. CORP: Space and Missile Systems Organization, Los Angeles Air Force Station, Calif.; Aerospace Corp., El Segundo, Calif In NASA. Lewis Res. Center Spacecraft Charging Technol., 1978 p 4-10 (SEE N79-24001 15-18)
ABS: The P78-2 spacecraft and its payloads are designed to measure the environment at near synchronous altitude and the interactions of the environment on the spacecraft. A brief description of each payload is provided. 79/00/00 79N24002

UTTL: A comparison of lightning and nuclear electromagnetic pulse response of a helicopter
AUTH: A/EASTERBROOK, C. C.; B/PERALA, R. A. CORP: Electro Magnetic Applications, Inc., Denver, Colo. In NASA. Langley Research Center Intern. Aerospace and Ground Conf. on Lightning and Static Elec. 7 p (SEE N85-16343 07-47)
ABS: A numerical modeling technique is utilized to investigate the response of a UH-60A helicopter to both lightning and nuclear electromagnetic pulses (NEMP). The analytical approach involves the three-dimensional time domain finite-difference solutions of Maxwell's equations. Both the external currents and charges as well as the internal electromagnetic fields and cable responses are computed. Results of the analysis indicate that, in general, the short circuit current on internal cables is larger for lightning, whereas the open-circuit voltages are slightly higher for NEMP. The lightning response is highly dependent upon the rise time of the injected current as was expected. The analysis shows that a coupling levels to cables in a helicopter are 20 to 30 dB larger than those observed in fixed-wing aircraft. 84/12/00 85N16349

UTTL: Atmospheric electricity hazards analytical model development and application. Volume 3: Electromagnetic coupling modeling of the lightning/aircraft interaction event
AUTH: A/ERIKSEN, F. J.; B/RUDOLPH, T. H.; C/PERALA, R. CORP: Electro Magnetic Applications, Inc., Denver, Colo.
ABS: The state of the art of coupling of electromagnetic fields to aircraft is reviewed. Assessing the electromagnetic interaction of lightning with aircraft is considered. The coupling process is explained and the modeling requirements implied by the lightning environment are discussed. The description of models selected and implemented is given.

RPT#: AD-A114017 EMA-81-R-21-VOL-3 AFWAL-TR-81-3084-VOL-3
81/06/00 82N29802

UTTL: Induced transients in a simulated lightning test of the fly-by-wire Jaguar aircraft
AUTH: A/EVANS, R. H.; B/BISHOP, J. CORP: Royal Aircraft Establishment, Farnborough (England). In FAA Eighth Intern. Aerospace and Ground Conf. on Lightning and Static Elec. 14 p (SEE N83-31163 19-47)
ABS: Simulated lightning tests were performed on the Jaguar aircraft modified for demonstrating fly-by-wire technology. A pulse generator injected currents of 100 kA maximum into the fuselage; measurements were made of induced voltage and current transients in cables, currents and magnetic fields in equipment bays, current density on the fuselage and wings, and rate of change of electrical field at two locations. Full-threat estimates were obtained by extrapolation. Some remarks are included on the consistency and accuracy of the results and their realism in relation to actual in-flight strikes. 83/06/00 83N31196

UTTL: The susceptibility of advanced filament organic matrix composites to damage by simulated lightning strikes
AUTH: A/FASSELL, W. M.; B/PENTON, A. P.; C/PLUMER, J. A. CORP: Philco-Ford Corp., Philadelphia, Pa. IN AFSC LIGHTNING AND STATIC ELEC. CONF., PT. 2 MAY 1969 P 530-570 /SEE N70-19027 07-02/ 69/05/00 70N19060

UTTL: Description of P78-2 (SCATHA) satellite and experiments
AUTH: A/FENNELL, J. F. CORP: Aerospace Corp., El Segundo, Calif. CSS: (Space Sciences Lab.)
ABS: The P78-2 (SCATHA) satellite was placed into a near synchronous orbit in early February 1979. The satellite was a part of a joint U.S. Air Force/NASA program to study spacecraft charging. The satellite has its spin axis approximately parallel to the Earth's equatorial plane. This allows good pitch angle coverage by the particle experiments. The experiment complement consists of a complete set of plasma, energetic particle, composition, field and wave experiments. The satellite has already provided over two years of data; about one year (February, 1979 to March, 1980) of it has been provided to the experimenters as formatted digital tapes. The data is of very high quality and the coverage is good (> 90%).
RPT#: AD-A118232 TR-0082(2940-05)-10 SD-TR-82-43 82/07/12 83N11171

UTTL: Analysis and calculations of lightning interactions with aircraft electrical circuits
AUTH: A/FISHER, F. A. CORP: General Electric Co., Schenectady, N. Y.
ABS: This report documents the results of a study performed to evaluate the indirect effects of lightning strikes - specifically, induced voltages - on the electrical systems of aircraft. Numerical methods for evaluating the fields produced by lightning currents flowing the skin of the aircraft are presented as a first analytical step. Additional numerical methods, for computing the voltages induced in wiring systems by the fields evaluated in the first step, are also presented, as are recommendations on the direction of further study.
RPT#: AD-A062606 SRD-78-044 AFFDL-TR-78-106 78/08/00 79N20108

UTTL: Development and use of types of construction employing fiber-reinforced materials
AUTH: A/FLEMMING, M. PAA: A/(Dornier GmbH, Friedrichshafen, West Germany) Deutsche Gesellschaft fuer Luft- und Raumfahrt, Jahrestagung, 7th, Kiel, West Germany, Sept. 17-19, 1974, 133 p. In German.
ABS: A report is presented of an investigation conducted jointly by a number of German aerospace firms to explore the possibility of a utilization of the new materials in aircraft. The use of structures utilizing fiber-reinforced materials involves a number of technical problems when compared to an employment of conventional structures. These problems are examined, giving attention to materials, approaches for affecting stiffness and strength, computation techniques, questions of stability and carrying capacity, design, and considerations concerning the operational life. Questions of impact bending strength are discussed along with aspects of erosion, corrosion, temperature characteristics, protection against lightning, inspection procedures, problems regarding material specifications, and the testing of materials in flying aircraft models. The costs of the new structures are compared with those of conventional structures.
RPT#: DGLR PAPER 74-117 74/09/00 75A24154

UTTL: Development and application possibilities of new construction techniques with fiberreinforced materials
AUTH: A/FLEMMING, M. CORP: European Space Agency, Paris (France).
ABS: The use of carbon and boron fiber reinforced materials in future aircraft design is discussed. A new construction method for use in primary structures will

succeed only if all technical problems are solved. The many construction possibilities and the limits of fiber technology are described, and weight reductions obtained are illustrated by practical examples. The design and calculation for strength and rigidity superseding that of conventional structures are discussed. The cost effectiveness of the new construction method is considered.
RPT#: ESA-TT-267 DGLR-PAPER-74-117 76/02/00 77N13165

UTTL: The PLACER: Assembly and operation
AUTH: A/GOODWIN, D. L. CORP: Harry Diamond Labs., Adelphi, Md.
ABS: This report describes the assembly and operation instructions of the PLACER, a test system for discovering and locating electromagnetic-pulse shielding flaws in underground conduits.
RPT#: AD-A039997 HDL-TM-77-7 77/04/00 77N30345

UTTL: EMP hardening of airborne systems through electro-optical techniques design guidelines
AUTH: A/GREENWELL, R. A. CORP: Naval Ocean Systems Center, San Diego, Calif.
ABS: This report examines the utilization of fiber optics technology as an alternative to system EMP hardening and provides design guidelines for airborne system applications. It also examines potential EMP vulnerabilities of the overall fiber optic data subsystems, defines and quantifies methods of protection against the EMP threat, and compares vulnerabilities with those of hard-wired data systems.
RPT#: AD-A080650 NOSC/TR-469 79/12/15 80N23146

UTTL: Fiber optics cost models for the A-7 aircraft
AUTH: A/GREENWELL, R. A. PAA: A/(U.S. Naval Electronics Laboratory Center, San Diego, Calif.) Fiber and Integrated Optics, vol. 1, no. 2, 1977, p. 197-225. Navy-sponsored research.
ABS: Presented in this article is a description of two cost models which compare fiber optic interface to alternative wire interconnect for the Airborne Light Optical Fiber Technology (ALOFT) project on the A-7 aircraft. Data for these models were collected on existing components of fiber optics and wire systems. The results of this study indicate that fiber optics, in comparison to most wire alternatives, achieves a significant reduction in total life-cycle cost and at the same time meets or exceeds the future requirements of Electromagnetic Interference (EMI), Electromagnetic Pulse (EMP), and lightning strike vulnerability. 77/00/00 77A36972

UTTL: Effect of precipitation static on general aviation digital avionics
AUTH: A/HENDRY, L. D. PAA: A/(Beech Aircraft Corp., Military Aircraft Group, Wichita, KS) IN: Digital Avionics Systems Conference, 6th, Baltimore, MD, December 3-6, 1984, Proceedings (A85-17801 06-01). New York, American Institute of Aeronautics and Astronautics, 1984, p. 190-192.
ABS: Design recommendations were made after a series of tests on the effects of precipitation (P-) static on general aviation electronic avionics. P-static arises from the fields produced by lightning, and was simulated by placing an aircraft in a high voltage (HV) facility. A HV cable was attached to one end of the aircraft, the other was attached to a grounding sphere which was moved around while various electrical systems were activated and monitored. Attention was also given to the occurrence of corona discharges. The tests revealed the need for static dischargers, which would remain closed with a current of 300 A, for the engines. Closed wheel doors were of great aid in assuring a uniform distribution of induced voltage around the aircraft. Conductive coatings were found necessary for all sharp extremities and nonconductive materials.
RPT#: AIAA PAPER 84-2641 84/00/00 85A17830

UTTL: Effects of simulated lightning on composite and metallic joints
AUTH: A/HOWELL, W. E.; B/PLUMER, J. A. PAA: B/(Lightning Technologies, Inc., Pittsfield, Mass.) CORP: National Aeronautics and Space Administration. Langley Research Center, Hampton, Va. Presented at the Army Symp. on Solid Mech., Cape Cod, Mass., 21-23 Sep. 1982
ABS: The effects of simulated lightning strikes and currents on aircraft bonded joints and access/inspection panels were investigated. Both metallic and composite specimens were tested. Tests on metal fuel feed through elbows in graphite/epoxy structures were evaluated. Sparking threshold and residual strength of single lap bonded joints and sparking threshold of access/inspection panels and metal fuel feed through elbows are reported.
RPT#: NASA-TM-84554 NAS 1.15:84554 82/10/00 83N14170

UTTL: Lightning test facilities measurement techniques
AUTH: A/HUBER, R. F.; B/KAWIECKI, C. J.; C/ROBB, J. D. IN- SOCIETY OF AUTOMOTIVE ENGINEERS AND U.S. AIR FORCE AVIONICS LAB., LIGHTNING AND STATIC ELECTRICITY CONFERENCE, SAN DIEGO, CALIF., DEC. 9-11, 1970, PROCEEDINGS. p. 39-46. /A71-19926 07-02/ 70/00/00

71A19931

UTTL: FAA lightning protection study: Lightning protection requirements for airport surveillance radar model ASR-7
AUTH: A/HUDDLESTON, G. K.; B/BUSH, G. G. CORP: Georgia Inst. of Tech., Atlanta.
ABS: The protection situations and requirements for the landlines of the ASR-7 radar in regard to lightning- and EMP-induced surges are presented. Gasfilled surge arrestors supplemented with avalanche diode transient suppressors with associated series line resistances are recommended to protect susceptible circuits connected to the buried landlines.
RPT#: AD-A019965 FAA-RD-75-180 75/07/00 76N21374

UTTL: Close-in magnetic fields of a lightning return stroke
AUTH: A/JONES, R. D.; B/WATTS, H. A. CORP: Sandia National Labs., Albuquerque, N. Mex.
ABS: The method of images is used to determine the time history of the close in magnetic field environment resulting from a lightning return stroke at a point on the earth's surface and at altitudes of 2,000 and 4,000 meters. The lightning channel is modeled after Uman and McLain, and a Dennis and Pierce-type current distribution in the channel is assumed. Particular attention is given to the initial lightning return stroke, in which the velocity of stroke propagation is time varying. A constant velocity of stroke propagation is used for subsequent return strokes. Results obtained from a simplified model are compared with those obtained from a model using retarded potentials. For close-in environments, excellent agreement is obtained between the two treatments. Some observations are made about the magnetic field variation with respect to altitude and the distance of the observer from the stroke, and a versatile, easily used computer code applicable to a wide range of lightning parameters is described.
RPT#: SAND-75-0114 75/06/00 76N22799

UTTL: The effect of the in-service environment on composite materials (resume of the April 1980 Athens conference)
AUTH: A/JUBE, G. CORP: Societe Nationale Industrielle Aerospatiale, Paris (France). In its Electromagnetic Effects of (Carbon) Composite Mater. Upon Avionics Systems 4 p (SEE N81-16144 07-24)
ABS: Reported experience of the effect of physical and mechanical aggressions (environment) on composite materials and structures is summarized. Topics covered include: (1) the physical chemistry of the environment and the sensitivity of the composite materials to humidity; (2) the behavior of composite materials in spatial ambience, particularly in vacuum; (3) rules for predicting damage to composite structures and the effect of accidental impact; (4) atmospheric physical phenomena, particularly lightning and rain erosion; and (5) the in service behavior of helicopter blades, NASA experience with transport aircraft structures, and USAF and Navy experience with boron and carbon fiber composites. 80/10/00 81N16146

UTTL: The 1981 NASA/ASEE Summer Faculty Fellowship Program: Research reports
AUTH: A/KARR, G. R.; B/DOZIER, J. B.; C/KENT, M. I.; D/BARFIELD, B. F. CORP: National Aeronautics and Space Administration. Marshall Space Flight Center, Huntsville, Ala.; Alabama Univ., University.; Alabama Univ., Huntsville.
RPT#: NASA-CR-161855 82/01/00 82N17043

UTTL: 757 lightning protection
AUTH: A/KING, C. H.; B/EAST, D. A.; C/MAKSIM, J. W. PAA: C/(Boeing Commercial Airplane Co., Seattle, WA) IN: NAECON 1983; Proceedings of the National Aerospace and Electronics Conference, Dayton, OH, May 17-19, 1983. Volume 1 (A84-16526 05-01). New York, Institute of Electrical and Electronics Engineers, 1983, p. 162-165.
ABS: The Boeing 757 is an advanced technology aircraft which incorporates multiple digital systems and makes extensive use of composite materials for secondary structure. Fiberglass, Kevlar, graphite, and graphite/Kevlar composites are used in the wing leading and trailing edges, engine nacelle and strut fairing, horizontal and vertical stabilizer tip fairings, rudder, and elevators. Aircraft power, signal, and control wiring run through structure covered by these composite materials. 83/00/00 84A16541

UTTL: Effects of electromagnetic radiofrequent emissions produced by detonating chemical explosives. Part 1: Experimental results
AUTH: A/KOCH, B.; B/HAENSEL, H.; C/KOHLMANN, R.; D/HORNY, G.; E/KOENIG, M. CORP: Institut Franco-Allemand de Recherches, St. Louis (France).
ABS: Energy and maximum performance of radiofrequent electromagnetic radiation impulses, produced by the detonation of shells of different caliber and of

explosion simulators of various sizes and wall materials, were measured. The recordings were made simultaneously with five calibrated receiver amplifiers in the 2.8 m and 40 cm wavelength region in the far field area of the radiation sources. Conclusions on the relationship between radiation energy and emission delay, detection distance, and overthermal nature of the radiation effects are summarized. In annexes a definition of the far field energy conservation on transfer of a block impulse across a lossfree threshold (passive integration), and an active integrator are discussed.
RPT#: ISL-5/74 74/02/27 76N24422

UTTL: Synthesis of a plume simulator for the MX missile
AUTH: A/LAM, J. CORP: Science Applications, Inc., Berkeley, Calif.; Dikewood Industries, Inc., Los Angeles, Calif.
ABS: A simulator for the exhaust plume of an MX missile is synthesized for use in the in-flight EMP hardness assessment of the missile in an EMP simulator. The synthesis is based on a set of results obtained in a numerical analysis of the interaction between the missile plume and an EMP which uses the Titan-III missile plume data scaled to the MX missile dimensions. It is found that, for this case, the plume simulator can be made entirely out of passive lumped LRC elements.
RPT#: AD-A068623 AD-E300507 DNA-4615T 78/05/31 79N29232

UTTL: Optoelectronic devices for flight vehicle control systems
AUTH: A/LAZAREV, L. P.; C/LAZAREV, V. L. Moscow, Izdatel'stvo Mashinostroenie, 1978. 175 p. In Russian.
ABS: The principles of operation and design of optoelectronic flight vehicle control systems are set forth. The design problem is treated as a problem in the design of large systems from the standpoint of systems engineering. Systems considered include scanning thermal direction finders, thermal autonavigation heads, and optical devices used by the operator in flight during landing and in training. Methods of increasing the effectiveness of the development process of electrooptic equipment based on rational organization of the development steps and use of computer modeling are studied. 78/00/00 79A20665

UTTL: Simulation of radiation from lightning return strokes - The effects of tortuosity
AUTH: A/LEVINE, D. M.; B/MENEGHINI, R. PAA: B/(NASA, Goddard Space Flight Center, Greenbelt, Md.) CORP: National Aeronautics and Space Administration. Goddard Space Flight Center, Greenbelt, Md. Radio Science, vol. 13, Sept.-Oct. 1978, p. 801-809.
ABS: A Monte Carlo simulation has been developed for the electromagnetic fields radiated from a tortuous lightning channel. This was done using a piecewise linear model for the channel and employing for each element the field radiated by a traveling wave on an arbitrarily oriented filament over a conducting plane. The simulation reproduces experimental data reasonably well and has been used to study the effects of tortuosity on the fields radiated by return strokes. Tortuosity can significantly modify the radiated waveform, tending to render it less representative of the current pulse and more nearly unipolar than one would expect based on the theory for a long straight channel. In the frequency domain the effect of tortuosity is an increase in high frequency energy as compared with an equivalent straight channel. The extent of this increase depends on the mean length of the elements comprising the channel and can be significant. 78/10/00 78A52356

UTTL: Evaluation of rocket triggered lightning for research and development
AUTH: A/LIPPERT, J. R. CORP: Air Force Inst. of Tech., Wright-Patterson AFB, Ohio. CSS: (School of Engineering.)
ABS: The feasibility of using rocket-triggered lightning as a research and development tool for testing hardware is investigated. Previous experimental work in the area is examined and used as the foundation for the experiments in this thesis to establish the significant factors of a successful lightning-triggering station. Using a point charge model, computer simulations were performed to determine the most probable locations of the charge centers associated with the triggered discharge. Five electric field records obtained from field mills were used to perform this simulation. A full scale test technique configuration is proposed for subjecting representative Air Force subsystems and components to the lightning threat. A conclusion is drawn that such a system is feasible at Mt. Baldy, New Mexico with minor augmentations of the existing facilities of the Langmuir laboratory.
RPT#: AD-A100548 AFIT/GE/EE/81J-5 81/05/00 81N28648

UTTL: Lightning transient research on an F-111E aircraft
AUTH: A/MANGOLD, V. L.; B/WALKO, L. C. CORP: Air Force Flight Dynamics Lab., Wright-Patterson AFB, Ohio.
ABS: A simulated lightning test was conducted on an F-111E aircraft (S/N 67-116A) to field test improved measurement techniques and to record and evaluate induced transient voltages on selected electrical circuits to determine their susceptibility to lightning. Technical improvements included (1) a pneumatic system to trigger the simulated lightning current-producing capacitor bank, (2) a change in configuration of current return leads, (3) specially designed breakout boxes and cables, (4) a fiber optics measurement system, and (5) a Tektronix transient digitizer data recording system. The standard 2 x 50 microsecond current pulse was applied to the aircraft (nose-to-tail) and induced voltages were measured and recorded both in the time and frequency domains on 17 different circuits with power off in the aircraft. The magnitude of the current pulse was varied from 0.5 to 5.5 kiloamperes, but most measurements were made at 2.5 kiloamperes. Measurements were made on flight critical circuits of the Altitude-Vertical Speed amplifiers, the Yaw and Roll computers, and the Roll Rate Gyro in the Feel and Trim assembly, on the tail light and right and left wing position light circuits, on the fuel indication circuits, and on the pitot heater circuit (with and without a transient suppressor device). Power-on measurements made on four damper servo circuits resulted in substantially higher induced voltage amplitudes than with power off. Changing aircraft ground points did not affect the magnitude or waveshape of induced transients.
RPT#: AD-A063765 AFFDL-TR-78-1 78/02/00 79N22066

UTTL: Modification of the aurora electromagnetic environment experiment and interpretation
AUTH: A/MANRIQUEZ, R. P.; B/MERKEL, G.; C/SPOHN, D. J. CORP: Harry Diamond Labs., Adelphi, Md.
ABS: In a series of experiments, it has been determined that a simple parallel plate transmission line would behave in a predictable manner when subjected to the 13-MeV-thick target bremsstrahlung produced by the AURORA flash X-ray machine. During the experiment, the following parameters were measured: current into the transmission line, current through the matched termination of the transmission line, the electric field at the bottom plate along the center of the transmission line, and a component of the magnetic field at the center of the transmission line. The experimental results were interpreted with a simple lumped parameter model of the transmission line.
RPT#: AD-A080804 HDL-PR-79-5 79/10/00 80N23534

UTTL: Calculations of lightning return stroke electric and magnetic fields above ground
AUTH: A/MASTER, M. J.; B/UMAN, M. A.; C/LING, Y. T.; D/STANDLER, R. B. PAA: D/(Florida, University, Gainesville, FL) CORP: Florida Univ., Gainesville.
Journal of Geophysical Research, vol. 86, Dec. 20, 1981, p. 12127-12132.
ABS: Lin et al., (1980) presented a lightning return stroke model with which return stroke electric and magnetic fields measured at ground level could be reproduced. This model and a modified version of it, in which the initial current peak decays with height above ground, are used to compute waveforms for altitudes from 0-10 km and at ranges of 20 m to 10 km. Both the original and modified models gave accurate predictions of measured ground-based fields. The use of the calculated fields in calibrating airborne field measurements from simultaneous ground and airborne data is discussed. 81/12/20 82A17714

UTTL: Protection of advanced composites against the direct effects of lightning strikes
AUTH: A/MCCLENAHAN, D. H.; B/PLUMER, J. A. PAA: A/(Lear Fan Corp., Reno, NV); B/(Lightning Technologies, Inc., Pittsfield, MA) IN: International Aerospace Conference on Lightning and Static Electricity, Oxford, England, March 23-25, 1982, Proceedings. Volume 2 (A84-18508 06-01). Abingdon, Oxon, England, Culham Laboratory, 1982, p. G3-1 to G3-9.
ABS: Protective measures must be incorporated to keep lightning strikes from causing severe damage in composite materials. The presently available methods of protection involve the application of a layer or ply of conductive material to a composite laminate, compromising the composite's prospective weight savings and imposing manufacture and repair difficulties. An effort has therefore been made to develop more efficient lightning protection methods. Attention is presently given to a carbon fiber-reinforced composite material which incorporates conductive (aluminum) filaments to disperse lightning strike energies and limit damage, while retaining the physical and structural properties of unprotected composites. The weight increase thus incurred is minimal, and no additional procedures are required in the course of aircraft manufacture. 82/00/00 84A18547

UTTL: Analytical and experimental validation of the lightning transient analysis technique
AUTH: A/MCCORMICK, W.; B/MAXWELL, K. J.; C/FINCH, R.
CORP: Technology, Inc., Dayton, Ohio. CSS: (Instruments and Controls Div.)
ABS: A research program was undertaken to analyze and experimentally validate the Lightning Transient Analysis (LTA) technique using Lightning Simulation Test (LST) data. Using linear systems theory, the LST has been shown to be a linear combination of three transfer functions. These transfer functions were derived and shown to be valid. Specifically, the linear transform of the output pulse (S sub LST (Omega)) was shown to be the product of linear transfer functions of the LST configuration (G sub LST (Omega)), an aperture coupling term (G sub ap (Omega)) and the aircraft wiring/measurement equipment (G sub a/c (Omega)). Recommendations are made to perform analytical and experimental studies to quantify configuration effects; small aperture spatial electromagnetic fields and shielding effects; the pulse response of a wide range of aircraft circuits; the complete nature of aperture coupling, including identification of the dominant and secondary apertures; the effects of possibly distributed versus local excitation points and methods of extending the technique to other aircraft cabling parameters (e.g., terminating impedances, non-linear devices and cable lengths) and to shielded cabling. The amplitude scaling technique should be incorporated into existing routines at the AFFDL Electromagnetic Hazards Group data acquisition and processing system.
RPT#: AD-A063991 AFFDL-TR-78-47 78/03/00 79N22358

UTTL: E and H fields measurements on the Transall C160 aircraft during lightning flashes
AUTH: A/MOREAU, J. P.; B/ALLIOT, J. C. PAA: B/(ONERA, Chatillon-sous-Bagneux, France) (International Conference on Lightning and Static Electricity, Paris, France, June 10-12, 1985) ONERA, TP, no. 1985-48, 1985, 8 p.
ABS: An airborne experiment was carried out to study the microphysical, dynamic, and thermodynamic properties of frontal systems and to determine the main parameters of electrical and electromagnetic phenomena associated with cloud discharges. It is found that a lightning flash lasts several hundred milliseconds and that there are two kinds of flashes, i.e., those beginning with a train of pulses lasting milliseconds and followed by solitary pulses (75 percent of the cases) and those beginning with solitary pulses. Typical E and H field waveforms for the duration of the flashes, recorded with a 2-MHz-bandwidth analog device, are presented, as are E and H waveforms obtained with 100-MHz-bandwidth transient digitizers and electromagnetic transfer functions of a well defined aperture installed on the aircraft fuselage.
RPT#: ONERA, TP NO. 1985-48 85/00/00 85A47259

UTTL: EMP hardening of aircraft by closing the points-of-entry
AUTH: A/MORGAN, G. E. PAA: A/(Rockwell International Corp., Anaheim, Calif.) In: International Symposium on Electromagnetic Compatibility, San Antonio, Tex., October 7-9, 1975, Record. (A77-15401 04-33) New York, Institute of Electrical and Electronics Engineers, Inc., 1975, p. 3AIId1-3AIId8.
ABS: EMP (electromagnetic pulse) couples radio frequency energy into aircraft cables by a series of interactions with the total system. In a series of trade studies it was concluded that to harden the C-130 aircraft against EMP, it would be most cost effective to begin by closing the points of entry into the fuselage. It was indicated that this would provide the greatest benefit in improving hardness with the least effect on cost, weight, reliability, and maintainability. A detailed investigation was begun to identify all the points of entry on the C-130, and to devise ways to close them. This paper presents preliminary results of this investigation. 75/00/00 77A15408

UTTL: Comparison of the electromagnetic properties of lightning and EMP (Electromagnetic pulse): Results of recent lightning studies
AUTH: A/NANEVICZ, J. E.; B/VANCE, E. F.; C/HAMM, J. M.; D/BUBENIK, D. M. CORP: SRI International Corp., Menlo Park, Calif.
ABS: This report presents the results of the first phase of a program conducted by SRI International in an effort to address and resolve issues concerning the comparative interactions of lightning and EMP with aircraft. The program concentrated on using recently generated analytical and experimental data and interacting with lightning workers in an effort to define the current state of knowledge regarding the electromagnetic properties of lightning. This program was motivated by suggestions that there might be sufficient similarity between the effects of lightning and EMP that consideration of the electromagnetic effects of one would also suffice for the other.
RPT#: AD-A154325 AD-E301685 DNA-TR-82-204 83/06/30 85N30560

UTTL: LTRI - Industry cooperative program research on the Concorde SST
AUTH: A/NEWMAN, M. M.; B/REYNOLDS, S. T. M. CORP: British Aircraft Corp. (Operating) Ltd., Bristol (England). IN AFSC LIGHTNING AND STATIC ELEC. CONF., PT 2 MAY 1969 P 104-110 /SEE N70-19027 07-02/ 69/05/00 70N19034

UTTL: The effects of high intensity electrical currents on advanced composite materials
AUTH: A/PENTON, A. P.; B/PERRY, J. L.; C/LLOYD, K. J. CORP: Philco-Ford Corp., Newport Beach, Calif.; General Electric Co., Pittsfield, Mass. CSS: (Aeronutronic Div.)
ABS: The objective of the program was to perform a research study to investigate high intensity electric current flow of such magnitude and waveform as might result from lightning strikes, and to characterize the resulting degradation in advanced composites and to investigate means of providing internal protection from such damage.
RPT#: AD-740822 U-5018 72/03/21 72N30514

UTTL: Induced effects of lightning on an all composite aircraft
AUTH: A/PERALA, R. A.; B/COOK, R.; C/LEE, K. PAA: B/(Electro Magnetic Applications, Inc., Golden, Colo.) ; C/(Mission Research Corp., Albuquerque, N. Mex.) In: Electromagnetic compatibility 1979; Proceedings of the Third Symposium and Technical Exhibition, Rotterdam, Netherlands, May 1-3, 1979. (A80-27753 10-32) Zurich, Eidgenoessische Technische Hochschule Zuerich, 1979, p. 421-424.
ABS: The paper presents results for lightning induced cable currents and voltages on typical cable runs inside an all composite aircraft. Consideration is given to both a direct stroke and a nearby stroke. Attention is also given to results for the case in which the aircraft is coated with 6-mil aluminum flame spray. Finally, it is shown that, as expected, the direct stroke induces the largest voltages, but that the effects of the nearby strike are not negligible. 79/00/00 80A27783

UTTL: Laboratory test procedures to determine lightning attachment points on actual aircraft parts /A qualification test/
AUTH: A/PLUMER, J. A. PAA: A/(Lightning Technologies, Inc., Pittsfield, Mass.) In: Conference on Certification of Aircraft for Lightning and Atmospheric Electricity Hazards, Chatillon-sous-Bagneux, Hauts-de-Seine, France, September 14-21, 1978. Proceedings. (A79-51126 23-09) Chatillon-sous-Bagneux, Hauts-de-Seine, France, Office National d'Etudes et de Recherches Aerospatiales, 1979, p. 12-1 to 12-12.
ABS: Lightning flashes initially attach to aircraft extremities such as the nose, wing tips or vertical fin cap. If these extremities are covered with non-metallic skins such as fiberglass radomes, wing tips, or plastic antenna fairings, the lightning flash may puncture the skin and attach to a conductor within. Conductive diverters or other means may be necessary to protect against such punctures. Whether punctures occur or not depends upon the geometry of the structure and diverter arrangement (if present), the dielectric strength of the non-metallic skin, and the rate of rise of the electric field presented by the advancing leader. A test in which this electric field is simulated and applied to a full size replica of the structure in question may be utilized to determine the need for protection or verify its adequacy. This test is also utilized to identify lightning strike zone boundaries on metallic or advanced composite surfaces, and to determine whether windshields or canopies may be punctured by re-strikes occurring in swept lightning flashes. Typical high voltage test circuits, electrode arrangements and other considerations are described. 79/00/00 79A51133

UTTL: Status of research into lightning effects on aircraft
AUTH: A/PLUMER, J. A. CORP: General Electric Co., New York. In NASA. Langley Res. Center Aircraft Safety and Operating Problems p 337-354 (SEE N77-18081 09-03)
ABS: Developments in aircraft lightning protection since 1938 are reviewed. Potential lightning problems resulting from present trends toward the use of electronic controls and composite structures are discussed, along with presently available lightning test procedures for problem assessment. The validity of some procedures is being questioned because of pessimistic results and design implications. An in-flight measurement program is needed to provide statistics on lightning severity at flight altitudes and to enable more realistic tests, and operators are urged to supply researchers with more details on electronic components damaged by lightning strikes. A need for review of certain aspects of fuel system vulnerability is indicated by several recent accidents, and specific areas for examination are identified. New educational materials and standardization activities are also noted. 76/00/00

77N18099

UTTL: Broadband electromagnetic environments simulator (EMES)
AUTH: A/POLLARD, N. CORP: Sandia Corp., Albuquerque, N. Mex. Presented at IEEE Intern. Symp. on Electromagnetic Compatibility, Seattle, 2 Aug. 1977
ABS: A test facility developed for determining the effects of electromagnetic environments on systems and components is described. The facility is capable of producing uniform, vertically polarized, continuous wave (CW) and pulsed fields over the frequency range of dc to 10 GHz. This broadband capability addresses the electromagnetic radiation (EMR) threat and is ideally suited to computer controlled sweeping and data acquisition. The facility is also capable of producing uniform transient fields having the wave shape and magnitude characteristic of a nuclear electromagnetic pulse (EMP) and near lightning. The design consists of a truncated, triplate, rectangular coaxial transmission line. At frequencies below the first resonance of the facility it behaves as a typical coaxial system. Above resonance, a wall of electromagnetic absorbing material provides a nonreflecting termination. Thus, EMES essentially combines the elements of a transmission line and an anechoic chamber.
RPT#: SAND-77-0039C CONF-770806-1 77/00/00 78N14233

UTTL: Lightning protection systems for fiber-composite structural components
AUTH: A/PROPP, H.-J. PAA: A/(Vereinigte Flugtechnische Werke-Fokker GmbH, Bremen, West Germany) Deutsche Gesellschaft fuer Luft- und Raumfahrt, Symposium ueber neue Bauweisen und Fertigungsverfahren in der Luftfahrt, Munich, West Germany, Sept. 17, 1976, 19 p. In German.
ABS: It is possible that aircraft during a flight can be struck by lightning. All components of an aircraft should, therefore, be designed and protected in such a way that they remain fully functional in case of an average lightning stroke. Emergency flight capabilities should be assured even in case of the worst possible conditions related to lightning hazards. Aircraft components made of materials with novel characteristics are to be tested under simulated lightning conditions which correspond to the actual conditions. Components made of glass-fiber reinforced plastics require only a protection if below them are systems which have to be protected. A lightning-protection strap can be used. In case of carbon or boron fibers as reinforcing agents more elaborate systems including a multilayer protective system have to be used. Tests have demonstrated that the described protective systems are fully effective.
RPT#: DGLR PAPER 76-234 76/09/00 77A43589

UTTL: A compendium of lightning effects on future aircraft electronic systems
AUTH: A/RASCH, N. O. CORP: Federal Aviation Administration, Atlantic City, N.J. Proc. of Conf. held at Hampton, Va., 4-6 Nov. 1981
ABS: This publication is a composite of presentations given at the NASA-Langley Research Center/FAA Technical Center 'Lightning Effects on Future Aircraft Systems Workshop' held on November 4-6, 1981, at the NASA-Langley Research Center Facility. The presentations encompassed the full spectrum of lightning research from lightning phenomonology, lightning modeling, electromagnetic issues associated with composite materials, to the lightning/aircraft electromagnetic interaction analysis. Also included are a total of five presentations assessing the Digital System upset phenomena.
RPT#: AD-A114117 DOT/FAA/CT-82/30 82/02/00 82N28293

UTTL: Transient penetration effects on aerospace vehicle electronics and fuel systems
AUTH: A/ROBB, J. D. CORP: Lightning and Transients Research Inst., Minneapolis, Minn. IN AFSC LIGHTNING AND STATIC ELEC. CONF., PT. 2 MAY 1969 P 145-154 /SEE N70-19027 07-02/ 69/05/00 70N19038

UTTL: Mechanisms of lightning damage to composite materials
AUTH: A/ROBB, J. D. CORP: Lightning and Transients Research Inst., Minneapolis, Minn. IN AFSC LIGHTNING AND STATIC ELEC. CONF., PT. 2 MAY 1969 P 520-529 /SEE N70-19027 07-02/ 69/05/00 70N19059

UTTL: Analysis and measurements of low frequency lightning component penetration through aerospace vehicle metal and graphite skins
AUTH: A/ROBB, J. D.; B/CHEN, T. PAA: B/(Texas Instruments, Inc.) CORP: Lightning and Transients Research Inst., Minneapolis, Minn. In NASA. Langley Res. Center Lightning Technol. p 431-448 (SEE N80-21927 12-47)
ABS: An analysis of the shielding properties of mixed metal and graphite composite structures has illustrated some important aspects of electromagnetic field penetration into the interior. These include: (1) that graphite

access doors on metallic structures will attenuate lightning magnetic fields very little; conversely, metal doors on a graphite structure will also attenuate fields from lightning strike currents very little, i.e., homogeneity of the shield is a critical factor in shielding and (2) that continuous conductors between two points inside a graphite skin such as an air data probe metallic tubing connection to an air data computer can allow large current penetrations into a vehicle interior. The true weight savings resulting from the use of composite materials can only be evaluated after the resulting electromagnetic problems such as current penetrations have been solved, and this generally requires weight addition in the form of cable shields, conductor bonding or external metallization. 80/04/00 80N21951

UTTL: EMP induced currents on a simplified missile theory and experiment
AUTH: A/RODGER, K. S. PAA: A/(Aeroplane and Armament Experimental Establishment, Boscombe Down, Wilts., England) In: Electromagnetic compatibility; Proceedings of the Second Symposium and Technical Exhibition, Montreux, Switzerland, June 28-30, 1977. (A78-39076 16-32) New York, Institute of Electrical and Electronics Engineers, Inc., 1977, p. 377-382.
ABS: To improve understanding of the EM pulse hazard to aircraft and airborne systems, experimental and theoretical investigations of the currents induced by a nuclear EM pulse in a simply modeled airborne missile have been conducted. The model includes a two-wire transmission line external to the cylindrical missile but terminating in two internal resistors. Frequency-domain expressions for the currents induced in the loads are transformed by analytical means into the time domain. The analytical evaluations are in adequate agreement with the experimental data, except for the first nanosec of the EM pulse. 77/00/00 78A39109

UTTL: An approach to EMP testing of complete strike aircraft
AUTH: A/RODGER, K. S. PAA: A/(Aeroplane and Armament Experimental Establishment, Boscombe Down, Wilts., England) In: Electromagnetic compatibility; Proceedings of the Second Symposium and Technical Exhibition, Montreux, Switzerland, June 28-30, 1977. (A78-39076 16-32) New York, Institute of Electrical and Electronics Engineers, Inc., 1977, p. 95-98.
ABS: Development of a nuclear EM pulse (NEMP) testing procedure for a strike aircraft is discussed. Difficulties arise in NEMP testing because of the low symmetry of aircraft with complex equipment, and because of allowances needed for the proximity of the simulator. Models for treating NEMP response of simple cavities, coupled cavities with wires, and wires behind screens without cavities are reviewed. Since transient NEMP causes many components to fail by energy overload, it may be possible to stipulate protection requirements with some ease. 77/00/00 78A39088

UTTL: Assessing the behavior of high modulus composite materials in lightning
AUTH: A/ROUCHON, J.; B/GALL, D. CORP: Centre d'Essais Aeronautique Toulouse (France). In AGARD Effect of Serv. Environ. on Composite Mater. 14 p (SEE N81-11128 02-24)
ABS: Lightning strikes of aircraft in flight are relatively frequent and result in damage and even destruction to both equipment and structures, particularly those made of composite materials. Generalities about lightning are reviewed and methods for measuring it during flight and simulating it on the ground are described. Results are presented for laboratory tests on carbon-epoxy monolithic and boron-epoxy coated sandwich specimens, and on the elements of real structures. Associated control processes are also considered. 80/08/00 81N11141

UTTL: Evaluation of the behavior of structures made of high modulus composite materials when struck by lightning
AUTH: A/ROUCHON, J.; B/GALL, D. CORP: National Aeronautics and Space Administration, Washington, D.C. Presented at 50th Reunion of the Struct. and Mater. Panel, Specialists Meeting on Effect of Service Environ. on Composite Mater., Athens, 13-18 Apr. 1980
ABS: Lightning strikes on aircraft are a relatively frequent phenomena which result in damage to the equipment as well as to structures, especially parts made of composite materials. General information about lightning (measurements of the characteristics of lightning during flight, simulation procedures on the ground) is followed by results of the tests carried out at the laboratory on samples (monolithic carbon epoxy samples, sandwich samples covered with boron epoxy covering) and tests with real structures. The associated control procedures are described.
RPT#: NASA-TM-75866 81/01/00 81N20188

UTTL: Extending and interfacing the MSEP semiconductor damage data bank for analysis and retrieval by DAMTRAC
AUTH: A/RUZIC, C. P. CORP: Harry Diamond Labs., Adelphi, Md.
ABS: Presented are four groups of programs to update, maintain, and list the diode and transistor data bases for use with circuit analysis codes. The data bases are specifically designed to work with the DAMTRAC code, but can work with other circuit analysis codes, too. Included in the data bases are the standard TRAC parameters, references to the sources of these parameters, and damage parameters with individual source references.
RPT#: AD-A050845 HDL-TR-1821 77/12/00 78N22752

UTTL: Foundation of the magnetic field integral equation code for the calculation of the electromagnetic pulse external interaction with aircraft
AUTH: A/SANCER, M. I.; B/SIEGEL, S.; C/VARVATSIS, A. D. CORP: TDR, Inc., Los Angeles, Calif.
ABS: This report presents the equations that are programmed along with their derivations and the underlying theory. The code determines the current density and charge density induced on a model of an aircraft. The equations that are programmed result from patch zoning the aircraft model in order to obtain a solution to the frequency domain representation of the magnetic field intergral equation. The intent is to obtain solutions for a continuous spectrum that includes the low and resonant range of frequencies corresponding to the bulk of the energy in a typical EMP spectrum.
RPT#: AD-A039953 AFWL-TR-76-279 77/04/00 77N31389

UTTL: System for radio remote control of dropping bombs
AUTH: A/SCHEIDEGGER, A.; B/ZELLWEGER, E. CORP: Autophon A.G., Solothurn (Switzerland).
ABS: A system for radio control of a series of bombs which have to be dropped shortly one after another was developed. The bombs are dropped at short intervals. The first contains a transmitter and serves as leading bomb; the other bombs contain a receiver. During its fall the leading bomb emits unmodulated and uncoded pulses, and the receivers avoid ignition as long as the pulses are received. The ignition occurs when the leading bomb reaches the ground and detonates, interrupting the pulse emission. An air propeller delivers the energy for transmitter and receivers.
RPT#: CH-639335-A5 INTL-CL.B64D-1/06 INTL-CL.F42C-15/40 INTL-CL.F42C-15/12 83/11/15 85N25371

UTTL: Fabrication of composite materials: Source book
AUTH: A/SCHWARTZ, M. M. PAA: A/(United Technologies Corp., Sikorsky Aircraft, Stratford, CT) Metals Park, OH, American Society for Metals, 1985, 414 p. No individual items are abstracted in this volume.
ABS: Practical engineering guidelines for the selection and manipulation of composite materials are presented in a collection of recently published reviews and reports, with a focus on polymer-reinforced composites and metal-reinforced metal-matrix composites. Consideration is given to joining, trimming and cutting, painting, drilling, and machining; and diagrams, photographs, micrographs, graphs, and tables of numerical data are provided. 85/00/00 85A42219

UTTL: Skynet applications software package (SASP) programmer's handbook
AUTH: A/SCOTT, W. J.; B/HILLER, J. R. CORP: Harry Diamond Labs., Adelphi, Md.
ABS: The objective of the Defense Nuclear Agency (DNA) sponsored SKYNET program is to develop a methodology for the assessment of satellite vulnerability to system generated electromagnetic pulse (SGEMP) effects from nuclear weapons. The approach includes a study of basic phenomenology and development of cost-effective simulation techniques, as well as improving SGEMP instrumentation and data acquisition and recording techniques. This report summarizes the software developed to acquire and reduce SGEMP data on satellite models for the SKYNET project. Included are comprehensive descriptions of the tasks, subroutines, and common areas. Accompanied by the source and task builder listings and the companion volume titled SKYNET Applications Software Package (SASP) Operator's and User's Handbook, this material provides the reader with a detailed explanation of the SGEMP Transportable Automated Recording System (STARS) operation.
RPT#: AD-A057116 HDL-TR-1828 77/11/00 79N10115

UTTL: SKYNET Applications Software Package (SASP) operator's and user's handbook
AUTH: A/SCOTT, W. J.; B/HILLER, J. R. CORP: Harry Diamond Labs., Adelphi, Md.
ABS: The objective of the Defense Nuclear Agency sponsored SKYNET program is to develop a methodology for the assessment of satellite vulnerability to system generated electromagnetic pulse (SGEMP) effects from nuclear weapons. The approach includes a study of basic phenomenology and development of cost-effective simulation techniques, as well as improving SGEMP instrumentation and data acquisition and recording techniques. This report presents a new procedure for

capturing and processing complex SGEMP transients. The method is incorporated into an SGEMP Transportable Automated Recording System (STARS). It reduces manual data handling significantly (a major source of errors); outputs data as computer compatible magnetic tapes, annotated hard copies, or both; and lessens the manpower requirements for data acquisition and processing. The software implementation, SKYNET Applications Software Package (SASP), is discussed here to provide STARS operators and users with the detailed information needed to effectively utilize the system. A companion volume, the SKYNET Applications Software Package (SASP) Programmer's Handbook, contains detailed summaries of all SASP source codes.
RPT#: AD-A044411 HDL-TR-1817 77/08/00 78N12120

UTTL: Electrical bonding of advanced airplane structures
AUTH: A/SHORT, L. E. CORP: Boeing Co., Seattle, Wash. IN AFSC LIGHTNING AND STATIC ELEC. CONF., PT. 2 MAY 1969 P 425-441 /SEE- N70-19027 07-02/ 69/05/00 70N19054

UTTL: Treatment of late time instabilities in finite-difference EMP scattering codes
AUTH: A/SIMPSON, L. T.; B/HOLLAND, R.; C/ARMAN, S. PAA: C/(Mission Research Corp., Albuquerque, NM) (IEEE, DOD, NASA, and DOE, Annual Conference on Nuclear and Space Radiation Effects, 19th, Las Vegas, NV, July 20-22, 1982.) IEEE Transactions on Nuclear Science, vol. NS-29, Dec. 1982, p. 1943-1948.
ABS: Constraints applicable to a finite difference mesh for solution of Maxwell's equations are defined. The equations are applied in the time domain for computing electromagnetic coupling to complex structures, e.g., rectangular, cylindrical, or spherical. In a spatially varying grid, the amplitude growth of high frequency waves becomes exponential through multiple reflections from the outer boundary in cases of late-time solution. The exponential growth of the numerical noise exceeds the value of the real signal. The correction technique employs an absorbing surface and a radiating boundary, along with tailored selection of the grid mesh size. High frequency noise is removed through use of a low-pass digital filter, a linear least squares fit is made to thy low frequency filtered response, and the original, filtered, and fitted data are merged to preserve the high frequency early-time response. 82/12/00 83A17532

UTTL: Electromagnetic coupling analysis of a learjet aircraft
AUTH: A/STRAWE, D. F.; B/OBYRNE, M.; C/SANDBERG, S. CORP: Boeing Co., Seattle, Wash.
ABS: This report presents the results of an electromagnetic modeling analysis of a Learjet aircraft. Coupling models were developed for the aircraft exterior and selected internal cabling. Calculations of pulse induced responses were made using the computer codes WIRANT and TRAFFIC. The calculated responses were compared to test data obtained by AFFDL. Lightning-induced responses were also calculated for a nearby 20 kiloampere stroke.
RPT#: AD-A062490 D180-24256-1 AFFDL-TR-78-121 78/09/00 79N20311

UTTL: Methods for reducing electrostatic hazards in space launchers
AUTH: A/TAILLET, J. PAA: A/(ONERA, Chatillon-sous-Bagneux, Hauts-de-Seine, France) In: Conference on Lightning and Static Electricity, Abingdon, Oxon, England, April 14-17, 1975, Proceedings. (A76-14402 03-01) London, Royal Aeronautical Society, 1975. 12 p.
ABS: A summary is presented of investigations concerned with a reduction of electrostatic hazards in the Europa II and Diamant-BP4 launchers. The origin of the work is related to the dramatic failure of the F11 Europa II launch on November 5, 1971. The cause of the failure was electrostatic charging of an ungrounded screen by a current of a few tens of microamperes flowing during three seconds. The nature and origin of electrostatic hazards in space launchers are discussed along with approaches for reducing these hazards.
RPT#: ONERA, TP NO. 1975-21 75/00/00 76A14441

UTTL: Protection of launch vehicles against electrostatic hazards
AUTH: A/TAILLET, J.; B/BOULAY, J.-L. PAA: B/(ONERA, Chatillon-sous-Bagneux, Hauts-de-Seine, France) L'Aeronautique et l'Astronautique, no. 83, 1980, p. 45-58. In French. Research supported by the European Space Agency.
ABS: After a brief review of electrostatic hazards in spacecraft flight, the paper examines the basic mechanisms that lead to the accumulation of static charge on launch vehicles and the transfer of charge to sensitive elements of the systems. The general principles for the protection of vehicles against electrostatic charge are described, with emphasis on the conditioning of insulating surfaces. Some applications concerning the Ariane launcher are described.

RPT#: ONERA, TP NO. 1980-138 80/00/00 81A15120

UTTL: Atmospheric electricity and air transport safety
AUTH: A/TAILLET, J. PAA: A/(ONERA, Chatillon-sous-Bagneux, Hauts-de-Seine, France) (Societe Francaise de Physique, Journees Physique et Industrie, Lyons, France, Sept. 13, 14, 1982.) ONERA, TP no. 1982-82, 1982. 13 p. In French.
ABS: Atmospheric electricity hazards to avionics and structural components of aircraft featuring computerized equipment and composite materials are reviewed, together with the level of knowledge of natural electrical threats to aircraft and investigative techniques. The threats comprise static charge build-up and lightning strikes. Electrostatic charging occurs over a period of time, and is caused by airframe contact with ice or particulate aerosols, or by passage through intense electromagnetic fields near cumulonimbus clouds. The charges accumulate around antennas and electronic components, producing degraded communications and navigational capabilities. Numerious hazards are present with lightning strikes, the most serious being wing rupture and subsequent crash of the aircraft. Composite materials are less conductive than metal, although lighter and therefore preferred for fuel efficiency. Various experimental efforts to characterize lightning, through its artificial generation and flights through storm clouds, and its effects, in terms of damage to materials and paths through structures and electronic circuitry, are described.
RPT#: ONERA, TP NO. 1982-82 82/00/00 83A14534

UTTL: Aircraft lightning protection
AUTH: A/TAILLET, J. PAA: A/(ONERA, Chatillon-sous-Bagneux, Hauts-de-Seine, France) L'Aeronautique et l'Astronautique, no. 93, 1982, p. 37-52. In French.
ABS: Currently known effects of lightning on aircraft and interior components are reviewed, along with measures which must be taken in order to make the broad use of composites acceptable in future aircraft. The types of accident lightning strikes have inflicted on USAF aircraft in the period 1970-1980 are examined, noting that catastrophic failures occurred due to damage to the control and navigation systems, electronics, and explosions of fuel or armaments. The introduction of increasing amounts of composite materials in the aircraft structures, parts which may cause resistance to the lightning path, and the use of electronic controls which can be degraded by electromagnetic pulses pose difficulties when the introduction of cost-saving measures is also life-endangering. The points of lightning attachment are examined, along with the effects on the aircraft components. It is recommended that composite parts be covered with a thin metallic film which conducts the current freely away from the composite, and that microelectronic circuitry be hardened against EMP.
RPT#: ONERA, TP NO. 1982-51 82/00/00 82A33544

UTTL: The past and future of lightning studies
AUTH: A/TAILLET, J. PAA: A/(ONERA, Chatillon-sous-Bagneux, Hauts-de-Seine, France) (Societe Francaise de Physique, Congres, Toulouse, France, June 25-30, 1979.) ONERA, TP no. 1979-92, 1979. 8 p. In French.
ABS: The historical background and current status of lightning research are reviewed. Attention is given to the possibility of developing a self-consistent theory of lightning physics, taking into account charge generation in clouds as well as the discharge process. Attention is given to the study of lightning in planetary atmospheres, with particular emphasis on Venera missions.
RPT#: ONERA, TP NO. 1979-92 79/00/00 79A49540

UTTL: External interaction of the nuclear EMP with aircraft and missiles
AUTH: A/TAYLOR, C. D. PAA: A/(Mississippi State University, Mississippi State, Miss.) IEEE Transactions on Antennas and Propagation, vol. AP-26, Jan. 1978, p. 64-76. USAF-supported research.
ABS: The external coupling of nuclear EMP to metal aircraft and missile structures is discussed, with particular attention given to the cases of the EC-135 and the B-1 aircraft. Experimental data for the skin current and charge densities induced on the two types of aircraft are presented; the experiments involve continuous wave testing and the construction of the response to the nuclear EMP through use of Fourier frequency superposition. The experimental results are compared with numerical calculations developed on the basis of aircraft models formed by bodies of revolution or intersecting sections of wires. 78/01/00 78A21989

UTTL: Internal interaction analysis. Topological concepts and needed model improvements
AUTH: A/TESCHE, F. M.; B/MORGAN, M. A.; C/FISHBINE, B. H.; D/PARKINSON, E. R. CORP: Science Applications, Inc., Berkeley, Calif.
ABS: This report introduces and formalizes various topological concepts for defining internal interaction problems. A preliminary examination of presently-used internal interaction models is made, and indications

of possible improvements are given. Finally, a brief discussion of possible statistical approaches to the internal interaction problem is presented.
RPT#: AD-A027047 AFWL-TR-75-282 76/05/00 77N15250

UTTL: Comparison of lightning flash rates from the PBE sensor and streak counting from the DMSP satellite
AUTH: A/TURMAN, B. N. CORP: Sandia National Labs., Albuquerque, N. Mex. Presented at 7th Conf. on Atmospheric Elec., Albany, 4 Jun. 1984
ABS: Lightning trigger rates from the PRE sensor and streaks recorded by the accompanying optical scanners were compared. The comparison provides a calibration between these two lightning detection techniques. The areal sensitivity of the optical scanner for lightning detection (2.6 x 10(4) km(2) is inferred from this calibration. Lightning flash density are calculated from equations 9 and 10, and global flash densities were calculated for dawn, dusk, and midnight for September to November 1977. The global flash rate was estimated to be about 50 s(-1). Lightning observations from a low altitude satellite are very limited. The measurements give a rough estimate of lightning flash density, averaged over large areas and long times. A more sophisticated lightning detector on a geosynchronous satellite platform is required for full time monitoring of lightning activity to generate more accurate flash density data.
RPT#: DE84-006722 SAND-83-2233C CONF-840668-1 84/00/00 84N30602

UTTL: A comparison of lightning electromagnetic fields with the nuclear electromagnetic pulse in the frequency range 10 to the 4th to 10 to the 7th Hz
AUTH: A/UMAN, M. A.; B/MASTER, M. J.; C/KRIDER, E. P. PAA: A/(Florida, University, Gainesville, FL; Lightning Location and Protection, Inc., Tucson, AZ); B/(Bell Telephone Laboratories, Inc., Holmdel, NJ); C/(Arizona, University; Lightning Location and Protection, Inc., Tucson, AZ) IEEE Transactions on Electromagnetic Compatibility, vol. EMC-24, Nov. 1982, p. 410-416. Research supported by SRI International
ABS: The electromagnetic fields produced by both direct lightning strikes and nearby lightning are compared with the nuclear electromagnetic pulse (NEMP) from an exoatmospheric burst. Model calculations indicate that, in the frequency range from 10 kHz to near 10 MHz, the Fourier amplitude spectra of the return stroke magnetic fields near ground 1 m from an average lightning strike will exceed that of the NEMP. Nearby first return strokes at a range of about 50 m, if they are severe, produce electric field spectra near ground which exceed that of the NEMP below about 1 MHz, while the spectra of average nearby first return strokes exceed that of the NEMP below about 300 kHz. Implications of these results for aircraft in flight are discussed. 82/11/00 83A14550

UTTL: Atmospheric electricity hazards analytical model development and application. Volume 1: Lightning environment modeling
AUTH: A/UMAN, M. A.; B/KRIDER, E. P. PAA: A/(Lightning Location and Protection, Inc.); B/(Lightning Location and Protection, Inc.) CORP: Electro Magnetic Applications, Inc., Denver, Colo.
ABS: The state of the art of lightning phenomenology and its electromagnetic environment is reviewed. All aspects and phases are discussed. A model is chosen for each phase which best describes what is currently known and understood. Computer models for predicting the electromagnetic environment for several of the processes are given, along with numerical predictions. A comprehensive bibliography is also provided.
RPT#: AD-A114015 EMA-81-R-21-VOL-1 AFWAL-TR-81-3084-VOL-1 81/08/00 82N29800

UTTL: Radiation-hardened integrated circuit amplifier: Nuclear weapon effects susceptibility study
AUTH: A/VAULT, W. L.; B/HARPER, L. CORP: Harry Diamond Labs., Adelphi, Md.
ABS: The objective of this program was to measure the permanent degradation and transient circuit response of a radiation-hardened operational amplifier, developed for long-wave infrared (LWIR) sensors, to simulate nuclear weapon effects environments. These included transient radiation effects (TRE), system-generated electromagnetic pulse (SGEMP), and combined nuclear radiation and electrical pulse effects.
RPT#: AD-A029026 HDL-TR-1759 76/08/00 77N16277

UTTL: Effects of lightning and nuclear electromagnetic pulse on an advanced composites aircraft
AUTH: A/VOLPE, V.; B/CARRI, R. PAA: B/(Grumman Aerospace Corp., Bethpage, NY) In: Fibrous composites in structural design. (A82-27126 12-05) New York, Plenum Press, 1980, p. 341-357.
ABS: Tests with a 1/2 scale model of the Advanced Design Composite Aircraft (ADCA) made of graphite/epoxy for the effects of lightning strikes and the development of a mathematical model to define the internal and external coupling for nuclear and EM pulses are reported. The lightning strike portion of the trails

determined the attachment points, their distribution, and the frequency of occurrence. Features of the test model are outlined, along with trial procedures which included directions of the emitting electrodes to simulate yaw, pitch, and roll. Each extremity drew an equal number of strikes, and some degradation of the composite structure was observed at locations of multiple strikes. Nuclear EM pulses were examined and it was found that external coupling is concerned only with composite conductivities parallel to the surface, the aircraft is an infinite conductor, and charge and current densities were quantified and are provided. 80/00/00 82A27144

UTTL: Lightning simulation facilities in the United States and Europe
AUTH: A/WALKO, L. C.; B/HEBERT, J. L. PAA: B/(USAF, Wright Aeronautical Laboratories, Wright-Patterson AFB, OH) American Institute of Aeronautics and Astronautics, Aerospace Sciences Meeting, 23rd, Reno, NV, Jan. 14-17, 1985. 7 p.
ABS: The use of sophisticated avionics systems and non-metallic structures has enhanced aircraft susceptibility to, and the need for protection from, the lightning threat. Some of the lightning aspects may be simulated and this has established lightning simulation as a valuable aid in aircraft design. This paper describes the lightning threat and existing lightning simulation standards. It overviews lightning simulation facilities in the United States and Europe.
RPT#: AIAA PAPER 85-0093 85/01/00 85A19515

UTTL: Full scale lightning test technique
AUTH: A/WALKO, L. C.; B/SCHNEIDER, J. G. PAA: B/(Technology/Scientific Service, Inc.) CORP: Air Force Wright Aeronautical Labs., Wright-Patterson AFB, Ohio. In NASA. Langley Res. Center Lightning Technol. p 449-450 (SEE N80-21927 12-47)
ABS: A test technique was developed for applying a full scale mean value (30 kiloampere peak) simulated lightning return stroke current on a complete flight ready aircraft to assess the threat of lightning to aircraft electrical circuits. A computer-aided generator design was used to establish the parameters of the test system. Data from previous work done on development of low inductance current paths determined the basic system configuration. 80/04/00 80N21952

UTTL: Electromagnetic coupling to advanced composite aircraft with application to trade-off and specification determination
AUTH: A/WALLENBERG, R.; B/BURT, E.; C/DIKE, G. CORP: Syracuse Research Corp., N. Y. In AGARD Electromagnetic Effects of (Carbon) Composite Mater. Upon Avionics Systems 22 p (SEE N81-16144 07-24)
ABS: A major concern with the increasing use of composite materials and low voltage electronics is the amount of electromagnetic coupling to the interior of an aircraft and to the cables and electronic devices within it. Simple methods are described for determining the shielding provided by an aircraft's exterior surface and the coupling of the interior fields to cables and transmission lines within aircraft cavities. The results can be used to determine tradeoffs between electromagnetic shielding, weight, and cost. 80/10/00 81N16166

UTTL: Advanced composite aircraft electromagnetic design and synthesis
AUTH: A/WALLENBERG, R. F.; B/BIRKEN, J. A.; C/MILTON, O. PAA: A/(Syracuse Research Corp., N.Y.); B/(Naval Air System Command, Washington, D.C.) CORP: Sandia National Labs., Albuquerque, N. Mex. CSS: (Div. 1556.) Presented at the IEEE Intern. Symp. on Electromagnetic Compatability Record, Boulder, Colo., 18-20 Aug. 1981
ABS: The ramifications of using advanced composite materials in more upcoming aircraft were investigated. Mission requirements include fly by wire systems surviving increased threats when contained in a composite material fuselage which generally provides poor electromagnetic shielding. The coupling of lightning and a nuclear electromagnetic pulse to aircraft comprised of composite materials are addressed.
RPT#: SAND-81-1278C CONF-810816-1 SRC-TR-81-1170 81/04/00 81N33200

UTTL: Design practices for EMP protection of military systems
AUTH: A/WOUTERS, L. F. CORP: California Univ., Livermore. Lawrence Radiation Lab. PRESENTED AT TECH. COOP. PROGRAM PANEL N-4 MEETING, LONDON, 3 APR. 1968
RPT#: UCRL-71024-REV-1 CONF-71024-1 68/04/10 69N17128

UTTL: Shielded enclosures for experimental studies of shielding topology

AUTH: A/YANG, F. C.; B/LEE, K. S. H.; C/KOKOROWSKI; S. A.; D/BAUM, C. E.; E/HAMM, J.; F/GRAF, W.; G/VANCE, E. F. CORP: Dikewood Corp., Albuquerque, N. Mex.

ABS: The report discusses the effort to provide shielded enclosures for EMP experimental studies of shielding topology. Section 1 discusses the theoretical modeling for which scattering matrices of subshields and their norms are used to relate the internal signals to the electromagnetic source environment. Both the line and aperture penetrations are included in the scattering matrix formulation. Experimental and analytical methods are proposed for estimating parameters of the scattering matrices. It is pointed out in the discussion that these methods can, in turn, be employed.to analyze the overall shielding performance and to synthesize the subshield requirements of a system. The discussion in Section 1 includes an illustrative example. Section 2 describes experiments to characterize and quantify the shielding performance of a rectangular metal enclosure containing various line and aperture penetrations. Experimental techniques and procedures are given for obtaining certain parameters involved in the theoretical model for bounding the shielding performance of an enclosure. Techniques for evaluation of the accuracy of the theoretical calculation and its comparison to measured data are also discussed. Section 3 describes specifications that were developed to construct two shielded enclosures, one with a single layer topology and one with a double layer topology. Details are given on the mechanical design of the two enclosures, and on the design of various replaceable panels that can be used to test the accuracy of the theoretical model. Section 4 describes the experimental results of the shielding performance of the two enclosures constructed by SRI International.

RPT#: AD-A149292 DC-FR-1026.610-1B AFWL-TR-84-11 84/11/00
85N20227

REPORT DOCUMENTATION PAGE

1. Recipient's Reference	2. Originator's Reference	3. Further Reference	4. Security Classification of Document
	AGARD-LS-144	ISBN 92-835-1528-5	UNCLASSIFIED

5. Originator Advisory Group for Aerospace Research and Development
North Atlantic Treaty Organization
7 rue Ancelle, 92200 Neuilly sur Seine, France

6. Title INTERACTION BETWEEN EMP, LIGHTNING AND STATIC ELECTRICITY WITH AIRCRAFT AND MISSILE AVIONICS SYSTEMS

7. Presented on 29—30 May 1986 in Ankara, Turkey, 2—3 June 1986 in Oberpfaffenhofen, Germany and 5—6 June 1986 in The Hague, The Netherlands.

8. Author(s)/Editor(s)	9. Date
Various	May 1986
10. Author's/Editor's Address	**11. Pages**
Various	148

12. Distribution Statement This document is distributed in accordance with AGARD policies and regulations, which are outlined on the Outside Back Covers of all AGARD publications.

13. Keywords/Descriptors

Electromagnetic pulses
Nuclear explosion effects
Lightning
Static electricity
Avionics

14. Abstract

This Lecture Series will describe interactions between transient electromagnetic waves with aircraft and missile avionics systems. Transient electromagnetic waves include electromagnetic pulses (EMP) from nuclear explosions, lightning, and static electricity. Interactions are introduced by coupling of EMP and lightning induced currents and voltages with avionics components. Shielding against these interactions is discussed with respect to induced currents and voltages from EMP and lightning, and induced voltages from static charging effects. Several examples of interactions, coupling, shielding, and measurement techniques are presented.

This Lecture Series, sponsored by the Avionics Panel of AGARD, has been implemented by the Consultant and Exchange Programme of AGARD.

AGARD Lecture Series No.144 Advisory Group for Aerospace Research and Development, NATO INTERACTION BETWEEN EMP, LIGHTNING AND STATIC ELECTRICITY WITH AIRCRAFT AND MISSILE AVIONICS SYSTEMS Published May 1986 148 Pages This Lecture Series will describe interactions between transient electromagnetic waves with aircraft and missile avionics systems. Transient electromagnetic waves include electromagnetic pulses (EMP) from nuclear explosions, lightning, and static electricity. Interactions are introduced by coupling of EMP and lightning induced currents and voltages with avionics components. Shielding against these P.T.O.	AGARD-LS-144 Electromagnetic pulses Nuclear explosion effects Lightning Static electricity Avionics	AGARD Lecture Series No.144 Advisory Group for Aerospace Research and Development, NATO INTERACTION BETWEEN EMP, LIGHTNING AND STATIC ELECTRICITY WITH AIRCRAFT AND MISSILE AVIONICS SYSTEMS Published May 1986 148 Pages This Lecture Series will describe interactions between transient electromagnetic waves with aircraft and missile avionics systems. Transient electromagnetic waves include electromagnetic pulses (EMP) from nuclear explosions, lightning, and static electricity. Interactions are introduced by coupling of EMP and lightning induced currents and voltages with avionics components. Shielding against these P.T.O.	AGARD-LS-144 Electromagnetic pulses Nuclear explosion effects Lightning Static electricity Avionics
AGARD Lecture Series No.144 Advisory Group for Aerospace Research and Development, NATO INTERACTION BETWEEN EMP, LIGHTNING AND STATIC ELECTRICITY WITH AIRCRAFT AND MISSILE AVIONICS SYSTEMS Published May 1986 148 Pages This Lecture Series will describe interactions between transient electromagnetic waves with aircraft and missile avionics systems. Transient electromagnetic waves include electromagnetic pulses (EMP) from nuclear explosions, lightning, and static electricity. Interactions are introduced by coupling of EMP and lightning induced currents and voltages with avionics components. Shielding against these P.T.O.	AGARD-LS-144 Electromagnetic pulses Nuclear explosion effects Lightning Static electricity Avionics	AGARD Lecture Series No.144 Advisory Group for Aerospace Research and Development, NATO INTERACTION BETWEEN EMP, LIGHTNING AND STATIC ELECTRICITY WITH AIRCRAFT AND MISSILE AVIONICS SYSTEMS Published May 1986 148 Pages This Lecture Series will describe interactions between transient electromagnetic waves with aircraft and missile avionics systems. Transient electromagnetic waves include electromagnetic pulses (EMP) from nuclear explosions, lightning, and static electricity. Interactions are introduced by coupling of EMP and lightning induced currents and voltages with avionics components. Shielding against these P.T.O.	AGARD-LS-144 Electromagnetic pulses Nuclear explosion effects Lightning Static electricity Avionics

interactions is discussed with respect to induced currents and voltages from EMP and lightning and induced voltages from static charging effects. Several examples of interactions, coupling, shielding, and measurement techniques are presented.

This Lecture Series, sponsored by the Avionics Panel of AGARD has been implemented by the Consultant and Exchange Programm of AGARD.

ISBN 92-835-1528-5

interactions is discussed with respect to induced currents and voltages from EMP and lightning and induced voltages from static charging effects. Several examples of interactions, coupling, shielding, and measurement techniques are presented.

This Lecture Series, sponsored by the Avionics Panel of AGARD has been implemented by the Consultant and Exchange Programm of AGARD.

ISBN 92-835-1528-5

interactions is discussed with respect to induced currents and voltages from EMP and lightning and induced voltages from static charging effects. Several examples of interactions, coupling, shielding, and measurement techniques are presented.

This Lecture Series, sponsored by the Avionics Panel of AGARD has been implemented by the Consultant and Exchange Programm of AGARD.

ISBN 92-835-1528-5

interactions is discussed with respect to induced currents and voltages from EMP and lightning and induced voltages from static charging effects. Several examples of interactions, coupling, shielding, and measurement techniques are presented.

This Lecture Series, sponsored by the Avionics Panel of AGARD has been implemented by the Consultant and Exchange Programm of AGARD.

ISBN 92-835-1528-5

AGARD
NATO OTAN
7 RUE ANCELLE · 92200 NEUILLY-SUR-SEINE
FRANCE
Telephone (1) 47.45.08.10 · Telex 610176

DISTRIBUTION OF UNCLASSIFIED AGARD PUBLICATIONS

AGARD does NOT hold stocks of AGARD publications at the above address for general distribution. Initial distribution of AGARD publications is made to AGARD Member Nations through the following National Distribution Centres. Further copies are sometimes available from these Centres, but if not may be purchased in Microfiche or Photocopy form from the Purchase Agencies listed below.

NATIONAL DISTRIBUTION CENTRES

BELGIUM
Coordonnateur AGARD – VSL
Etat-Major de la Force Aérienne
Quartier Reine Elisabeth
Rue d'Evere, 1140 Bruxelles

CANADA
Defence Scientific Information Services
Dept of National Defence
Ottawa, Ontario K1A 0K2

DENMARK
Danish Defence Research Board
Ved Idraetsparken 4
2100 Copenhagen Ø

FRANCE
O.N.E.R.A. (Direction)
29 Avenue de la Division Leclerc
92320 Chatillon

GERMANY
Fachinformationszentrum Energie,
Physik, Mathematik GmbH
Kernforschungszentrum
D-7514 Eggenstein-Leopoldshafen

GREECE
Hellenic Air Force General Staff
Research and Development Directorate
Holargos, Athens

ICELAND
Director of Aviation
c/o Flugrad
Reykjavik

ITALY
Aeronautica Militare
Ufficio del Delegato Nazionale all'AGARD
3 Piazzale Adenauer
00144 Roma/EUR

LUXEMBOURG
See Belgium

NETHERLANDS
Netherlands Delegation to AGARD
National Aerospace Laboratory, NLR
P.O. Box 126
2600 AC Delft

NORWAY
Norwegian Defence Research Establishment
Attn: Biblioteket
P.O. Box 25
N-2007 Kjeller

PORTUGAL
Portuguese National Coordinator to AGARD
Gabinete de Estudos e Programas
CLAFA
Base de Alfragide
Alfragide
2700 Amadora

TURKEY
Department of Research and Development (ARGE)
Ministry of National Defence, Ankara

UNITED KINGDOM
Defence Research Information Centre
Kentigern House
65 Brown Street
Glasgow G2 8EX

UNITED STATES
National Aeronautics and Space Administration (NASA)
Langley Research Center
M/S 180
Hampton, Virginia 23665

THE UNITED STATES NATIONAL DISTRIBUTION CENTRE (NASA) DOES NOT HOLD STOCKS OF AGARD PUBLICATIONS, AND APPLICATIONS FOR COPIES SHOULD BE MADE DIRECT TO THE NATIONAL TECHNICAL INFORMATION SERVICE (NTIS) AT THE ADDRESS BELOW.

PURCHASE AGENCIES

Microfiche or Photocopy
National Technical
Information Service (NTIS)
5285 Port Royal Road
Springfield
Virginia 22161, USA

Microfiche
ESA/Information Retrieval Service
European Space Agency
10, rue Mario Nikis
75015 Paris, France

Microfiche or Photocopy
British Library Lending
Division
Boston Spa, Wetherby
West Yorkshire LS23 7BQ
England

Requests for microfiche or photocopies of AGARD documents should include the AGARD serial number, title, author or editor, and publication date. Requests to NTIS should include the NASA accession report number. Full bibliographical references and abstracts of AGARD publications are given in the following journals:

Scientific and Technical Aerospace Reports (STAR)
published by NASA Scientific and Technical
Information Branch
NASA Headquarters (NIT-40)
Washington DC, 20546, USA

Government Reports Announcements (GRA)
published by the National Technical
Information Services, Springfield
Virginia 22161, USA

Printed by Specialised Printing Services Limited
40 Chigwell Lane, Loughton, Essex IG10 3TZ

ISBN-92-835-1528-5